Cognition in healthy aging and Parkinson's disease: Structural and functional integrity of neural circuits

by

David A. Ziegler

B.S., Pyschobiology
Denison University, 1999

Submitted to the Department of Brain and Cognitive Sciences
in partial fulfillment of the requirements for the degree of

Doctor of Philosophy in Neuroscience

at the

Massachusetts Institute of Technology

September, 2011

© Massachusetts Institute of Technology. All rights reserved

Signature of Author _____
David Ziegler
Department of Brain and Cognitive Sciences

Certified by_____
Suzanne Corkin
Professor of Behavioral Neuroscience, MIT
Thesis Supervisor

Accepted by _____
Earl K. Miller
Picower Professor of Neuroscience
Director, BCS Graduate Program

Cognition in healthy aging and Parkinson's disease: Structural and functional integrity of neural circuits

by

David A. Ziegler

Submitted to the Department of Brain and Cognitive Sciences
on August 5, 2011 in partial fulfillment of the requirements for the degree of
Doctor of Philosophy in Neuroscience

Abstract

This dissertation documents how healthy aging and Parkinson's disease (PD) affect brain anatomy and physiology and how these neural changes relate to measures of cognition and perception. While healthy aging and PD are both accompanied by a wide-range of cognitive impairments, the neural underpinnings of cognitive decline in each is likely mediated by deterioration of different systems. The four chapters of this dissertation address specific aspects of how healthy aging and PD affect the neural circuits that support sensory processes and high-level cognition.

The experiments in **Chapters 2** and **3** examine the effects of healthy aging on the integrity of neural circuits that modulate cognitive control processes. In **Chapter 2**, we test the hypothesis that the patterns of age-related change differ between white matter and gray matter regions, and that changes in the integrity of anterior regions correlate most strongly with performance on cognitive control tasks. In **Chapter 3**, we build upon the structural findings by examining the hypothesis that age-related changes in white matter integrity are associated with disrupted oscillatory dynamics observed during a visual search task. **Chapter 4** investigates healthy age-related changes in somatosensory mu rhythms and evoked responses and uses a computational model of primary somatosensory cortex to predict the underlying cellular and neurophysiolgical bases of these alterations.

In contrast to the widespread cortical changes seen in healthy OA, the cardinal motor symptoms of PD are largely explained by degeneration of the dopaminergic substantia nigra, pars compacta (SNc). Cognitive sequelae of PD, however, likely result from disruptions in multiple neurotransmitter systems, including nondopaminergic nuclei, but research on these aspects of the disease has been hindered by a lack of sensitive MRI biomarkers for the affected structures. **Chapter 5** presents new multispectral MRI tools that visualize the SNc and the cholinergic basal forebrain (BF). We applied these methods to test the hypothesis that degenerative processes in PD affect the SNc before the BF. This experiment lays important groundwork for future studies that will examine the relative contribution of the SNc and BF to cognitive impairments in PD.

Thesis Supervisor: Suzanne Corkin
Title: Professor of Behavioral Neuroscience

Table of Contents

Chapter 1: Introduction

Structural integrity of cognitive control networks in healthy aging.

Healthy aging is characterized by functional declines that cross multiple cognitive domains, including attention, working memory, and long-term declarative memory (Craik & Salthouse, 2000; Hedden & Gabrieli, 2004; Glisky, 2007; Piguet & Corkin, 2007). Common to many of the tasks that reveal the effects of age is a reliance on cognitive control processes. Cognitive control encompasses a collection of top-down processes that enable us to modulate the impact of sensory inputs on our brain. These processes include planning a series of actions, managing goals, coordinating and monitoring automatic processes, inhibiting prepotent responses, focusing attention selectively, and suppressing irrelevant sensory inputs (Salthouse & Meinz, 1995; Spencer & Raz, 1995; Fuster, 2000; Miller, 2000; Braver *et al.*, 2001; Miller & Cohen, 2001). This ability to manage the barrage of sensory information that we encounter in the world allows us to engage in complex, goal-directed behaviors, and it is exactly these processes that are most susceptible to breakdown during the course of healthy aging (Buckner, 2004; Gazzaley & D'Esposito, 2007). Notably, older adults (OA) consistently show reduced performance on tasks that place high demands on cognitive control, including multi-tasking (Jimura & Braver, 2010; Clapp *et al.*, 2011), attention (McDowd, 1986; Hawkins *et al.*, 1992; Milham *et al.*, 2002; West, 2004), episodic and source memory (Craik & McDowd, 1984; Spencer & Raz, 1994), and working memory (Hasher & Zacks, 1988; Salthouse, 1994; Gazzaley *et al.*, 2005; Emery *et al.*, 2008), or on tasks such as free recall, which provide relatively little

environmental support during encoding or retrieval (Craik, 1990). In contrast, OA appear to remain relatively unimpaired on most measures of nondeclarative or implicit memory, which are believed to rely on more automatic and less attention-demanding processes (Light & Singh, 1987; La Voie & Light, 1994; Fleischman & Gabrieli, 1998; Bergerbest *et al.*, 2009). Consequently, an emerging theme is that impaired or inefficient deployment of cognitive control processes may be a common mechanism underlying many of the cognitive deficits in healthy aging (Miyake *et al.*, 2000; Fletcher & Henson, 2001; Braver & Barch, 2002; Salthouse *et al.*, 2003; Braver & Ruge, 2006; Glisky, 2007).

Cognitive control processes are supported by broadly distributed networks within association areas, including prefrontal (PFC) and posterior parietal cortex, that exert top-down control over posterior sensory and motor areas (Goldman-Rakic, 1988; Wise *et al.*, 1996; Miller, 2000; Miller & Cohen, 2001; Stuss & Knight, 2002; Koechlin *et al.*, 2003; Tanji & Hoshi, 2008). Degeneration of any of the nodes or links of these networks could interfere with efficient deployment of cognitive control processes in OA. Evidence for age-related changes in the structural integrity of frontoparietal control regions come from a variety of sources and point toward changes in both cortical gray matter and its underlying white matter. Based on the patterns of neuroanatomical change observed during the course of healthy aging, the frontal aging hypothesis has been proposed as a theoretically parsimonious explanation of deficits in cognitive control processes in OA (West, 1996; Tisserand & Jolles, 2003), although this hypothesis is not universally embraced (Greenwood, 2000; Van Petten *et al.*, 2004; Raz & Rodrigue, 2006).

Magnetic resonance imaging (MRI)-based studies consistently reveal a global age-related decline in gray matter volumes (Pfefferbaum *et al.*, 1994; Raz *et al.*, 1997; Salat *et al.*, 1999; Bartzokis *et al.*, 2001; Allen *et al.*, 2005; Raz *et al.*, 2005; Walhovd *et al.*, 2005), but regional differences exist in terms of the relative rate and magnitude of change. An ever-growing literature documents the most dramatic volume losses in PFC (Jernigan *et al.*, 1991; Raz *et al.*, 1997; Salat *et al.*, 1999; Sowell *et al.*, 2003; Raz *et al.*, 2004; Grieve *et al.*, 2005; Raz & Rodrigue, 2006), while more posterior areas tend to show less shrinkage with age (Raz *et al.*, 1997; Salat *et al.*, 1999; Bartzokis *et al.*, 2001; Resnick *et al.*, 2003; Allen *et al.*, 2005; Raz *et al.*, 2005). Within PFC, lateral PFC and orbital cortices show the greatest degree of volumetric decline (Raz *et al.*, 2004; Raz *et al.*, 2005). Newer methods for examining the thickness of discrete areas across the cerebral cortex provide confirmatory evidence of pronounced thinning of the superior and inferior frontal gyri, but also reveal thinning in occipital and parietal lobes (Salat *et al.*, 2004; Fjell *et al.*, 2009; Lemaitre *et al.*, 2010). A postmortem study confirmed that age-related thinning of the frontal and temporal lobes, with greater atrophy in the frontal lobe (Freeman *et al.*, 2008). Futher, cortical thinning was not associated with decreased neuron number or density, suggesting that changes in neuropil, decreased dendritic arborization, or a loss of ascending projections account for age-related cortical thinning. Thus, while strong evidence shows that the detrimental effects of aging occur earlier and have a greater magnitude of effect on frontal lobe gray matter, compared to posterior cortices, significant degeneration has also been documented in all four lobes of the brain bilaterally (Cowell *et al.*, 1994; Bartzokis *et al.*, 2001; Tisserand *et al.*, 2002; Raz *et al.*, 2004; Van Petten, 2004; Van Petten *et al.*, 2004; Allen *et al.*, 2005),

Postmortem studies indicate that healthy aging is also associated with marked degradation of white matter (Double *et al.*, 1996; Guttmann *et al.*, 1998; Peters, 2002; Hinman & Abraham, 2007; Ikram *et al.*, 2007; Piguet *et al.*, 2009), but the evidence for volumetric decline remains equivocal: Some studies report reduced global and regional white matter volumes (Guttmann *et al.*, 1998; Salat *et al.*, 1999; Courchesne *et al.*, 2000; Bartzokis *et al.*, 2001; Jernigan *et al.*, 2001; Allen *et al.*, 2005; Piguet *et al.*, 2009), whereas others fail to find such decreases (Pfefferbaum *et al.*, 1994; Good *et al.*, 2001; Sullivan *et al.*, 2004). More compelling in vivo evidence of white matter decline comes from other MRI markers of degeneration, including diffusion-tensor imaging (DTI)-based measures of white matter integrity. Like cortical thickness, declines in white matter integrity are widespread (Good *et al.*, 2001; Salat *et al.*, 2004; Lutz *et al.*, 2007; Yoon *et al.*), but tend to be most striking in anterior areas, such as the genu of the corpus callosum and the white matter underlying the PFC (O'Sullivan *et al.*, 2001; Head *et al.*, 2004; Pfefferbaum *et al.*, 2005; Salat *et al.*, 2005; Sullivan & Pfefferbaum, 2006; Ardekani *et al.*, 2007; Madden *et al.*, 2007; Yoon *et al.*).

While the patterns of age-related cognitive and neuroanatomical change are relatively well characterized, linking these measures to unmask the specific neural bases of cognitive decline has proven more difficult. In OA, diminished attention and executive function are associated with decreased global cortical volumes and reduced volumes of lateral PFC and OFC (Zimmerman *et al.*, 2006; Kramer *et al.*, 2007). In addition, PFC volume was inversely correlated with perseverative errors in OA (Raz *et al.*, 1998; Gunning-Dixon & Raz, 2003). In contrast,

spatial and object working memory correlated with occipital lobe volume (Raz *et al.*, 1998), but neither spatial, object, nor verbal working memory showed significant correlations with PFC volume (Gunning-Dixon & Raz, 2003). Thus, direct evidence in support of an association between cortical atrophy and age-related cognitive decline remains equivocal.

Stronger support for a link between frontal lobe integrity and cognition comes from studies of white matter. One study of older rhesus monkeys found a correlation between measures of executive function and DTI-based measures of white matter integrity (e.g., FA and diffusivity) in long-distance corticocortical association pathways (Makris *et al.*, 2007). Several investigations in OA have linked deficits in processing speed, executive function, immediate and delayed recall, and overall cognition to an increased burden of white matter hypertintensities (Gunning-Dixon & Raz, 2000; Gunning-Dixon & Raz, 2003; Soderlund *et al.*, 2003; Smith *et al.*, 2011). White matter abnormalities were also associated with decreased frontal lobe metabolism (DeCarli *et al.*, 1995; Tullberg *et al.*, 2004), and with diminished BOLD responses in PFC during performance of episodic and working memory tasks (Nordahl *et al.*, 2006). Functional correlates of decreased FA include working memory impairments (Charlton *et al.*, 2006), slowed processing speed (Sullivan *et al.*, 2006; Bucur *et al.*, 2007), and executive dysfunction (O'Sullivan *et al.*, 2001; Deary *et al.*, 2006; Grieve *et al.*, 2007). These results suggest that degeneration of white matter pathways contributes to the etiology of age-related cognitive decline to an equal or greater extent than gray matter atrophy (O'Sullivan *et al.*, 2001; Hinman & Abraham, 2007).

In summary, evidence of morphological and microstructural changes in anterior areas appears consistently in the literature on aging. In addition, regional alterations have been noted across wide regions of gray and white matter, but the exact nature and magnitude of these changes remain a topic of debate. To explicitly test whether gray and white matter exhibit similar or distinct patterns of age-related change, measures of both regions must be examined in a single group of participants. **Chapter 1** accomplishes this goal by using advanced MRI techniques to examine high-resolution measures of white matter integrity and cortical thickness in healthy young adults (YA) and OA. Further, we tested the prediction that performance on tests of cognitive control is correlated with integrity of anterior regions, while episodic memory and semantic memory are associated with changes in posterior cortices.

The role of oscillatory activity in top-down control.

A growing body of literature supports the idea that oscillatory synchronization is one mechanism underlying efficient deployment of cognitive control processes. The first report of oscillatory activity in the human brain came from Hans Berger who recorded electrical potentials over the posterior scalp using a string galvanometer (Berger, 1929). Berger observed oscillatory signals over the occipital cortex, the most prominent being the ~10 Hz alpha rhythm, which was strongest when participants closed their eyes. Berger's invention of the electroencephalogram ushered in an era of active investigation of the origins and functional significance of brain rhythms (Bremer, 1958). Additional technological advances, such as the development of high-resolution whole-head magnetoencephalography in humans (Hämäläinen *et al.*, 1993; Cohen, 2004), as well as the advent of multi-electrode recordings in non-human

animals (Nicolelis & Ribeiro, 2002; Miller & Wilson, 2008), have led to a greater understanding of the range and pervasiveness of cortical oscillations, with frequencies ranging from <1 Hz up to several hundred Hz being observed in the cerebral cortex of virtually every mammal studied (Buzsaki, 2006). It is now well established that oscillations occur throughout the brain and are believed to be a fundamental mechanism of neural information processing, likely mediating high-level cognition (Hari & Salmelin, 1997; Kahana, 2006; Fries, 2009), but the underlying mechanisms of these rhythms and their complex dynamic modulation remain topics of intense scrutiny (Whittington & Traub, 2003; Bartos *et al.*, 2007; Wang, 2010).

Neural rhythms are thought to be critical for a number of cognitive processes including working memory (Howard *et al.*, 2003; Jensen, 2006; Kahana, 2006; Jokisch & Jensen, 2007), visual attention (Buschman & Miller, 2007; Jensen *et al.*, 2007; Gregoriou *et al.*, 2009), top-down anticipatory biasing of sensory cortices (Schadow *et al.*, 2009), motor planning (Van Der Werf *et al.*, 2008; Van Der Werf *et al.*, 2010), complex spatial navigation (Kahana *et al.*, 1999), and long-term memory encoding (Klimesch *et al.*, 1996; Sederberg *et al.*, 2003) and retrieval (Klimesch *et al.*, 2006). Oscillations may bind information across brain regions (Singer, 1999) or facilitate communication between disparate cortical sites (Salinas & Sejnowski, 2001). In particular, oscillations may provide a mechanism for facilitating top-down modulation, possibly by enhancing stimulus representations or regulating communication between high-order control areas and sensory and motor cortices (Engel *et al.*, 2001; Salinas & Sejnowski, 2001; Jensen *et al.*, 2007).

Mounting evidence suggests an important role for high-frequency, or gamma (~30-100 Hz), oscillations in working memory and attention (Tallon-Baudry *et al.*, 2001; Howard *et al.*, 2003; Jensen *et al.*, 2007; Fries, 2009), and some have proposed that such oscillations provide a mechanism for sustaining information "online" (Jensen, 2006). Gamma oscillations occur locally in primary sensory and motor areas during performance of attention demanding tasks and are believed to be mediated by local network interactions between excitatory pyramidal neurons and inhibitory interneurons (McBain & Fisahn, 2001; Whittington & Traub, 2003; Bartos *et al.*, 2007; Cardin *et al.*, 2009). Oscillations in the beta (~15-30 Hz) range likely facilitate top-down influences from association cortices during performance of tasks that require a high degree of cognitive control (Buschman & Miller, 2007; Siegel *et al.*, 2008; Schroeder & Lakatos, 2009). This effect may depend on synchronization of neural firing between distant executive control areas and primary sensory and motor areas, thus requiring efficient long-distance communication via white matter tracts. Low-frequency alpha oscillations (~7-14 Hz) block modality-specific distracters, and are commonly observed during working memory tasks (Jokisch & Jensen, 2007; Tuladhar *et al.*, 2007). In contrast, event-related decreases in alpha power (alpha desynchronizations) are often seen in occipital areas when participants perform tasks that require active visual processing (Capotosto *et al.*, 2009), such as during visual search tasks.

Age-related declines in white matter integrity could interfere with long-range synchronization of lower frequency alpha and beta oscillations, while cortical thinning, which likely reflects a loss of interneurons or synapses (Peters *et al.*, 1998; Peters *et al.*, 2008), may disrupt local

gamma oscillations. These changes in neural rhythms likely impact cognition in OA. In **Chapter 3**, we describe a multimodal neuroimaging experiment that combines magnetoencephalography (MEG) and MRI to study the effects of aging on oscillatory activity associated with visual attention.

Age-related changes in primary sensory rhythms.

Oscillations in primary sensory cortices, such as the somatosensory mu rhythm, also appear to play important roles in facilitating sensory processing. In addition to declines in high-level cognitive processes, healthy aging is also accompanied by decrements in somatosensory perceptual abilities (Baltes & Lindenberger, 1997; Schneider & Pichora-Fuller, 2000), including declines in tactile perception. OA exhibit significantly higher detection thresholds for vibrations delivered to the hand (Verrillo, 1982; Gescheider *et al.*, 1996; Verrillo *et al.*, 2002). This change is accompanied by a decrease in the subjective magnitude of vibrotactile sensation (Verrillo, 1982; Verrillo *et al.*, 2002) and decreased discrimination abilities (Gescheider *et al.*, 1996).

The neural underpinnings of these age-related changes in somatosensory function remain elusive. One hypothesis is that decreased discrimination thresholds are consistent with a reduction in the amount of afferent input to cortical somatosensory areas (Gescheider *et al.*, 1996). This decrease in afferent drive could stem from a reduced density of tactile receptors in the skin (Cauna, 1965). In contrast, other studies in OA have documented age-related increases in peak magnitudes of somatosensory responses following median nerve stimulation (Luders, 1970; Desmedt & Cheron, 1980; Adler & Nacimiento, 1988; Kakigi & Shibasaki, 1991; Ferri *et al.*,

1996; Stephen *et al.*, 2006) and increased amplitude of tactile evoked potentials (Ogata *et al.*, 2009). Further, many of these changes are apparent by middle-age, and anatomical studies suggest that age-related thinning of primary somatosensory cortex begins at this time (Salat *et al.*, 2004).

An expanding body of literature has shown that somatosensory evoked responses are inextricably linked to ongoing neural rhythms (Nikulin *et al.*, 2007; Mazaheri & Jensen, 2008; Jones *et al.*, 2009; Zhang & Ding, 2010), and that these modulations are correlated with perception and attention (Linkenkaer-Hansen *et al.*, 2004; Fries, 2009; Zhang & Ding, 2010). The predominant rhythm in pre- and postcentral cortex is the somatosensory mu rhythm, which manifests as a complex of alpha and beta oscillations when recorded with MEG (Tiihonen *et al.*, 1989; Narici *et al.*, 1990; Cheyne *et al.*, 2003). One study reported concomitant age-related increases in induced alpha and high beta (22-23 Hz) power in anterior sensorimotor electrodes during a simple finger extension task (Sailer *et al.*, 2000), but few studies have examined the effects of aging on this commonly observed somatosensory rhythm. Because age-related changes in somatosensory evoked responses and cortical thickness are observed in middle-age, these alterations should also impact the somatosensory mu rhythm. In **Chapter 4,** we use MEG to examine age-related changes in spontaneous cortical rhythms and evoked responses from the primary somatosensory cortices (SI) of healthy YA and middle-aged adults during a tactile detection task. We then apply a biophysically realistic computational neural model of SI (Jones *et al.*, 2007) to examine possible neural mechanisms underlying the age-related effects.

***Neuropathological and neuroimaging studies of Parkinson's disease*.**

In contrast to healthy aging, which is by definition aging in the absence of overt pathology, Parkinson's disease (PD) is an age-related neurodegenerative disorder that is typically characterized by its cardinal motor symptoms: resting tremor, muscular rigidity, bradykinesia, postural instability, and gait abnormality (Shulman *et al.*, 2011). Cognitive impairments are common in PD, but differ from those that characterize healthy aging.

The major neuropathologic feature of idiopathic PD is selective loss of dopaminergic neurons and accumulation of Lewy bodies and neurites in the substantia nigra pars compacta (Wichmann & DeLong, 2002; Jellinger, 2005). In healthy brains, neurons from the substantia nigra project to the striatum and other basal ganglia nuclei. Functionally segregated circuits link the basal ganglia and neocortex in a topographical manner (Alexander *et al.*, 1986; Middleton & Strick, 2000), and include dense reciprocal fronto-striatal connections (Alexander *et al.*, 1986; Saint-Cyr, 2003). Because of neuronal loss in the substanita nigra, PD patients show markedly reduced dopamine neurotransmission in the striatum, which likely accounts for the majority of the primary motor symptoms. Loss of dopamineric cells in the substantia nigra also disrupts the function of frontostriatal circuits. The pattern of dopamine loss in the striatum occurs according to a lateral-medial/dorsal-ventral gradient, corresponding inversely to the gradient of cell loss in the substantia nigra: Cells projecting to the putamen are lost first, followed by those that project to the caudate nucleus and nucleus accumbens (Jellinger, 2005). Thus, many of the cognitive deficits in PD—working memory, attention, and processing speed—have been attributed to loss of dopamine inputs to nonmotor circuits of the basal ganglia, which may be

affected by dopamine loss in the same way as basal ganglia motor circuits (Alexander *et al.*, 1986; Saint-Cyr, 2003).

Neuropathological studies indicate, however, that cell loss and neuropathology in PD are not limited to the basal ganglia (Halliday *et al.*, 1990; Laakso *et al.*, 1996; Henderson *et al.*, 2000; Harding *et al.*, 2002). Degeneration of the cholinergic basal forebrain also occurs (Javoy-Agid *et al.*, 1981; Rogers *et al.*, 1985; Mufson *et al.*, 1991), and may account for some cognitive impairments (Pillon *et al.*, 1989; Rye & DeLong, 2003; Calabresi *et al.*, 2006), including deficits in attention and cognitive control (Dubois *et al.*, 1990). PD patients who show early pathological insults in non-dopaminergic nuclei may exhibit cognitive decline earlier in the course of the disease and may be more likely to develop dementia, while PD patients with more targeted degeneration of the substantia nigra may show a more subtle pattern of cognitive change.

A major limitation to studies of brain-behavior correlations in PD is that conventional structural MRI techniques provide relatively poor contrast for the structures that are affected by the disease, and thus are not typically used in experimental studies of PD (Schrag *et al.*, 1998; Marek & Jennings, 2009). This ineffectiveness is due predominantly to the limited contrast of most current MRI methods, which are unable to detect PD abnormalities. In **Chapter 5**, we describe a new multispectral MRI method that provides excellent contrast for the substantia nigra and basal forebrain and apply these methods to data from PD patients and controls to show that these structures display different trajectories of volume loss early in the disease.

References

Adler G & Nacimiento AC (1988) Age-dependent changes of short-latency somatosensory evoked potentials in healthy adults. *Appl Neurophysiol* **51**, 55-59.

Alexander GE, DeLong MR & Strick PL (1986) Parallel organization of functionally segregated circuits linking basal ganglia and cortex. *Annu Rev Neurosci* **9**, 357-381.

Allen JS, Bruss J, Brown CK & Damasio H (2005) Normal neuroanatomical variation due to age: the major lobes and a parcellation of the temporal region. *Neurobiol Aging* **26**, 1245-1260; discussion 1279-1282.

Ardekani S, Kumar A, Bartzokis G & Sinha U (2007) Exploratory voxel-based analysis of diffusion indices and hemispheric asymmetry in normal aging. *Magn Reson Imaging* **25**, 154-167.

Baltes PB & Lindenberger U (1997) Emergence of a powerful connection between sensory and cognitive functions across the adult life span: a new window to the study of cognitive aging? *Psychol Aging* **12**, 12-21.

Bartos M, Vida I & Jonas P (2007) Synaptic mechanisms of synchronized gamma oscillations in inhibitory interneuron networks. *Nat Rev Neurosci* **8**, 45-56.

Bartzokis G, Beckson M, Lu PH, Nuechterlein KH, Edwards N & Mintz J (2001) Age-related changes in frontal and temporal lobe volumes in men: a magnetic resonance imaging study. *Arch Gen Psychiatry* **58**, 461-465.

Berger H (1929) Ueber das Elektroenkephalogramm des Menschen. *Arch Psychiatr Nervenkrankh* **87**.

Bergerbest D, Gabrieli JD, Whitfield-Gabrieli S, Kim H, Stebbins GT, Bennett DA & Fleischman DA (2009) Age-associated reduction of asymmetry in prefrontal function and preservation of conceptual repetition priming. *Neuroimage* **45**, 237-246.

Braver TS & Barch DM (2002) A theory of cognitive control, aging cognition, and neuromodulation. *Neurosci Biobehav Rev* **26**, 809-817.

Braver TS, Barch DM, Keys BA, Carter CS, Cohen JD, Kaye JA, Janowsky JS, Taylor SF, Yesavage JA, Mumenthaler MS, Jagust WJ & Reed BR (2001) Context processing in older adults: evidence for a theory relating cognitive control to neurobiology in healthy aging. *J Exp Psychol Gen* **130**, 746-763.

Braver TS & Ruge H (2006) Functional Neuroimaging of Executive Functions. In *Handbook of Functional Neuroimaging of Cognition, 2nd Edition*, pp. 307-347 [R Cabeza and A Kingstone, editors]. Cambridge, MA: MIT Press.

Bremer F (1958) Cerebral and cerebellar potentials. *Physiol Rev* **38**, 357-388.

Buckner RL (2004) Memory and executive function in aging and AD: multiple factors that cause decline and reserve factors that compensate. *Neuron* **44**, 195-208.

Bucur B, Madden DJ, Spaniol J, Provenzale JM, Cabeza R, White LE & Huettel SA (2007) Age-related slowing of memory retrieval: Contributions of perceptual speed and cerebral white matter integrity. *Neurobiol Aging*.

Buschman TJ & Miller EK (2007) Top-down versus bottom-up control of attention in the prefrontal and posterior parietal cortices. *Science* **315**, 1860-1862.

Buzsaki G (2006) *Rhythms of the Brain*. New York: Oxford University Press.

Calabresi P, Picconi B, Parnetti L & Di Filippo M (2006) A convergent model for cognitive dysfunctions in Parkinson's disease: the critical dopamine-acetylcholine synaptic balance. *Lancet Neurol* **5**, 974-983.

Capotosto P, Babiloni C, Romani GL & Corbetta M (2009) Frontoparietal cortex controls spatial attention through modulation of anticipatory alpha rhythms. *J Neurosci* **29**, 5863-5872.

Cardin JA, Carlen M, Meletis K, Knoblich U, Zhang F, Deisseroth K, Tsai LH & Moore CI (2009) Driving fast-spiking cells induces gamma rhythm and controls sensory responses. *Nature* **459**, 663-667.

Cauna N (1965) The effects of aging on the receptor organs of the human dermis. In *Advances in Biology of the Skin: Aging*, pp. 63-96 [W Montagna, editor]. Elmsford, NY: Pergamon Press.

Charlton RA, Barrick TR, McIntyre DJ, Shen Y, O'Sullivan M, Howe FA, Clark CA, Morris RG & Markus HS (2006) White matter damage on diffusion tensor imaging correlates with age-related cognitive decline. *Neurology* **66**, 217-222.

Cheyne D, Gaetz W, Garnero L, Lachaux JP, Ducorps A, Schwartz D & Varela FJ (2003) Neuromagnetic imaging of cortical oscillations accompanying tactile stimulation. *Brain Res Cogn Brain Res* **17**, 599-611.

Clapp WC, Rubens MT, Sabharwal J & Gazzaley A (2011) Deficit in switching between functional brain networks underlies the impact of multitasking on working memory in older adults. *Proc Natl Acad Sci U S A* **108**, 7212-7217.

Cohen D (2004) Boston and the history of biomagnetism. *Neurol Clin Neurophysiol* **2004**, 114.

Courchesne E, Chisum HJ, Townsend J, Cowles A, Covington J, Egaas B, Harwood M, Hinds S & Press GA (2000) Normal brain development and aging: quantitative analysis at in vivo MR imaging in healthy volunteers. *Radiology* **216**, 672-682.

Cowell PE, Turetsky BI, Gur RC, Grossman RI, Shtasel DL & Gur RE (1994) Sex differences in aging of the human frontal and temporal lobes. *J Neurosci* **14**, 4748-4755.

Craik FI (1990) Changes in memory with normal aging: a functional view. *Adv Neurol* **51**, 201-205.

Craik FI & McDowd JM (1984) Age differences in recall and recognition. *Journal of Experimental Psychology: Learning, Memory, and Cognition* **13**, 474-479.

Craik FIM & Salthouse TA (2000) *The Handbook of Aging and Cognition*. Mahwah, NJ: Lawrence Erlbaum Associates.

Deary IJ, Bastin ME, Pattie A, Clayden JD, Whalley LJ, Starr JM & Wardlaw JM (2006) White matter integrity and cognition in childhood and old age. *Neurology* **66**, 505-512.

DeCarli C, Murphy DG, Tranh M, Grady CL, Haxby JV, Gillette JA, Salerno JA, Gonzales-Aviles A, Horwitz B, Rapoport SI & et al. (1995) The effect of white matter hyperintensity volume on brain structure, cognitive performance, and cerebral metabolism of glucose in 51 healthy adults. *Neurology* **45**, 2077-2084.

Desmedt JE & Cheron G (1980) Somatosensory evoked potentials to finger stimulation in healthy octogenarians and in young adults: wave forms, scalp topography and transit times of parietal and frontal components. *Electroencephalogr Clin Neurophysiol* **50**, 404-425.

Double KL, Halliday GM, Kril JJ, Harasty JA, Cullen K, Brooks WS, Creasey H & Broe GA (1996) Topography of brain atrophy during normal aging and Alzheimer's disease. *Neurobiol Aging* **17**, 513-521.

Dubois B, Pillon B, Sternic N, Lhermitte F & Agid Y (1990) Age-induced cognitive disturbances in Parkinson's disease. *Neurology* **40**, 38-41.

Emery L, Heaven TJ, Paxton JL & Braver TS (2008) Age-related changes in neural activity during performance matched working memory manipulation. *Neuroimage* **42**, 1577-1586.

Engel AK, Fries P & Singer W (2001) Dynamic predictions: oscillations and synchrony in top-down processing. *Nat Rev Neurosci* **2**, 704-716.

Ferri R, Del Gracco S, Elia M, Musumeci SA, Spada R & Stefanini MC (1996) Scalp topographic mapping of middle-latency somatosensory evoked potentials in normal aging and dementia. *Neurophysiol Clin* **26**, 311-319.

Fjell AM, Westlye LT, Amlien I, Espeseth T, Reinvang I, Raz N, Agartz I, Salat DH, Greve DN, Fischl B, Dale AM & Walhovd KB (2009) High consistency of regional cortical thinning in aging across multiple samples. *Cereb Cortex* **19**, 2001-2012.

Fleischman DA & Gabrieli JD (1998) Repetition priming in normal aging and Alzheimer's disease: a review of findings and theories. *Psychol Aging* **13**, 88-119.

Fletcher PC & Henson RN (2001) Frontal lobes and human memory: insights from functional neuroimaging. *Brain* **124**, 849-881.

Freeman SH, Kandel R, Cruz L, Rozkalne A, Newell K, Frosch MP, Hedley-Whyte ET, Locascio JJ, Lipsitz LA & Hyman BT (2008) Preservation of neuronal number despite age-related cortical brain atrophy in elderly subjects without Alzheimer disease. *J Neuropathol Exp Neurol* **67**, 1205-1212.

Fries P (2009) Neuronal gamma-band synchronization as a fundamental process in cortical computation. *Annu Rev Neurosci* **32**, 209-224.

Fuster JM (2000) Executive frontal functions. *Exp Brain Res* **133**, 66-70.

Gazzaley A, Cooney JW, Rissman J & D'Esposito M (2005) Top-down suppression deficit underlies working memory impairment in normal aging. *Nat Neurosci* **8**, 1298-1300.

Gazzaley A & D'Esposito M (2007) Top-down modulation and normal aging. *Ann N Y Acad Sci* **1097**, 67-83.

Gescheider GA, Edwards RR, Lackner EA, Bolanowski SJ & Verrillo RT (1996) The effects of aging on information-processing channels in the sense of touch: III. Differential sensitivity to changes in stimulus intensity. *Somatosens Mot Res* **13**, 73-80.

Glisky EL (2007) Changes in Cognitive Function in Human Aging. In *Brain Aging: Models, Methods, and Mechanisms*, pp. Chapter 1. [DR Riddle, editor]. Boca Raton (FL): CRC Press.

Goldman-Rakic PS (1988) Topography of cognition: parallel distributed networks in primate association cortex. *Annu Rev Neurosci* **11**, 137-156.

Good CD, Johnsrude IS, Ashburner J, Henson RN, Friston KJ & Frackowiak RS (2001) A voxel-based morphometric study of ageing in 465 normal adult human brains. *Neuroimage* **14**, 21-36.

Greenwood PM (2000) The frontal aging hypothesis evaluated. *J Int Neuropsychol Soc* **6**, 705-726.

Gregoriou GG, Gotts SJ, Zhou H & Desimone R (2009) High-frequency, long-range coupling between prefrontal and visual cortex during attention. *Science* **324**, 1207-1210.

Grieve SM, Clark CR, Williams LM, Peduto AJ & Gordon E (2005) Preservation of limbic and paralimbic structures in aging. *Hum Brain Mapp* **25**, 391-401.

Grieve SM, Williams LM, Paul RH, Clark CR & Gordon E (2007) Cognitive aging, executive function, and fractional anisotropy: a diffusion tensor MR imaging study. *AJNR Am J Neuroradiol* **28**, 226-235.

Gunning-Dixon FM & Raz N (2000) The cognitive correlates of white matter abnormalities in normal aging: a quantitative review. *Neuropsychology* **14**, 224-232.

Gunning-Dixon FM & Raz N (2003) Neuroanatomical correlates of selected executive functions in middle-aged and older adults: a prospective MRI study. *Neuropsychologia* **41**, 1929-1941.

Guttmann CR, Jolesz FA, Kikinis R, Killiany RJ, Moss MB, Sandor T & Albert MS (1998) White matter changes with normal aging. *Neurology* **50**, 972-978.

Halliday GM, Blumbergs PC, Cotton RG, Blessing WW & Geffen LB (1990) Loss of brainstem serotonin- and substance P-containing neurons in Parkinson's disease. *Brain Res* **510**, 104-107.

Hämäläinen M, Hari R, Ilmoniemi R, Knuutila J & Lounasmaa O (1993) Magnetoencephalography--theory, instrumentation, and applications to noninvasive studies of the working human brain. *Rev Mod Phys* **65**, 1-93.

Harding AJ, Stimson E, Henderson JM & Halliday GM (2002) Clinical correlates of selective pathology in the amygdala of patients with Parkinson's disease. *Brain* **125**, 2431-2445.

Hari R & Salmelin R (1997) Human cortical oscillations: a neuromagnetic view through the skull. *Trends Neurosci* **20**, 44-49.

Hasher L & Zacks RT (1988) Working memory, comprehesion, and aging: A review and a new view. In *The Psychology of Learning and Motivation*, pp. 193 [GH Bower, editor]. New York: Academic Press.

Hawkins HL, Kramer AF & Capaldi D (1992) Aging, exercise, and attention. *Psychol Aging* **7**, 643-653.

Head D, Buckner RL, Shimony JS, Williams LE, Akbudak E, Conturo TE, McAvoy M, Morris JC & Snyder AZ (2004) Differential vulnerability of anterior white matter in nondemented aging with minimal acceleration in dementia of the Alzheimer type: evidence from diffusion tensor imaging. *Cereb Cortex* **14**, 410-423.

Hedden T & Gabrieli JD (2004) Insights into the ageing mind: a view from cognitive neuroscience. *Nat Rev Neurosci* **5**, 87-96.

Henderson JM, Carpenter K, Cartwright H & Halliday GM (2000) Loss of thalamic intralaminar nuclei in progressive supranuclear palsy and Parkinson's disease: clinical and therapeutic implications. *Brain* **123 (Pt 7)**, 1410-1421.

Hinman JD & Abraham CR (2007) What's behind the decline? The role of white matter in brain aging. *Neurochem Res* **32**, 2023-2031.

Howard MW, Rizzuto DS, Caplan JB, Madsen JR, Lisman J, Aschenbrenner-Scheibe R, Schulze-Bonhage A & Kahana MJ (2003) Gamma oscillations correlate with working memory load in humans. *Cereb Cortex* **13**, 1369-1374.

Ikram MA, Vrooman HA, Vernooij MW, van der Lijn F, Hofman A, van der Lugt A, Niessen WJ & Breteler MM (2007) Brain tissue volumes in the general elderly population The Rotterdam Scan Study. *Neurobiol Aging*.

Javoy-Agid F, Taquet H, Ploska A, Cherif-Zahar C, Ruberg M & Agid Y (1981) Distribution of catecholamines in the ventral mesencephalon of human brain, with special reference to Parkinson's disease. *J Neurochem* **36**, 2101-2105.

Jellinger K (2005) The pathology of Parkinson's disease-recent advances. In *Scientific basis for the treatment of parkinson's disease.*, pp. 53-86 [N Galvez-Jimenez, editor]. New York: Taylor & Francis.

Jensen O (2006) Maintenance of multiple working memory items by temporal segmentation. *Neuroscience* **139**, 237-249.

Jensen O, Kaiser J & Lachaux JP (2007) Human gamma-frequency oscillations associated with attention and memory. *Trends Neurosci* **30**, 317-324.

Jernigan TL, Archibald SL, Berhow MT, Sowell ER, Foster DS & Hesselink JR (1991) Cerebral structure on MRI, Part I: Localization of age-related changes. *Biol Psychiatry* **29**, 55-67.

Jernigan TL, Archibald SL, Fennema-Notestine C, Gamst AC, Stout JC, Bonner J & Hesselink JR (2001) Effects of age on tissues and regions of the cerebrum and cerebellum. *Neurobiol Aging* **22**, 581-594.

Jimura K & Braver TS (2010) Age-related shifts in brain activity dynamics during task switching. *Cereb Cortex* **20**, 1420-1431.

Jokisch D & Jensen O (2007) Modulation of gamma and alpha activity during a working memory task engaging the dorsal or ventral stream. *J Neurosci* **27**, 3244-3251.

Jones SR, Pritchett DL, Sikora MA, Stufflebeam SM, Hamalainen M & Moore CI (2009) Quantitative analysis and biophysically realistic neural modeling of the MEG mu rhythm: rhythmogenesis and modulation of sensory-evoked responses. *J Neurophysiol* **102**, 3554-3572.

Jones SR, Pritchett DL, Stufflebeam SM, Hamalainen M & Moore CI (2007) Neural correlates of tactile detection: a combined magnetoencephalography and biophysically based computational modeling study. *J Neurosci* **27**, 10751-10764.

Kahana MJ (2006) The cognitive correlates of human brain oscillations. *J Neurosci* **26**, 1669-1672.

Kahana MJ, Sekuler R, Caplan JB, Kirschen M & Madsen JR (1999) Human theta oscillations exhibit task dependence during virtual maze navigation. *Nature* **399**, 781-784.

Kakigi R & Shibasaki H (1991) Effects of age, gender, and stimulus side on scalp topography of somatosensory evoked potentials following median nerve stimulation. *J Clin Neurophysiol* **8**, 320-330.

Klimesch W, Doppelmayr M, Russegger H & Pachinger T (1996) Theta band power in the human scalp EEG and the encoding of new information. *Neuroreport* **7**, 1235-1240.

Klimesch W, Hanslmayr S, Sauseng P, Gruber W, Brozinsky CJ, Kroll NE, Yonelinas AP & Doppelmayr M (2006) Oscillatory EEG correlates of episodic trace decay. *Cereb Cortex* **16**, 280-290.

Koechlin E, Ody C & Kouneiher F (2003) The architecture of cognitive control in the human prefrontal cortex. *Science* **302**, 1181-1185.

Kramer JH, Mungas D, Reed BR, Wetzel ME, Burnett MM, Miller BL, Weiner MW & Chui HC (2007) Longitudinal MRI and cognitive change in healthy elderly. *Neuropsychology* **21**, 412-418.

La Voie D & Light LL (1994) Adult age differences in repetition priming: a meta-analysis. *Psychol Aging* **9**, 539-553.

Laakso MP, Partanen K, Riekkinen P, Lehtovirta M, Helkala EL, Hallikainen M, Hanninen T, Vainio P & Soininen H (1996) Hippocampal volumes in Alzheimer's disease, Parkinson's disease with and without dementia, and in vascular dementia: An MRI study. *Neurology* **46**, 678-681.

Lemaitre H, Goldman AL, Sambataro F, Verchinski BA, Meyer-Lindenberg A, Weinberger DR & Mattay VS (2010) Normal age-related brain morphometric changes: nonuniformity across cortical thickness, surface area and gray matter volume? *Neurobiol Aging*.

Light LL & Singh A (1987) Implicit and explicit memory in young and older adults. *J Exp Psychol Learn Mem Cogn* **13**, 531-541.

Linkenkaer-Hansen K, Nikulin VV, Palva S, Ilmoniemi RJ & Palva JM (2004) Prestimulus oscillations enhance psychophysical performance in humans. *J Neurosci* **24**, 10186-10190.

Luders H (1970) The effect of aging on the wave form of the somatosensory cortical evoked potential. *Electroencephalogr Clin Neurophysiol* **29**, 450-460.

Lutz J, Hemminger F, Stahl R, Dietrich O, Hempel M, Reiser M & Jager L (2007) Evidence of subcortical and cortical aging of the acoustic pathway: a diffusion tensor imaging (DTI) study. *Acad Radiol* **14**, 692-700.

Madden DJ, Spaniol J, Whiting WL, Bucur B, Provenzale JM, Cabeza R, White LE & Huettel SA (2007) Adult age differences in the functional neuroanatomy of visual attention: a combined fMRI and DTI study. *Neurobiol Aging* **28**, 459-476.

Makris N, Papadimitriou GM, van der Kouwe A, Kennedy DN, Hodge SM, Dale AM, Benner T, Wald LL, Wu O, Tuch DS, Caviness VS, Moore TL, Killiany RJ, Moss MB & Rosene DL (2007) Frontal connections and cognitive changes in normal aging rhesus monkeys: a DTI study. *Neurobiol Aging* **28**, 1556-1567.

Marek K & Jennings D (2009) Can we image premotor Parkinson disease? *Neurology* **72**, S21-26.

Mazaheri A & Jensen O (2008) Asymmetric amplitude modulations of brain oscillations generate slow evoked responses. *J Neurosci* **28**, 7781-7787.

McBain CJ & Fisahn A (2001) Interneurons unbound. *Nat Rev Neurosci* **2**, 11-23.

McDowd JM (1986) The effects of age and extended practice on divided attention performance. *J Gerontol* **41**, 764-769.

Middleton FA & Strick PL (2000) Basal ganglia output and cognition: evidence from anatomical, behavioral, and clinical studies. *Brain Cogn* **42**, 183-200.

Milham MP, Erickson KI, Banich MT, Kramer AF, Webb A, Wszalek T & Cohen NJ (2002) Attentional control in the aging brain: insights from an fMRI study of the stroop task. *Brain Cogn* **49**, 277-296.

Miller EK (2000) The prefrontal cortex and cognitive control. *Nat Rev Neurosci* **1**, 59-65.

Miller EK & Cohen JD (2001) An integrative theory of prefrontal cortex function. *Annu Rev Neurosci* **24**, 167-202.

Miller EK & Wilson MA (2008) All my circuits: using multiple electrodes to understand functioning neural networks. *Neuron* **60**, 483-488.

Miyake A, Friedman NP, Emerson MJ, Witzki AH, Howerter A & Wager TD (2000) The unity and diversity of executive functions and their contributions to complex "Frontal Lobe" tasks: a latent variable analysis. *Cognit Psychol* **41**, 49-100.

Mufson EJ, Presley LN & Kordower JH (1991) Nerve growth factor receptor immunoreactivity within the nucleus basalis (Ch4) in Parkinson's disease: reduced cell numbers and co-localization with cholinergic neurons. *Brain Res* **539**, 19-30.

Narici L, Pizzella V, Romani GL, Torrioli G, Traversa R & Rossini PM (1990) Evoked alpha- and mu-rhythm in humans: a neuromagnetic study. *Brain Res* **520**, 222-231.

Nicolelis MA & Ribeiro S (2002) Multielectrode recordings: the next steps. *Curr Opin Neurobiol* **12**, 602-606.

Nikulin VV, Linkenkaer-Hansen K, Nolte G, Lemm S, Muller KR, Ilmoniemi RJ & Curio G (2007) A novel mechanism for evoked responses in the human brain. *Eur J Neurosci* **25**, 3146-3154.

Nordahl CW, Ranganath C, Yonelinas AP, Decarli C, Fletcher E & Jagust WJ (2006) White matter changes compromise prefrontal cortex function in healthy elderly individuals. *J Cogn Neurosci* **18**, 418-429.

O'Sullivan M, Jones DK, Summers PE, Morris RG, Williams SC & Markus HS (2001) Evidence for cortical "disconnection" as a mechanism of age-related cognitive decline. *Neurology* **57**, 632-638.

Ogata K, Okamoto T, Yamasaki T, Shigeto H & Tobimatsu S (2009) Pre-movement gating of somatosensory-evoked potentials by self-initiated movements: the effects of ageing and its implication. *Clin Neurophysiol* **120**, 1143-1148.

Peters A (2002) The effects of normal aging on myelin and nerve fibers: a review. *J Neurocytol* **31**, 581-593.

Peters A, Sethares C & Luebke JI (2008) Synapses are lost during aging in the primate prefrontal cortex. *Neuroscience* **152**, 970-981.

Peters A, Sethares C & Moss MB (1998) The effects of aging on layer 1 in area 46 of prefrontal cortex in the rhesus monkey. *Cereb Cortex* **8**, 671-684.

Pfefferbaum A, Adalsteinsson E & Sullivan EV (2005) Frontal circuitry degradation marks healthy adult aging: Evidence from diffusion tensor imaging. *Neuroimage* **26**, 891-899.

Pfefferbaum A, Mathalon DH, Sullivan EV, Rawles JM, Zipursky RB & Lim KO (1994) A quantitative magnetic resonance imaging study of changes in brain morphology from infancy to late adulthood. *Arch Neurol* **51**, 874-887.

Piguet O & Corkin S (2007) The aging brain. In *Learning and the Brain: A Comprehensive Guide for Educators, Parents, and Teachers* [S Feinstein, editor]. Lanham, MD: Rowman & Littlefield Education.

Piguet O, Double KL, Kril JJ, Harasty J, Macdonald V, McRitchie DA & Halliday GM (2009) White matter loss in healthy ageing: a postmortem analysis. *Neurobiol Aging* **30**, 1288-1295.

Pillon B, Dubois B, Cusimano G, Bonnet AM, Lhermitte F & Agid Y (1989) Does cognitive impairment in Parkinson's disease result from non-dopaminergic lesions? *J Neurol Neurosurg Psychiatry* **52**, 201-206.

Raz N, Gunning-Dixon F, Head D, Rodrigue KM, Williamson A & Acker JD (2004) Aging, sexual dimorphism, and hemispheric asymmetry of the cerebral cortex: replicability of regional differences in volume. *Neurobiol Aging* **25**, 377-396.

Raz N, Gunning-Dixon FM, Head D, Dupuis JH & Acker JD (1998) Neuroanatomical correlates of cognitive aging: evidence from structural magnetic resonance imaging. *Neuropsychology* **12**, 95-114.

Raz N, Gunning FM, Head D, Dupuis JH, McQuain J, Briggs SD, Loken WJ, Thornton AE & Acker JD (1997) Selective aging of the human cerebral cortex observed in vivo: differential vulnerability of the prefrontal gray matter. *Cereb Cortex* **7**, 268-282.

Raz N, Lindenberger U, Rodrigue KM, Kennedy KM, Head D, Williamson A, Dahle C, Gerstorf D & Acker JD (2005) Regional brain changes in aging healthy adults: general trends, individual differences and modifiers. *Cereb Cortex* **15**, 1676-1689.

Raz N & Rodrigue KM (2006) Differential aging of the brain: patterns, cognitive correlates and modifiers. *Neurosci Biobehav Rev* **30**, 730-748.

Resnick SM, Pham DL, Kraut MA, Zonderman AB & Davatzikos C (2003) Longitudinal magnetic resonance imaging studies of older adults: a shrinking brain. *J Neurosci* **23**, 3295-3301.

Rogers JD, Brogan D & Mirra SS (1985) The nucleus basalis of Meynert in neurological disease: a quantitative morphological study. *Ann Neurol* **17**, 163-170.

Rye D & DeLong MR (2003) Time to focus on the locus. *Arch Neurol* **60**, 320.

Sailer A, Dichgans J & Gerloff C (2000) The influence of normal aging on the cortical processing of a simple motor task. *Neurology* **55**, 979-985.

Saint-Cyr JA (2003) Frontal-striatal circuit functions: context, sequence, and consequence. *J Int Neuropsychol Soc* **9**, 103-127.

Salat DH, Buckner RL, Snyder AZ, Greve DN, Desikan RS, Busa E, Morris JC, Dale AM & Fischl B (2004) Thinning of the cerebral cortex in aging. *Cereb Cortex* **14**, 721-730.

Salat DH, Kaye JA & Janowsky JS (1999) Prefrontal gray and white matter volumes in healthy aging and Alzheimer disease. *Arch Neurol* **56**, 338-344.

Salat DH, Tuch DS, Hevelone ND, Fischl B, Corkin S, Rosas HD & Dale AM (2005) Age-related changes in prefrontal white matter measured by diffusion tensor imaging. *Ann N Y Acad Sci* **1064**, 37-49.

Salinas E & Sejnowski TJ (2001) Correlated neuronal activity and the flow of neural information. *Nat Rev Neurosci* **2**, 539-550.

Salthouse TA (1994) The aging of working memory. *Neuropsychology* **8**, 535-543.

Salthouse TA, Atkinson TM & Berish DE (2003) Executive functioning as a potential mediator of age-related cognitive decline in normal adults. *J Exp Psychol Gen* **132**, 566-594.

Salthouse TA & Meinz EJ (1995) Aging, inhibition, working memory, and speed. *J Gerontol B Psychol Sci Soc Sci* **50**, P297-306.

Schadow J, Lenz D, Dettler N, Frund I & Herrmann CS (2009) Early gamma-band responses reflect anticipatory top-down modulation in the auditory cortex. *Neuroimage* **47**, 651-658.

Schneider BA & Pichora-Fuller MK (2000) Implications of perceptual deterioration for cognitive aging research. In *The Handbook of Aging adn Cognition*, pp. 155-219 [FI Craik and TA Salthouse, editors]. Mahwah, NJ: Lawrence Erlbaum Associates.

Schrag A, Kingsley D, Phatouros C, Mathias CJ, Lees AJ, Daniel SE & Quinn NP (1998) Clinical usefulness of magnetic resonance imaging in multiple system atrophy. *J Neurol Neurosurg Psychiatry* **65**, 65-71.

Schroeder CE & Lakatos P (2009) Low-frequency neuronal oscillations as instruments of sensory selection. *Trends Neurosci* **32**, 9-18.

Sederberg PB, Kahana MJ, Howard MW, Donner EJ & Madsen JR (2003) Theta and gamma oscillations during encoding predict subsequent recall. *J Neurosci* **23**, 10809-10814.

Shulman JM, De Jager PL & Feany MB (2011) Parkinson's disease: genetics and pathogenesis. *Annu Rev Pathol* **6**, 193-222.

Siegel M, Donner TH, Oostenveld R, Fries P & Engel AK (2008) Neuronal synchronization along the dorsal visual pathway reflects the focus of spatial attention. *Neuron* **60**, 709-719.

Singer W (1999) Neuronal synchrony: a versatile code for the definition of relations? *Neuron* **24**, 49-65, 111-125.

Smith EE, Salat DH, Jeng J, McCreary CR, Fischl B, Schmahmann JD, Dickerson BC, Viswanathan A, Albert MS, Blacker D & Greenberg SM (2011) Correlations between MRI white matter lesion location and executive function and episodic memory. *Neurology* **76**, 1492-1499.

Soderlund H, Nyberg L, Adolfsson R, Nilsson LG & Launer LJ (2003) High prevalence of white matter hyperintensities in normal aging: relation to blood pressure and cognition. *Cortex* **39**, 1093-1105.

Sowell ER, Peterson BS, Thompson PM, Welcome SE, Henkenius AL & Toga AW (2003) Mapping cortical change across the human life span. *Nat Neurosci* **6**, 309-315.

Spencer WD & Raz N (1994) Memory for facts, source, and context: can frontal lobe dysfunction explain age-related differences? *Psychol Aging* **9**, 149-159.

Spencer WD & Raz N (1995) Differential effects of aging on memory for content and context: a meta-analysis. *Psychol Aging* **10**, 527-539.

Stephen JM, Ranken D, Best E, Adair J, Knoefel J, Kovacevic S, Padilla D, Hart B & Aine CJ (2006) Aging changes and gender differences in response to median nerve stimulation measured with MEG. *Clin Neurophysiol* **117**, 131-143.

Stuss DT & Knight RT (2002) *Principles of Frontal Lobe Function*. New York: Oxford University Press.

Sullivan EV, Adalsteinsson E & Pfefferbaum A (2006) Selective age-related degradation of anterior callosal fiber bundles quantified in vivo with fiber tracking. *Cereb Cortex* **16**, 1030-1039.

Sullivan EV & Pfefferbaum A (2006) Diffusion tensor imaging and aging. *Neurosci Biobehav Rev* **30**, 749-761.

Sullivan EV, Rosenbloom M, Serventi KL & Pfefferbaum A (2004) Effects of age and sex on volumes of the thalamus, pons, and cortex. *Neurobiol Aging* **25**, 185-192.

Tallon-Baudry C, Bertrand O & Fischer C (2001) Oscillatory synchrony between human extrastriate areas during visual short-term memory maintenance. *J Neurosci* **21**, RC177.

Tanji J & Hoshi E (2008) Role of the lateral prefrontal cortex in executive behavioral control. *Physiol Rev* **88**, 37-57.

Tiihonen J, Kajola M & Hari R (1989) Magnetic mu rhythm in man. *Neuroscience* **32**, 793-800.

Tisserand DJ & Jolles J (2003) On the involvement of prefrontal networks in cognitive ageing. *Cortex* **39**, 1107-1128.

Tisserand DJ, Pruessner JC, Sanz Arigita EJ, van Boxtel MP, Evans AC, Jolles J & Uylings HB (2002) Regional frontal cortical volumes decrease differentially in aging: an MRI study to compare volumetric approaches and voxel-based morphometry. *Neuroimage* **17**, 657-669.

Tuladhar AM, ter Huurne N, Schoffelen JM, Maris E, Oostenveld R & Jensen O (2007) Parieto-occipital sources account for the increase in alpha activity with working memory load. *Hum Brain Mapp* **28**, 785-792.

Tullberg M, Fletcher E, DeCarli C, Mungas D, Reed BR, Harvey DJ, Weiner MW, Chui HC & Jagust WJ (2004) White matter lesions impair frontal lobe function regardless of their location. *Neurology* **63**, 246-253.

Van Der Werf J, Jensen O, Fries P & Medendorp WP (2008) Gamma-band activity in human posterior parietal cortex encodes the motor goal during delayed prosaccades and antisaccades. *J Neurosci* **28**, 8397-8405.

Van Der Werf J, Jensen O, Fries P & Medendorp WP (2010) Neuronal synchronization in human posterior parietal cortex during reach planning. *J Neurosci* **30**, 1402-1412.

Van Petten C (2004) Relationship between hippocampal volume and memory ability in healthy individuals across the lifespan: review and meta-analysis. *Neuropsychologia* **42**, 1394-1413.

Van Petten C, Plante E, Davidson PS, Kuo TY, Bajuscak L & Glisky EL (2004) Memory and executive function in older adults: relationships with temporal and prefrontal gray matter volumes and white matter hyperintensities. *Neuropsychologia* **42**, 1313-1335.

Verrillo RT (1982) Effects of aging on the suprathreshold responses to vibration. *Percept Psychophys* **32**, 61-68.

Verrillo RT, Bolanowski SJ & Gescheider GA (2002) Effect of aging on the subjective magnitude of vibration. *Somatosens Mot Res* **19**, 238-244.

Walhovd KB, Fjell AM, Reinvang I, Lundervold A, Dale AM, Eilertsen DE, Quinn BT, Salat D, Makris N & Fischl B (2005) Effects of age on volumes of cortex, white matter and subcortical structures. *Neurobiol Aging* **26**, 1261-1270; discussion 1275-1268.

Wang XJ (2010) Neurophysiological and computational principles of cortical rhythms in cognition. *Physiol Rev* **90**, 1195-1268.

West R (2004) The effects of aging on controlled attention and conflict processing in the Stroop task. *J Cogn Neurosci* **16**, 103-113.

West RL (1996) An application of prefrontal cortex function theory to cognitive aging. *Psychol Bull* **120**, 272-292.

Whittington MA & Traub RD (2003) Interneuron diversity series: inhibitory interneurons and network oscillations in vitro. *Trends Neurosci* **26**, 676-682.

Wichmann T & DeLong MR (2002) Neurocircuitry of Parkinson's disease. In *Neuropsychopharmacology: the difth generation of progress* [K Davis, D Charney, J Coyle and C Nemeroff, editors]. Philadelphia: Lippincott, Williams and Wilkins.

Wise SP, Murray EA & Gerfen CR (1996) The frontal cortex-basal ganglia system in primates. *Crit Rev Neurobiol* **10**, 317-356.

Yoon B, Shim YS, Lee KS, Shon YM & Yang DW (2008) Region-specific changes of cerebral white matter during normal aging: a diffusion-tensor analysis. *Arch Gerontol Geriatr* **47**, 129-138.

Zhang Y & Ding M (2010) Detection of a Weak Somatosensory Stimulus: Role of the Prestimulus Mu Rhythm and Its Top-Down Modulation. *J Cogn Neurosci* **22**, 307-322.

Zimmerman ME, Brickman AM, Paul RH, Grieve SM, Tate DF, Gunstad J, Cohen RA, Aloia MS, Williams LM, Clark CR, Whitford TJ & Gordon E (2006) The relationship between frontal gray matter volume and cognition varies across the healthy adult lifespan. *Am J Geriatr Psychiatry* **14**, 823-833.

Chapter 2

Cognition in healthy aging is related to regional white matter integrity, but not cortical thickness

David A. Ziegler[1], Olivier Piguet[1], David H. Salat[2],
Keyma Prince[1], Emily Connally[1], Suzanne Corkin[1,2]

1. Department of Brain & Cognitive Sciences, MIT, Cambridge, MA
2. Athinoula A. Martinos Center for Biomedical Imaging, Charlestown, MA

This article is published in *Neurobiology of Aging*. Volume 31(11):1912-26.
© 2008 Elsevier Inc.

Abstract

It is well established that healthy aging is accompanied by structural changes in many brain regions and functional decline in a number of cognitive domains. The goal of this study was to determine 1) whether the regional distribution of age-related brain changes is similar in gray matter (GM) and white matter (WM) regions, or whether these two tissue types are affected differently by aging, and 2) whether measures of cognitive performance are more closely linked to alterations in the cerebral cortex or in the underlying WM in older adults (OA). To address these questions, we collected high-resolution MRI data from a large sample of healthy young adults (YA; aged 18-28) and OA (aged 61-86 years). In addition, the OA completed a series of tasks selected to assess cognition in three domains: cognitive control, episodic memory, and semantic memory. Using advanced techniques for measuring cortical thickness and WM integrity, we found that healthy aging was accompanied by deterioration of both GM and WM, but with distinct patterns of change: Cortical thinning occurred primarily in primary sensory and motor cortices, whereas WM changes were localized to regions underlying association cortices. Further, in OA, we found a striking pattern of region-specific correlations between measures of cognitive performance and WM integrity, but not cortical thickness. Specifically, cognitive control correlated with integrity of frontal lobe WM, whereas episodic memory was related to integrity of temporal and parietal lobe WM. Thus, age-related impairments in specific cognitive capacities may arise from degenerative processes that affect the underlying connections of their respective neural networks.

Introduction

Healthy aging is characterized by myriad cognitive changes. Some of the most pronounced and consistently reported deficits are on tasks that require long-term memory or that challenge cognitive control processes and working memory (Hedden & Gabrieli, 2004; Piguet & Corkin, 2007). While the pattern of age-related cognitive changes is relatively well characterized, less is known about the neural bases of age-related changes in cognition.

Age-related structural changes in gray matter

Age-related cognitive decline is frequently attributed to deterioration of cortical gray matter (GM) structures. Magnetic resonance imaging (MRI)-based studies point to reduced global GM volumes in OA (Pfefferbaum *et al.*, 1994; Raz *et al.*, 1997; Salat *et al.*, 1999; Bartzokis *et al.*, 2001; Allen *et al.*, 2005; Raz *et al.*, 2005; Walhovd *et al.*, 2005). Several studies that examined regional effects of age found that frontal areas showed greater volumetric reduction than posterior regions (Raz *et al.*, 1997; Salat *et al.*, 1999; Bartzokis *et al.*, 2001; Allen *et al.*, 2005). Particularly notable are volumetric losses in prefrontal cortex (PFC) (Raz *et al.*, 1997; Salat *et al.*, 1999; Raz *et al.*, 2004a; Grieve *et al.*, 2005). These findings have led to the hypothesis that age-related GM loss occurs along an anterior-to-posterior gradient (Jernigan *et al.*, 1991; Raz *et al.*, 1997; Sowell *et al.*, 2003; Raz & Rodrigue, 2006). While this hypothesis tends to dominate the aging literature, degeneration has also been documented in all of the major lobes of the brain (Cowell *et al.*, 1994; Bartzokis *et al.*, 2001; Tisserand *et al.*, 2002; Raz *et al.*, 2004a; Van Petten, 2004; Van Petten *et al.*, 2004; Allen *et al.*, 2005).

Advanced methods now allow assessment of changes in cortical thickness across the lifespan (Fischl & Dale, 2000). Similar to results from volumetric studies, cortical thickness of lateral PFC is reduced in OA. At the same time, cortical thinning is also found in the occipital lobe and precentral gyrus—areas that have not generally been associated with volumetric decline (Salat *et al.*, 2004). The histopathological underpinnings of these macroscopic changes in cortical GM remain elusive: While early studies reported a loss of cortical neurons and decreased cell packing density (Pakkenberg & Gundersen, 1997), more advanced methods indicate that cell loss is relatively minimal in old age, overshadowed by a drastic loss of neuropil (Peters *et al.*, 1998a).

Age-related structural changes in white matter

In addition to GM degeneration, WM changes likely play an important role in explaining age-related cognitive deficits (Peters, 2002; Hinman & Abraham, 2007). Many volumetric studies have documented reduced global and regional WM volumes in OA (Guttmann *et al.*, 1998; Salat *et al.*, 1999; Courchesne *et al.*, 2000; Bartzokis *et al.*, 2001; Jernigan *et al.*, 2001; Allen *et al.*, 2005; Piguet *et al.*, 2009), but see (Pfefferbaum *et al.*, 1994; Good *et al.*, 2001; Sullivan *et al.*, 2004). Evidence that WM volume loss is greatest in the frontal lobes is equivocal (Raz *et al.*, 1997; Salat *et al.*, 1999; Raz *et al.*, 2004b; Allen *et al.*, 2005; Piguet *et al.*, 2009).

Other MRI-based markers of WM degeneration include an increase in hyperintensities on T2- and proton density-weighted images, with the greatest volume of hyperintensities typically found in the WM underlying the frontal lobes (DeCarli *et al.*, 1995; de Groot *et al.*, 2000;

Gunning-Dixon & Raz, 2000; Pfefferbaum *et al.*, 2000; Tullberg *et al.*, 2004; Nordahl *et al.*, 2006; Yoshita *et al.*, 2006). In addition, microstructural deterioration of WM has been assessed using diffusion tensor imaging (DTI), with numerous studies documenting widespread age-related decreases in fractional anisotropy (FA) (O'Sullivan *et al.*, 2001; Sullivan & Pfefferbaum, 2003; Madden *et al.*, 2004; Salat *et al.*, 2005a; Benedetti *et al.*, 2006; Charlton *et al.*, 2006). FA measures the degree to which the diffusion of water molecules is restricted by microstructural elements, such as cell bodies, axons, or myelin and other glial cells (Beaulieu, 2002). Like WM hyperintensities, FA reductions tend to be most prominent anteriorly, such as in the genu and anterior portions of the corpus callosum and in the WM underlying PFC (O'Sullivan *et al.*, 2001; Head *et al.*, 2004; Pfefferbaum *et al.*, 2005; Salat *et al.*, 2005b; Sullivan & Pfefferbaum, 2006; Ardekani *et al.*, 2007; Madden *et al.*, 2007; Yoon *et al.*, 2008). Other notable loci of decreased integrity include the internal capsule (Good *et al.*, 2001; Salat *et al.*, 2004), auditory pathways of the temporal lobes (Lutz *et al.*, 2007), and cingulum bundle (Yoon *et al.*, 2008). Postmortem studies reveal a number of pathologic factors that may cause changes in FA, including loss of small myelinated fibers (Tang *et al.*, 1997; Marner *et al.*, 2003) and myelin degradation (Peters, 2002), which likely contribute to volumetric change (Double *et al.*, 1996; Guttmann *et al.*, 1998; Ikram *et al.*, 2008; Piguet *et al.*, 2009).

In summary, evidence of morphological and microstructural changes in frontal areas appears consistently in the aging literature. In addition, regional alterations have been noted across wide regions of GM and WM, although the exact nature and magnitude of these changes remains a topic of debate. To explicitly test whether WM and GM exhibit similar or distinct

patterns of age-related change, measures of both structures must be examined in a single group of participants. The present study achieved that goal.

Linking GM changes to cognitive performance in OA

A prevalent view contends that age-related decline in episodic memory is related to deterioration of the hippocampus and other medial temporal lobe structures, and that cortical losses are more highly correlated with decrements in cognitive control processes (i.e., the frontal aging hypothesis) (West, 1996; Tisserand & Jolles, 2003). While a number of studies have reported correlations between hippocampal volume and episodic memory (Golomb *et al.*, 1996; Kramer *et al.*, 2007), some concerns have been raised about the robustness of the effect (Van Petten, 2004). Direct evidence in favor of the frontal aging hypothesis has also been difficult to demonstrate in humans (Greenwood, 2000; Van Petten *et al.*, 2004; Raz & Rodrigue, 2006). Diminished attention and executive function in OA have been associated with decreased global cortical volumes and reduced volumes of lateral PFC and OFC (Zimmerman *et al.*, 2006; Kramer *et al.*, 2007), although an inverse correlation between working memory function and OFC volume has also been reported (Salat *et al.*, 2002). In addition, PFC volume has been inversely correlated with perseverative errors in OA (Raz *et al.*, 1998; Gunning-Dixon & Raz, 2003). In contrast, spatial and object working memory correlated with visual cortex volume (Raz *et al.*, 1998), but neither spatial and object or verbal working memory (Gunning-Dixon & Raz, 2003) showed significant correlations with PFC volume.

Less is known about the cognitive correlates of cortical thinning. An experiment in monkeys found that age-related cortical thinning was associated with deficits in recognition memory and overall cognitive function (Peters *et al.*, 1998b). In humans, OA with high fluid intelligence scores had large regions of thicker cortex in the right hemisphere, most notably in posterior cingulate cortex, compared to OA with average scores (Fjell *et al.*, 2006). In contrast, the same study found virtually no thickness differences between high and low performers on tests of executive function.

Linking WM changes to cognitive performance in OA

Given the distributed nature of the neural networks that support the cognitive functions that decline most with age, degradation of the connections in these networks could have a dramatic effect on the processing abilities of OA. One study of older rhesus monkeys found a correlation between measures of executive function and DTI-based measures of WM integrity in long-distance corticocortical association pathways (Makris *et al.*, 2007). Similarly, several investigations of humans have linked deficits in processing speed, executive function, immediate and delayed recall, and overall cognition to an increased burden of periventricular WM hypertintensities in OA (Gunning-Dixon & Raz, 2000; Gunning-Dixon & Raz, 2003; Soderlund *et al.*, 2003). WM hyperintensities have also been associated with decreased frontal lobe metabolism (DeCarli *et al.*, 1995; Tullberg *et al.*, 2004), and with diminished BOLD responses in PFC during performance of episodic and working memory tasks (Nordahl *et al.*, 2006). When measured using DTI, functional correlates of decreased WM integrity included working memory impairments (Charlton *et al.*, 2006), slowed processing speed (Sullivan *et al.*,

2006; Bucur *et al.*, 2008), and executive dysfunction (O'Sullivan *et al.*, 2001; Deary *et al.*, 2006; Grieve *et al.*, 2007). In one study of OA, WM integrity was negatively correlated with the magnitude of the BOLD response in PFC in individuals performing an episodic memory task (Persson *et al.*, 2006). While these studies suggest that degeneration of WM pathways may contribute to the etiology of age-related cognitive decline to an equal or greater extent than GM atrophy (O'Sullivan *et al.*, 2001; Hinman & Abraham, 2007), a strong test of this hypothesis requires measures of GM and WM integrity in the same group of participants, and then relating those measures to cognitive test scores. To date, no study has provided a direct test of the hypothesis that cognitive performance in OA correlates more strongly with WM than with GM changes.

The present study

Our study was asked two specific questions: 1) Do the patterns of age-related change differ between WM and GM structures, and 2) Are changes in discrete regions of GM and WM related to specific cognitive measures in OA? To address the first question, we used high-resolution structural MRI to obtain measures of cortical thickness and DTI-based indices of WM integrity in a single sample of young adults (YA) and OA. We hypothesized that the patterns of change in WM and GM would largely overlap, with frontal regions showing the most widespread losses. At the same time, we expected the patterns to diverge slightly, with cortical thinning also extending to primary sensory and motor cortices, while loss of WM integrity was expected to be more restricted to frontal areas. We chose not to limit our DTI analyses to WM regions and intentionally performed exploratory analyses of GM regions as well. This decision was based on

emerging evidence that DTI data contain rich information about microstructural characteristics of all brain tissues (Rose *et al.*, 2008), and may be capable of detecting age-related changes in GM structures (Abe *et al.*, 2008). To answer the second question, our sample of OA completed a series of tasks designed to measure three cognitive domains: cognitive control, episodic memory, and semantic memory. We predicted that cognitive control and episodic memory in OA would correlate with cortical thickness in PFC and association areas of parietal and temporal lobes, respectively, as well as with the integrity of WM underlying these cortical areas. Because semantic memory tends to remain relatively stable throughout the lifespan, we did not expect to find robust structure-function correlations for this domain.

Methods

Participants

The participants in this study were 36 YA (16F/20M), aged 18-28 years (mean age = 21.9 ± 2.6 years), and 38 OA (20F/18M), aged 61-86 years (mean age = 70.3 ± 7.2) (Table 1). Most of the YA were recruited from the MIT and Harvard communities; OA came primarily from the MIT and Harvard alumni associations. OA had more years of education (17 ±3.0) than YA (15 ±2.0), due to the fact that the majority of YA had not completed their education. Our exclusion criteria were: history of neurological or psychiatric disease, use of psychoactive medications, substance misuse, and presence of serious medical conditions, including history of heart disease, diabetes, and untreated hypertension. Those participants whose hypertension was controlled by prescription medication were admitted into the study. All participants were screened for dementia using the Mini Mental State Examination (MMSE) (Folstein *et al.*, 1975),

and any individual scoring below 26 was excluded from the study. The two groups were well matched on MMSE scores (mean scores: YA = 29.2 ±1.0; OA = 29.2 ±2.0). All participants gave informed consent using methods approved by the MIT Committee on the Use of Humans as Experimental Subjects and by the Partners Human Research Committee (Massachusetts General Hospital).

MRI acquisitions

We collected whole-head MRI scans using a 1.5 Tesla Siemens Sonata imaging system (Siemens Medical Systems, Iselin, NJ). Tightly padded clamps attached to the head coil minimized head motion during the scan. For analyses of WM integrity, we obtained high-resolution DTI scans from each participant (TR = 9100 ms, TE = 68 ms, slice thickness = 2 mm, 60 slices, acquisition matrix 128 mm x 128 mm, FOV 256 mm x 256 mm yielding 2 mm^3 isotropic voxels, seven averages of eight directions with *b*-value = 700 s/mm^2, and 5 T2-weighted images with no diffusion weighting, *b*-value = 0 s/mm^2). The effective diffusion gradient spacing was Δ = 64 ms with a bandwidth of 1445 Hz/pixel. Images were collected in an oblique axial plane. The DTI acquisition used a twice-refocused balanced echo, developed to reduce eddy current distortions (Reese *et al.*, 2003). For morphometric analyses of cortical thickness, we collected two high-resolution T1-weighted anatomical (MPRAGE) scans from each participant (voxel size = 1.0 x 1.0 x 1.33 mm, TR = 2530 ms, TE = 2.6 ms, TI = 7100 degrees, flip angle = 7 degrees).

DTI analyses

We chose FA as an indirect measure of the integrity of WM fiber bundles and GM structures because FA values are dependant upon the microstructural composition of different tissues (Beaulieu, 2002). We tested for differences in FA between YA and OA using a whole-brain atlas-based analysis, and by comparing mean FA values derived from manually delineated regions of interest *(*ROIs).

Processing of DTI data. All DTI data were processed using tools from the FSL (http://www.fmrib.ox.ac.uk/fsl) and FreeSurfer (http://surfer.nmr.mgh.harvard.edu) image analysis packages. We first applied motion and eddy current correction to all DTI scans. To this end, we registered each participant's diffusion-weighted images to the T2-weighted image using FMRIB's Linear Image Registration Tool (FLIRT), available as part of the FSL analysis package (Jenkinson & Smith, 2001; Jenkinson *et al.*, 2002). FLIRT employs a 12-parameter affine transformation and a mutual information cost function to achieve a globally optimized registration. Diffusion tensor and FA metrics were derived as described previously (Basser *et al.*, 1994; Pierpaoli & Basser, 1996). For atlas-based statistical analyses, we used trilinear interpolation to resample all maps and nearest-neighbor resampling for ROI analyses. To avoid partial volume effects associated with the inclusion of cerebrospinal fluid in WM voxels, all voxels with trace diffusion values greater than 6 μm^2/ms were excluded from the analyses.

Whole-brain Statistical Analyses of DTI data. To perform voxelwise statistical analyses of DTI data, FA volumes were spatially normalized to MNI space with FLIRT (Jenkinson & Smith, 2001;

Jenkinson *et al.*, 2002) by registering each participant's T2-weighted volume to the MNI's 152-subject T2-weighted template (Mazziotta *et al.*, 1995) and then applying this transformation to individual FA maps. To increase statistical power, we performed minimal spatial smoothing of FA maps using a 3D Gaussian kernel with 4-mm full width at half maximum. Independent *t* tests were calculated at each voxel to test for differences in FA between groups. The tools that we used to perform statistical analyses of our DTI data were developed in-house and are not equipped with a False Discovery Rate correction procedure that is appropriate for voxel-wise analyses of WM regions. We did, however, enforce a strict cutoff of $p < .001$ for all statistical comparisons of FA measures to minimize the potential confound of multiple comparisons.

ROI analysis of DTI data. We manually defined 14 ROIs (Figure 1b) that were either selected a priori, based on age-related changes previously documented in the literature, or to confirm the results from our whole-brain analyses of FA, thereby ensuring that any group differences were not confounded by registration or smoothing procedures. Based on previous reports (O'Sullivan *et al.*, 2001; Madden *et al.*, 2004; Salat *et al.*, 2005a; Sullivan *et al.*, 2006; Lutz *et al.*, 2007; Abe *et al.*, 2008), we expected FA to be decreased in OA in the following regions: the genu of the corpus callosum, posterior sagittal striatum, and radiate WM regions underlying PFC and OFC. In contrast, we expected to find little or no age-related change in FA values in the splenium of the corpus callosum and in the radiate WM underlying occipital, temporal, and parietal areas (Head *et al.*, 2004; Salat *et al.*, 2005a; Sullivan *et al.*, 2006), and increased FA in OA in the putamen (Abe *et al.*, 2008). All ROIs were placed individually in each participant's native, unsmoothed FA volume, thus avoiding any errors due to misregistration and any

confounding effects of spatial smoothing. With the exception of callosal labels, all ROIs were drawn separately in each hemisphere. Each label contained the same number of voxels in each participant. We provide detailed anatomical descriptions of ROI placement and label size online as Supplementary Material. To help ensure that no GM voxels were included in any of the WM ROIs, we created individual WM masks by thresholding each participant's FA volume at 0.25, thus masking out the majority of GM voxels. To further minimize partial volume effects, we positioned all labels near the center of each WM region or tract, avoiding border voxels. The GM ROIs were drawn in participants' native, unthresholded maps; to ensure that these labels contained only GM voxels, we did not include any voxels with FA values above 0.5, essentially masking out most WM voxels. A multivariate repeated measures general linear model (GLM) tested for significant differences between YA and OA in mean FA for each ROI. In order to compare the magnitude of effects across ROIs, we calculated effect sizes ([OA mean – YA mean]/pooled standard deviation) for the differences in means between OA and YA.

Cortical thickness analyses

We used advanced tools to derive measures of cortical thickness across the entire cortical mantle. We tested for regional differences in cortical thickness between YA and OA using an automated, surface-based approach, as well as by analyzing cortical thickness measures derived from manually delineated ROIs.

Analyses of regional cortical thinning. T1-weighted MRI data were processed using the FreeSurfer (http://surfer.nmr.mgh.harvard.edu) morphometric analysis tools. We performed

motion correction and averaged the two scans from each participant, yielding a single volume with high contrast- and signal-to-noise ratios. Cortical surfaces were reconstructed using a semi-automated procedure that has been described at length in previous work (Dale *et al.*, 1999; Fischl *et al.*, 1999a; Fischl *et al.*, 2001). We derived thickness measures at each vertex along the reconstructed surface by calculating the shortest distance from the gray/white border to the outer cortical (pial) surface (Fischl & Dale, 2000). Thickness measures were then mapped back onto each participant's inflated cortical surface and were averaged across all participants using a spherical averaging procedure (Fischl *et al.*, 1999b).

Statistical Analyses of cortical thickness data. For analyses of differences between OA and YA, an average surface was derived using our entire sample. The average surface ensures that the data are displayed on a model that is representative of the overall population, but lacks individual anatomical idiosyncrasies, thus maximizing the chance of accurate regional localization of effects. For correlations between cortical thickness and measures of cognition, a separate average surface was derived using only the sample of OA who completed the cognitive tasks. All statistical comparisons were performed in a vertex-wise fashion across the entire cortical surface. We tested for group differences and for correlations between thickness and measures of cognition using GLMs. For correlations between thickness and cognitive performance, age and years of education were included as continuous covariates. Between-group comparisons and correlations were subject to False Discovery Rate correction (q = .05) for multiple comparisons (Benjamini & Hochberg, 1995; Genovese *et al.*, 2002).

ROI analysis of cortical thinning. In addition to the cortex-wide comparisons of cortical thickness between YA and OA, we manually defined ROIs (Figure 2b) in regions that we predicted would show the greatest degree of thinning (precentral gyrus, calcarine, PFC, OFC) (Raz *et al.*, 1997; Salat *et al.*, 2004; Fjell *et al.*, 2006), in two regions that were not expected to show reduced cortical thickness in OA (middle temporal gyrus and anterior cingulate cortex)(Salat *et al.*, 2004; Fjell *et al.*, 2006), and in two regions (inferior temporal gyrus and posterior cingulate cortex) that have been associated with inconsistent results based on the volumetric and thickness literatures (Raz *et al.*, 1997; Salat *et al.*, 2004). We tested each ROI for differences in mean cortical thickness between YA and OA using a multivariate repeated measures GLM. We then calculated an ES for each ROI.

Cognitive testing

Participants who underwent MRI scanning were asked to return for a second visit to complete a series of cognitive tasks. Over 90% of the OA returned to complete the cognitive tasks, compared to 60% of the YA. This difference resulted in a less representative YA sample and reduced statistical power for brain-behavior correlations. Thus, correlations between cognitive scores and neuroanatomical measures were restricted to the OA group.

We selected a series of tasks to assess frontal lobe and long-term memory functions in OA (Table 2). For frontal lobe function, we chose tasks that require working memory or cognitive control processes; within the realm of long-term memory, we included tasks to assess episodic and semantic memory capacities. The cognitive control composite was designed to provide and

index of a range of frontal lobe functions and included several tests that are know to be sensitive to aging (Glisky et al., 1995). The cognitive control composite included a measure robustly associated with inhibitory control, the Stroop interference score (i.e., difference between the color-word card score and the color card score) (Stroop, 1935), and two tests of working memory, the total raw score from the Wechsler Memory Scale-III Backward Digit Span (Wechsler, 1997b) and the Trail Making Test, B-A score (Reitan, 1958). In addition, to provide an index of abstract mental operations, we included the total number of words produced in the Controlled Oral Word Association Test (COWAT) (Benton & Hamsher, 1989), a test of verbal fluency that is thought to rely on search strategies rather than on semantic knowledge (Lezak, 1995). The episodic memory composite was comprised of two measures known to be sensitive to impairment in long-term memory: the delayed recall scores for the Wechsler Memory Scale-III Logical Memory and Word List subtests (Wechsler, 1997b). To achieve a broad assessment of semantic memory function in OA, this composite included scores for the Wechsler Adult Intelligence Scale-III Vocabulary subtest (Wechsler, 1997a), which tend to remain stable or even improve with age, and the total number of words for the Boston Naming Test (Kaplan *et al.*, 1983), which tends to show some variability across the lifespan (Zec *et al.*, 2005; Zec *et al.*, 2007). All test scores were converted to *z* scores and then averaged to create a composite score for each of the three cognitive domains: cognitive control processes, long-term episodic memory, and semantic memory

Brain-behavior correlations in OA

For the OA group, we performed whole-brain and ROI-based multiple regression analyses to examine correlations between each cognitive composite score and measures of FA and cortical thickness. The whole brain analyses consisted of voxelwise correlations between FA or cortical thickness and cognitive composite scores. The ROI-based regression models included age as a continuous covariate. To ensure that any observed correlations were not simply the result of individual differences in FA values, we took the following approach: For any ROI that showed a correlation between FA and a cognitive measure, we calculated the correlation between age and FA in that ROI and then calculated partial correlation coefficients for FA and age from the multiple regression model. We then computed squared partial correlation coefficients to determine the percentage of variance in the cognitive measure that was due to FA, age, or both.

Results

Differences between YA and OA in WM integrity

We found widespread reductions in FA values in OA, compared to YA (Figure 1a , yellow and red areas). As anticipated, FA was reduced in anterior regions, including the genu and anterior body of the corpus callosum, and in the WM underlying the superior and middle frontal gyri and OFC. We also noted reduced FA in the WM underlying the middle and superior temporal gyri and posterior parietal cortex. In contrast, FA values in the putamen were significantly greater in OA than in YA (blue areas).

In our ROI analysis (Figure 1b) of FA values, a multivariate repeated measures GLM revealed a significant main effect of age ($F_{1,61}$ = 17.2, p < .001) and a significant age by region interaction ($F_{11,61}$ = 9.1, p = .004). Effect sizes for each ROI are presented in Figure 1c. Post-hoc comparisons confirmed our predictions: FA was lower in OA relative to YA in the following ROIs: radiate OFC on the left (p < .001) and right (p , 0.001); genu of the corpus callosum (p < .001); sagittal striatum on the left (p = .008) and right (p < .001); and radiate PFC on the left (p = .02) and right (p = .01). In contrast, FA was significantly greater in OA, compared to YA, in the putamen on the left (p = .04) and right (p = .02). We found no significant differences between YA and OA for mean FA values in the splenium of the corpus callosum or in the radiate occipital WM bilaterally.

Differences between YA and OA in cortical thickness

A surface-based GLM revealed regional changes in cortical thickness between YA and OA (Figure 2a); all areas reported showed significant differences that survived False Discovery Rate correction for multiple comparisons (q < .05). Cortical thinning was found bilaterally in the following regions: the lateral aspect of the superior frontal gyrus, the precentral gyrus and banks of the central sulcus, and in the calcarine sulcus and cuneus in the occipital lobeand in lateral PFC and inferior parietal cortex. We also found age-related thinning in the transverse temporal gyri , but with a rightward predominance. A small, circumscribed region of cortex in the right posterior cingulate gyrus was thicker in OA.

We used a multivariate repeated measures GLM to test for differences in mean thickness in selected ROIs (Figure 2b). These analyses revealed a significant main effect of age ($F_{1,69}$ = 12.9, p < .001) and a significant age by region interaction ($F_{15,69}$ = 10.9, p = .001). Effect sizes for each ROI are presented in Figure 2c. Post-hoc comparisons indicated the greatest degree of thinning occurred, bilaterally, in the precentral gyrus, followed by OFC, calcarine sulcus, and PFC (all p < .01). In contrast, OA showed significantly thicker cortex in the anterior cingulate on the right (p < .001), but not on the left (p = .06), and in the inferior temporal gyrus on the right (p = .01), but not on the left (p = .22). No significant differences were found in thickness of the middle temporal gyrus on the left (p = .25) or right (p = .33) or in the posterior cingulate on the left (p = .33) or right (p = .27). The pattern of these results agreed largely with the predicted pattern of change, as well as with the results from our map-based cortical thickness analysis.

Brain-behavior correlations in OA

To determine whether changes in discrete regions of GM and WM were associated with specific cognitive impairments in OA, we tested for correlations between each cognitive composite score and measures of FA and cortical thickness. For each measure, we used an automated, whole-brain approach, and a complimentary ROI-based approach.

Correlations with DTI data. Voxel-based regression analyses revealed a significant positive correlation between performance on cognitive control tasks and FA in frontal lobe WM (Figure 3a). By contrast, performance on episodic memory tasks correlated positively with FA in more posterior regions, in particular the WM underlying the temporal and parietal lobes (Figure 3b).

No significant correlations were found between semantic memory composite scores and FA. Multiple regression analyses of FA values derived from manually delineated ROIs revealed significant, regionally-specific, correlations between cognitive composite scores and FA in two ROIs (Figure 3c): episodic memory composite scores correlated significantly with mean FA in the temporoparietal WM on the left (R^2 = .46, p = .003; $r^2_{[FA]}$ = .40; $r^2_{[age]}$ = .10) and right (R^2 = .29, p = .04; $r^2_{[FA]}$ = .27; $r^2_{[age]}$ = .05). FA in the temporoparietal ROI was negatively correlated with age on both the left (r^2= .14, p = .002) and right (r^2= .23, p = .001). In contrast, cognitive control scores were positively correlated with mean FA in the PFC on the left (R^2 = .36, p = .01; $r^2_{[FA]}$ = .29; $r^2_{[age]}$ = .09) and right (R^2 = .30, p = .04; $r^2_{[FA]}$ = .19; $r^2_{[age]}$ = .10). FA in the PFC ROI was negatively correlated with age on both the left (r^2= .13, p = .003) and right (r^2= .18, p < .001).

To test the regional specificity of these brain-behavior correlations, we performed additional multiple regression analyses for each of these two cognitive measures, including FA values from both the anterior and posterior ROIs as regressors. These models demonstrated that FA in left (p = .018) and right (p = .028) PFC correlated with performance on cognitive control tasks, independently of any contribution from temporoparietal WM on the left (p = .59) or right (p = .51). In contrast, episodic memory scores were correlated with FA values in left (p = .004) and right (p = .021) temporoparietal WM, but not PFC WM on the left (p = .32) or right (p = .6).

Correlations with cortical thickness. Surface-based regressions revealed a few modest correlations between semantic and episodic memory performance and measures of cortical thickness in OA. None of these correlations, however, exceeded our significance cutoff of p <

.001. Further, we found no significant correlations between thickness in any manually defined cortical ROI and any cognitive composite score (all $p > .06$).

Discussion

This study addressed two open questions about cognitive aging: 1) Do the distributions of age-related change in cortical thickness and WM integrity overlap, or are these brain regions affected differently; and 2) What are the cognitive effects of these brain changes? Here we consider the specific age-related alterations in brain structure, discuss the possible implications of the brain-behavior correlations, and relate our findings to the literature on microstructural factors that may contribute to the etiology of cognitive and neural decline in aging.

Age-related changes in WM integrity

Our predictions concerning age-related differences in WM were largely confirmed: We found widespread regions of reduced FA in the WM underlying the frontal lobes, including OFC, the genu of the corpus callosum, forceps major, and the anterior corona radiata of PFC. The finding of lower FA in the frontal lobes of OA is compatible with the results of several other studies that used a combination of ROI and voxel-based analyses similar to those employed here (Salat *et al.*, 2005a), or that used ROI- or tractography-based methods (Head et al., 2004; Nusbaum et al., 2001; O'Sullivan et al., 2001; Ota et al., 2006; Pfefferbaum et al., 2005). The observed pattern of change in FA also parallels studies that report reduced frontal WM volumes (Guttmann *et al.*, 1998; Salat *et al.*, 1999; Courchesne *et al.*, 2000; Bartzokis *et al.*, 2001; Jernigan *et al.*, 2001; Allen *et al.*, 2005) and increased WM hyperintensities on FLAIR and T2-

weighted images (DeCarli *et al.*, 1995; de Groot *et al.*, 2000; Gunning-Dixon & Raz, 2000; Tullberg *et al.*, 2004; Nordahl *et al.*, 2006; Yoshita *et al.*, 2006). An increased burden of WM hyperintensities is associated with decreased FA values, both within the hyperintense regions, as well as in normal appearing WM (O'Sullivan *et al.*, 2004; Taylor *et al.*, 2007). The present study did not exclude areas of hyperintense signal from FA analyses. While it is possible that a similar relation exists in the present sample, we have examined the quantitative effects of hyperintense signal on DTI measures using statistical models, and found that this variable did not have a significant effect on patterns of FA change in patients with Alzheimer's disease (Salat *et al.*, 2010).

We also found age-related decreases in WM adjacent to temporal and parietal cortices. The few DTI-based studies that have examined temporoparietal WM regions have reported mixed results. In agreement with our findings, one study showed a modest decrease in temporal and parietal lobe FA, but this decline was not proportionate to that in frontal lobe areas (Head *et al.*, 2004). Our results indicate that age-related changes in FA are particularly widespread in WM regions underlying multimodal association cortices. In support of this view, histopathological evidence points toward a degenerative process whereby small diameter myelinated fibers are more vulnerable to aging than larger diameter axons (Tang *et al.*, 1997). The interhemispheric callosal connections between frontal and temporoparietal areas appear to consist predominantly of small diameter fibers (Aboitiz & Montiel, 2003). Thus, the age-related vulnerability of the WM connecting association areas may reflect the high sensitivity of these small diameter fibers to aging processes.

In contrast to the significant decreases noted above, occipital FA values did not differ reliably between OA and YA, but FA values in the putamen were significantly greater in OA compared to YA. This finding is similar to one other report of reduced striatal FA (Abe *et al.*, 2008). Studies using T2-weighted MRI have documented signal changes that are believed to arise from an accumulation of heavy metals in the striatum with increasing age (Ketonen, 1998). Iron deposition in neural tissue has been associated with neurodegenerative disorders, such as Parkinson's disease (Ke & Ming Qian, 2003; Zecca *et al.*, 2004), and there is some evidence that a notable amount of buildup also occurs in subcortical GM structures during the course of healthy aging (Hallgren & Sourander, 1958; Bartzokis *et al.*, 1994; Ketonen, 1998; Bartzokis *et al.*, 2007). While the mechanism by which iron deposition would cause a change in the FA metric is not entirely understood, a well-documented decrease or shortening of the T2 signal has been linked to heavy metal accumulation in the putamen in the sixth decade of life (Ketonen, 1998). T2 shortening is typically found using gradient echo sequences, which are related to the DTI acquisitions used here (i.e., pulsed-gradient, spin-echo sequences). Thus, iron deposition in the putamen provides a putative explanation for the increased striatal FA that we see in our sample of OA.

Parallels between reduced FA and microstructural changes in aging

Our results indicate that DTI-based measures of WM integrity are sensitive to pathological changes that occur with advanced age. While we do not yet fully understand which specific tissue-level properties give rise to the MR signals used to derive FA values (Beaulieu, 2002),

evidence from histopathological studies suggests that alterations in myelin structure and integrity likely contribute to the age-related differences in FA values reported here. Studies of aged monkey brains show numerous abnormalities in myelin (Peters, 2002), including the formation of cytoplasmic inclusions following splitting of the myelin lamellae, the accumulation of "balloons" or holes inside the myelin sheath, formation of redundant myelin sheaths (Rosenbluth, 1966; Sturrock, 1976), and loss of small myelinated fibers (Kemper, 1994; Tang *et al.*, 1997; Sandell & Peters, 2001; Marner *et al.*, 2003). Further, myelin abnormalities have been linked to cognitive dysfunction in aged monkeys (Moss & Killiany, 1999). Thus, although the evidence is indirect, decreased FA values in the present study are likely due to cellular changes in myelin. Conclusive evidence will require further investigation combining MRI and histopathological techniques in the same brains.

Age-related changes in cortical thickness

Consistent with another study (Salat *et al.*, 2004), we found large regions of cortical thinning in sensory and motor areas, including the precentral gyrus, the pericalcarine region, and the medial aspect of the superior frontal gyrus. We also noted smaller regions of thinning in the lateral PFC, inferior parietal cortex, and transverse temporal gyri. In contrast, other frontal and temporal areas were largely devoid of significant age-related cortical thinning, and small areas of the right anterior cingulate and right inferior temporal gyrus showed modestly increased thickness in OA. These findings are in partial agreement with previous studies that documented significant age-related GM decrements in primary sensory and motor cortices using voxel- or ROI-based approaches (Good *et al.*, 2001; Resnick *et al.*, 2003; Raz *et al.*, 2004a; Salat *et al.*,

2004; Tisserand *et al.*, 2004; Lemaitre *et al.*, 2005), as well as with one study that used the same cortical thickness tools employed here (Salat *et al.*, 2004). Other studies, however, reported the greatest degree of volumetric loss in frontal areas, with primary sensory and motor cortices showing less age-related degeneration (Jernigan *et al.*, 1991; Raz *et al.*, 1997; Sowell *et al.*, 2003; Raz & Rodrigue, 2006), possibly reflecting a pattern of atrophy that occurs in reverse of the developmental trajectory of growth (Raz *et al.*, 1997).

The discrepancy in findings could be the result of differences in analytic techniques, whereby measures of cortical thickness and volume are detecting separate degenerative processes. Because cortical volume is a product of thickness and surface area, degenerative processes that selectively affect surface area would not necessarily be detected using measures of cortical thickness. For example, age-related sulcal expansion (Kemper, 1994) could, in theory, be related to changes in cortical volume but not thickness. Alternatively, the discrepancy across laboratories may be related to differences in participant characteristics, such as exclusionary criteria or the ages of the OA groups. Several studies indicate that some frontal lobe damage is more closely related to vascular disease than to healthy aging processes (Artero *et al.*, 2004; Raz *et al.*, 2007). Thus, results from studies such as the present one, which excluded any OA with untreated hypertension, should include fewer changes that are specifically related to vascular disease processes.

We also found several small areas where cortical thickness was greater in OA compared to YA. While not directly comparable to the present study, which examined differences between YA

and OA, one study did report a regionally specific increase in cortical thickness in high functioning OA, compared to OA with average fluid intelligence scores (Fjell *et al.*, 2006). The high functioning group had thicker cortex in the right posterior cingulate gyrus. Although slightly more posterior to the area of the cingulate gyrus where we found increased thickness in OA, these two regions are adjacent. Taken together, these findings support the idea that some areas of cortex do not show age-related loss, and that thickening in specific cortical regions may impart some protective advantage to OA in terms of performance in selected cognitive domains.

Cognitive correlates of decreased WM integrity

We found a reliable pattern of correlations between WM integrity and cognitive performance in this sample of healthy OA. These results are striking because the ROI-based analysis showed a putative double dissociation between cognitive control and episodic memory function vis-à-vis WM integrity in anterior and posterior regions, respectively. Namely, we found a positive correlation between FA in anterior WM regions, including PFC, and scores on tasks that assessed cognitive control processes. In contrast, episodic memory performance correlated positively with the integrity of WM underlying temporal and posterior parietal areas, but not frontal areas, in our sample of OA. It is important to note that, in a cross-sectional study, one cannot completely disentangle the effects of age and the effects of inherent variability in a brain measure when the brain measure itself is negatively correlated with age. From careful analysis of our data, however, we find that age has a negative effect on FA (both through our group comparisons and correlations with age in selected ROIs) and that cognition is predicted

by FA. Strengthening this conclusion is our finding that the correlations between cognition and FA were found in brain areas in which OA also showed significantly lower FA, when compared to YA.

The findings of a DTI study of WM in old rhesus monkeys support our conclusion: Age-related decline in executive function was significantly correlated with FA in long-distance corticocortical association pathways, including the anterior corpus callosum and the superior longitudinal fasciculus (Makris *et al.*, 2007). In older humans, increased numbers of WM hyperintensities in PFC are associated with greater executive dysfunction (Gunning-Dixon & Raz, 2003), and FA in anterior WM correlates with selected measures of executive function and mnemonic control (O'Sullivan *et al.*, 2001; Sullivan *et al.*, 2006). The present results confirm and extend these previous reports suggesting a link between the integrity of frontal lobe WM and performance on tests requiring the top-down control of cognition. By virtue of our combined whole-brain and ROI-based approach, we have also demonstrated that performance on these tasks is not correlated with WM integrity in more posterior regions. The brain-behavior correlations described here underscore the necessity of frontal lobe WM in supporting cognitive control processes in OA.

Other evidence supporting the association between temporoparietal areas and episodic memory performance comes from functional neuroimaging studies that have demonstrated a critical role for parietal lobe GM in mediating episodic memory retrieval (Buckner & Wheeler, 2001; Rugg *et al.*, 2002; Shannon & Buckner, 2004; Wagner *et al.*, 2005). The cortical loci that

are consistently implicated include lateral posterior parietal cortex (including the intraparietal sulcus and inferior parietal lobule), precuneus, posterior cingulate, and retrosplenial cortices (Wagner *et al.*, 2005). In the present study, the locus of the correlation between temporoparietal WM and episodic memory fell at the junction of several WM tracts that connect these previously identified brain regions. This WM region includes the sagittal stratum, which originates in the caudal portions of the superior and inferior parietal lobules and superior temporal gyrus, and the inferior longitudinal fasciculus, which contains projections that connect posterior parietal cortex with the inferior temporal gyrus and occipital lobe (Schmahmann & Pandya, 2006). One would expect this area to include fibers that link many of the cortical areas that are active during episodic retrieval, and it is, therefore, not surprising that decreased integrity of this WM region is associated with lower episodic memory performance in OA.

Cognitive correlates of age-related cortical thinning

Contrary to our expectations, we found no significant correlations between measures of cortical thickness and composite scores from any of the three cognitive domains examined. Prior evidence suggesting a link between age-related cortical changes and cognitive decline comes from a variety of sources. Functional neuroimaging studies in OA show dramatic changes in cortical activity during performance of tasks that require cognitive control (Gazzaley *et al.*, 2005; Grady *et al.*, 2006; Velanova *et al.*, 2007), episodic memory (Cabeza *et al.*, 1997; Grady *et al.*, 1999; Stebbins *et al.*, 2002), and semantic memory processes (Madden *et al.*, 1996; Cabeza, 2001; Dennis *et al.*, 2007). Such studies, however, rely on indirect measures of neural activity, and not structural integrity per se. Thus, these fMRI studies cannot rule out

contributions from other factors, such as decreased integrity of the connections between nodes in these functional networks, similar to the pattern we report here using DTI-based indices of WM integrity.

More direct evidence for a link between cortical thinning and cognitive decline comes from a study in monkeys, showing that cortical thinning in PFC was a good predictor of performance on a delayed non-match to sample memory test (Peters *et al.*, 1998b).

In humans, however, the evidence for a relation between cortical atrophy and cognitive decline is equivocal. A review of the literature on structure-function correlations in aging concluded that "the magnitude of the observed associations is modest" and "not easily replicated" (Raz & Rodrigue, 2006). One experiment that was limited to YA suggested a link between cortical thickness and verbal recall (Walhovd *et al.*, 2006), but at delay intervals (months) much longer than those employed here (minutes). Consistent with our results, another study found no association between cortical thickness and measures of executive function (Fjell *et al.*, 2006). Although some investigators have advocated searching for a link between memory decline and changes in the size of the hippocampus or other medial temporal lobe structures (Golomb *et al.*, 1996), a meta-analysis of volumetric studies found little evidence for an association between hippocampal atrophy and memory decline in healthy OA (Van Petten, 2004). Unfortunately, our thickness analyses are limited to cortical regions, and thus is is not possible to determine whether hippocampus proper is related to episodic memory function in our sample of OA. Our analyses do, however, include other medial temporal lobe structures, such

as entorhinal and parahippocampal cortices, and we did not find evidence for age-related changes or correlations with episodic memory scores in these areas.

These negative findings with respect to correlations between cortical thickness and cognition raise the possibility that MRI-based measures of thickness or volume are simply not sensitive enough to detect the age-related alterations that are functionally significant. It is important to note, however, that unlike many previous studies, the methods employed here are not constrained by the size of ROIs selected a priori (i.e., we did not rely on pre-defined cortical parcellation units), but rather combined an ROI analysis with a point-by-point examination of cognitive correlations across the entire cortical surface. Thus, we would have been capable of detecting correlations between cognitive scores and changes in small, discrete areas of cortex, had such correlations existed. It is possible that the cognitive processes that are measured by our three composite scores do not rely on the function of easily localizable cortical foci, but instead tend to recruit numerous nodes, distributed across large regions of cortex (Mesulam, 1990; McIntosh, 2000). Because efficient communication is essential for the proper function of such large scale networks, disruption in the integrity of the links could introduce catastrophic interference. This hypothesis is in accordance with our finding of stronger structure-function correlations when considering WM integrity.

Conclusions

Our data suggest that WM degeneration, rather than cortical (i.e., GM) thinning, may contribute more to explaining age-related deterioration of cognitive control processes and

episodic memory. While healthy aging was associated with cortical thinning and loss of WM integrity, the loci of these changes were distinct. WM changes occurred in tissue underlying association cortices, whereas cortical thinning was greatest in primary sensory and motor cortices. Thus, the contribution of cortical thinning to decline in the domains of episodic memory and cognitive control may be secondary to deterioration of WM integrity, or may instead correlate with lower-level processes that rely more on the primary sensory areas where cortical thinning is most pronounced. Further, this spatial dissociation suggests that separate degenerative processes may be at play in GM and WM. These processes may follow different time courses, and GM and WM abnormalities may even respond to different therapeutic interventions. The identification of new therapeutic opportunities applicable to healthy aging will require interdisciplinary research efforts that combine theoretical perspectives from cognitive science with histology, neuroimaging, genetics, and psychopharmacology.

Acknowledgements

This work was supported by NIH grants: AG021525 (SC), K01 AG24898 (DS), and T32 GM007484 (DZ). Imaging facilities at the Athinoula A. Martinos Center for Biomedical Imaging are supported by grants from the NCRR (P41RR14075) and the MIND Institute. Oliver Piguet was supported by a National Health and Medical Research Council of Australia Neil Hamilton Fairley Postdoctoral Fellowship (ID# 222909). He is now at now at the Prince of Wales Medical Research Institute, Sydney, Australia. Emily Connally is now at the University of Arizona. We thank Meredith Brown for helpful editorial comments, Julie Proulx for help with data collection, Nicholas Harrington for help with data analysis, and Joseph Locascio and Paymon Ashourian for statistical consultation.

References

Abe O, Yamasue H, Aoki S, Suga M, Yamada H, Kasai K, Masutani Y, Kato N, Kato N & Ohtomo K (2008) Aging in the CNS: comparison of gray/white matter volume and diffusion tensor data. *Neurobiol Aging* **29**, 102-116.

Aboitiz F & Montiel J (2003) One hundred million years of interhemispheric communication: the history of the corpus callosum. *Braz J Med Biol Res* **36**, 409-420.

Allen JS, Bruss J, Brown CK & Damasio H (2005) Normal neuroanatomical variation due to age: the major lobes and a parcellation of the temporal region. *Neurobiol Aging* **26**, 1245-1260; discussion 1279-1282.

Ardekani S, Kumar A, Bartzokis G & Sinha U (2007) Exploratory voxel-based analysis of diffusion indices and hemispheric asymmetry in normal aging. *Magn Reson Imaging* **25**, 154-167.

Artero S, Tiemeier H, Prins ND, Sabatier R, Breteler MM & Ritchie K (2004) Neuroanatomical localisation and clinical correlates of white matter lesions in the elderly. *J Neurol Neurosurg Psychiatry* **75**, 1304-1308.

Bartzokis G, Beckson M, Lu PH, Nuechterlein KH, Edwards N & Mintz J (2001) Age-related changes in frontal and temporal lobe volumes in men: a magnetic resonance imaging study. *Arch Gen Psychiatry* **58**, 461-465.

Bartzokis G, Mintz J, Sultzer D, Marx P, Herzberg JS, Phelan CK & Marder SR (1994) In vivo MR evaluation of age-related increases in brain iron. *AJNR Am J Neuroradiol* **15**, 1129-1138.

Bartzokis G, Tishler TA, Lu PH, Villablanca P, Altshuler LL, Carter M, Huang D, Edwards N & Mintz J (2007) Brain ferritin iron may influence age- and gender-related risks of neurodegeneration. *Neurobiol Aging* **28**, 414-423.

Basser PJ, Mattiello J & LeBihan D (1994) Estimation of the effective self-diffusion tensor from the NMR spin echo. *J Magn Reson B* **103**, 247-254.

Beaulieu C (2002) The basis of anisotropic water diffusion in the nervous system - a technical review. *NMR Biomed* **15**, 435-455.

Benedetti B, Charil A, Rovaris M, Judica E, Valsasina P, Sormani MP & Filippi M (2006) Influence of aging on brain gray and white matter changes assessed by conventional, MT, and DT MRI. *Neurology* **66**, 535-539.

Benjamini Y & Hochberg Y (1995) Controlling the false discovery rate: a practical and powerful approach to multiple testing. *Journal of the Royal Statistical Society B* **57**, 289-300.

Benton AL & Hamsher Kd (1989) *Multilingual aphasia examination*. Iowa City, Iowa: AJA Associates.

Buckner RL & Wheeler ME (2001) The cognitive neuroscience of remembering. *Nat Rev Neurosci* **2**, 624-634.

Bucur B, Madden DJ, Spaniol J, Provenzale JM, Cabeza R, White LE & Huettel SA (2008) Age-related slowing of memory retrieval: contributions of perceptual speed and cerebral white matter integrity. *Neurobiol Aging* **29**, 1070-1079.

Cabeza R (2001) Cognitive neuroscience of aging: contributions of functional neuroimaging. *Scand J Psychol* **42**, 277-286.

Cabeza R, Grady CL, Nyberg L, McIntosh AR, Tulving E, Kapur S, Jennings JM, Houle S & Craik FI (1997) Age-related differences in neural activity during memory encoding and retrieval: a positron emission tomography study. *J Neurosci* **17**, 391-400.

Charlton RA, Barrick TR, McIntyre DJ, Shen Y, O'Sullivan M, Howe FA, Clark CA, Morris RG & Markus HS (2006) White matter damage on diffusion tensor imaging correlates with age-related cognitive decline. *Neurology* **66**, 217-222.

Courchesne E, Chisum HJ, Townsend J, Cowles A, Covington J, Egaas B, Harwood M, Hinds S & Press GA (2000) Normal brain development and aging: quantitative analysis at in vivo MR imaging in healthy volunteers. *Radiology* **216**, 672-682.

Cowell PE, Turetsky BI, Gur RC, Grossman RI, Shtasel DL & Gur RE (1994) Sex differences in aging of the human frontal and temporal lobes. *J Neurosci* **14**, 4748-4755.

Dale AM, Fischl B & Sereno MI (1999) Cortical surface-based analysis. I. Segmentation and surface reconstruction. *Neuroimage* **9**, 179-194.

de Groot JC, de Leeuw FE, Oudkerk M, van Gijn J, Hofman A, Jolles J & Breteler MM (2000) Cerebral white matter lesions and cognitive function: the Rotterdam Scan Study. *Ann Neurol* **47**, 145-151.

Deary IJ, Bastin ME, Pattie A, Clayden JD, Whalley LJ, Starr JM & Wardlaw JM (2006) White matter integrity and cognition in childhood and old age. *Neurology* **66**, 505-512.

DeCarli C, Murphy DG, Tranh M, Grady CL, Haxby JV, Gillette JA, Salerno JA, Gonzales-Aviles A, Horwitz B, Rapoport SI & et al. (1995) The effect of white matter hyperintensity volume on brain structure, cognitive performance, and cerebral metabolism of glucose in 51 healthy adults. *Neurology* **45**, 2077-2084.

Dennis NA, Daselaar S & Cabeza R (2007) Effects of aging on transient and sustained successful memory encoding activity. *Neurobiol Aging* **28**, 1749-1758.

Double KL, Halliday GM, Kril JJ, Harasty JA, Cullen K, Brooks WS, Creasey H & Broe GA (1996) Topography of brain atrophy during normal aging and Alzheimer's disease. *Neurobiol Aging* **17**, 513-521.

Fischl B & Dale AM (2000) Measuring the thickness of the human cerebral cortex from magnetic resonance images. *Proc Natl Acad Sci U S A* **97**, 11050-11055.

Fischl B, Liu A & Dale AM (2001) Automated manifold surgery: constructing geometrically accurate and topologically correct models of the human cerebral cortex. *IEEE Trans Med Imaging* **20**, 70-80.

Fischl B, Sereno MI & Dale AM (1999a) Cortical surface-based analysis. II: Inflation, flattening, and a surface-based coordinate system. *Neuroimage* **9**, 195-207.

Fischl B, Sereno MI, Tootell RB & Dale AM (1999b) High-resolution intersubject averaging and a coordinate system for the cortical surface. *Hum Brain Mapp* **8**, 272-284.

Fjell AM, Walhovd KB, Reinvang I, Lundervold A, Salat D, Quinn BT, Fischl B & Dale AM (2006) Selective increase of cortical thickness in high-performing elderly--structural indices of optimal cognitive aging. *Neuroimage* **29**, 984-994.

Folstein MF, Folstein SE & McHugh PR (1975) "Mini-mental state". A practical method for grading the cognitive state of patients for the clinician. *J Psychiatr Res* **12**, 189-198.

Gazzaley A, Cooney JW, Rissman J & D'Esposito M (2005) Top-down suppression deficit underlies working memory impairment in normal aging. *Nat Neurosci* **8**, 1298-1300.

Genovese CR, Lazar NA & Nichols T (2002) Thresholding of statistical maps in functional neuroimaging using the false discovery rate. *Neuroimage* **15**, 870-878.

Golomb J, Kluger A, de Leon MJ, Ferris SH, Mittelman M, Cohen J & George AE (1996) Hippocampal formation size predicts declining memory performance in normal aging. *Neurology* **47**, 810-813.

Good CD, Johnsrude IS, Ashburner J, Henson RN, Friston KJ & Frackowiak RS (2001) A voxel-based morphometric study of ageing in 465 normal adult human brains. *Neuroimage* **14**, 21-36.

Grady CL, McIntosh AR, Rajah MN, Beig S & Craik FI (1999) The effects of age on the neural correlates of episodic encoding. *Cereb Cortex* **9**, 805-814.

Grady CL, Springer MV, Hongwanishkul D, McIntosh AR & Winocur G (2006) Age-related changes in brain activity across the adult lifespan. *J Cogn Neurosci* **18**, 227-241.

Greenwood PM (2000) The frontal aging hypothesis evaluated. *J Int Neuropsychol Soc* **6**, 705-726.

Grieve SM, Clark CR, Williams LM, Peduto AJ & Gordon E (2005) Preservation of limbic and paralimbic structures in aging. *Hum Brain Mapp* **25**, 391-401.

Grieve SM, Williams LM, Paul RH, Clark CR & Gordon E (2007) Cognitive aging, executive function, and fractional anisotropy: a diffusion tensor MR imaging study. *AJNR Am J Neuroradiol* **28**, 226-235.

Gunning-Dixon FM & Raz N (2000) The cognitive correlates of white matter abnormalities in normal aging: a quantitative review. *Neuropsychology* **14**, 224-232.

Gunning-Dixon FM & Raz N (2003) Neuroanatomical correlates of selected executive functions in middle-aged and older adults: a prospective MRI study. *Neuropsychologia* **41**, 1929-1941.

Guttmann CR, Jolesz FA, Kikinis R, Killiany RJ, Moss MB, Sandor T & Albert MS (1998) White matter changes with normal aging. *Neurology* **50**, 972-978.

Hallgren B & Sourander P (1958) The effect of age on the non-haemin iron in the human brain. *J Neurochem* **3**, 41-51.

Head D, Buckner RL, Shimony JS, Williams LE, Akbudak E, Conturo TE, McAvoy M, Morris JC & Snyder AZ (2004) Differential vulnerability of anterior white matter in nondemented aging with minimal acceleration in dementia of the Alzheimer type: evidence from diffusion tensor imaging. *Cereb Cortex* **14**, 410-423.

Hedden T & Gabrieli JD (2004) Insights into the ageing mind: a view from cognitive neuroscience. *Nat Rev Neurosci* **5**, 87-96.

Hinman JD & Abraham CR (2007) What's behind the decline? The role of white matter in brain aging. *Neurochem Res* **32**, 2023-2031.

Ikram MA, Vrooman HA, Vernooij MW, van der Lijn F, Hofman A, van der Lugt A, Niessen WJ & Breteler MM (2008) Brain tissue volumes in the general elderly population. The Rotterdam Scan Study. *Neurobiol Aging* **29**, 882-890.

Jenkinson M, Bannister P, Brady M & Smith S (2002) Improved optimization for the robust and accurate linear registration and motion correction of brain images. *Neuroimage* **17**, 825-841.

Jenkinson M & Smith S (2001) A global optimisation method for robust affine registration of brain images. *Med Image Anal* **5**, 143-156.

Jernigan TL, Archibald SL, Berhow MT, Sowell ER, Foster DS & Hesselink JR (1991) Cerebral structure on MRI, Part I: Localization of age-related changes. *Biol Psychiatry* **29**, 55-67.

Jernigan TL, Archibald SL, Fennema-Notestine C, Gamst AC, Stout JC, Bonner J & Hesselink JR (2001) Effects of age on tissues and regions of the cerebrum and cerebellum. *Neurobiol Aging* **22**, 581-594.

Kaplan E, Goodglass H & Weintraub S (1983) *The Boston Naming Test*. Philadelphia.

Ke Y & Ming Qian Z (2003) Iron misregulation in the brain: a primary cause of neurodegenerative disorders. *Lancet Neurol* **2**, 246-253.

Kemper TL (1994) Neuroanatomical and neuropathological changes during aging and dementia. In *Clinical Neurology of Aging*, pp. 3-67 [ML Albert and JE Knoefel, editors]. New York: Oxford University Press.

Ketonen LM (1998) Neuroimaging of the aging brain. *Neurol Clin* **16**, 581-598.

Kramer JH, Mungas D, Reed BR, Wetzel ME, Burnett MM, Miller BL, Weiner MW & Chui HC (2007) Longitudinal MRI and cognitive change in healthy elderly. *Neuropsychology* **21**, 412-418.

Lemaitre H, Crivello F, Grassiot B, Alperovitch A, Tzourio C & Mazoyer B (2005) Age- and sex-related effects on the neuroanatomy of healthy elderly. *Neuroimage* **26**, 900-911.

Lezak MD (1995) *Neuropsychological assessment*, 3rd ed. New York: Oxford University Press.

Lutz J, Hemminger F, Stahl R, Dietrich O, Hempel M, Reiser M & Jager L (2007) Evidence of subcortical and cortical aging of the acoustic pathway: a diffusion tensor imaging (DTI) study. *Acad Radiol* **14**, 692-700.

Madden DJ, Spaniol J, Whiting WL, Bucur B, Provenzale JM, Cabeza R, White LE & Huettel SA (2007) Adult age differences in the functional neuroanatomy of visual attention: a combined fMRI and DTI study. *Neurobiol Aging* **28**, 459-476.

Madden DJ, Turkington TG, Coleman RE, Provenzale JM, DeGrado TR & Hoffman JM (1996) Adult age differences in regional cerebral blood flow during visual world identification: evidence from H215O PET. *Neuroimage* **3**, 127-142.

Madden DJ, Whiting WL, Huettel SA, White LE, MacFall JR & Provenzale JM (2004) Diffusion tensor imaging of adult age differences in cerebral white matter: relation to response time. *Neuroimage* **21**, 1174-1181.

Makris N, Papadimitriou GM, van der Kouwe A, Kennedy DN, Hodge SM, Dale AM, Benner T, Wald LL, Wu O, Tuch DS, Caviness VS, Moore TL, Killiany RJ, Moss MB & Rosene DL (2007) Frontal connections and cognitive changes in normal aging rhesus monkeys: a DTI study. *Neurobiol Aging* **28**, 1556-1567.

Marner L, Nyengaard JR, Tang Y & Pakkenberg B (2003) Marked loss of myelinated nerve fibers in the human brain with age. *J Comp Neurol* **462**, 144-152.

Mazziotta JC, Toga AW, Evans A, Fox P & Lancaster J (1995) A probabilistic atlas of the human brain: theory and rationale for its development. The International Consortium for Brain Mapping (ICBM). *Neuroimage* **2**, 89-101.

McIntosh AR (2000) Towards a network theory of cognition. *Neural Netw* **13**, 861-870.

Mesulam MM (1990) Large-scale neurocognitive networks and distributed processing for attention, language, and memory. *Ann Neurol* **28**, 597-613.

Moss MB & Killiany RJ (1999) Age-related cognitive decline in rhesus monkey. In *Cerebral Cortex Vol. 14: Neurodegenerative and Age-Related Changes in Structure and Function of the*

Cerebral Cortex, pp. 21-48 [A Peters and JH Morrison, editors]. New York: Kluwer Academic/Plenum Publishers.

Nordahl CW, Ranganath C, Yonelinas AP, Decarli C, Fletcher E & Jagust WJ (2006) White matter changes compromise prefrontal cortex function in healthy elderly individuals. *J Cogn Neurosci* **18**, 418-429.

O'Sullivan M, Jones DK, Summers PE, Morris RG, Williams SC & Markus HS (2001) Evidence for cortical "disconnection" as a mechanism of age-related cognitive decline. *Neurology* **57**, 632-638.

O'Sullivan M, Morris RG, Huckstep B, Jones DK, Williams SC & Markus HS (2004) Diffusion tensor MRI correlates with executive dysfunction in patients with ischaemic leukoaraiosis. *J Neurol Neurosurg Psychiatry* **75**, 441-447.

Pakkenberg B & Gundersen HJ (1997) Neocortical neuron number in humans: effect of sex and age. *J Comp Neurol* **384**, 312-320.

Persson J, Nyberg L, Lind J, Larsson A, Nilsson LG, Ingvar M & Buckner RL (2006) Structure-function correlates of cognitive decline in aging. *Cereb Cortex* **16**, 907-915.

Peters A (2002) The effects of normal aging on myelin and nerve fibers: a review. *J Neurocytol* **31**, 581-593.

Peters A, Morrison JH, Rosene DL & Hyman BT (1998a) Feature article: are neurons lost from the primate cerebral cortex during normal aging? *Cereb Cortex* **8**, 295-300.

Peters A, Sethares C & Moss MB (1998b) The effects of aging on layer 1 in area 46 of prefrontal cortex in the rhesus monkey. *Cereb Cortex* **8**, 671-684.

Pfefferbaum A, Adalsteinsson E & Sullivan EV (2005) Frontal circuitry degradation marks healthy adult aging: Evidence from diffusion tensor imaging. *Neuroimage* **26**, 891-899.

Pfefferbaum A, Mathalon DH, Sullivan EV, Rawles JM, Zipursky RB & Lim KO (1994) A quantitative magnetic resonance imaging study of changes in brain morphology from infancy to late adulthood. *Arch Neurol* **51**, 874-887.

Pfefferbaum A, Sullivan EV, Hedehus M, Lim KO, Adalsteinsson E & Moseley M (2000) Age-related decline in brain white matter anisotropy measured with spatially corrected echo-planar diffusion tensor imaging. *Magn Reson Med* **44**, 259-268.

Pierpaoli C & Basser PJ (1996) Toward a quantitative assessment of diffusion anisotropy. *Magn Reson Med* **36**, 893-906.

Piguet O & Corkin S (2007) The aging brain. In *Learning and the Brain: A Comprehensive Guide for Educators, Parents, and Teachers* [S Feinstein, editor]. Lanham, MD: Rowman & Littlefield Education.

Piguet O, Double KL, Kril JJ, Harasty J, Macdonald V, McRitchie DA & Halliday GM (2009) White matter loss in healthy ageing: a postmortem analysis. *Neurobiol Aging* **30**, 1288-1295.

Raz N, Gunning-Dixon F, Head D, Rodrigue KM, Williamson A & Acker JD (2004a) Aging, sexual dimorphism, and hemispheric asymmetry of the cerebral cortex: replicability of regional differences in volume. *Neurobiol Aging* **25**, 377-396.

Raz N, Gunning-Dixon FM, Head D, Dupuis JH & Acker JD (1998) Neuroanatomical correlates of cognitive aging: evidence from structural magnetic resonance imaging. *Neuropsychology* **12**, 95-114.

Raz N, Gunning FM, Head D, Dupuis JH, McQuain J, Briggs SD, Loken WJ, Thornton AE & Acker JD (1997) Selective aging of the human cerebral cortex observed in vivo: differential vulnerability of the prefrontal gray matter. *Cereb Cortex* **7**, 268-282.

Raz N, Lindenberger U, Rodrigue KM, Kennedy KM, Head D, Williamson A, Dahle C, Gerstorf D & Acker JD (2005) Regional brain changes in aging healthy adults: general trends, individual differences and modifiers. *Cereb Cortex* **15**, 1676-1689.

Raz N & Rodrigue KM (2006) Differential aging of the brain: patterns, cognitive correlates and modifiers. *Neurosci Biobehav Rev* **30**, 730-748.

Raz N, Rodrigue KM, Head D, Kennedy KM & Acker JD (2004b) Differential aging of the medial temporal lobe: a study of a five-year change. *Neurology* **62**, 433-438.

Raz N, Rodrigue KM, Kennedy KM & Acker JD (2007) Vascular health and longitudinal changes in brain and cognition in middle-aged and older adults. *Neuropsychology* **21**, 149-157.

Reese TG, Heid O, Weisskoff RM & Wedeen VJ (2003) Reduction of eddy-current-induced distortion in diffusion MRI using a twice-refocused spin echo. *Magn Reson Med* **49**, 177-182.

Reitan RM (1958) Validity of the Trail Making Test as an indicator of brain damage. *Perceptual & Motor Skills* **8**, 271-276.

Resnick SM, Pham DL, Kraut MA, Zonderman AB & Davatzikos C (2003) Longitudinal magnetic resonance imaging studies of older adults: a shrinking brain. *J Neurosci* **23**, 3295-3301.

Rose SE, Janke AL & Chalk JB (2008) Gray and white matter changes in Alzheimer's disease: a diffusion tensor imaging study. *J Magn Reson Imaging* **27**, 20-26.

Rosenbluth J (1966) Redundant myelin sheaths and other ultrastructural features of the toad cerebellum. *J Cell Biol* **28**, 73-93.

Rugg MD, Otten LJ & Henson RN (2002) The neural basis of episodic memory: evidence from functional neuroimaging. *Philos Trans R Soc Lond B Biol Sci* **357**, 1097-1110.

Salat DH, Buckner RL, Snyder AZ, Greve DN, Desikan RS, Busa E, Morris JC, Dale AM & Fischl B (2004) Thinning of the cerebral cortex in aging. *Cereb Cortex* **14**, 721-730.

Salat DH, Kaye JA & Janowsky JS (1999) Prefrontal gray and white matter volumes in healthy aging and Alzheimer disease. *Arch Neurol* **56**, 338-344.

Salat DH, Kaye JA & Janowsky JS (2002) Greater orbital prefrontal volume selectively predicts worse working memory performance in older adults. *Cereb Cortex* **12**, 494-505.

Salat DH, Tuch DS, Greve DN, van der Kouwe AJ, Hevelone ND, Zaleta AK, Rosen BR, Fischl B, Corkin S, Rosas HD & Dale AM (2005a) Age-related alterations in white matter microstructure measured by diffusion tensor imaging. *Neurobiol Aging* **26**, 1215-1227.

Salat DH, Tuch DS, Hevelone ND, Fischl B, Corkin S, Rosas HD & Dale AM (2005b) Age-related changes in prefrontal white matter measured by diffusion tensor imaging. *Ann N Y Acad Sci* **1064**, 37-49.

Salat DH, Tuch DS, van der Kouwe AJ, Greve DN, Pappu V, Lee SY, Hevelone ND, Zaleta AK, Growdon JH, Corkin S, Fischl B & Rosas HD (2010) White matter pathology isolates the hippocampal formation in Alzheimer's disease. *Neurobiol Aging* **31**, 244-256.

Sandell JH & Peters A (2001) Effects of age on nerve fibers in the rhesus monkey optic nerve. *J Comp Neurol* **429**, 541-553.

Schmahmann JD & Pandya DN (2006) *Fiber Pathways of the Brain*. Oxford, UK: Oxford University Press.

Shannon BJ & Buckner RL (2004) Functional-anatomic correlates of memory retrieval that suggest nontraditional processing roles for multiple distinct regions within posterior parietal cortex. *J Neurosci* **24**, 10084-10092.

Soderlund H, Nyberg L, Adolfsson R, Nilsson LG & Launer LJ (2003) High prevalence of white matter hyperintensities in normal aging: relation to blood pressure and cognition. *Cortex* **39**, 1093-1105.

Sowell ER, Peterson BS, Thompson PM, Welcome SE, Henkenius AL & Toga AW (2003) Mapping cortical change across the human life span. *Nat Neurosci* **6**, 309-315.

Stebbins GT, Carrillo MC, Dorfman J, Dirksen C, Desmond JE, Turner DA, Bennett DA, Wilson RS, Glover G & Gabrieli JD (2002) Aging effects on memory encoding in the frontal lobes. *Psychol Aging* **17**, 44-55.

Stroop J (1935) Studies of interference in serial verbal reactions. *J Exp Psychol Gen* **18**, 643-662.

Sturrock RR (1976) Changes in neuroglia and myelination in the white matter of aging mice. *J Gerontol* **31**, 513-522.

Sullivan EV, Adalsteinsson E & Pfefferbaum A (2006) Selective age-related degradation of anterior callosal fiber bundles quantified in vivo with fiber tracking. *Cereb Cortex* **16**, 1030-1039.

Sullivan EV & Pfefferbaum A (2003) Diffusion tensor imaging in normal aging and neuropsychiatric disorders. *Eur J Radiol* **45**, 244-255.

Sullivan EV & Pfefferbaum A (2006) Diffusion tensor imaging and aging. *Neurosci Biobehav Rev* **30**, 749-761.

Sullivan EV, Rosenbloom M, Serventi KL & Pfefferbaum A (2004) Effects of age and sex on volumes of the thalamus, pons, and cortex. *Neurobiol Aging* **25**, 185-192.

Tang Y, Nyengaard JR, Pakkenberg B & Gundersen HJ (1997) Age-induced white matter changes in the human brain: a stereological investigation. *Neurobiol Aging* **18**, 609-615.

Taylor WD, Bae JN, MacFall JR, Payne ME, Provenzale JM, Steffens DC & Krishnan KR (2007) Widespread effects of hyperintense lesions on cerebral white matter structure. *AJR Am J Roentgenol* **188**, 1695-1704.

Tisserand DJ & Jolles J (2003) On the involvement of prefrontal networks in cognitive ageing. *Cortex* **39**, 1107-1128.

Tisserand DJ, Pruessner JC, Sanz Arigita EJ, van Boxtel MP, Evans AC, Jolles J & Uylings HB (2002) Regional frontal cortical volumes decrease differentially in aging: an MRI study to compare volumetric approaches and voxel-based morphometry. *Neuroimage* **17**, 657-669.

Tisserand DJ, van Boxtel MP, Pruessner JC, Hofman P, Evans AC & Jolles J (2004) A voxel-based morphometric study to determine individual differences in gray matter density associated with age and cognitive change over time. *Cereb Cortex* **14**, 966-973.

Tullberg M, Fletcher E, DeCarli C, Mungas D, Reed BR, Harvey DJ, Weiner MW, Chui HC & Jagust WJ (2004) White matter lesions impair frontal lobe function regardless of their location. *Neurology* **63**, 246-253.

Van Petten C (2004) Relationship between hippocampal volume and memory ability in healthy individuals across the lifespan: review and meta-analysis. *Neuropsychologia* **42**, 1394-1413.

Van Petten C, Plante E, Davidson PS, Kuo TY, Bajuscak L & Glisky EL (2004) Memory and executive function in older adults: relationships with temporal and prefrontal gray matter volumes and white matter hyperintensities. *Neuropsychologia* **42**, 1313-1335.

Velanova K, Lustig C, Jacoby LL & Buckner RL (2007) Evidence for frontally mediated controlled processing differences in older adults. *Cereb Cortex* **17**, 1033-1046.

Wagner AD, Shannon BJ, Kahn I & Buckner RL (2005) Parietal lobe contributions to episodic memory retrieval. *Trends Cogn Sci* **9**, 445-453.

Walhovd KB, Fjell AM, Dale AM, Fischl B, Quinn BT, Makris N, Salat D & Reinvang I (2006) Regional cortical thickness matters in recall after months more than minutes. *Neuroimage* **31**, 1343-1351.

Walhovd KB, Fjell AM, Reinvang I, Lundervold A, Dale AM, Eilertsen DE, Quinn BT, Salat D, Makris N & Fischl B (2005) Effects of age on volumes of cortex, white matter and subcortical structures. *Neurobiol Aging* **26**, 1261-1270; discussion 1275-1268.

Wechsler D (1997a) *Wechsler Adult Intelligence Scale--Third Edition*. San Antonio, TX: Harcourt Assessment.

Wechsler D (1997b) *Wechsler Memory Scale--Third Edition*. San Antonio, TX: Harcourt Assessment.

West RL (1996) An application of prefrontal cortex function theory to cognitive aging. *Psychol Bull* **120**, 272-292.

Yoon B, Shim YS, Lee KS, Shon YM & Yang DW (2008) Region-specific changes of cerebral white matter during normal aging: a diffusion-tensor analysis. *Arch Gerontol Geriatr* **47**, 129-138.

Yoshita M, Fletcher E, Harvey D, Ortega M, Martinez O, Mungas DM, Reed BR & DeCarli CS (2006) Extent and distribution of white matter hyperintensities in normal aging, MCI, and AD. *Neurology* **67**, 2192-2198.

Zec RF, Burkett NR, Markwell SJ & Larsen DL (2007) A cross-sectional study of the effects of age, education, and gender on the Boston Naming Test. *Clin Neuropsychol* **21**, 587-616.

Zec RF, Markwell SJ, Burkett NR & Larsen DL (2005) A longitudinal study of confrontation naming in the "normal" elderly. *J Int Neuropsychol Soc* **11**, 716-726.

Zecca L, Youdim MB, Riederer P, Connor JR & Crichton RR (2004) Iron, brain ageing and neurodegenerative disorders. *Nat Rev Neurosci* **5**, 863-873.

Zimmerman ME, Brickman AM, Paul RH, Grieve SM, Tate DF, Gunstad J, Cohen RA, Aloia MS, Williams LM, Clark CR, Whitford TJ & Gordon E (2006) The relationship between frontal gray matter volume and cognition varies across the healthy adult lifespan. *Am J Geriatr Psychiatry* **14**, 823-833.

Tables and Figures

Table 1. Participant characteristics : mean ± *SD* and (range)

Group	Age (yrs)	Education (yrs)	MMSE[a]
Young Adults (YA)	21.9 ±2.6	15 ±2.0	29.2 ±1.0
(*n* = 36, 16F)	(18–28)	(12–18)	(27–30)
Older Adults (OA)	70.3 ±7.2	17 ±3.0	29.2 ±1.2
(*n* = 38, 20F)	(61–86)	(14–23)	(27–30)

[a] Mini Mental State Examination

Table 2. Scores for OA on the individual cognitive comprising each composite score.

Composite score	Test	Mean	*SD*	Range
Episodic memory	Word lists	8.0	3.0	(3 - 12)
	Logical memory	29.9	8.2	(13 - 45)
Semantic memory	Boston naming	40.6	1.7	(36 - 42)
	Vocabulary	59.1	6.1	(44-66)
Cognitive control	COWAT	49.6	11.8	(30 - 76)
	Trails B-A	47.4	30.5	(8 - 129)
	Digit span backward	8.8	2.8	(3 - 14)
	Stroop interference	101.8	8.2	(86 - 115)

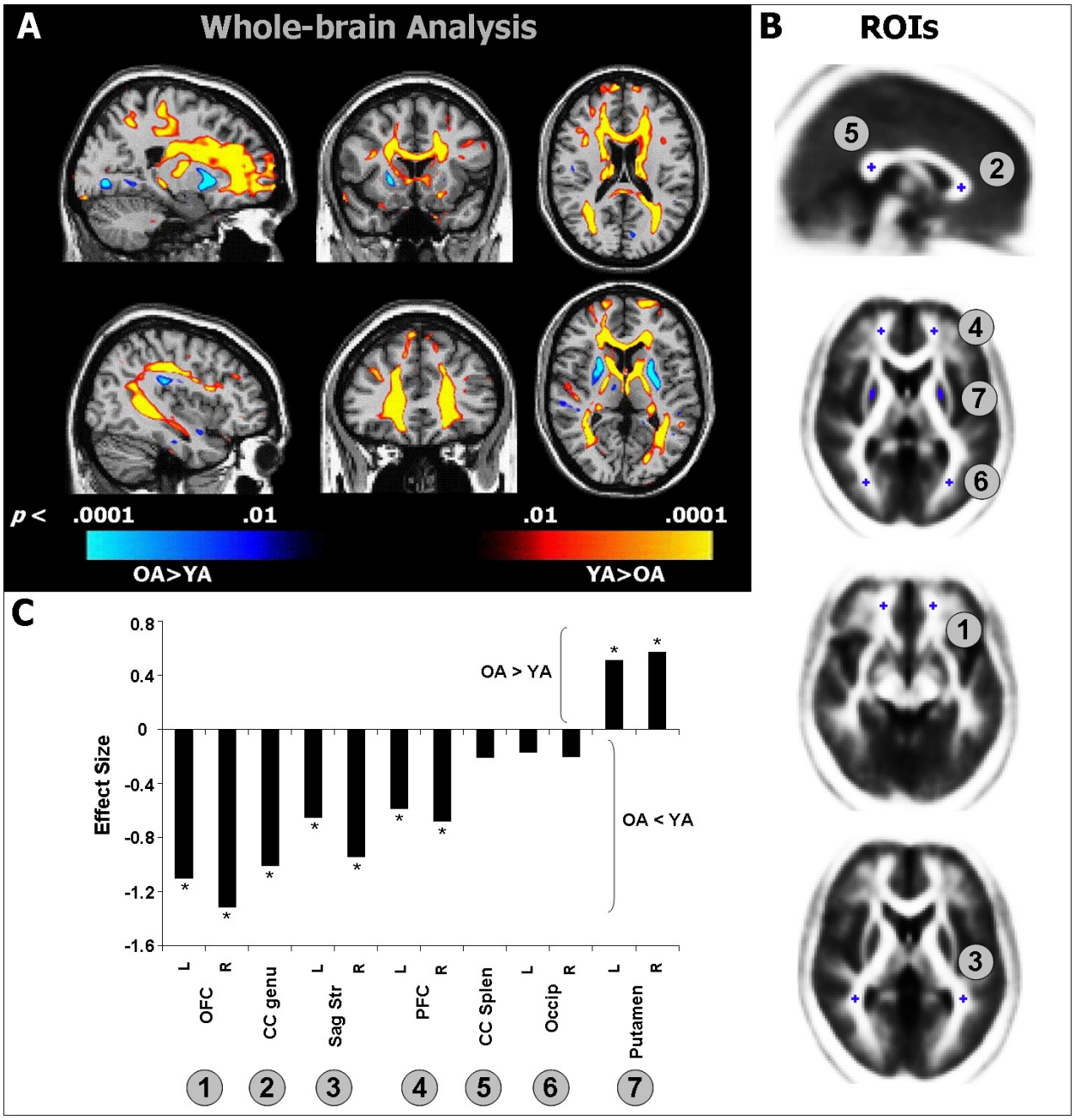

Figure 1. A) Voxel-wise *t* maps showing differences between YA and OA in FA overlaid on representative sagittal (left), coronal (middle), and axial (right) slices. Regions depicted in red-yellow indicate areas where FA was lower in OA compared to YA; regions depicted in blue indicate areas where FA was higher in OA compared to YA. **B)** Placement of manually defined ROIs. **C)** Effect sizes ([OA mean – YA mean]/pooled *SD*) for all ROIs; negative values are regions where FA was lower in OA compared to YA and positive values are area where FA was greater in OA; asterisks indicate significant differences between OA and YA ($p < .05$). Abbreviations: CC, corpus callosum; PFC, prefrontal cortex; OFC, orbitofrontal cortex; Sag Str, sagittal stratum.

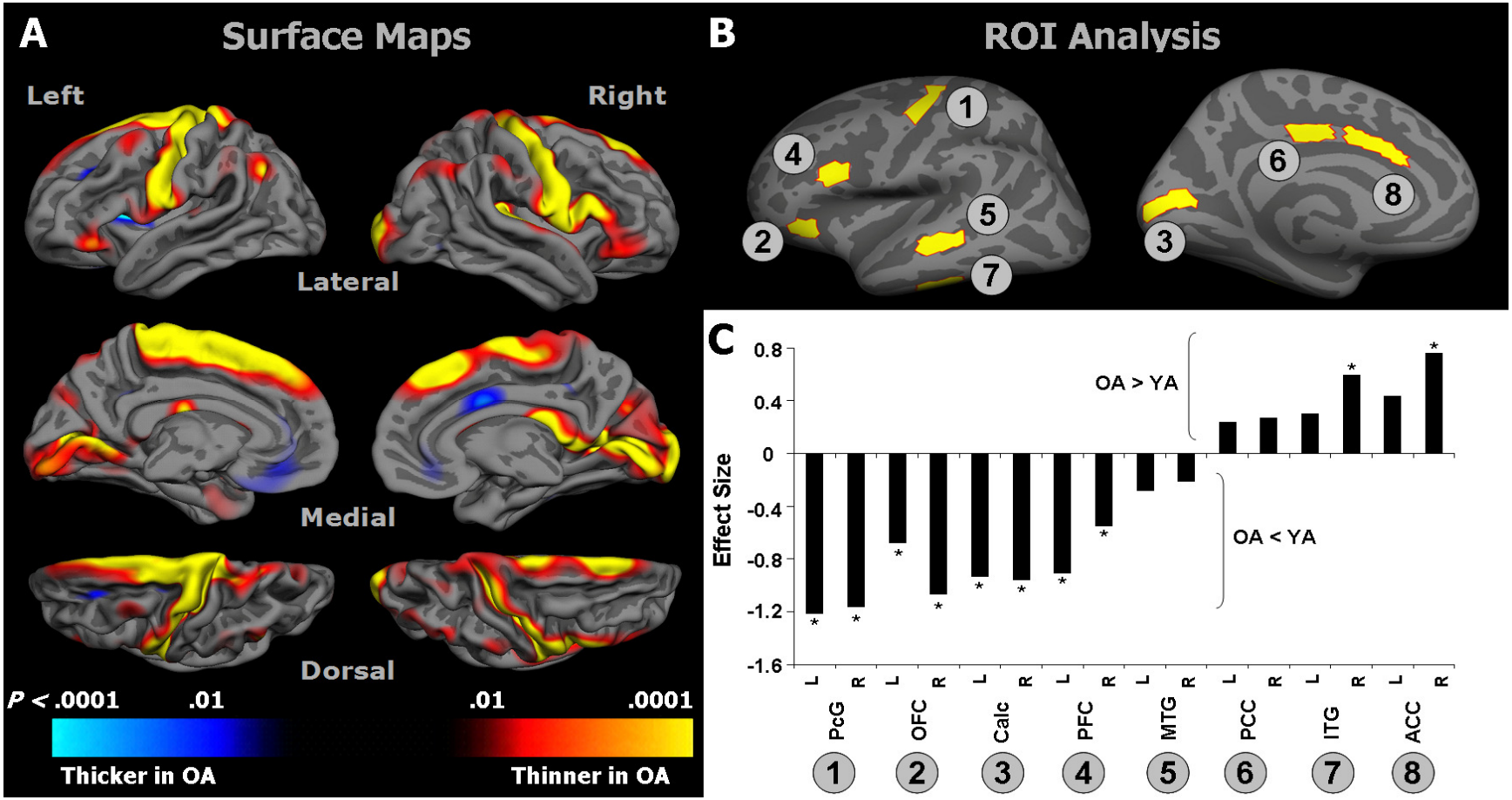

Figure 2. A) Surface-based vertex-wise GLM maps showing differences between OA and YA in cortical thickness. Regions depicted in red-yellow indicate areas where cortex was thinner in OA compared to YA; regions depicted in blue indicate areas where cortex was thicker in OA compared to YA. **B)** Placement of manually defined cortical ROIs. **C)** Effect sizes ([OA mean – YA mean]/pooled *SD*) for all ROIs; negative values indicate regions with thinner cortex in OA, compared to YA, and positive values represent regions with thicker cortex in OA; asterisks indicate significant differences between OA and YA ($p < .05$). Abbreviations: MTG, middle temporal gyrus; ITG, inferior temporal gyrus; PFC, prefrontal cortex; OFC, orbitofrontal cortex; ACC, anterior cingulate cortex; PCC, posterior cingulate cortex; PcG, precentral gyrus; Calc, calcarine cortex.

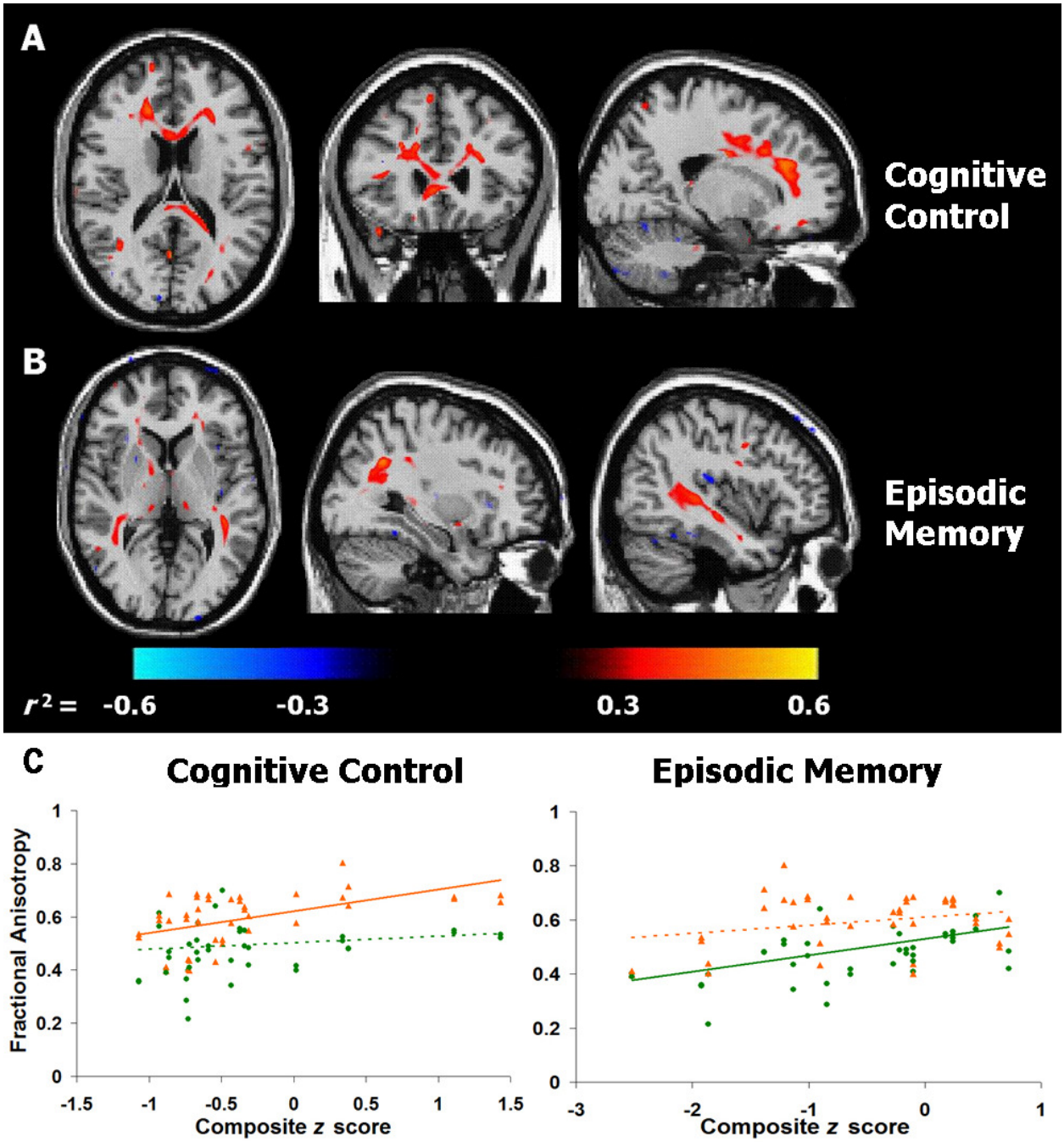

Figure 3. Voxel-wise signed-r^2 maps for correlations between FA and composite scores on **A)** cognitive control tasks, and **B)** episodic memory tasks in OA. Positive correlations are shown in red, negative correlations in blue. **C)** Composite *z* scores on cognitive control and episodic memory tasks plotted against mean FA for frontal (▲, orange lines) and temporo-parietal (●, green lines) ROIs, bilaterally (see text for anatomical definitions). Significant correlations ($p < 0.01$) are indicated by solid lines, non-significant correlations by dashed lines. Due to the similar patterns of correlation, right and left ROIs are combined for graphical purposes.

Supplementary Material

***Detailed description of WM ROI placement*.**

With the exception of the putamen, all ROIs consisted of a seven voxel, 3D crosshairs. The genu and splenium of the corpus callosum were initially identified in sagittal sections, one slice lateral to the midline. ROIs were drawn in the axial view as close as possible to the center of the structure. The ROIs were then viewed in the sagittal plane to ensure that they were as close to the center of each region as possible. The radiate PFC ROIs, underlying the middle frontal gyrus, were defined in axial sections at the point where the callosal projections from the genu could clearly be seen branching out into the forceps minor. A label was placed in the middle of the intersection of the forceps minor with the anterior thalamic radiations. The radiate OFC ROIs, underlying the inferior frontal gyrus, were defined in axial section as one slice lateral to the last section in which the genu of the callosum was visible (i.e., at the point where the callosal decussation disappeared). A label was placed in the middle of the circumscribed hyperintense region defined by the merging of the outer callosal fibers with the uncinate fasciculus and anterior thalamic radiations. The posterior radiate ROIs, underlying the occipital lobe, were defined in axial view as the intersection between forceps major and the outer segment of the splenium of the corpus callosum.

The putamen, the only non-WM ROI, was identified in axial section where the splenium of the callosum was still visible, but at its most lateral extent. A single rectangular label, approximately 2 x 2 x 3 voxels, was placed in the middle of the circumscribed hypointense region falling between the internal and external capsules. The superior sagittal striatum ROI

was defined in sagittal section as the region just anterior to the intersection of the sagittal stratum, inferior longitudinal fasciculus, and inferior fronto-occipital fasciculus. A single crosshair label was placed near the center of this intersection. To minimize the possibility of WM-CSF partial volume effects, we avoided any voxels that appeared to flank the ventricles.

Based on the loci of significant correlations between FA and composite scores on cognitive control and episodic memory tasks, two additional ROIs were drawn for the OA. To capture the regions with the highest correlations and to minimize the number of statistical comparisons, we chose a single frontal and single posterior ROI to label in both hemispheres. The anterior ROI was placed in the WM underlying PFC, but was placed more medially than the above PFC label. That is, on an axial section superficial to the slice used earlier, a label was placed at the base of the forceps minor before it fully branched out into the anterior corona radiata. The posterior ROI was drawn in the WM underlying the parietal lobe. An axial slice was chosen in which the decussation of the body of the corpus callosum was clearly visible. Moving medially to the posterior callosum, the posterior segment of the cingulum bundle was identified, and a line connecting the left and right cingulum, but extending out laterally, was used as an anterior-posterior landmark. Along this reference line, a seven-voxel 3D crosshairs label was placed in the middle of the largest lateral WM tract, most likely corresponding to the superior longitudinal fasciculus.

Chapter 3

Age-related changes in white matter integrity disrupt top-down modulation of oscillations during visual search

David A. Ziegler[1], Paymon Hosseini[1], Erica Y. Griffith[1], Leslie A. Hansen[1], Matti Hämäläinen[2], Suzanne Corkin[1,2]

1. Department of Brain & Cognitive Sciences, MIT, Cambridge, MA
2. Athinoula A. Martinos Center for Biomedical Imaging, Massachusetts General Hospital, Charlestown, MA

Abstract

Healthy older adults (OA) often show diminished performance on attention-demanding tasks, such as effortful visual search, and these impairments have been linked to decreased integrity of white matter pathways. Neuronal synchronization has emerged as an important mechanism underlying selective attention, but we do not know how healthy aging affects oscillatory activity associated with top-down and bottom-up attention. The present study used magnetoencephalography (MEG) and diffusion tensor imaging (DTI) to test the hypothesis that altered oscillatory dynamics underly diminished top-down processing in OA and that these effects are mediated by decreased integrity of frontoparietal white matter tracts. We found that in young adults (YA), top-down and bottom-up attention were associated with relative increases in beta and gamma activity, respectively, but we did not observe this specialization of frequency bands in OA. Instead, OA showed little modulation of beta or gamma activity as a function of search difficultly. Integrity of anterior, but not posterior, white matter tracts was decreased in OA. Further, the integrity of the frontoparietal superior longitudinal fasciculus, which was reduced in OA, significantly predicted the magnitude of beta activity during effortful search. These results are the first to document age-related changes in the modulation of top-down oscillatory activity and suggest that these effects may be mediated by the strength of connections between frontal and parietal cortices.

Introduction

Research on cognitive aging has identified areas of decline in healthy older adults (OA) that bridge multiple domains, including attention, working memory, and long-term declarative memory (Craik & Salthouse, 2000; Buckner, 2004; Hedden & Gabrieli, 2004; Gazzaley & D'Esposito, 2007; Glisky, 2007; Piguet & Corkin, 2007). An emerging theme is that impaired or inefficient deployment of cognitive control processes may be a common mechanism underlying many of the cognitive deficits seen in healthy aging (Miyake *et al.*, 2000; Fletcher & Henson, 2001; Braver & Barch, 2002; Salthouse *et al.*, 2003; Braver & Ruge, 2006; Glisky, 2007). Cognitive control encompasses a collection of top-down processes that enable us to modulate the impact of sensory inputs on our brain. This ability to manage and filter a constant barrage of environmental stimuli enables us to engage in complex, goal-directed behaviors (Salthouse & Meinz, 1995; Spencer & Raz, 1995; Fuster, 2000; Miller, 2000; Braver *et al.*, 2001; Miller & Cohen, 2001). Notably, when compared to young adults (YA), OA consistently show reduced performance on tasks that place high demands on cognitive control, including multi-tasking (Jimura & Braver, 2010; Clapp *et al.*, 2011), attention (McDowd, 1986; Hawkins et al., 1992; Milham et al., 2002; West, 2004), and working memory tasks (Hasher & Zacks, 1988; Salthouse, 1994; Gazzaley *et al.*, 2005; Emery *et al.*, 2008).

Attention is a fundamental component process of virtually all aspects of cognitive control (Knudsen, 2007; Buschman & Miller, 2010; Baluch & Itti, 2011), and thus a complete understanding of how aging affects cognitive control requires careful examination of age-related changes in attention. The process engaged to indentify a subset of available information

for more extensive analysis, while ignoring irrelevant items is termed selective attention (Desimone & Duncan, 1995; Wolfe & Horowitz, 2004). Because this subset of attended items could be selected either from stimuli in the external environment or from internal memory stores, attentional processes can be divided into bottom-up and top-down components (Desimone & Duncan, 1995; Yantis & Egeth, 1999; Buschman & Miller, 2010; Baluch & Itti, 2011). Bottom-up processes are stimulus-driven mechanisms that are deployed rapidly and automatically, such as when the loud screeching of brakes causes us to stop in our tracks at a crosswalk. In contrast, top-down attention is comprised of slower, internally generated signals that guide the focus of our attention in a volitional manner, such as when we strive to pay attention to the road while driving in heavy rain.

These two types of attention are often studied using visual search paradigms (Wolfe *et al.*, 1989; Baluch & Itti, 2011) that incorporate both pop-out (bottom-up) and effortful (top-down) search trials. In a typical experiment, participants view an array of stimuli on a screen and are instructed to detect a target item. If the target is distinct from the distractors (i.e., differing from the other items along a single dimension), the item captures the subject's attention and "pops out." In contrast, if the target and distractors can be distinguished only by taking into account the conjunction of their features on multiple dimensions, the target will not automatically grab attention, and the participant must engage in a volitional search of the visual array (Wolfe *et al.*, 1989; Baluch & Itti, 2011). Thus, pop-out relies heavily on bottom-up processing, whereas effortful search places more demands on attention, and thus requires a greater degree of top-down control. As a result, set-size effects, in which response times

increase and accuracy decreases as a function of the number of distractors, is typically seen only for effortful search trials, while response times and accuracy are largely independent of the search array size in pop-out trials (Palmer, 1994; Gilbert & Sigman, 2007; Baluch & Itti, 2011).

One mechanism by which top-down areas may exert control over more posterior sensory and motors cortices is through the modulation of oscillatory activity (Hari & Salmelin, 1997; Kahana, 2006; Fries, 2009). Researchers have begun to document the role of oscillations in visual attention, suggesting a complex, dynamic interplay between rhythms at different frequencies and at different spatial scales, with each frequency playing a specific role (Palva & Palva, 2007; Siegel *et al.*, 2008; Gregoriou *et al.*, 2009). Local high-frequency oscillations in the gamma range (~30-100 Hz) have been documented in a number of attention and cognitive control tasks (Fries et al., 2001; Bauer et al., 2006; Womelsdorf et al., 2006; Gregoriou et al., 2009). It has been proposed that synchronizing neural activity at a high-frequency range may serve to heighten the fidelity of local stimulus representations or increase the tuning of neurons to a particular target stimulus, facilitating the transmission of task-relevant information to downstream sensory areas (Aertsen et al., 1989; Tiesinga et al., 2002; Saalmann et al., 2007).

Modulation of oscillations at lower frequences, such as alpha (~5-14 Hz) and beta (~15-30 Hz), is also associated with attentional processes. Beta rhythms are thought to be particularly well suited to mediating inter-areal communication, and thus may also facilitate top-down processes (von Stein *et al.*, 2000; Buschman & Miller, 2007; Schroeder & Lakatos, 2009b). In

contrast, alpha rhythms are observed in parietal and occipital areas in the absence of task-relevant visual inputs, but show a marked desynchronization when visual processes are brought online (Klimesch et al., 1998). Posterior alpha desynchronizations are modified by attention (Sauseng et al., 2005; Thut et al., 2006) and are actively modulated by activity in frontoparietal control regions (Capotosto et al., 2009). Thus, alpha, beta, and gamma rhythms appear to play important roles in attention, with the relative recruitment of each frequency is driven by the specific requirements of the task at hand.

Visual search tasks have highlighted age-related changes in visual attention. The most common behavioral finding is a greater effect of set-size in OA for trials that require effortful search (Madden, 2007). Specifically, the slope of the increase in response times and decline in accuracy from trials with few distractors to those with many distractors is significantly greater in OA compared to YA (Folk & Lincourt, 1996; McDowd & Shaw, 2000; Hommel *et al.*, 2004; Madden & Whiting, 2004). But despite a general slowing of perceptual processing speed in OA (Salthouse, 1996), they do not show set-size effects in terms of accuracy on pop-out search trials, in which target detection is driven predominantly by bottom-up processes. ERP studies have found neural correlates of age-related visual search impairments in temporo-occipital areas (Lorenzo-Lopez et al., 2011), prefrontal cortex (PFC), and anterior cingulate cortex (Lorenzo-Lopez et al., 2008), while fMRI and PET studies have documented age-related increases in frontoparietal activation associated with selective visual attention (Madden et al., 1997; Madden et al., 2002; Madden et al., 2004; Madden et al., 2007). To our knowledge, no

studies have examined the effects of healthy aging on the oscillatory dynamics of attentional modulation.

We have shown that performance on tasks that require the engagement of cognitive control processes correlates with the integrity of frontal white matter tracts in healthy OA (Ziegler et al., 2010). These age-related declines in white matter integrity could interfere with synchronization in alpha and beta ranges, which likely mediate inter-areal communication and, in turn, impair cognition in older adults. The purpose of the present study was to test the hypothesis that age-related decrements in effortful search are associated with altered oscillatory dynamics, and that these changes correlate with decreased integrity of white matter tracts connecting frontoparietal attention networks. We collected multimodal neuroimaging data from healthy YA and OA, including magnetoencephalography (MEG) data to examine oscillatory activity while participants performed a visual search task and diffusion tensor imaging (DTI) data to assess the integrity of major white matter tracts. MEG is a functional neuroimaging technique that measures the magnetic fields that are generated when groups of cortical neurons exhibit synchronous dendritic potentials (Baillet *et al.*, 2001; Hämäläinen & Hari, 2002). As a direct measure of the neural currents, MEG has high temporal resolution (i.e., on the order of msec), making the method particularly well suited for studying high-frequency neural oscillations.

Methods

Participants. We recruited 12 YA (7F), aged 21-31 years (mean age = 25 ± 2 years), and 13 OA (8F), aged 55-73 years (mean age = 67 ± 6) (**Table 1**). Our exclusion criteria were: history of neurological or psychiatric disease, use of psychoactive medications, substance misuse, and presence of serious medical conditions, including history of heart disease, diabetes, untreated hypertension, and cancer. We also screened participants for any contraindication for MRI scanning (claustrophobia, mechanical or electromagnetic implants, ferromagnetic or non-static metal implants, or tattoos with metal ink) or contraindications for MEG recordings (permanently affixed ferrous dental work such as non-removable bridges, dentures, or a large number of crowns or fillings). In four cases, we were made aware of the presence of dental work only after the start of the MEG session, and attempted to use degaussers to reduce the electromagnetic noise. Because this effort was unsuccessful in 1 YA and 1 OA, they were excluded from our sample (these participants are not included in Table 1). All participants had a minimum corrected visual acuity of 20-40; those with corrected vision were provided MEG compatible glasses prior to testing. We screened all participants for dementia using the Mini Mental State Examination (MMSE) (Folstein et al., 1975), and any individual scoring below 27 was excluded from the study. The young and older groups did not differ significantly in terms of MMSE scores (mean scores: YA = 29.1; OA = 29.2). OA had more years of education (17.9 ±7.4) than YA (15 ±1.6), due to the fact that the majority of YA had not completed their education. All participants gave informed consent using procedures approved by the MIT Committee on the Use of Humans as Experimental Subjects and by the Partners Human Research Committee (Massachusetts General Hospital).

Behavioral task. During MEG recordings, participants performed a visual search task that contained both pop-out and effortful search conditions: They tried to detect an X among Ls (pop-out) or a T among Ls (effortful search). Participants performed the task seated in a magnetically shielded room and viewed the stimuli on a screen projector. The distance of the screen from the chair was the same for all participants. On each trial, a central red fixation dot appeared and remained on the screen for 1,000 msec before the start of the trial (**Figure 1**). Participants were then presented with a search array that remained on the screen for 2000 msec and was followed by a 500 msec visual mask. The ITI varied from 2000-8000 msec. The search duration, determined through pilot studies, was chosen to give OA a long enough window in which to respond. The stimuli were light grey capital letters X, L, and T that were rotated 45, 135, 225, or 315 degrees. The letters were presented on a black background at pseudorandomly determined positions on the circumference of an imaginary circle with a visual angle radius of 3º. The number of letters in each search array (set size) was either 4 or 10 items. A target was present among the distractors on 50% of the trials. Participants were instructed to indicate when a target was present by pressing a button with their right index finger and to indicate the absence of a target by pressing a button with their right middle finger. To avoid a potential confound of age-related changes in set-shifting ability, pop-out and effortful search trials were presented in separate blocks, each preceded by the words “Is there an X?” or “Is there a T?.” Each block lasted 6 min 40 sec and consisted of 64 trials. Participants completed 3 blocks of pop-out and 3 blocks of effortful search trials, yielding a total of 96 trials per condition. For analyses of MEG data, all X and all T trials were combined, yieldind a total of 192

trials of each per participant. Participants rested for a few minutes between each block. Within each block, the ordering of 4- versus 10-item displays, the presence or absence of a target, and the variable length of the ISI was determined using Optseq, a tool for automatically scheduling events and for introducing jitter for rapid-presentation event-related experiments, in anticipation of an additional fMRI experiment.

MEG acquisition and preprocessing. MEG data were recorded at the Massachusetts General Hospital's Athinoula A. Martinos Center for Biomedial imaging using a whole-head 306-channel Elekta NeuroMag VectorView system with 102 sensor units, each composed of a triplet of two planar gradiometers and a magnetometer. Vertical and horizontal electro-oculogram signals were recorded to be used for artifact rejection. Head position in the MEG helmet was monitored using four head position indicator coils. The MEG data were sampled at 600 Hz and were analyzed with Neuromag software and the Fieldtrip (Oostenveld et al., 2011) and Brainstorm (Tadel et al., 2011) MATLAB toolboxes. The raw data were preprocessed using Maxfilter to realign each individual's data to a standard sensor space derived from an average of all participants. We identified segments of MEG data containing blinks and excessive eye movements, muscle artifacts, and sensor jumps and removed them using Fieldtrip's semiautomatic artifact rejection procedure.

Spectral analysis. We performed a sensor-level analysis of the planar gradiometer data. Our index of oscillatory activity was the time-varying spectral energy, or power, defined as the variance of the MEG signal at each frequency (e.g., the amplitude of an ongoing oscillation in

the MEG signal). To optimize the spectral resolution in each frequency band, we computed time-frequency representations (TFR) of power separately for low (5-30 Hz) and high (30-100 Hz) frequency ranges using Hanning taper and wavelet methods, respectively (Percival & Walden, 1993; Tallon-Baudry & Bertrand, 1999). To achieve a frequency resolution of 2 Hz for the low frequency TFR, we used a fixed 500 msec time window that slid from 500 msec prestimulus to 1000 msec after the onset of the search array in 50 msec increments. The wavelet cycle width constant defining the compromise between time and frequency resolution was 7 for the high-frequency TFR. We generated TFRs of power for the first 1000 msec following search array onset for each gradiometer and then averaged across sensor pairs; combined planar gradient TFRs were then averaged across participants in each group to create a grand average TFR. Power values for each trial were baseline corrected relative to the last 500 msec of the fixation period prior to the search array onset. Thus an increase in power represents an event-related synchronization, while a decrease in power relative to the prestimulus period represents an event-related desynchronization (Jensen & Hesse, 2010).

MRI data acquisitions. On a separate visit, we collected structural MRI data for each participant at MIT's Athinoula A. Martinos Imaging Center at the McGovern Institute for Brain Research using a Siemens 3 Tesla Trio MRI system with a 32-channel head coil. For each participant, we collected a series of high-resolution multiecho MPRAGE (ME-MPRAGE) with T1-weighting. Each 3D slab consisted of 176 sagittal slices, 1.0 mm thick. The in-plane field of view was 256 mm sampled on a 256 x 256 matrix, giving an in-plane resolution of 1.0 x 1.0 mm. For T1 weighting, we used the following parameters: flip angle = 7˚, TR = 2530 msec, and inversion time (TI) =

1100 msec, during which four echoes were collected after non-selective excitation, TE = 1.58 + (n x 1.74) ms (n = 0,..,3). A final volume was generated from a root mean square average of acquisitions. We previously showed that, for the purposes of morphometric analyses, high-bandwidth T1-weighted ME-MPRAGE data are as good or better than are conventional T1-weighted images (Wonderlick et al., 2009). Further, multiecho sequences are less prone to distortion and have a higher contrast-to-noise ratio for subcortical structures (Fischl et al., 2004; van der Kouwe et al., 2008).

We acquired diffusion-weighted images (DWI) with axial in-plane isotropic resolution 2 mm, slice thickness 2 mm, 128 x 128 x 60 image matrix, TR = 8900 msec, TE = 80 msec, NEX = 1, and bandwidth = 1860 Hz/pixel. The series included images acquired with diffusion weighting along 60 non-colinear directions (b = 700 s/mm^2) and 10 images without diffusion weighting (b = 0). We were unable to collect DTI data for one YA because the participant arrived late, and one OA experienced discomfort and asked to be removed from the scanner during the DWI acquisition.

MRI Processing. We used the FreeSurfer (version 5.0) software package (http://www.surfer.nmr.mgh.harvard.edu/) to reconstruct cortical surfaces from the T1-weighted MRI data. This semi-automated procedure included grey-white segmentation, subcortical segmentation, and cortical parcellation (Dale et al., 1999; Fischl et al., 1999; Fischl et al., 2001; Desikan et al., 2006). The outputs were used as masks and seed regions for tractography analyses of DTI data. All DTI data were processed using FreeSurfer's TRACULA (TRActs Constrained by UnderLying Anatomy) algorithm and FMRIB's Diffusion Toolbox (FDT),

available as part of the FSL package. TRACULA performed fully automated probabilistic tractography of 18 major white matter bundles by taking advantage of prior tract information derived from a manually labeled training atlas (Yendiki et al., in review). This prior anatomical knowledge was then used to constrain the tract reconstruction in our sample, allowing the process to be applied to data from a large group without the need for manual intervention. Preprocessing of DTI data was performed with FDT and consisted of registering the DWI to the b = 0 images to remove motion and eddy current distortions. We next performed a two-step linear registration whereby each participant's b = 0 image was registered to his or her ME-MPRAGE, which in turn was registered to the MNI-152 template. We produced cortical and white matter masks from each individual's FreeSurfer segmentation and fit diffusion tensors to each voxel of the DWIs using FSL's DTIFIT. TRACULA then generated priors for each major pathway based on a manually labeled training atlas; ball-and-stick model fitting of the DWIs was performed with FSL's bedpostx. The probability distributions for the 18 tracts were computed by simultaneously fitting the shape of each pathway to the ball-and-stick diffusion model while constraining the solution based on the training atlas priors. Following reconstruction, we performed a visual check of all paths in each participant and computed, for each individual, values of fractional anisotropy (FA), axial diffusivity (AD), and radial diffusivity (RD), averaged over the entire path. We analyzed paths associated with frontoparietal attention networks—the superior longitudinal fasciculus (SLF) and inferior longitudinal fasciculus (ILF), and connections mediating interhemispheric communication between association cortices—forceps major (fmajor) and minor (fminor).

Statistical Analyses. We tested for differences in behavioral performance between YA and OA using two 2 x 4 mixed between- and within-subjects repeated-measures general linear models (GLMs): one for response time and one for accuracy. In each model, the between-subject factor was group and the within-subject factor was search condition (4X, 10X, 4T, 4L). Multivariate GLMs examined group differences in white matter integrity. We performed two separate GLMs: a primary analysis of FA, followed by a secondary analysis of RD and AD. In each model, the independent variables were the tract-average values for the six white matter paths. Although YA and OA were well matched in terms of sex distribution, this variable was included in each model to mitigate against the effect of any underlying sex differences in white matter integrity. Post-hoc tests of group differences in individual tracts used a Sidak correction for multiple comparisons.

We compared spectral power within-subjects (popout vs effortful search conditions) and between-subjects (YA vs OA) at the sensor level using a Monte Carlo permutation method to compute exact independent *t* statistics and probabilities, with a cluster-based correction for multiple comparisons (Nichols & Holmes, 2002; Maris & Oostenveld, 2007). For each frequency range of interest (alpha, 7-12Hz; beta, 15-30Hz; gamma, 40-60 Hz), nonparametric cluster statistics were computed by thresholding those sensors with a *t* value above the critical level ($\alpha = .05$). These values were then pooled among clusters of sensors that were selcted on the basis of temporal, spatial and spectral adjacency. Exact *p* values were then calculated by comparing the cluster statistics to a null distribution generated through 500 random permutations of the

data between conditions or between groups, thus controlling the overall Type I error rate over for all sensors.

We also tested for associations between white matter integrity and oscillatory activity and between oscillatory activity and search task performance. For this analysis, we identified the sensors that contributed to significant differences between OA and YA in the sensor-level analyses of spectral power in the alpha and gamma ranges. For the beta range, because no clusters showed significant group differences, we used those sensors that showed significant differences in power between pop-out and effortful search conditions. For each group of sensors, power in each frequency range was averaged for each participant over a period of 200-800 ms after the appearance of the search array. Because these power averages did not meet the assumption of normality, we performed a log transformation of the data, which resulted in normally distributed data for all variables.

Two additional steps minimized the total number of statistical comparisons: first, we used a multiple stepwise regression approach with backward elimination (as opposed to a series of simple bivariate correlations) to determine what tracts contributed significantly to explaining the variance in average power values; and second, we examined only correlations between white matter integrity and average power for effortful search trials because these trials were associated with the largest group differences in performance. Backward-elimination regression models included all of the independent variables in the initial model and successively tested each variable for significance, eliminating non-predictive variables in a stepwise fashion. We

performed a separate regression for each frequency band of interest, with average power over all T trials serving as the dependent variable and FA values for each of the six white matter tracts included as independent variables. We performed four regression analyses to test the significance of relations between average power and behavioral performance, each with a single dependent variable: all X-trial accuracy, all T-trial accuracy, all X-trial response times, and all T-trial response times. The independent variables in each model were average alpha, beta, and gamma power for the respective search condition.

Results

Age-related differences in visual search performance. We found a significant main effect of age on response times (F = 27.1, p > .0001; **Figure 2a**), with OA responding more slowly than YA, regardless of set-size or search condition. In addition, a significant age by search condition interaction (F = 8.8, p = .007) indicated that response times increased more rapidly as a function of increasing set-size for OA compared to YA. For search accuracy, the main effect of age did not reach significance (F = 3.6, p = .072). We found a significant group by search condition interaction (F = 5.6, p = .002; **Figure 2b**), such that YA and OA differed in terms of accuracy on X trials, but OA showed a steeper decline in accuracy from 10T to 4T trials than YA.

Age-related differences in oscillatory power. Relative to the prestimulus period, YA and OA exhibited an event-related desynchronization in the alpha range (7-12 Hz) over posterior sensors during both search (**Figure 3**) and popout (not shown) trials, which was sustained throughout the entire search period. Alpha power did not differ significantly between search

and popout conditions. Compared to YA, however, OA showed a more diffuse desynchronization with the decrease in alpha power extending anteriorly into parieto-occipital sensors, where a cluster of sensors showed significantly lower alpha power in OA compared to YA (**Figure 3,** right).

In the beta (15-30 Hz) band, we found significant task-related modulation of power and this modulation differed between YA and OA. Our within-subjects comparison revealed significantly greater beta power in frontal sensors during search trials, compared to popout trials, in YA (**Figure 4**), with little modulation of beta power in posterior parietal and occipital sensors. In contrast, beta band power was relatively high in frontal sensors during both types of trials in OA and even showed a small cluster of frontoparietal sensors in which beta power was significantly greater for popout trials compared to search trials. While YA and OA showed different, and nearly opposite, patterns of beta band modulation for search versus popout trials, the overall levels of beta power did not differ significantly between YA and OA. Thus, both groups were able to engage beta oscillations, but that aging affects the relative recruitment of beta rhythms as a function of task demands.

In the gamma range (40-60 Hz), we found both within- and between-group differences for power. For YA, gamma power was significantly greater during popout than search in two clusters of sensors: a larger cluster over posterior parietal sensors and a smaller cluster over frontal sensors (**Figure 5,** top). OA showed a different pattern: gamma power was highest over posterior sensors during both popout and search trials, and this effect extended into

occipitotemporal areas (**Figure 5,** middle). One cluster of temporoparietal sensors showed a trend toward greater power in search relative to popout trials, but this effect did not reach significance (cluster-corrected p = .078). Gamma power in temporooccipital sensors was significantly higher in OA compared to YA (**Figure 5**, bottom) during popout and search trials, suggesting OA rely more on gamma activity to a greater degree than beta activity, regardless of search condition.

Age-related decreases in white matter integrity. A multivariate GLM revealed an significant omnibus difference in white matter integrity over all tracts between YA and OA ($F_{6,22}$ = 4.5, p = .004). Post-hoc tests revealed significantly decreased FA values of fminor, left and right ILF, and right SLF, with no significant difference between groups for fmajor and left SLF (**Table 2**). A secondary GLM of AD and RD values was also significant at the omnibus level ($F_{12,22}$ = 4.5, p = .003), and post-hoc tests showed that the age-related changes in FA were driven entirely by increases in RD (**Table 2**), while AD did not differ between groups, suggesting the age-related decreases in white matter integrity are linked to myelin degredation.

Correlations between oscillatory power and white matter integrity. A backward stepwise elimination multiple linear regression ($F_{1,21}$ = 5.1, p = .035) showed that FA in the right SLF was the only significant predictor of beta power during effortful search trials (β = .44, p = .035), with higher FA associated with increased power (**Figure 6a**). The next highest predictor was left SLF, but this effect was not significant (β = .23, p = .25). For gamma power, the regression model did not reach significance ($F_{1,21}$ = 3.7, p = .07), but the white matter tract with the highest predictive

value was right SLF (β = .39, p = .07). Of the six white matter tracts examined, the single significant ($F_{1,21}$ = 16.3, p = .001) predictor of alpha power was fmajor (β = .66, p = .001), with higher FA associated with a greater event-related desynchronization (**Figure 6b**).

Correlations between oscillatory power and task performance. None of the three frequency ranges predicted accuracy on popout trials ($F_{1,21}$ = 0.9, p = .35) or effortful search trials ($F_{1,21}$ = 0.8, p = .37). Beta power significantly predicted response times on effortful search trials ($F_{1,21}$ = 4.9, p = .038, β = -.42), such that increased power led to reduced response times. Gamma power significantly predicted response times on popout trials ($F_{1,21}$ = 3.7, p = .066, β = -.37), with higher power being associated with faster responses.

Discussion

We tested the hypothesis that age-related declines in visual search performance would be associated with changes in event-related modulation of cortical oscillations and white matter integrity, and that these effects would differ for top-down and bottom-up attentional processes. We report three primary findings. First, we discovered a complex pattern of frequency-specific changes in oscillatory dynamics between popout and effortful search conditions and between YA and OA. For high-frequency rhythms, YA showed differential engagement of beta and gamma rhythms as a function of search condition: Beta power was greater in frontal areas during effortful search, while gamma power was increased in frontoparietal sensors during popout trials. OA did not show this pattern of frequency band modulation as a function of search condition. Intead, during all trials in OA, beta activity was

high in frontalparietal areas and gamma activity was high in occipitotemporal areas. Further, overall levels of gamma were increased in OA, compared to YA. Both groups showed a robust event-related alpha desynchronization in occipital sensors that was not modulated by search condition and this desynchronization extended into parietal areas in OA.

Second, as predicted, OA showed a loss of white matter integrity in frontoparietal white matter tracts, and levels of FA in the right SLF correlated with beta power on effortful search trials. In contrast, white matter integrity in the splenium of the corpus callosum (forceps major) correlated with the magnitude of alpha desynchronization, but the integrity of this tract did not differ between YA and OA. These results support the idea that integrity of frontoparietal connections mediates attention-related oscillatory activity, and degeneration of myelin integrity in OA may reduce the efficiency of cognitive control networks.

Third, levels of beta power correlated with response times on effortful search trials, while gamma power showed a marginally significant negative correlation with response times on popout trials. In contrast, alpha synchronization did not correlate with response times, suggesting that beta and gamma rhythms were the primary oscillatory mechanisms underlying attentional modulation.

Age-related changes in attention-related cortical oscillations. The present finding of differential engagement of gamma oscillations during popout trials and beta oscillations during effortful search is consistent with a growing literature examining the relative roles of these two rhythms

on different aspects of visual attention. A study in monkeys that used a visual search task with popout and effortful search conditions found that bottom-up processes were associated with synchronization between frontal and posterior parietal areas at high gamma frequencies (36-56 Hz), whereas top-down search was characterized by frontoparietal synchrony at lower gamma or high beta (22-34 Hz) frequencies (Buschman & Miller, 2007). This pattern is similar to the present results. Similarly, other researchers have reported that oscillatory synchrony between relatively distant visual areas was greater at low frequencies (4-12 Hz) during internally guided trials, while high-frequency oscillations were generated locally in primary visual cortices, likely mediated by networks of monosynaptic connections, and were associated with bottom-up processing (von Stein et al., 2000). Subsequent studies have partially confirmed this dissociation in humans using EEG recordings. Phillips and Takeda (2009) reported greater frontoparietal synchrony at low gamma/high beta during effortful search trials, compared to popout, but failed to find a significant condition-dependant modulation of high gamma power. Another study in humans found attentional modulation in the 4-24 Hz range, with power in this range elevated in parietal areas during popout trials and in frontal areas during effortful search (Li et al., 2010).

This dissociation between beta and gamma suggests that each frequency is better suited for a specific type of neural computation: high gamma oscillations increase the general excitability of visual areas and aid in feature binding, increasing the likelihood of stimulus detection (Fries, 2009; Ray & Maunsell, 2010; Donner & Siegel, 2011). By contrast, lower frequency alpha or beta rhythms may facilitate top-down communication between higher-order multimodal areas

to primary sensory cortices (Schroeder & Lakatos, 2009a; Buschman & Miller, 2010; Engel & Fries, 2010). This distinction would explain the finding of more beta synchrony on tasks that require top-down modulation, while bottom-up attentional processes, such as popout trials, would be associated with gamma oscillations.

Other researchers have proposed that attentional processes can be divided into two modes, a continuous, or vigilance, mode and an entrainment mode (Schroeder & Lakatos, 2009b). By this view, gamma activity, associated with a high degree of neuronal excitability, supports a vigilance mode, while lower frequency oscillations would allow a system to entrain to rhythmic aspects of important sensory inputs. Such an interpretation is compatible with the notion that beta oscillations support top-down processes, while gamma mediates bottom-up attention, and also suggests that these rhythms represent separate mechanisms underlying sensory selection in a modality-independent fashion. Thus, the functional distinction between gamma and beta rhythms may extend beyond the realm of attentional control and can be thought of as more general tools for successful information processing under different task or environmental conditions.

The present finding of significant age-related changes in the modulation of beta and gamma rhythms provides new information about how aging affects the relative reliance on top-down and bottom-up processes. We found that YA relied on beta rhythms during effortful search trials and gamma rhythms during popout trials, whereas OA did not show such an efficient division of labor. One interpretation of this result is that OA are less efficient at deploying

cognitive control processes when faced with greater attentional demands and, as a result, rely more heavily on gamma-mediated bottom-up processing. Further support for this view comes from the finding of greater overall levels of gamma power in OA compared to YA. Functional MRI and PET studies have documented age-related increases in activations of frontal and parietal areas during performance of cognitive control tasks (McIntosh *et al.*, 1999; Cabeza, 2002; Rajah & D'Esposito, 2005). These increases are typically observed on tasks where performance is equal between YA and OA (Hedden, 2007), suggesting that this effect is compensatory, such that OA activate additional areas in an attempt to overcome processing difficulties, leading to improved performance (Cabeza *et al.*, 1997; Reuter-Lorenz *et al.*, 2000; Park & Reuter-Lorenz, 2009). Other researchers have found decreased levels of PFC activity in OA when the cognitive control demands were high and where performance in OA was below YA levels (Rypma et al., 2001; Rypma et al., 2005).

We lack a firm understanding of how oscillatory activity correlates with fMRI activation, but some evidence points to a link between the BOLD response and high-frequency oscillations in local field potentials (Niessing et al., 2005) and in synchronized activity recorded with EEG and MEG (Lachaux et al., 2007; Winterer et al., 2007). An interesting parallel to the present result comes from a PET study of age-related changes in visual search in which YA showed increased activity in occipitoremporal cortex for guided (i.e., effortful) search trials compared to feature (i.e., pop-out) search trials, but OA did not show this effect (Madden *et al.*, 2002). This difference was driven largely by the fact that OA showed greater activity in this region on

feature trials, compared to YA, and thus the difference between feature and guided conditions was washed out in OA.

We also found an age-related increase in gamma power in occipitotemporal sensors in popout and in search trials. This result raises the possibility that some of the observed increases in neural activity measured with PET and fMRI may be related to higher levels of gamma power, consistent with the notion that gamma rhythms represent increased cortical excitability. We did not find a correlation between oscillatory power and search accuracy in the present study, possibly due to the relatively high level of overall performance (although OA did perform significantly worse on effortful search trials, compared to YA). We did, however, observe a significant negative correlation between beta power and response times, and a trend toward a negative association between gamma power and response times, suggesting that increased power in OA led to improved performance. Additional studies of oscillatory power with tasks that yields a greater range of test scores is needed to address the question of whether increases in gamma activity are compensatory in OA.

Age-related changes in white matter integrity.

As expected, we found a significant age-related reduction in the integrity of associational white matter tracts, with sparing of more posterior tracts that subserve low-level sensory processing. This finding is consistent with a vast literature documenting greater declines in frontal white matter than in white matter underlying posterior cortices (O'Sullivan *et al.*, 2001; Head *et al.*,

2004; Pfefferbaum *et al.*, 2005; Salat *et al.*, 2005; Sullivan & Pfefferbaum, 2006; Ardekani *et al.*, 2007; Madden *et al.*, 2007; Yoon *et al.*, 2007; Ziegler *et al.*, 2010).

FA is a complex average of three diffusion eigenvalues that does not distinguish between the relative contributions of myelin or axonal integrity. Two new measures, RD and AD, allow us to separate the radial and axial components of diffusion tensor eigenvalues. Studies in mice and in patients with well-characterized neurodegenerative diseases that target specific components of white matter, such as multiple sclerosis, indicate that RD is a specific index of myelin integrity and that AD measures axonal integrity (Song et al., 2002; Song et al., 2005; Budde et al., 2009; Klawiter et al., 2011). These new tools have advanced our understanding of the microstructural changes that give rise to age-related reductions in FA values. We found that in all tracts where FA values were lower in OA than in YA, RD, but not AD, was also increased significantly. This finding is consistent with several other reports that have examined age-related changes in RD and AD (Davis et al., 2009; Madden et al., 2009; Sullivan et al., 2010; Bennett et al., 2011) and with postmortem studies that documented significant myelin degradation in older humans and monkeys (Tang et al., 1997; Peters, 2002; Marner et al., 2003). The specific indices of the cellular changes that occur in white matter during the course of healthy aging, revealed by RD and AD, suggest that the alterations in OA are predominantly the result of decreased myelin integrity.

Correlations between white matter integrity and oscillatory power.

We hypothesized that compromised integrity of connections, such as that observed in OA, could lead to destabilization in the large-scale networks that support cognitive control processes, causing changes in oscillatory activity. In support of this idea, we found a significant correlation between beta power and FA values in the right SLF and a trend toward a significant correlation between FA in this white matter tract and gamma power. In addition, we found an unexpected negative correlation between alpha power and FA values in the splenium of the corpus callosum. To our knowledge, no other studies have sought to link measures of white matter integrity to oscillatory activity, and few have examined correlations with any measures of MEG activity. One MEG study examined evoked responses during a memory-guided saccade task and found an inverse correlation between peak latencies in visual areas and FA values in regions underlying posterior parietal cortex and frontal eye fields (Stufflebeam et al., 2008); this study did not measure oscillatory activity. A study of age-related changes in visual search examined relations between fMRI activity and white matter integrity (Madden et al., 2007). While these authors found a significant age-related increase in response times and heighted activations in frontal and parietal cortices in OA, compared to YA, as well as decreased FA in anterior regions, they did not find a significant correlation between white matter integrity and BOLD responses in any frontal or parietal area. The present study, therefore, is the first to document an explicit link between white matter integrity and a neurophysiological marker of visual search performance. Further, we found that FA values and beta and gamma power were significantly altered in OA. These results suggest that differences in white matter integrity have a greater impact on modulation of oscillatory activity than on general measures of brain

activity, such as BOLD responses, and thus provide a more sensitive index of age-related changes.

Our finding of a strong correlation between the magnitude of posterior alpha desynchronization with FA in the posterior corpus callosum raises interesting questions. The putative role of alpha rhythms in visual areas is one of suppression, whereby high levels of alpha are associated with disengagement of task-irrelevant visual areas (Vanni et al., 1997; Bollimunta et al., 2011). Decreased alpha activity is associated with heightened cortical excitability (Jones *et al.*, 2000; Worden *et al.*, 2000; Rajagovindan & Ding, 2011). Consistent with this distinction are findings of increased alpha activity in sensory areas whose receptive fields correspond to distractor items that need to be ignored (Vanni et al., 1997; Foxe et al., 1998; Worden et al., 2000). In contrast, event-related alpha descynchronizations are commonly observed in tasks that require active visual processing and the degree of desynchronization correlated with the magnitude of stimulus-induced evoked responses (Worden *et al.*, 2000; Palva & Palva, 2007; Rajagovindan & Ding, 2011). New studies that used transcranial magnetic stimulation to selectively inactivate discrete cortical areas demonstrated that frontoparietal areas play a causal role in the modulation of posterior alpha oscillations (Capotosto et al., 2009; Zanto et al., 2011). Our finding of a strong correlation between FA values in fmajor and the level of alpha desynchronization in occipital sensors suggests that this white matter tract is important for mediating the top-down control over this visual rhythm. The splenium of the corpus callosum is a major white matter tract that contains fibers that support interhemispheric communication between the left and right occipital and parietal lobes (Schmahmann & Pandya,

2006). It is not surprising, therefore, that this white matter tract would correlate with physiological markers of visual attention, which relies on communication between frontoparietal and occipital cortices. We did not, however, find a significant correlation between alpha power and visual search performance, nor did we find a significant age-related reduction in the integrity of the posterior corpus callosum. It is, therefore, unclear whether this structure-function relation is specific to visual attention processes or whether it represents a more general marker of heightened activity in visual cortices, possibly as a byproduct of the covert direction of attention. Indeed, numerous studies have documented associations between alpha band modulations in occipital areas and visual discrimination in tasks that did not specifically manipulate the attentional demands (Brandt & Jansen, 1991; Ergenoglu *et al.*, 2004; Hanslmayr *et al.*, 2007; Romei *et al.*, 2008)

Conclusions.

We have demonstrated that visual search performance in YA is accompanied by a dynamic modulation of oscillatory activity, with beta activity associated with top-down direction of attention and gamma activity relating to bottom-up processes. This modulation is lacking in OA, who tended to rely more on gamma-mediated bottom-up processing during all trials. Oscillatory power in these frequency ranges was associated with the integrity of white matter in the SLF. Decreased integrity of this white matter tract in OA is the result of an increase in radial diffusivity, a DTI-based marker of myelin integrity. Thus, these results are consistent with our hypothesis that disruption of white matter myelination in healthy aging leads to interference in rapid cortical communication, leading OA to engage a less efficient processing

mechanism on trials that require a high degree of selective attention. An important question for future studies is to determine how these changes in cortical oscillations relate to patterns of fMRI activity and to measures of functional connectivity between frontal, parietal, and occipital cortices, how these relations are affected by aging, and whether the age-related changes can be modified through cognitive training or the use of more effective strategies by OA.

References

Aertsen AM, Gerstein GL, Habib MK & Palm G (1989) Dynamics of neuronal firing correlation: modulation of "effective connectivity". *J Neurophysiol* **61**, 900-917.

Ardekani S, Kumar A, Bartzokis G & Sinha U (2007) Exploratory voxel-based analysis of diffusion indices and hemispheric asymmetry in normal aging. *Magn Reson Imaging* **25**, 154-167.

Baillet S, Mosher JC & Leahy RM (2001) Electromagnetic brain mapping. *iEEE Signal Processing Magazine* **18**, 14-30.

Baluch F & Itti L (2011) Mechanisms of top-down attention. *Trends Neurosci* **34**, 210-224.

Bauer M, Oostenveld R, Peeters M & Fries P (2006) Tactile spatial attention enhances gamma-band activity in somatosensory cortex and reduces low-frequency activity in parieto-occipital areas. *J Neurosci* **26**, 490-501.

Bennett IJ, Motes MA, Rao NK & Rypma B (2011) White matter tract integrity predicts visual search performance in young and older adults. *Neurobiol Aging*.

Bollimunta A, Mo J, Schroeder CE & Ding M (2011) Neuronal mechanisms and attentional modulation of corticothalamic alpha oscillations. *J Neurosci* **31**, 4935-4943.

Brandt ME & Jansen BH (1991) The relationship between prestimulus-alpha amplitude and visual evoked potential amplitude. *Int J Neurosci* **61**, 261-268.

Braver TS & Barch DM (2002) A theory of cognitive control, aging cognition, and neuromodulation. *Neurosci Biobehav Rev* **26**, 809-817.

Braver TS, Barch DM, Keys BA, Carter CS, Cohen JD, Kaye JA, Janowsky JS, Taylor SF, Yesavage JA, Mumenthaler MS, Jagust WJ & Reed BR (2001) Context processing in older adults: evidence for a theory relating cognitive control to neurobiology in healthy aging. *J Exp Psychol Gen* **130**, 746-763.

Braver TS & Ruge H (2006) Functional Neuroimaging of Executive Functions. In *Handbook of Functional Neuroimaging of Cognition, 2nd Edition*, pp. 307-347 [R Cabeza and A Kingstone, editors]. Cambridge, MA: MIT Press.

Buckner RL (2004) Memory and executive function in aging and AD: multiple factors that cause decline and reserve factors that compensate. *Neuron* **44**, 195-208.

Budde MD, Xie M, Cross AH & Song SK (2009) Axial diffusivity is the primary correlate of axonal injury in the experimental autoimmune encephalomyelitis spinal cord: a quantitative pixelwise analysis. *J Neurosci* **29**, 2805-2813.

Buschman TJ & Miller EK (2007) Top-down versus bottom-up control of attention in the prefrontal and posterior parietal cortices. *Science* **315**, 1860-1862.

Buschman TJ & Miller EK (2010) Shifting the spotlight of attention: evidence for discrete computations in cognition. *Front Hum Neurosci* **4**, 194.

Cabeza R (2002) Hemispheric asymmetry reduction in older adults: the HAROLD model. *Psychol Aging* **17**, 85-100.

Cabeza R, Grady CL, Nyberg L, McIntosh AR, Tulving E, Kapur S, Jennings JM, Houle S & Craik FI (1997) Age-related differences in neural activity during memory encoding and retrieval: a positron emission tomography study. *J Neurosci* **17**, 391-400.

Capotosto P, Babiloni C, Romani GL & Corbetta M (2009) Frontoparietal cortex controls spatial attention through modulation of anticipatory alpha rhythms. *J Neurosci* **29**, 5863-5872.

Clapp WC, Rubens MT, Sabharwal J & Gazzaley A (2011) Deficit in switching between functional brain networks underlies the impact of multitasking on working memory in older adults. *Proc Natl Acad Sci U S A* **108**, 7212-7217.

Craik FIM & Salthouse TA (2000) *The Handbook of Aging and Cognition*. Mahwah, NJ: Lawrence Erlbaum Associates.

Dale AM, Fischl B & Sereno MI (1999) Cortical surface-based analysis. I. Segmentation and surface reconstruction. *Neuroimage* **9**, 179-194.

Davis SW, Dennis NA, Buchler NG, White LE, Madden DJ & Cabeza R (2009) Assessing the effects of age on long white matter tracts using diffusion tensor tractography. *Neuroimage* **46**, 530-541.

Desikan RS, Segonne F, Fischl B, Quinn BT, Dickerson BC, Blacker D, Buckner RL, Dale AM, Maguire RP, Hyman BT, Albert MS & Killiany RJ (2006) An automated labeling system for subdividing the human cerebral cortex on MRI scans into gyral based regions of interest. *Neuroimage* **31**, 968-980.

Desimone R & Duncan J (1995) Neural mechanisms of selective visual attention. *Annu Rev Neurosci* **18**, 193-222.

Donner TH & Siegel M (2011) A framework for local cortical oscillation patterns. *Trends Cogn Sci* **15**, 191-199.

Emery L, Heaven TJ, Paxton JL & Braver TS (2008) Age-related changes in neural activity during performance matched working memory manipulation. *Neuroimage* **42**, 1577-1586.

Engel AK & Fries P (2010) Beta-band oscillations--signalling the status quo? *Curr Opin Neurobiol* **20**, 156-165.

Ergenoglu T, Demiralp T, Bayraktaroglu Z, Ergen M, Beydagi H & Uresin Y (2004) Alpha rhythm of the EEG modulates visual detection performance in humans. *Brain Res Cogn Brain Res* **20**, 376-383.

Fischl B, Liu A & Dale AM (2001) Automated manifold surgery: constructing geometrically accurate and topologically correct models of the human cerebral cortex. *IEEE Trans Med Imaging* **20**, 70-80.

Fischl B, Salat DH, van der Kouwe AJ, Makris N, Segonne F, Quinn BT & Dale AM (2004) Sequence-independent segmentation of magnetic resonance images. *Neuroimage* **23 Suppl 1**, S69-84.

Fischl B, Sereno MI & Dale AM (1999) Cortical surface-based analysis. II: Inflation, flattening, and a surface-based coordinate system. *Neuroimage* **9**, 195-207.

Fletcher PC & Henson RN (2001) Frontal lobes and human memory: insights from functional neuroimaging. *Brain* **124**, 849-881.

Folk CL & Lincourt AE (1996) The effects of age on guided conjunction search. *Exp Aging Res* **22**, 99-118.

Folstein MF, Folstein SE & McHugh PR (1975) "Mini-mental state". A practical method for grading the cognitive state of patients for the clinician. *J Psychiatr Res* **12**, 189-198.

Foxe JJ, Simpson GV & Ahlfors SP (1998) Parieto-occipital approximately 10 Hz activity reflects anticipatory state of visual attention mechanisms. *Neuroreport* **9**, 3929-3933.

Fries P (2009) Neuronal gamma-band synchronization as a fundamental process in cortical computation. *Annu Rev Neurosci* **32**, 209-224.

Fries P, Reynolds JH, Rorie AE & Desimone R (2001) Modulation of oscillatory neuronal synchronization by selective visual attention. *Science* **291**, 1560-1563.

Fuster JM (2000) Executive frontal functions. *Exp Brain Res* **133**, 66-70.

Gazzaley A, Cooney JW, Rissman J & D'Esposito M (2005) Top-down suppression deficit underlies working memory impairment in normal aging. *Nat Neurosci* **8**, 1298-1300.

Gazzaley A & D'Esposito M (2007) Top-down modulation and normal aging. *Ann N Y Acad Sci* **1097**, 67-83.

Gilbert CD & Sigman M (2007) Brain states: top-down influences in sensory processing. *Neuron* **54**, 677-696.

Glisky EL (2007) Changes in Cognitive Function in Human Aging.

Gregoriou GG, Gotts SJ, Zhou H & Desimone R (2009) High-frequency, long-range coupling between prefrontal and visual cortex during attention. *Science* **324**, 1207-1210.

Hämäläinen M & Hari R (2002) Magnetoencephalographic characterization of dynamic brain activation: basic principles and methods of data collection and source analysis. In *Brain Mapping: The Methods* [AW Toga and JC Mazziotta, editors]. Boston: Academic Press.

Hanslmayr S, Aslan A, Staudigl T, Klimesch W, Herrmann CS & Bauml KH (2007) Prestimulus oscillations predict visual perception performance between and within subjects. *Neuroimage* **37**, 1465-1473.

Hari R & Salmelin R (1997) Human cortical oscillations: a neuromagnetic view through the skull. *Trends Neurosci* **20**, 44-49.

Hasher L & Zacks RT (1988) Working memory, comprehesion, and aging: A review and a new view. In *The Psychology of Learning and Motivation*, pp. 193 [GH Bower, editor]. New York: Academic Press.

Hawkins HL, Kramer AF & Capaldi D (1992) Aging, exercise, and attention. *Psychol Aging* **7**, 643-653.

Head D, Buckner RL, Shimony JS, Williams LE, Akbudak E, Conturo TE, McAvoy M, Morris JC & Snyder AZ (2004) Differential vulnerability of anterior white matter in nondemented aging with minimal acceleration in dementia of the Alzheimer type: evidence from diffusion tensor imaging. *Cereb Cortex* **14**, 410-423.

Hedden T (2007) Imaging cognition in the aging human brain. In *Brain Aging: Models, Methods, and Mechanisms* [DR Riddle, editor]. Boca Raton, FL: CRC Press.

Hedden T & Gabrieli JD (2004) Insights into the ageing mind: a view from cognitive neuroscience. *Nat Rev Neurosci* **5**, 87-96.

Hommel B, Li KZ & Li SC (2004) Visual search across the life span. *Dev Psychol* **40**, 545-558.

Jensen O & Hesse C (2010) Estimating distributed representations of evoked responses and oscillatory activity. In *MEG: An Introduction to Methods*, pp. 156-187 [PC Hansen, ML Kringelback and R Salmelin, editors]. New York: Oxford University Press.

Jimura K & Braver TS (2010) Age-related shifts in brain activity dynamics during task switching. *Cereb Cortex* **20**, 1420-1431.

Jones SR, Pinto DJ, Kaper TJ & Kopell N (2000) Alpha-frequency rhythms desynchronize over long cortical distances: a modeling study. *J Comput Neurosci* **9**, 271-291.

Kahana MJ (2006) The cognitive correlates of human brain oscillations. *J Neurosci* **26**, 1669-1672.

Klawiter EC, Schmidt RE, Trinkaus K, Liang HF, Budde MD, Naismith RT, Song SK, Cross AH & Benzinger TL (2011) Radial diffusivity predicts demyelination in ex vivo multiple sclerosis spinal cords. *Neuroimage* **55**, 1454-1460.

Klimesch W, Doppelmayr M, Russegger H, Pachinger T & Schwaiger J (1998) Induced alpha band power changes in the human EEG and attention. *Neurosci Lett* **244**, 73-76.

Knudsen EI (2007) Fundamental components of attention. *Annu Rev Neurosci* **30**, 57-78.

Lachaux JP, Fonlupt P, Kahane P, Minotti L, Hoffmann D, Bertrand O & Baciu M (2007) Relationship between task-related gamma oscillations and BOLD signal: new insights from combined fMRI and intracranial EEG. *Hum Brain Mapp* **28**, 1368-1375.

Li L, Gratton C, Yao D & Knight RT (2010) Role of frontal and parietal cortices in the control of bottom-up and top-down attention in humans. *Brain Res* **1344**, 173-184.

Lorenzo-Lopez L, Amenedo E, Pascual-Marqui RD & Cadaveira F (2008) Neural correlates of age-related visual search decline: a combined ERP and sLORETA study. *Neuroimage* **41**, 511-524.

Lorenzo-Lopez L, Gutierrez R, Moratti S, Maestu F, Cadaveira F & Amenedo E (2011) Age-related occipito-temporal hypoactivation during visual search: Relationships between mN2pc sources and performance. *Neuropsychologia* **49**, 858-865.

Madden DJ (2007) Aging and Visual Attention. *Curr Dir Psychol Sci* **16**, 70-74.

Madden DJ, Spaniol J, Costello MC, Bucur B, White LE, Cabeza R, Davis SW, Dennis NA, Provenzale JM & Huettel SA (2009) Cerebral white matter integrity mediates adult age differences in cognitive performance. *J Cogn Neurosci* **21**, 289-302.

Madden DJ, Spaniol J, Whiting WL, Bucur B, Provenzale JM, Cabeza R, White LE & Huettel SA (2007) Adult age differences in the functional neuroanatomy of visual attention: a combined fMRI and DTI study. *Neurobiol Aging* **28**, 459-476.

Madden DJ, Turkington TG, Provenzale JM, Denny LL, Langley LK, Hawk TC & Coleman RE (2002) Aging and attentional guidance during visual search: functional neuroanatomy by positron emission tomography. *Psychol Aging* **17**, 24-43.

Madden DJ, Turkington TG, Provenzale JM, Hawk TC, Hoffman JM & Coleman RE (1997) Selective and divided visual attention: age-related changes in regional cerebral blood flow measured by H2(15)O PET. *Hum Brain Mapp* **5**, 389-409.

Madden DJ & Whiting WL (2004) Age-related changes in visual attention. In *Recent advances in psychology and aging*, pp. 41-88 [PT Costa and IC Siegler, editors]. Amsterdam: Elsevier.

Madden DJ, Whiting WL, Cabeza R & Huettel SA (2004) Age-related preservation of top-down attentional guidance during visual search. *Psychol Aging* **19**, 304-309.

Maris E & Oostenveld R (2007) Nonparametric statistical testing of EEG- and MEG-data. *J Neurosci Methods* **164**, 177-190.

Marner L, Nyengaard JR, Tang Y & Pakkenberg B (2003) Marked loss of myelinated nerve fibers in the human brain with age. *J Comp Neurol* **462**, 144-152.

McDowd JM (1986) The effects of age and extended practice on divided attention performance. *J Gerontol* **41**, 764-769.

McDowd JM & Shaw RJ (2000) Attention and aging: a functional perspective. In *The Handbook of Aging and Cognition, 2nd Edition*, pp. 221-292 [FIM Craik and TA Salthouse, editors]. Mahwah, NH: Erlbaum.

McIntosh AR, Sekuler AB, Penpeci C, Rajah MN, Grady CL, Sekuler R & Bennett PJ (1999) Recruitment of unique neural systems to support visual memory in normal aging. *Curr Biol* **9**, 1275-1278.

Milham MP, Erickson KI, Banich MT, Kramer AF, Webb A, Wszalek T & Cohen NJ (2002) Attentional control in the aging brain: insights from an fMRI study of the stroop task. *Brain Cogn* **49**, 277-296.

Miller EK (2000) The prefrontal cortex and cognitive control. *Nat Rev Neurosci* **1**, 59-65.

Miller EK & Cohen JD (2001) An integrative theory of prefrontal cortex function. *Annu Rev Neurosci* **24**, 167-202.

Miyake A, Friedman NP, Emerson MJ, Witzki AH, Howerter A & Wager TD (2000) The unity and diversity of executive functions and their contributions to complex "Frontal Lobe" tasks: a latent variable analysis. *Cognit Psychol* **41**, 49-100.

Nichols TE & Holmes AP (2002) Nonparametric permutation tests for functional neuroimaging: a primer with examples. *Hum Brain Mapp* **15**, 1-25.

Niessing J, Ebisch B, Schmidt KE, Niessing M, Singer W & Galuske RA (2005) Hemodynamic signals correlate tightly with synchronized gamma oscillations. *Science* **309**, 948-951.

O'Sullivan M, Jones DK, Summers PE, Morris RG, Williams SC & Markus HS (2001) Evidence for cortical "disconnection" as a mechanism of age-related cognitive decline. *Neurology* **57**, 632-638.

Oostenveld R, Fries P, Maris E & Schoffelen JM (2011) FieldTrip: Open source software for advanced analysis of MEG, EEG, and invasive electrophysiological data. *Comput Intell Neurosci* **2011**, 156869.

Palmer J (1994) Set-size effects in visual search: the effect of attention is independent of the stimulus for simple tasks. *Vision Res* **34**, 1703-1721.

Palva S & Palva JM (2007) New vistas for alpha-frequency band oscillations. *Trends Neurosci* **30**, 150-158.

Park DC & Reuter-Lorenz P (2009) The adaptive brain: aging and neurocognitive scaffolding. *Annu Rev Psychol* **60**, 173-196.

Percival DB & Walden AT (1993) *Spectral analysis for physical applications: Multitaper and conventional univariate techniques*. New York: Cambridge University Press.

Peters A (2002) The effects of normal aging on myelin and nerve fibers: a review. *J Neurocytol* **31**, 581-593.

Pfefferbaum A, Adalsteinsson E & Sullivan EV (2005) Frontal circuitry degradation marks healthy adult aging: Evidence from diffusion tensor imaging. *Neuroimage* **26**, 891-899.

Piguet O & Corkin S (2007) The aging brain. In *Learning and the Brain: A Comprehensive Guide for Educators, Parents, and Teachers* [S Feinstein, editor]. Lanham, MD: Rowman & Littlefield Education.

Rajagovindan R & Ding M (2011) From prestimulus alpha oscillation to visual-evoked response: an inverted-U function and its attentional modulation. *J Cogn Neurosci* **23**, 1379-1394.

Rajah MN & D'Esposito M (2005) Region-specific changes in prefrontal function with age: a review of PET and fMRI studies on working and episodic memory. *Brain* **128**, 1964-1983.

Ray S & Maunsell JH (2010) Differences in gamma frequencies across visual cortex restrict their possible use in computation. *Neuron* **67**, 885-896.

Reuter-Lorenz PA, Jonides J, Smith EE, Hartley A, Miller A, Marshuetz C & Koeppe RA (2000) Age differences in the frontal lateralization of verbal and spatial working memory revealed by PET. *J Cogn Neurosci* **12**, 174-187.

Romei V, Brodbeck V, Michel C, Amedi A, Pascual-Leone A & Thut G (2008) Spontaneous fluctuations in posterior alpha-band EEG activity reflect variability in excitability of human visual areas. *Cereb Cortex* **18**, 2010-2018.

Rypma B, Berger JS, Genova HM, Rebbechi D & D'Esposito M (2005) Dissociating age-related changes in cognitive strategy and neural efficiency using event-related fMRI. *Cortex* **41**, 582-594.

Rypma B, Prabhakaran V, Desmond JE & Gabrieli JD (2001) Age differences in prefrontal cortical activity in working memory. *Psychol Aging* **16**, 371-384.

Saalmann YB, Pigarev IN & Vidyasagar TR (2007) Neural mechanisms of visual attention: how top-down feedback highlights relevant locations. *Science* **316**, 1612-1615.

Salat DH, Tuch DS, Hevelone ND, Fischl B, Corkin S, Rosas HD & Dale AM (2005) Age-related changes in prefrontal white matter measured by diffusion tensor imaging. *Ann N Y Acad Sci* **1064**, 37-49.

Salthouse TA (1994) The aging of working memory. *Neuropsychology* **8**, 535-543.

Salthouse TA (1996) The processing-speed theory of adult age differences in cognition. *Psychol Rev* **103**, 403-428.

Salthouse TA, Atkinson TM & Berish DE (2003) Executive functioning as a potential mediator of age-related cognitive decline in normal adults. *J Exp Psychol Gen* **132**, 566-594.

Salthouse TA & Meinz EJ (1995) Aging, inhibition, working memory, and speed. *J Gerontol B Psychol Sci Soc Sci* **50**, P297-306.

Sauseng P, Klimesch W, Stadler W, Schabus M, Doppelmayr M, Hanslmayr S, Gruber WR & Birbaumer N (2005) A shift of visual spatial attention is selectively associated with human EEG alpha activity. *Eur J Neurosci* **22**, 2917-2926.

Schmahmann JD & Pandya DN (2006) *Fiber Pathways of the Brain*. Oxford, UK: Oxford University Press.

Schroeder CE & Lakatos P (2009a) The gamma oscillation: master or slave? *Brain Topogr* **22**, 24-26.

Schroeder CE & Lakatos P (2009b) Low-frequency neuronal oscillations as instruments of sensory selection. *Trends Neurosci* **32**, 9-18.

Siegel M, Donner TH, Oostenveld R, Fries P & Engel AK (2008) Neuronal synchronization along the dorsal visual pathway reflects the focus of spatial attention. *Neuron* **60**, 709-719.

Song SK, Sun SW, Ramsbottom MJ, Chang C, Russell J & Cross AH (2002) Dysmyelination revealed through MRI as increased radial (but unchanged axial) diffusion of water. *Neuroimage* **17**, 1429-1436.

Song SK, Yoshino J, Le TQ, Lin SJ, Sun SW, Cross AH & Armstrong RC (2005) Demyelination increases radial diffusivity in corpus callosum of mouse brain. *Neuroimage* **26**, 132-140.

Spencer WD & Raz N (1995) Differential effects of aging on memory for content and context: a meta-analysis. *Psychol Aging* **10**, 527-539.

Stufflebeam SM, Witzel T, Mikulski S, Hamalainen MS, Temereanca S, Barton JJ, Tuch DS & Manoach DS (2008) A non-invasive method to relate the timing of neural activity to white matter microstructural integrity. *Neuroimage*.

Sullivan EV & Pfefferbaum A (2006) Diffusion tensor imaging and aging. *Neurosci Biobehav Rev* **30**, 749-761.

Sullivan EV, Rohlfing T & Pfefferbaum A (2010) Quantitative fiber tracking of lateral and interhemispheric white matter systems in normal aging: relations to timed performance. *Neurobiol Aging* **31**, 464-481.

Tadel F, Baillet S, Mosher JC, Pantazis D & Leahy RM (2011) Brainstorm: A User-Friendly Application for MEG/EEG Analysis. *Comput Intell Neurosci* **2011**, Article ID 879716, 879713 pages. doi:879710.871155/872011/879716.

Tallon-Baudry C & Bertrand O (1999) Oscillatory gamma activity in humans and its role in object representation. *Trends Cogn Sci* **3**, 151-162.

Tang Y, Nyengaard JR, Pakkenberg B & Gundersen HJ (1997) Age-induced white matter changes in the human brain: a stereological investigation. *Neurobiol Aging* **18**, 609-615.

Thut G, Nietzel A, Brandt SA & Pascual-Leone A (2006) Alpha-band electroencephalographic activity over occipital cortex indexes visuospatial attention bias and predicts visual target detection. *J Neurosci* **26**, 9494-9502.

Tiesinga PH, Fellous JM, Jose JV & Sejnowski TJ (2002) Information transfer in entrained cortical neurons. *Network* **13**, 41-66.

van der Kouwe AJ, Benner T, Salat DH & Fischl B (2008) Brain morphometry with multiecho MPRAGE. *Neuroimage* **40**, 559-569.

Vanni S, Revonsuo A & Hari R (1997) Modulation of the parieto-occipital alpha rhythm during object detection. *J Neurosci* **17**, 7141-7147.

von Stein A, Chiang C & Konig P (2000) Top-down processing mediated by interareal synchronization. *Proc Natl Acad Sci U S A* **97**, 14748-14753.

West R (2004) The effects of aging on controlled attention and conflict processing in the Stroop task. *J Cogn Neurosci* **16**, 103-113.

Winterer G, Carver FW, Musso F, Mattay V, Weinberger DR & Coppola R (2007) Complex relationship between BOLD signal and synchronization/desynchronization of human brain MEG oscillations. *Hum Brain Mapp* **28**, 805-816.

Wolfe JM, Cave KR & Franzel SL (1989) Guided search: an alternative to the feature integration model for visual search. *J Exp Psychol Hum Percept Perform* **15**, 419-433.

Wolfe JM & Horowitz TS (2004) What attributes guide the deployment of visual attention and how do they do it? *Nat Rev Neurosci* **5**, 495-501.

Womelsdorf T, Fries P, Mitra PP & Desimone R (2006) Gamma-band synchronization in visual cortex predicts speed of change detection. *Nature* **439**, 733-736.

Wonderlick JS, Ziegler DA, Hosseini-Varnamkhasti P, Locascio JJ, Bakkour A, van der Kouwe A, Triantafyllou C, Corkin S & Dickerson BC (2009) Reliability of MRI-derived cortical and subcortical morphometric measures: effects of pulse sequence, voxel geometry, and parallel imaging. *Neuroimage* **44**, 1324-1333.

Worden MS, Foxe JJ, Wang N & Simpson GV (2000) Anticipatory biasing of visuospatial attention indexed by retinotopically specific alpha-band electroencephalography increases over occipital cortex. *J Neurosci* **20**, RC63.

Yantis S & Egeth HE (1999) On the distinction between visual salience and stimulus-driven attentional capture. *J Exp Psychol Hum Percept Perform* **25**, 661-676.

Yendiki A, Panneck P, Stevens A, Zollei L, Augustinack J, Wang R, Salat D, Ehrlich S, Behrens TE, Jbabdi S, Gollub R & Fischl B (in review) Automated probabilistic reconstruction of white-matter pathways in health and disease using an atlas of the underlying anatomy. *Frontiers in Neuroinformatics*.

Yoon B, Shim YS, Lee KS, Shon YM & Yang DW (2007) Region-specific changes of cerebral white matter during normal aging: A diffusion-tensor analysis. *Arch Gerontol Geriatr*.

Zanto TP, Rubens MT, Thangavel A & Gazzaley A (2011) Causal role of the prefrontal cortex in top-down modulation of visual processing and working memory. *Nat Neurosci* **14**, 656-661.

Ziegler DA, Piguet O, Salat DH, Prince K, Connally E & Corkin S (2010) Cognition in healthy aging is related to regional white matter integrity, but not cortical thickness. *Neurobiol Aging* **31**, 1912-1926.

Tables and Figures

Table 1. Participant characteristics: mean ± SD (range)

Group	*N*	Age	Edu	MMSE
YA	12 (7F)	25 *± 2.4*	15 *± 1.6*	29.1 *± 1.3*
		(20–31)	(12–18)	(27–30)
OA	13 (8F)	67 *± 5.9*	17.9 *± 7.4*	29.2 *± 1.2*
		(55–73)	(14–23)	(27–30)

Table 2. Age group differences in white matter integrity

	FA			RD (x 10^{-4} mm^2/sec)			AD (x 10^{-3} mm^2/sec)		
Tract	**YA**	**OA**	***p***	**YA**	**OA**	***p***	**YA**	**OA**	***p***
fmajor	0.56 ± 0.17	0.63 ± 0.09	0.211	5.4 ± 2.5	4.7 ± 1.1	0.290	1.5 ± 0.3	1.6 ± 0.1	0.789
fminor	0.52 ± 0.06	0.46 ± 0.04	0.004	5.9 ± 0.9	6.8 ± 0.9	0.008	1.4 ± 0.07	1.5 ± 0.1	0.583
SLF left	0.40 ± 0.05	0.38 ± 0.04	0.326	5.8 ± 0.5	6.1 ± 0.4	0.137	1.1 ± 0.06	1.1 ± 0.06	0.359
SLF right	0.41 ± 0.06	0.36 ± 0.03	0.017	5.9 ± 0.4	6.3 ± 0.6	0.024	1.1 ± 0.05	1.1 ± 0.07	0.905
ILF left	0.48 ± 0.06	0.43 ± 0.04	0.028	5.7 ± 0.5	6.1 ± 0.5	0.038	1.2 ± 0.07	1.2 ± 0.08	0.854
IFL right	0.48 ± 0.04	0.42 ± 0.04	0.001	5.9 ± 0.3	6.7 ± 0.8	0.001	1.3 ± 0.06	1.3 ± 0.08	0.679

Means ± SD for values of fractional anisotropy (FA), radial diffusivity (RD), and axial diffusivity (AD) for each white matter tract for YA and OA. Abbreviations: fmajor, forceps major; fminor, forceops minor; SLF, superior longitudinal fasiculus; IFL, inferior longitudinal fasciculus.

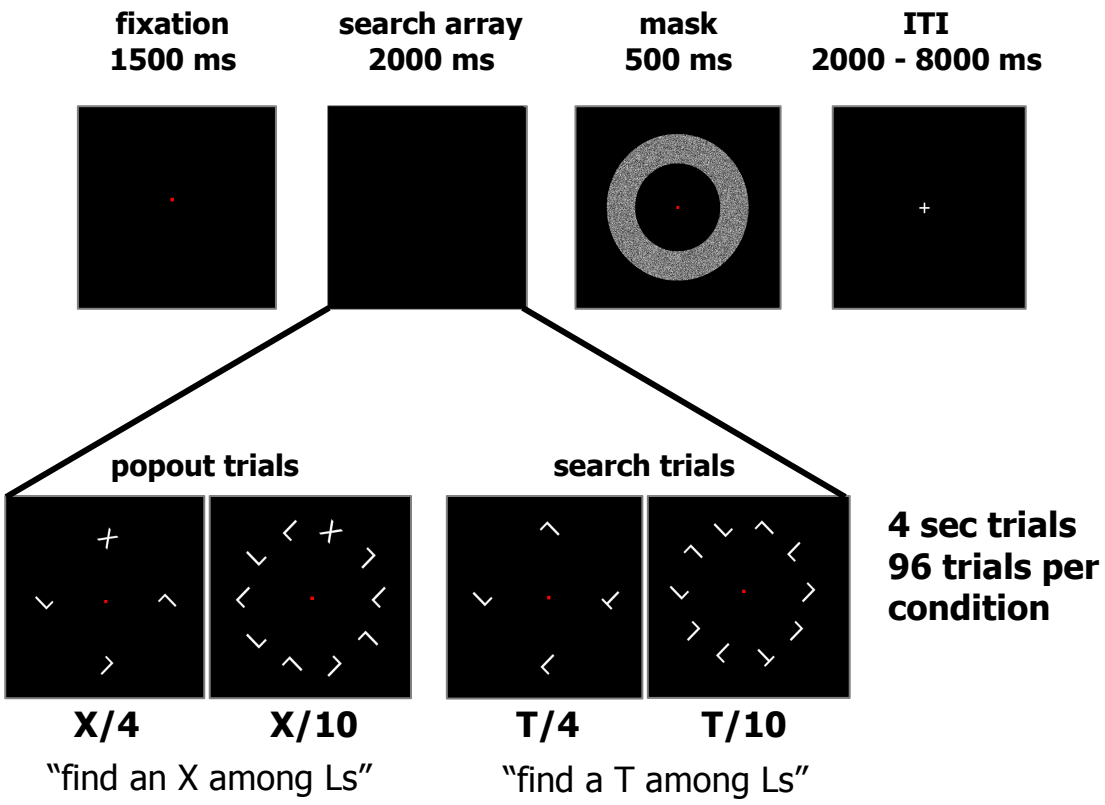

Figure 1. The visual search task.

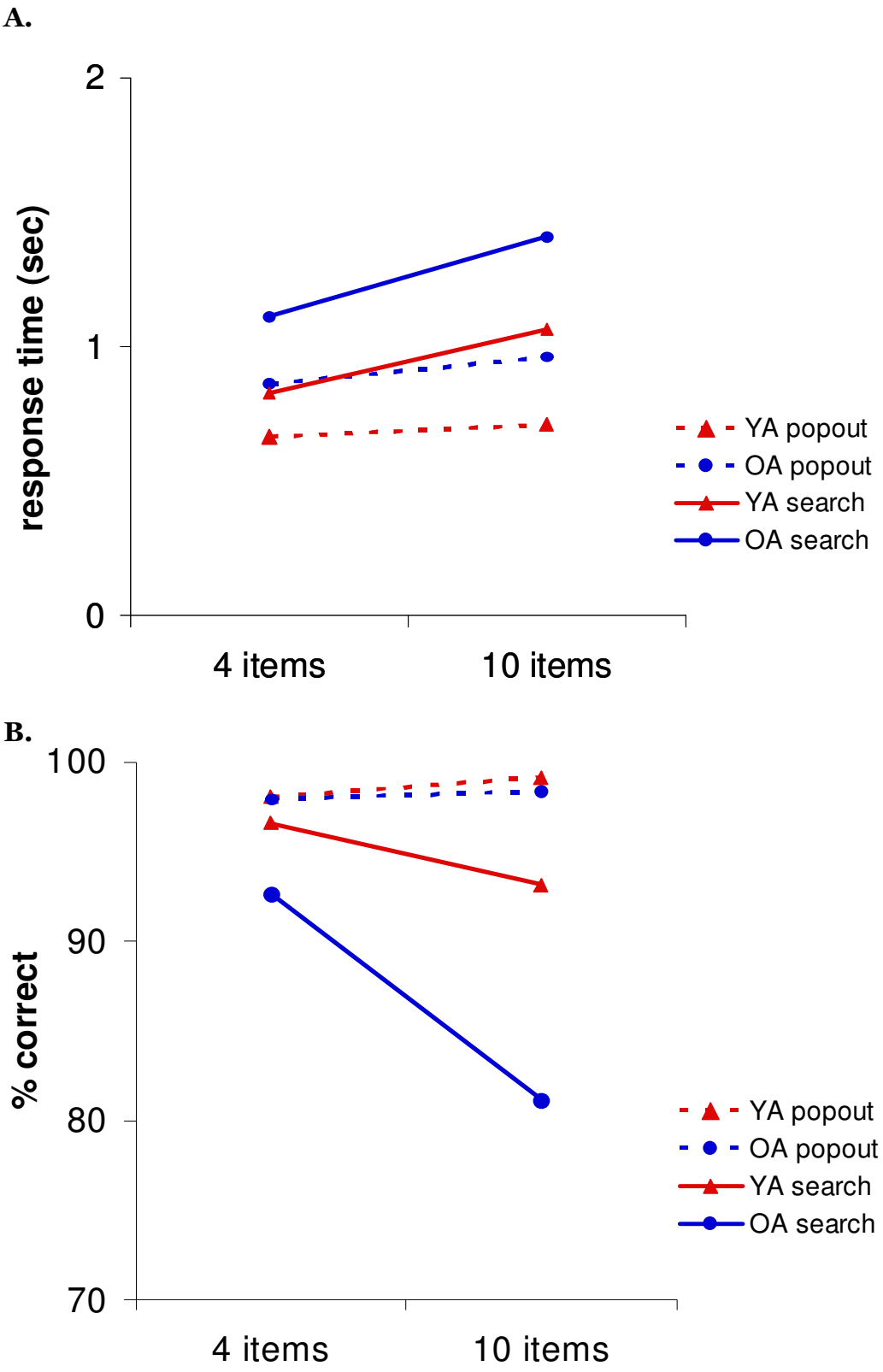

Figure 2. Measures of **A**) response times and **B**) accuracy for popout (dotted lines) and search trials (solid lines) in YA (blue) and OA (red) for 4- and 10-item arrays.

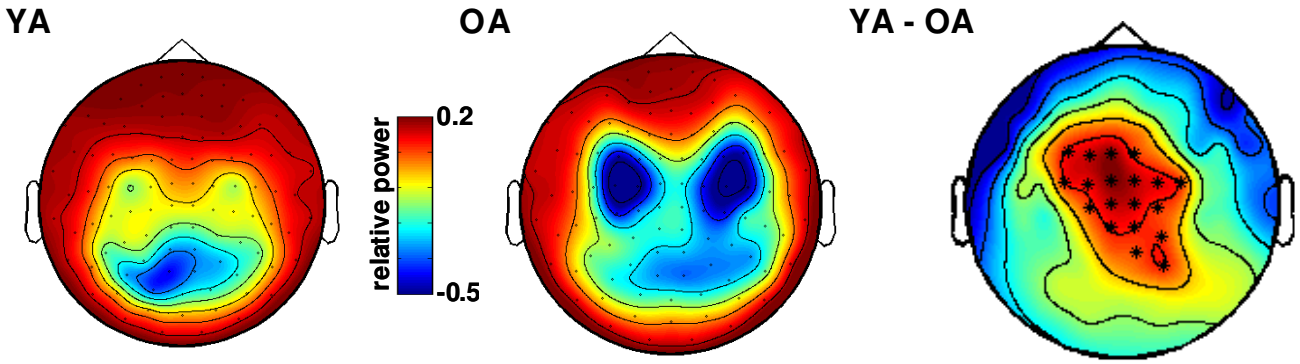

Figure 3. Topographic plots of sensor-level alpha band activity during effortful search trials. Values of power from 200-800 msec are plotted relative to activity in the prestimulus fixation period 500 ms prior to search array onset. Topographic plots of alpha power are shown for YA (left), OA (middle), and for differences between YA and OA (right). Asterisks denote clusters of significant differences (cluster-corrected $p < .05$)**.**

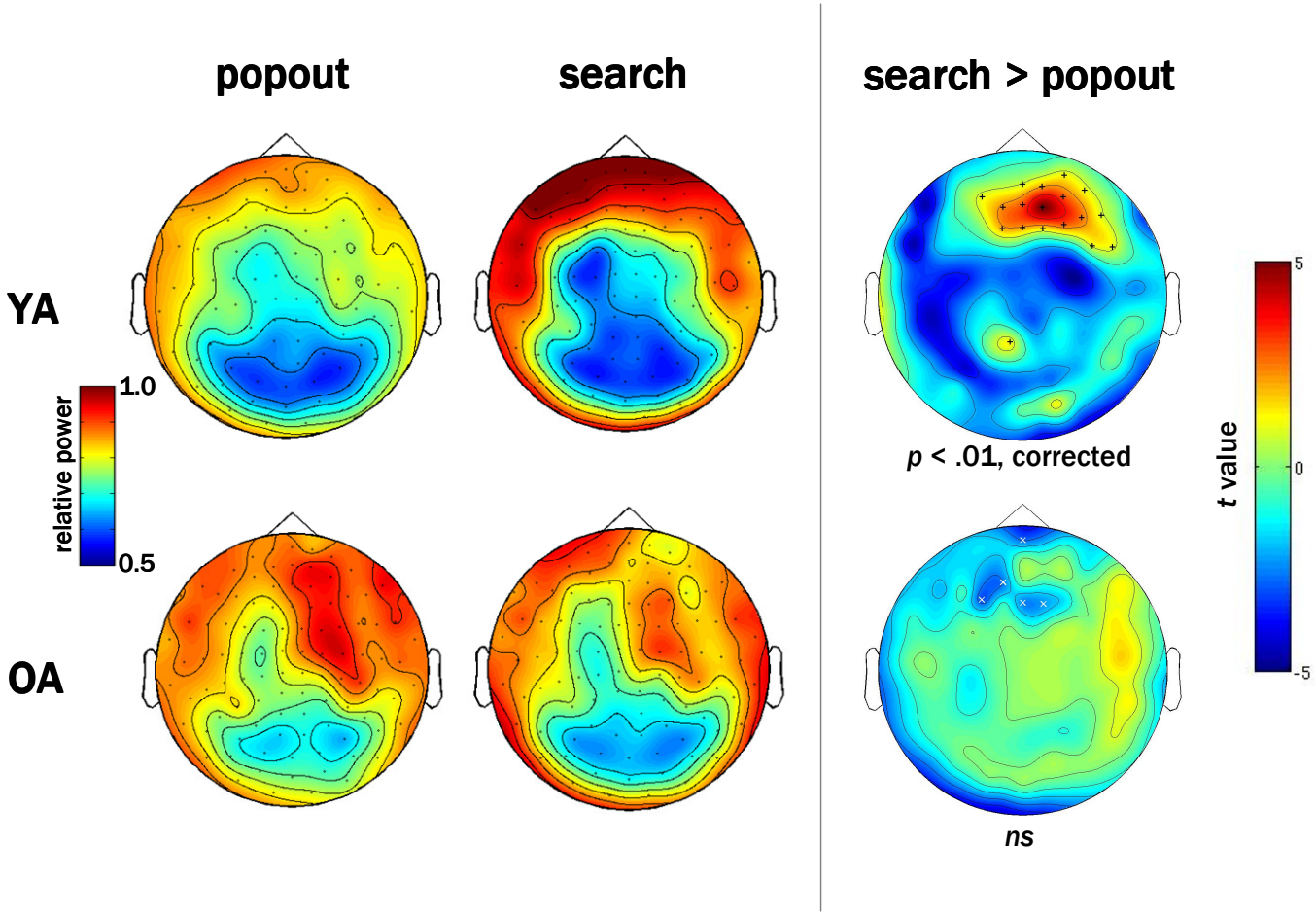

Figure 4. Topographic plots of sensor-level beta band activity during popout (left) and effortful (middle) search trials from 200-800 ms. Values of power are plotted relative to activity in the prestimulus fixation period 500 ms prior to search array onset. Topographic plots of beta power are shown for YA (top), OA (bottom), and differences between popout and search trials for each group (right). Asterisks denote sensors with a cluster-corrected $p < .05$.

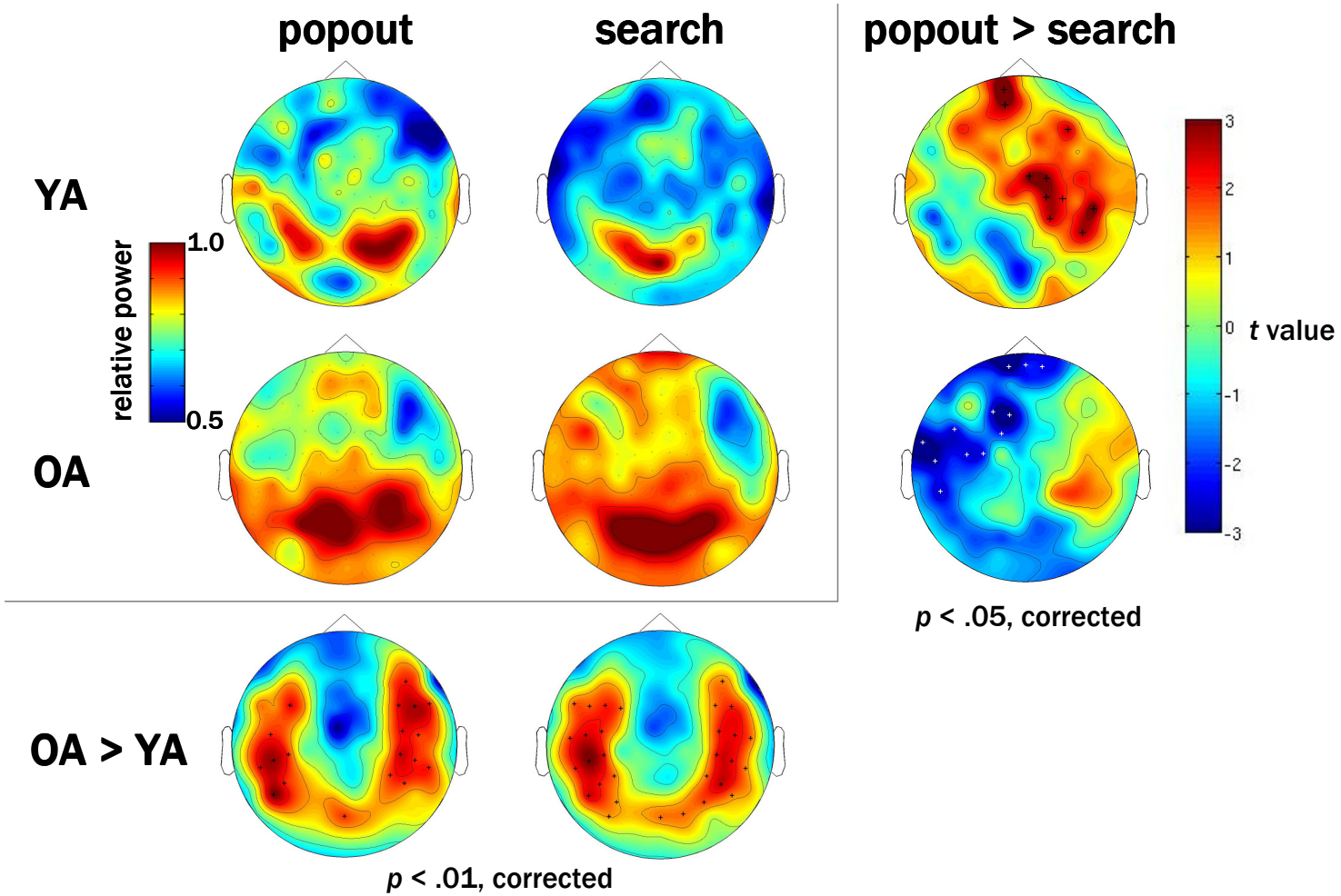

Figure 5. Topographic plots of sensor-level gamma band activity during popout (left column) and effortful (middle column) search trials from 200-800 msec. Values of power are plotted relative to activity in the prestimulus fixation period 500 ms prior to search array onset. Topographic plots of gamma power are shown for YA (top row), OA (middle row), differences in gamma power between popout and search trials (right column) and differences between YA and OA (bottom row). Asterisks denote sensors with a cluster-corrected $p < .05$, open circles denote sensors with a cluster-corrected $p < .1$.

A.

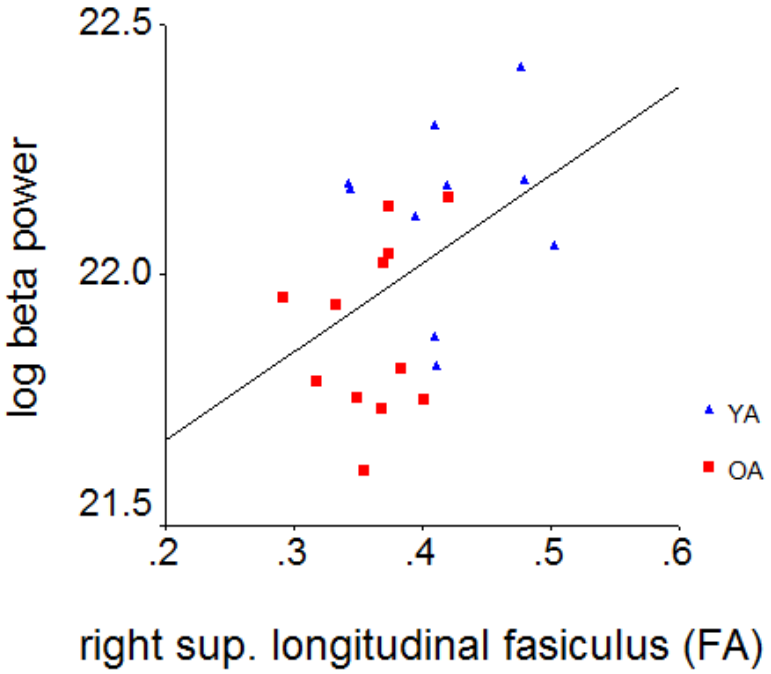

B.

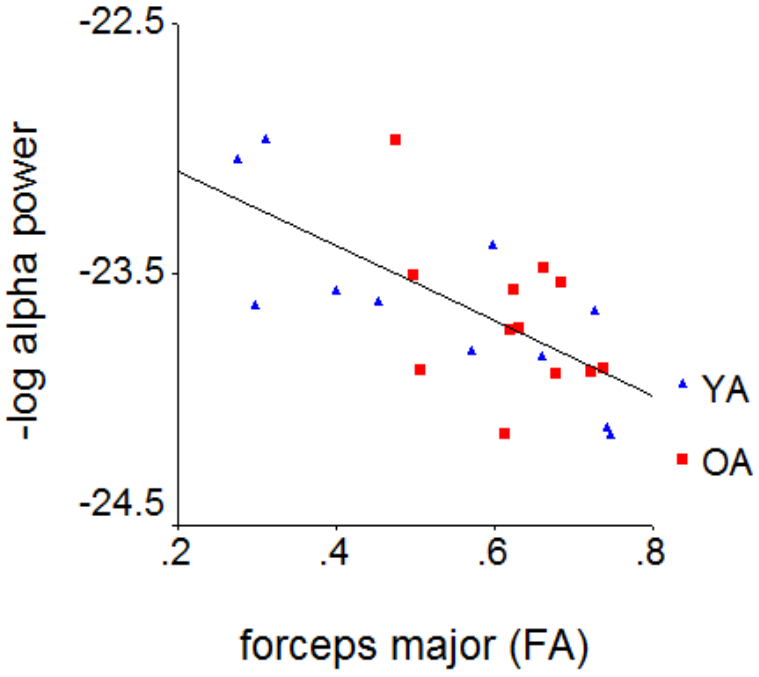

Figure 6. Scatterplots and regression lines showing significant (p < .05) correlations between FA values in the **A**) left superior longitudinal fasciculus and log-transformed beta power and **B**) between FA in the forceps major and log-transformed alpha power for YA (black squares) and OA (grey squares).

Chapter 4

Transformations in Oscillatory Activity and Evoked Responses in Primary Somatosensory Cortex in Middle Age: A Combined Computational Neural Modeling and MEG Study

David A. Ziegler[1], Dominique L. Pritchett[1,2], Paymon Hosseini-Varnamkhasti[1], Suzanne Corkin[1,3], Matti Hämäläinen[3], Christopher I. Moore[1,2], Stephanie R. Jones[3*]

[1]Department of Brain & Cognitive Sciences, MIT, Cambridge, MA;
[2]McGovern Institute for Brain Research, MIT, Cambridge, MA;
[3]Athinoula A. Martinos Center for Biomedical Imaging, Massachusetts General Hospital, Charlestown, MA;

This article is published in *NeuroImage*, Volume 52(3):897-912.
© 2010 Elsevier Inc.

Abstract

Oscillatory brain rhythms and evoked responses are widely believed to impact cognition, but relatively little is known about how these measures are affected by healthy aging. The present study used MEG to examine age-related changes in spontaneous oscillations and tactile evoked responses in primary somatosensory cortex (SI) in healthy young (YA) and middle-aged (MA) adults. To make specific predictions about neurophysiological changes that mediate age-related MEG changes, we applied a biophysically realistic model of SI that accurately reproduces SI MEG mu rhythms, containing alpha (7-14Hz) and beta (15-30Hz) components, and evoked responses. Analyses of MEG data revealed a significant increase in prestimulus mu power in SI, driven predominately by greater mu-beta dominance, and a larger and delayed M70 peak in the SI evoked response in MA. Previous analysis with our computational model showed that the SI mu rhythm could be reproduced with a stochastic sequence of rhythmic ~10Hz feedforward (FF) input to the granular layers of SI (representative of lemniscal thalamic input) followed nearly simultaneously by ~10Hz feedback (FB) input to the supragranular layers (representative of input from high order cortical or non-specific thalamic sources) (Jones et al., 2009). In the present study, the model further predicted that the rhythmic FF and FB inputs become stronger with age. Further, the FB input is predicted to arrive more synchronously to SI on each cycle of the 10Hz input in MA. The simulated neurophysiological changes are sufficient to account for the age-related differences in both prestimulus mu rhythms and evoked responses. Thus, the model predicts that a single set of neurophysiological changes intimately links these age-related changes in neural dynamics.

Introduction

Healthy aging is accompanied by widespread and systematic neuroanatomical changes (Raz & Rodrigue, 2006; Walhovd *et al.*, 2011) that have been linked to alterations in perceptual and cognitive abilities in older adults (Ziegler *et al.*, 2010). In addition, MEG and EEG studies have revealed age-related changes in brain dynamics on fast (ms) time-scales, such as changes in ongoing neural oscillations and in stimulus-locked evoked responses (Roubicek, 1977; Kononen & Partanen, 1993; Marciani *et al.*, 1994; d'Onofrio *et al.*, 1996; Niedermeyer, 1997; Kolev *et al.*, 2002; Babiloni *et al.*, 2006; Rossini *et al.*, 2007). Less is known about the effects of middle age on these phenomena.

Most of the work examining age related changes in neural rhythms has focused on the spontaneous or resting state 'alpha rhythm' measured with EEG, typically defined as 7-14Hz activity. In EEG sensor data, a generalized decrease in alpha power occurs with increasing age in parietal, temporal, and occipital cortices (Niedermeyer, 1997; Babiloni *et al.*, 2006; Rossini *et al.*, 2007). Further, older participants show decreases in alpha and low beta power (13-25 Hz), but increased high beta power (25-30 Hz) (Roubicek, 1977). A contradictory pattern emerges from studies of task-related rhythms, which show age-related decreases in alpha power in posterior sources, but increases in alpha power in anterior sources (Niedermeyer, 1997). Such a shift has been documented in the auditory (Yordanova *et al.*, 1998) and visual (Kononen & Partanen, 1993; Marciani *et al.*, 1994; d'Onofrio *et al.*, 1996; Kolev *et al.*, 2002) systems, with many of these changes seen in middle age. Few studies have examined the effects of aging on the commonly observed somatosensory mu rhythm, which is composed of a complex of alpha

and beta components (Hari, 2006; Jones *et al.*, 2009). One EEG study used a finger extension task and found age-related increases in mu-alpha and high mu-beta (22-23 Hz) power in anterior sensorimotor electrodes (Sailer *et al.*, 2000).

Other studies have examined age-related changes in evoked responses driven by median nerve stimulation and have found increases in the amplitudes and latencies of somatosensory-evoked potentials with advancing age (Luders, 1970; Desmedt & Cheron, 1980; Adler & Nacimiento, 1988; Kakigi & Shibasaki, 1991; Ferri *et al.*, 1996; Stephen *et al.*, 2006; Ogata *et al.*, 2009) These age-related increases in peak magnitudes occur in the first 100 ms following median nerve stimulation, with the greatest differences observed between 40-90 ms. Many of the changes are apparent by middle-age. The neural mechanism underlying these changes is typically attributed to a decline in cortical inhibition with advancing age (Drechsler, 1978; Simpson & Erwin, 1983; Stephen *et al.*, 2006), but no direct evidence supports this conclusion.

An expanding body of literature has shown that ongoing brain rhythms are causally related to changes in evoked response activity (Nikulin *et al.*, 2007; Mazaheri & Jensen, 2008; Jones *et al.*, 2009; Zhang & Ding, 2010), and that these modulations are correlated with changes in behavioral states, such as attention and perception (Fries *et al.*, 2001; Linkenkaer-Hansen *et al.*, 2004; Zhang & Ding, 2010). Despite the growing accumulation of studies showing age-dependent changes in neural rhythms, evoked response activity, and cognitive abilities, an open question is whether these measures change over the lifespan (e.g., from young to middle age). Further, there is little mechanistic understanding of the underlying neurophysiological

changes related to human aging. An obvious difficulty in achieving a mechanistic understanding is that the microscopic neural activity underlying macroscopically measured MEG/EEG signals is largely unknown and difficult to derive in humans without invasive recordings. Biophysically principled neural models can be used as powerful non-invasive tools to study the underlying neural dynamics generating these signals (Okada *et al.*, 1997; Murakami *et al.*, 2003; Murakami & Okada, 2006; Jones *et al.*, 2007; Jones *et al.*, 2009).

We have recently developed a neurophysiologically-grounded laminar neural model of primary somatosensory cortex (SI) that accurately reproduces spontaneous somatosensory mu rhythms and tactile evoked responses measured with human MEG (Jones *et al.*, 2007; Jones *et al.*, 2009). The model contains a network of morphologically and physiologically principled excitatory pyramidal neurons and inhibitory interneurons spanning multiple cortical laminae. The model includes extrinsic feedforward and feedback excitatory synaptic inputs, defined by their laminar location of postsynaptic effects. These inputs represent feedforward (FF) lemniscal thalamic input to the granular layers of SI, and feedback (FB) input to the supragranular layers from intracortical sources or nonspecific thalamic nuclei (Felleman & Van Essen, 1991; O'Sullivan *et al.*, 2001). This model can be used to identify the changes in network parameters, which have a direct neurophysiological interpretation, that produce observed changes MEG measured SI dynamics.

Here, we describe novel initial analyses of the impact of healthy aging on somatosensory dynamics, using a data set collected to address more general questions of dynamics, perception

and rhythmogenesis in neocortex (Jones et al., 2007; Jones et al., 2009). We then applied computational modeling to disambiguate possible interpretations of these data. Specifically, we used MEG to examine age-related changes in spontaneous mu rhythms and tactile evoked responses from localized SI activity in healthy young adults (YA) and early middle aged adults (MA). Our main findings from the MEG data are that the beta component of the spontaneous mu rhythm is greater in MA, and that the ~70ms peak (M70) in the tactile evoked response is also enhanced. These results provide initial evidence that both prestimulus SI mu rhythms and tactile evoked response magnitudes are increased in MA, compared to YA.

We then applied our biophysically realistic computational model of SI to predict the neural mechanisms underlying these changes. Our previous model results showed that the SI mu-rhythm could be reproduced by driving the SI network with two alternating ~10Hz inputs that contacted SI in FF and FB connection patterns, respectively. The relative alpha to beta power expressed in SI depended on the delay between and relative strength of the inputs (Jones et al., 2009). Based on these previous model results and our current MEG findings, we set forth to test two alternative predictions for the observed increase in mu-beta in MA: (A) that mu-beta dominance in MA, relative to YA, results from a decrease in the delay between 10Hz FF and FB inputs, or that (B) the FF-FB delay is the same in both groups and the mu-beta dominance arises from “stronger” FB inputs. Comparison of model results and MEG data supported prediction (B), leading to specific hypotheses about the cellular-level neural events that intimately link modulations in ongoing rhythmic activity with evoked response magnitudes in MA.

Methods

MEG experiment

MEG data were collected from 10 right-handed healthy adults aged 23-43 years (mean = 31 years; 6 female) with no known neurological or psychiatric conditions during performance of a tactile detection paradigm. All of the participants in our study had either obtained a Ph.D. or were enrolled in a doctoral-level graduate program at the time of the study, yielding a relatively homogeneous cohort in terms of educational demographics. In addition to MEG recordings, a high-resolution T1-weighted structural (MPRAGE) MRI scan was collected for each participant for dipole source localization analysis. The experimental protocol was approved by the Massachusetts General Hospital Internal Review Board and each participant gave informed consent prior to data acquisition. Previous publications have described the stimulus delivery system, behavioral paradigm, MEG data acquisition, and MEG source analysis (Jones *et al.*, 2007; Jones *et al.*, 2009). We summarize them here.

Stimulus paradigm

A piezoelectric device delivered single 100Hz sine wave taps (10 ms duration) to digit 3 of the right hand; participants responded with a button press using their left hand to indicate whether they had detected the stimulus on each trial. Stimulus strength was dynamically maintained at a perceptual threshold level (50% detection) using a dynamic algorithm (Jones et al., 2007). Supra-threshold stimuli (10% of all trials; 350 µm deflection; 100% detection) and null trials (20% of all trials) were randomly interleaved. Trial duration was 3 sec. Each participant completed 8 runs with 120 trials. The beginning of each trial was indicated by a binaural 60dB,

2kHz auditory cue, which remained constant during the entire 2 sec trial duration. During the auditory cue, the 10 ms finger tap was delivered between 500–1500 ms from trial onset in a randomized event-related design. The number of trials of a given latency to tap was randomly distributed during each run. The auditory cue ended $\geq$ 500 ms after the tactile stimulus and 1000 ms before the next trial began.

MEG data acquisition

Neuromagnetic responses were recorded using a 306-channel Elekta NeuroMag VectorView MEG system with 102 sites, each composed of a triplet of two planar gradiometers and a magnetometer. To record vertical and horizontal electro-oculogram (EOG) signals, two pairs of bipolar electrodes were placed above and below the left eye and lateral to the right and left eyes. To coregister each participant's anatomical MRI scan with the MEG sensors, four head position indicator (HPI) coils were placed on each participant's head. The MEG data were sampled at 600Hz with the bandpass set to 0.01 – 200 Hz. Responses were averaged on-line for quality control. During the off-line analysis, we re-averaged the data using a bandpass of 0.1 – 200 Hz. The chosen high-pass filter corner frequency was low enough to retain possible slow variations in the dc level of the neural signals while eliminating low-frequency environmental noise. Epochs with EOG peak-to-peak amplitude exceeding 150 µV were excluded from the analysis.

MEG source analysis

Isolation of the SI contribution to the field data was described in detail in two previous studies (Jones et al., 2007, Jones et al., 2009) and we summarize these methods here.

We used equivalent current dipole (ECD) source analysis to locate a primary ECD in SI contralateral to the side of stimulus presentation and all analyses were performed on the time course of activity from this source. We initially modeled the data with two dipoles in contralateral SI and SII determined by a supra-threshold tactile evoked response as described below (consistent evoked activity was not observed in ipsilateral SII, or in other brain areas), and then considered the forward solution from only the SI source. The 2-dipole fit to the field data was optimized using signal-space projection (SSP) (Tesche *et al.*, 1995; Uusitalo & Ilmoniemi, 1997), and a least-squares fit with the dipole forward solution was calculated using the spherically symmetric conductor model (Hamalainen and Sarvas, 1989; Sarvas, 1987). We began by fitting a contralateral SI ECD at the time peak activity in the average response from a suprathreshold stimulus (avg. 12 trials; mean= 68ms s.d.=8ms). We then removed the SI ECD contribution to the field using SSP, and fit a second ECD to the residual ECD in contralateral SII (Nishitani and Hari 2000; Tesche et al., 1995; Uusitalo and Ilmoniemi 1997). Confirmation of dipole locations in the hand area 3b of SI, and SII, were confirmed with anatomical MRI registration in 7 out of 10 participants. Dipoles were manually placed in 2 of the remaining 3 participants such the SI source was placed in the finger representation of area 3b within the anterior bank of the post-central gyrus (Moore et al. 2000; Penfield and Rasmusson 1950; Sastre-Janer et al. 1998; Uematsu et al. 1992; White et al. 1997; Yousry et al. 1997), and the SII

dipole source was placed in the parietal operculum. Both of these subjects belonged to the MA group (36 and 43 yrs). For one of the 10 subjects, anatomical MRI data could not be obtained. In this case, SI dipole localization was determined by field contours on the spherical head model consistent with the predicted position of contralateral SI. This subject belonged to the YA group (31 yrs). The goodness-of-fit of the two-dipole model was larger than 70% in all fit data during peak responses. The effect of the second ECD was then removed using SSP and we refit the SI ECD to the residual. The forward solution from SI ECD location was used to model all responses.

We cannot rule out the possibility that the presence of a continuous auditory mask in our task affected our source localizations or some other aspect of somatosensory oscillations or evoked responses, because of the close proximity between auditory cortex and SII. To mediate localization confounds, we visually inspected the SI and SII localizations on MRI data in 9 of the participants, as described above. Further, we employed an event-related random designed in our tactile stimulation paradigm so that the somatosensory stimuli were not time-locked to the auditory cue. Thus, it is unlikely that the presence of the auditory cue affected the significance of our age-related or between-group comparisons.

MEG spectral analysis

We computed time-frequency representations (TFRs) of the SI ECD timecourses by convolving the SI signals with a complex Morlet wavelet of the form $w(t, f_0) = A\exp(-t^2/2\sigma_t^2)\exp(2i\pi f_0 t)$, for each frequency of interest f_0, where $\sigma_t = m/2\pi f_0$, and i is the imaginary unit. The constant *m* defining the compromise between time and frequency resolution was 7 and the

normalization factor was $A = 1/(\sigma_t\sqrt{2\pi})$. The normalization factor used is the same as that in our previous study (Jones et al., 2009) and is such that the sum of the magnitude of the wavelet coefficients for all frequencies is one, unlike that preserving sum of squared magnitudes of the wavelet coefficients used in, e.g., (Tallon-Baudry *et al.*, 1997), which allowed for better visualization of higher frequency beta activity. The choice of normalization factor did not affect the significance of our age-related results (see **Supplementary Figure 1**). TFRs of power were calculated as the squared magnitude of the complex wavelet-transformed data, as in our previous study (Jones et al., 2009). We generated TFRs for each participant over the entire mu frequency range 7-29Hz for 1000 ms prior to stimulus onset and, in each figure except Figures 1C and 9D, measures of mu (7-29Hz), mu-alpha (7-14Hz) and mu-beta (15-29Hz) power were determined from these TFRs. In Figures 1C and 9D, we calculated power spectral densities (PSDs) using Welch's periodogram method, implemented in Matlab, for frequencies from 3-30 Hz with overlapping 0.5 sec windows. Identical TFR and Welch's calculation methods were employed on both the MEG and model data allowing us to relate the model predictions directly to the experimental observations.

MEG waveform analysis

To uncover age-related differences in the amplitude and symmetry of SI ECD oscillations, we bandpass filtered the SI signal for 1000 ms prior to stimulus onset for each trial over the mu frequency range (7-29 Hz). We then found the local maxima (peaks) and minima (troughs) in the filtered data over the prestimulus period and calculated peak-to-trough time differences (illustration in Jones et al., 2009). To calculate the amplitude of the oscillations, we identified

the time points corresponding to each peak and trough, used these to obtain signal values from the unfiltered SI data, and measured the distance between the absolute value of each peak and trough. We then computed a symmetry index on the absolute values of the unfiltered peak and trough data using the equation (peak – trough)/(peak + trough). Thus, a positive symmetry index indicates greater amplitude peaks and a negative value indicates greater amplitude troughs, whereas a value close to zero indicates that an oscillation was symmetric around zero.

SI ECD evoked responses were averaged over threshold-level stimulation trials (n=200 trials per *participant*) for each participant and then averaged across YA and MA groups (see group definitions in statistical analysis section below). For comparisons of M50 and M70 peak response amplitudes, these values were calculated as the mean from 45-55ms, and 75-90ms, respectively. For comparison of M70 peak latencies, the M70 response was calculated as the minimum in 60-90 ms; we then calculated the slope of the response from the M70 minimum to 100 ms.

Statistical analysis

For each measure of interest in the MEG data (mu/alpha/beta power, TFR alpha to beta ratio, oscillation symmetry index, oscillation amplitude, and evoked response parameters) significance of age related changes was determined by sorting the data by increasing age across the 10 participants and performing a linear regression analysis. In addition, for direct comparison to computational model results, we tested group differences in the MEG data from the 5 youngest (YA; mean age = 26 yrs) and 5 oldest (MA; mean age = 36 yrs) participants using

two-tailed independent sample *t*-tests. Group membership was assigned based on a median split of age. Significance persisted in these group comparisons despite the small group sample sizes. Paired *t*-tests were similarly used to assess significant differences across trials in the YA and MA model simulations.

Computational Neural Model

The computational neural modeling used in the present study was previously developed and used for studies of the neural basis of MEG measured SI tactile evoked responses and spontaneous rhythmic activity (Jones *et al.*, 2007; Jones *et al.*, 2009). The details of the model, methods, supporting literature, and the code for our original smaller network model (Jones *et al.*, 2007) is available to the public on the NEURON modelDB website at http://senselab.med.yale.edu/modeldb/ShowModel.asp?model=113732. Here, we describe key features of the model construction.

Local Network Configuration

The SI cortical column network model consisted of a 2-dimensional grid 100 multiple-compartment excitatory pyramidal neurons (PNs) with 35 single compartment inhibitory interneurons (INs) evenly interleaved per layer in layers II/III and V (Jones *et al.*, 2009). **Supplementary Figure 2** shows a schematic illustration of the local network structure. Fast and slow excitatory (AMPA/NMDA) and inhibitory (GABAA/GABAB) synapses were simulated with a symmetric 2-dimensional Gaussian spatial spread and inverse Gaussian delay with rise/decay time constants and reversal potentials, respectively as: AMPA 0.5/5ms, 0mV; NMDA 1/20ms,

0mV; GABAA 0.5/5ms, -80mV; GABAB 1/20ms, -80mV. The maximum synaptic conductances and Gaussian weight space constants are described in Table 1 of Jones et al., 2009.

Morphology and physiology of individual cells

The IN in each layer were simulated with single compartments and contained instrinsic current kinetics (sodium, potassium, and leak currents) that created spiking activity. Layers II/III and V PN were simulated with 8 and 9 segments, respectively, and contained active currents in both the somatic and dendritic compartments, such that layer II/III PNs produced adapting spike trains (via sodium, potassium, adaptation M-current, and a leak current) and the layer V PNs produced bursting responses to injected current (via the addition of two types of calcium currents, a mixed cation h-current, and a potassium-activated calcium current).

Exogenous drive to the SI network

We modeled ongoing mu rhythms and SI evoked responses by stimulating the network with sequences of exogenous inputs to the local SI model. A full description and default parameters for these drives are summarized in Tables 1 and 2 and in (Jones *et al.*, 2009). Here, we briefly detail important features for the current analysis.

Architecture of feedforward (FF) and feedback (FB) drive

FF drive emerged from layer IV (modeled to reflect lemniscal thalamic input) and contacted the layer II/III neurons, with a delayed and weaker connection to layer V neurons (see **Supplementary Figure 2B** for illustration and poststimulus dendritic compartments). For all FF

inputs, the maximal conductance onto INs was twice as strong as that onto PNs. FB drive (representative of input from high-order cortices or nonspecific thalamic sources) contacted the distal apical dendrites of each PN neural population and layer II/III INs (**Supplementary Figure 2C**).

Stochastic ongoing rhythmic FF and FB drive

We have previously shown that SI mu rhythms analogous to those observed experimentally can be simulated with ongoing ~10Hz FF followed by FB input to the SI network (Jones *et al.*, 2009). A schematic illustration of this input is shown in **Supplementary Figure 3** and is described here in detail. The ongoing rhythmic input was simulated by delivering 10 "burst" spike trains, each consisting of 2 spikes with an ISI = 10 ms to the SI network in a FF synaptic activation pattern. All 10 bursts arrived approximately every 100 ms such that the arrival time for each burst was chosen from a Gaussian random distribution (mean ISI 100 ms, default of variance of 10 input bursts = 400 ms). On each cycle, an input patter with the same number of bursts and arrival time statistics reached the SI network in a FB synaptic activation pattern. This input, however, was delayed from the FF input by 5 or 50 ms for the simulations in the present study. Changes in the effective strength of the ongoing rhythmic FF and FB input were simulated by varying the number of "bursts" (i.e., number of 2-spike burst events) on each cycle, the variance of the arrival time of each "burst" at the SI network on each cycle of the 10Hz input, or the maximal postsynaptic conductance of the inputs.

Each simulation was stochastically regulated by the arrival time of each of the FF and FB input bursts as follows. On each cycle of the rhythmic input, the timing of each 2-spike burst event was chosen from gaussian distributions with means fixed at 100 ms intervals (e.g., 0, 100, 200 ms, etc) and a variance of 400 ms. All other parameters were fixed during each simulation with the following default values: FF-FB delay = 5 ms, number of input bursts = 10, variance of input bursts = 400 ms, maximal FF and FB postsynaptic conductances 0.4 pS onto PN and 2 x 0.4=0.8 pS onto IN. Synaptic weights and delays were distributed by a symmetric 2-D Gaussian spatial profile with maximal weight and minimal delay (0 ms) for FF inputs to layer II/III and 1 ms to layer V) in the center and weight space constant = 100 and delay space constant = 100 for all connections.

Evoked response inputs

SI tactile evoked response were simulated with a sequence of FF input, followed by FB, followed by a re-emergent late FF (LFF) input (see **Table 2** for timing and post-synaptic conductance) at various phases in a simulated mu-alpha and mu-beta cycles and averaged (Jones *et al.*, 2007; Jones *et al.*, 2009).

Calculation of net current dipole

The SI ECD moment was calculated as the net sum across the PN populations of the intracellular currents flowing in a direction perpendicular to the longitudinal axis of the apical dendrite multiplied by the corresponding length of the dendrite (Murakami et al., 2003, Murakami and Okada, 2006, Jones et al., 2007, Jones et al., 2009).

Simulations

All simulations used the shareware software program NEURON available at http://www.neuron.yale.edu/neuron/. The fixed-time-step-implicit-Euler integration had a time increment of dt=0.05 ms. Simulated evoked responses were smoothed by convolution with a 15 ms box filter. Upon publication, the code that produced all simulated data in this paper will be available on the ModelDB website http://senselab.med.yale.edu/senselab/modeldb/.

Results.

MEG experiment

Mu rhythm changes with age

To examine the effects of middle age on the spontaneous mu rhythm in SI, we computed the average power in the calculated TFRs over all trials for the entire mu range (7-29Hz) from the 1000 ms prestimulus time period, as well as for the mu-alpha (7-14Hz) and mu-beta (15-29Hz) subcomponents. All references to power in our results were derived from this TFR calculation and the same analysis was used in all participants, except in **Figure 1C** where power spectral densities (PSDs) were calculated with Welch's methods (see Methods). Regression analyses showed a significant age-related increase in average mu power (**Figure 1A,** top left panel; r^2 = .58, p = 0.002). The change in mu power was largely driven by an age-related increase in mu-beta (**Figure 1A**, bottom left panel; r^2 = .71, p = 0.001). Mu-alpha power showed only a trend toward a positive correlation with age (r^2 = .21, p = 0.07, data not shown). Group comparison of time-averaged TFR power between the 5 YA and5 MA confirmed an age-related increase in

mu ($t_{(8)}$ = -2.6, p = 0.03) and mu-beta ($t_{(8)}$ = -2.4, p = 0.04), but not mu-alpha ($t_{(8)}$ = -1.7, p = 0.12) power (**Figure 1A**, right panels). These age-related changes are visible in average prestimulus TFRs for the grouped YA and MA (**Figure 1B**). The average TFRs showed a clear predominance of mu-alpha in the YA, whereas the MA showed enhanced mu-beta in addition to slightly increased mu-alpha power. Age related increases in mu-power, and specific enhancement of mu-beta activity, are also apparent in PSD calculations averaged across groups (**Figure 1C,** mean and s.e.). A large peak near 10Hz and a small peak near 20Hz are apparent in the PSD from the MA adults, while only a smaller 10Hz peak is prevalent in the YA.

Effects of age on relative dominance of mu-alpha and mu-beta

To compare the relative dominance of mu-alpha vs. mu-beta power with age, we calculated the ratio of TFR mu-alpha to mu-beta power in small time windows. Specifically, we calculated a TFR for each 1 sec prestimulus epoch. We then divided the prestimulus TFR into 10 bins (100 ms each) for each epoch and computed the mean power in the mu-alpha and mu-beta ranges in each bin, averaged these measures over all trials, and then computed a ratio of mean mu-alpha to mean mu-beta power for each participant (referred to as the TFR ratio). We found a marginally significant negative correlation between the ratio of mu-alpha to mu-beta power and age (r = -.52, p = 0.06, data not shown), indicating that YA showed dominant mu-alpha, while MA showed a dominant mu-beta, and that these changed almost linearly with age We then computed group average ratios for the 5 YA and 5 MA (**Figure 1D**) and found a trend toward a decrease in the ratio in the MA, compared to YA ($t_{(8)}$ = 2.1, p = 0.07).

Effects of age on oscillation symmetry and amplitude

We investigated two additional features of the SI mu rhythm, the symmetry of the oscillation waveform around zero and the amplitude of the oscillation. We first identified the peaks and troughs of oscillations occurring during each 1000 ms prestimulus period and calculated a peak-to-trough symmetry index for each trial. We previously reported that the symmetry index did not differ significantly from zero when grouped across all 10 participants (Jones *et al.*, 2007; Jones *et al.*, 2009). Here, we present a similar analysis with the data grouped by age. **Figure 2A** shows a grand total histogram (200 trials per participant) of the symmetry index values color coded for each group (red YA, blue MA**).** A one-sample *t*-test confirmed that the mean symmetry index over all trials was not significantly different from zero for either group (YA, p = 0.22; OA, p = 0.41). Further, the mean symmetry indices did not differ significantly between the two groups ($t_{(8)}$ = -0.92, p = 0.38). Linear regression analysis confirmed that the symmetry indices did not correlate significantly with age (r = .26, p = 0.46).

We then used similar analysis to examine peak-to-trough amplitudes between the groups (**Figure 2B**), and found that the mean amplitudes over all trials were significantly greater in the MA, when compared to YA ($t_{(8)}$ = -3.4, p = 0.01; **Figure 2C**). Linear regression analyses confirmed that amplitudes increased significantly with age (r = .75, p = 0.01; **Figure 2D**). This increase in oscillatory amplitude contributed to the increase in mu power with age. **Figure 2E** depicts example single trial 1Sec waveform and TFR time-course calculations for a YA and MA. The oscillation waveforms emphasize the difference in the amplitude of the oscillations across groups. The single trial TFR time-courses highlight the fact that the alpha and beta components

are variable in time and power on single trials and often non-overlapping, a measure that was quantified in (Jones et al, 2009). These single trial features are directly comparable to the model data (**Figure 7E**).

Effects of age on early evoked responses

To investigate the effect of middle age on post-stimulus SI dynamics, we computed average evoked responses from a threshold-level tactile stimulus (175 ms poststimulus, n = 200 trials per participant) for each participant. Previous results have shown that the tactile stimulus employed created a waveform from 0 - 175 ms post-stimulus with consistent characteristics across participants. This evoked response is dominated by a negative polarity peak at ~70ms (M70) and positive polarity peaks at ~50, ~100 and ~135ms (M50, M100 and M135, respectively) (Jones et al., 2007, Jones et al., *2009*). These peaks persisted in the current analysis when averaged across YA and MA groups (**Figure 3**). When compared to YA, MA showed a significantly greater M70 peak (M70 = mean 75-90 ms, $t_{(8)}$ = -3.1, p = 0.01) and a trend toward a greater M50 peak (M50 = mean 45-55 ms, $t_{(8)}$ = -2.1, p = 0.06). A regression analysis on the M70 peak response confirmed that the M70 peak amplitude showed a trend toward increasing significantly with age (r = .6 , p = 0.10). Further, MA showed a significantly longer latency of the M70 minimum (defined as the minimum between 60-90 ms: YA mean = 79.9 ± 11.1 ms, MA mean = 63.3 ± 4.3 ms, $t_{(8)}$ = 2.5, p = 0.03) and exhibited a trend toward a steeper slope from the M70 minimum to the M100 peak (M100 = 100 ms response; YA mean = 2.0 ± 1.0, MA mean = 4.7 ± 2.5, $t_{(8)}$ = -1.9, p = 0.09).

Summary of changes in MEG SI activity with age

In summary, we found that SI activity in MA was characterized by a preferential increase in mu-beta power (**Figure 1A-C**), resulting in a trend toward a TFR mu-alpha to mu-beta ratio > 1 in YA but < 1 in MA (**Figure 1D**). In addition, while the SI oscillation waveform remained symmetric around zero in both groups, the amplitude of the oscillation was significantly increased in MA compared to YA (**Figure 2**). These changes occurred in conjunction with a corresponding increase in evoked response magnitudes and timings (**Figure 3**), suggesting that the neural mechanisms that cause changes in the spontaneous mu rhythm may modulate changes in the evoked response. Below we use a biophysically realistic computational neural model of SI to predict the neural mechanisms underlying these changes.

Predictions Generated by Computational Neural Model

Previous Modeling Results

We developed a laminar model of SI to study the neural origin of the MEG measured SI tactile evoked responses and spontaneous mu rhythms (Jones et al., 2007, 2009). Here we review details of our previous results that are pertinent to our current study on the effects of middle age.

The model contained a local synaptically coupled network of 100 excitatory pyramidal neurons and 35 inhibitory interneurons in infra- and supra-granular layers. It was driven exogenously with feedforward (FF) and feedback (FB) excitatory inputs that contact all neurons in layer II/III and layer VI, respectively (**Supplementary Figure 2**). The SI current dipole signal that we

recorded with MEG was simulated as the net intracellular current flow across the pyramidal neuron populations (Okada *et al.*, 1997; Murakami *et al.*, 2003; Jones *et al.*, 2007; Jones *et al.*, 2009). This model accurately reproduced characteristic features of the recorded spontaneous SI mu rhythm when driven with a stochastic sequence of ~10Hz FF input followed by ~10Hz FB input (Jones et al., 2009, see **Supplementary Figure 3** for schematic illustration of rhythmic input). The relative mu-alpha to mu-beta power expressed in the network depended on the delay between the rhythmic inputs and on the relative strength of those inputs. Nearly equal mu-alpha to mu-beta expression occurred when the ~10Hz rhythmic FF and FB arrived at the network almost synchronously (5 ms delay), whereas asynchronous inputs (50 ms delay) created a predominantly mu-alpha frequency rhythm. These results were derived previously by calculating averaged ratio of mu-beta/mu-alpha power over a 1 sec time window (Jones et al., 2009).

Figure 4 shows the time course of the expressed mu rhythm with a 1 sec TFR when the mean delay between the rhythmic FF and FB inputs was set to 5 ms (**Figure 4A**) or 50 ms (**Figure 4B**) (other parameters were set on each cycle of the rhythmic input at FF and FB input number = 10, input variance = 400, and postsynaptic conductance=0.4e-5 milli-Siemens). **Figures 4C** and **D** show the corresponding waveforms of the oscillations, and **Figures 4E** and **F** show mean mu-alpha and mu-beta powers over the 1 sec time window. When the FF-FB delay was 5 ms, the expressed mu-alpha and mu-beta powers were nearly equal and the oscillation waveform was small in amplitude and 'jagged,' reflecting higher frequency components. When the delay was 50 ms, the oscillation was larger in amplitude and smoother with mu-alpha power dominance.

Our previous study also reported that, with a fixed delay between FF and FB inputs, increasing the strength of the rhythmic FF inputs enhanced mu-alpha power, while increasing the strength of the FB inputs enhanced mu-beta power. The strength of the input was modulated in three ways: increased synchrony of the 'input burst' on each cycle of the 10Hz input; more spikes in the 'input burst'; and greater post-synaptic conductances of the driving inputs (**Supplementary Figure 3)**. These results were also derived previously by calculating averaged ratio of mu-beta/mu-alpha power over a 1 sec time window (Jones et al., 2009). For further illustration of the effects of increased FF and FB input strength on mu-alpha and mu-beta expression, the TFRs and waveforms over the entire 1 sec window are shown in **Supplementary Figure 4**, over various changes in input strength.

Predictions on the neural origin of differences in the mu rhythm with age

Based on the previous model results, we arrived at two predictions as to the neural origin of increased mu-beta expression in the MA group. One prediction, referred to as Prediction A, is that the mu-beta dominance occurs from a decrease in the delay between the 10Hz FF and FB input creating the rhythm, from a near 50ms delay in YA to a near 5ms delay in MA. An alternate prediction, referred to as Prediction B, is that in both groups the FF-FB delay is 5 ms, but MA have effectively 'stronger' FB inputs compared to FF inputs creating mu-beta dominance.

We tested these two predictions to see which would reproduce the mu-beta increase MA and meet other defining characteristics of the oscillation, including a maintained symmetry index near zero, larger amplitude oscillations in MA, and a TFR mu-alpha to mu-beta ratio greater than 1 in YA and less than 1 in MA.

Testing Prediction A

To test prediction A, we began with a parameter regime that reproduced a mu rhythm consistent with the SI MEG data pooled across the entire sample (Jones et al., 2009, FF = FB conductance = 0.4e-5 mS, FF = FB number of input spikes = 10, FF = FB variance of input spikes = 400 ms). We then compared the effects of 5 ms and 50 ms delays between the rhythmic ~10Hz FF and FB input on the symmetry index and TFR mu-alpha to mu-beta ratios of the produced oscillation. Consistent with the MEG data, we found that both delays produced a symmetry index that was not significantly different from zero. In addition, the 5 ms delay created a TFR mu-alpha to mu-beta ratio that was < 1, and the 50 ms delay created a TFR mu-alpha to mu-beta ratio that was > 1 (**Figure 5**), consistent with the YA vs MA MEG data (**Figure 1D**). With at 50 ms delay, however, the TFR ratio was more than five times larger than the TFR ratios in the MEG data (**Figure 1D**). This difference in TFR ratios came from the fact that this simulation showed virtually no mu-beta and only large amplitude alpha oscillations (**Figures 4B** and **4D**), which was not consistent with the MEG results. Further, the model TFR ratio was more than five times greater than the experimental data over a range of FF and FB postsynaptic input conductances (data not shown).

Thus, predication A, that the mu-beta dominance in MA arises from a decrease in the delay between the 10Hz FF and FB inputs from ~50 ms to ~5ms, was not supported, because the TFR mu-alpha to mu-beta ratios and oscillation amplitudes were excessively large when a 50 ms delay was used. Next, we tested whether prediction B that YA and MA each had near synchronous FF-FB rhythm input (i.e., 5 ms delay), with effectively stronger FB inputs in MA, could reproduce each of the observed age-related features of the MEG SI signal.

Testing Prediction B

To test prediction B, we assumed that the delay between the FF and FB inputs remained constant near synchrony at 5 ms for both groups. We then asked whether a biophysical change in the relative strength of the FF and FB inputs could cause the TFR ratio to go from a value above 1 for YA to below 1 for MA while the symmetry index remained fixed near zero for both groups. We calculated the symmetry index and TFR mu-alpha to mu-beta ratio for various FF and FB input strengths simulated as changes in parameters controlling the effective strength of the FF and FB 'input burst' on each cycle of the ongoing ~10Hz rhythm (**Supplementary Figure 3**). These changes were simulated with increases in the relative weight of the postsynaptic conductance of the 'input burst' (**Figure 6A**), number of spikes in the 'input burst' on each cycle (**Figure 6B**), and variance of spikes in the 'input burst' on each cycle (**Figure 6C**).

We found that increasing the postsynaptic conductance of the FB input relative to a fixed FF post-synaptic conductance decreased the symmetry index from above to below zero, and drove the TFR mu-alpha to mu-beta ratio from a value greater than 1 to a value less than 1 (**Figure 6A**

left panel). When we increased the FF weight relative to a fixed FB weight (**Figure 6A right panel**), the opposite effect emerged.

The symmetry index was above zero when the FF input conductance was stronger, because on each cycle of the rhythmic ~10Hz input the intracellular current flow (our measure of MEG current dipole activity) was being driven more strongly up the pyramidal neuron apical dendrites, creating an oscillation that shifted toward more positive polarity. In contrast, the symmetry index was below zero when the FB input conductance was stronger, because intracellular current flow was driven more strongly down the pyramidal neuron apical dendrites, creating an oscillation that shifted toward more negative polarity (compare oscillation waveforms in the left and right hand middle panels of **Supplementary Figure 4A**). When the FF and FB input conductance were equal the symmetry index was near zero. The TFR ratio was above 1 when the FF input conductance was stronger because alpha power exceeded beta power, but the TFR ratio was below 1 when the FB input conductance was stronger due to greater beta than alpha power (compare TFR spectrograms and bar plots of power in **Supplementary Figure 4A**).

While the described increase in relative postsynaptic conductance of the ongoing rhythmic FB input created changes in TFR mu-alpha to mu-beta ratios that mimicked differences between YA and MA (i.e., TFR ratios from > 1 to < 1 with increased FB conductance, **Figure 6A**), the symmetry index did not remain fixed near zero, which is inconsistent with the MEG data.

We then tested whether changes in the number or variance of spikes in the 'input bursts' on each cycle of the rhythmic ~10Hz FF and FB input (**Supplementary Figure 3**) could create the observed change in the TFR ratio in MA, while maintaining a stable symmetry index. We found that increasing the number of FB inputs relative to a fixed number of FF inputs decreased the TFR mu-alpha to mu-beta ratio from above 1 to below 1, as occurred in MA (**Figure 6B**). This change, however, also decreased the symmetry index. In contrast, increasing the FB input variance (decreasing the synchrony of the inputs bursts) compared to a fixed FF input variance, and vice versa, maintained a relatively stable symmetry index ($p<0.01$) (**Figure 6B**), while also increasing the TFR mu-alpha to mu-beta ratio from below 1 to above 1. Thus, we conclude that, for a fixed 5 ms delay between the 10Hz FF and FB input, increase in synchrony of the FB input bursts on each cycle of the input (i.e., decrease in variance) can drive the TFR mu-alpha to mu-beta ratio from above to below one while maintaining a stable symmetry index near zero, in agreement with changes that occur from YA to MA in the MEG data.

Reproducing amplitude differences

The remaining age-related difference in SI activity that we investigated the neural source of with our computational model was the change in the amplitudes of the oscillations with age, which were about two times greater in MA, compared to YA (**Figure 2**). We began by testing whether the simulated changes in the relative FF and FB variance that thus far accurately reproduced the different TFR ratios and symmetry indices in the two groups (YA, FF input variance = 400, FB input variance = 600; MA, FF input variance = 400, FB input variance = 200) also created a difference in the oscillation amplitudes. We found that, for a fixed FF variance,

increasing the FB variance, which decreased the mu-beta power and was consistent with the YA simulations thus far, slightly increased the amplitude of the oscillations (**Supplementary Figure 4**), and vise versa. This effect is the opposite of that seen in the MEG data, where YA had smaller amplitude oscillations.

Next, we simulated the decrease in the amplitude of the oscillations in YA by decreasing the strength of both the FF and FB inputs (via the postsynaptic conductance), while maintaining a larger FB input variance in YA. We found that when the weight of postsynaptic conductances of FF and FB inputs were 50% smaller, the amplitude of the oscillations were approximately two times smaller, consistent with the MEG data for YA (**Figure 7A** compared to **Figure 2C**).

Thus, our model showed that the observed age-related differences in the SI mu rhythm could be reproduced by maintaining a fixed and almost synchronous delay (5 ms) between the ongoing ~10Hz FF and FB inputs in YA and MA. Further, in MA the strength of both the rhythm FF and FB inputs were increased, and the variance of the FB inputs was decreased (increased synchrony). **Table 1** describes the parameter regime that reproduced these results. **Figures 7A-D** show results from simulations using these parameters averaged over 25 trials (mean and s.e.) for the calculated amplitudes, TFR ratios, symmetry indices, PSDs, and time-averaged TFR power estimates in YA and MA, each of which is consistent with the MEG data.

Figure 7A (compare to **Figure 2C**) shows that the mean oscillations amplitudes are significantly smaller in the YA compared to MA simulations ($p < 0.001$). The actual amplitude of the

simulated SI ECD oscillation in the model was multiplied by a scaling factor of 60,000 (see also **Figure 7E**) and predicts that on the order of 60,000 X 200 PNs (100 in each layer) = 1.2 million PNs contribute to the observed SI mu rhythm. This prediction is in line with an estimated cortical space that lies within the volume of the human hand representation, defined as the omega shaped bend in the postcentral gyrus (Moore et al., 2000). **Figure 7B** (compare to **Figure 1D**) shows that the mean TFR mu-alpha to mu-beta ratio is significantly larger in the YA compared to MA simulations ($p < 0.001$), while this effect was marginally significant in the MEG data ($p = 0.06$). We found that the symmetry indices for the YA and MA simulations were significantly different ($p < 0.001$), unlike the MEG data. As in the MEG data, however, neither group means differed significantly from zero. **Figure 7C** (compare to **Figure 1C**) shows PSDs calculated for each group. Similar to the MEG data, the MA simulations have overall greater mu power than the YA simulations, and the model MA data has peaks near 10 and 20Hz while the YA data only has a clear peak near 10Hz. **Figure 7D** (compare to **Figure 1A**, right panel) shows that time-averaged TFR power significantly increases between YA and MA simulations in the mu, alpha and beta ranges ($p<0.001$, in each case). **Figure 7E** (compare to **Figure 2E**) shows the variability on single 1 sec trials in the model SI waveform and TFR time-courses. As in the MEG data, on single trials, the oscillation amplitudes are clearly smaller and TFR alpha and beta components are variable in time and power.

Next, we examined how the YA and MA parameter regimes influenced the SI evoked response in the model.

Predicted neural origin of age dependent difference in evoked responses

We have previously shown that the observed tactile evoked response can be reproduced in the model by simulating a sequence of driving inputs to the network that consists of a FF input at ~25 ms poststimulus, followed by a FB input at ~70 ms, and a subsequent late FF input at ~135 ms (Jones *et al.*, 2007). This sequence could be interpreted as initial lemniscal thalamic input arriving to the cortex at ~25 ms, followed by a feedback input from a high-order cortical area or a nonspecific thalamic source to the supragranular layers at ~70 ms, followed by a re-emergent lemniscal thalamic input at ~135ms. In simulating the evoked response in this manner, we reproduced the timing, magnitude and polarity of peaks in the SI ECD tactile evoked responses (Jones *et al.*, 2007).

Previous model results also showed that the power of the prestimulus mu rhythm directly influenced the magnitude of the evoked response (Jones et al., 2009). Specifically, the model showed that higher prestimulus mu-alpha and mu-beta increased the amplitude of an early response at approximately 50 ms (M50) via increased depolarization in pyramidal and inhibitory neurons, and decreased the subsequent M70 peak response due to a preferential recruitment of inhibition (Jones et al., 2009). The prestimulus mu power did not affect the later > 70 ms components of the evoked response. These predictions were confirmed in the MEG data (Jones et al., 2009).

In the current study, we tested whether differences in the parameters of the model that reproduced the age differences in the prestimulus mu rhythm could also account for the age differences in the evoked response.

We simulated an evoked response during an ongoing mu rhythm in YA and MA parameter regimes described in **Table 1**. The evoked response input conductances were consistent with those that gave accurate amplitudes of a threshold level response in our previous paper (Jones et al., 2009). However, analogous to the simulated differences in the ongoing mu rhythm for YA vs MA, in the YA simulations the postsynaptic conductances of the evoked FF-FB-LFF input sequence were decreased by 50% (**Table 2**). We simulated an evoked response to begin at 20 equally spaced 'starting phases' in a mu-alpha cycle and 10 in a mu-beta cycle for each group (Jones et al., 2009) and averaged the results. The 'starting phase' was defined as the time of the initial FF leminiscal thalamic input to the network that was followed 45ms later by a FB input, and 65ms later by a LFF input.

The described changes in the prestimulus mu rhythm and in the evoked response conductances were sufficient to produce the observed age-related changes in the MEG evoked response data (compare **Figure 8** to **Figure 3**). Specifically, compared to the YA simulations, the MA simulations showed a significantly greater M70 peak (M70 = mean 75-90 ms, $p = 0.01$; **Figure 8**) and a trend toward a greater M50 peak (M50 = mean 45-55 ms, $p = 0.08$). Further, the MA simulations showed a significantly steeper slope from the minimum M70 response (defined as the minimum between 60-90 ms for each trial) to the 100 ms M100 peak (YA model mean = 1.1

± 1.7, MA model mean = 5.7 ± 2.2 , $p < .0001$). While the latency of the M70 minimum was slightly later in the MA model data, this difference was not significant in the model data (YA model mean = 77.8 ± 8.2, MA model mean = 79.5 ± 6.5, $p = 0.39$). Notably, there is an apparent discrepancy between the MEG and model data in that the amplitude of the evoked response after 100 ms appears to remains larger in the simulated MA compared to YA data. However, this effect did not reach significance.

Summary of predicted neural origin of changes in MEG SI activity in middle age.

Our model predicted that the delay between the 10Hz FF and FB inputs that created the ongoing SI mu rhythm was relatively stable with age and nearly synchronous (~5 ms). In MA, the variance of the FB 'input bursts' became smaller relative to the variance of the FF inputs (i.e., the FB inputs arrive more synchronously to the SI network), and the strength of both the FF and FB inputs, simulated as increased post-synaptic conductance, was larger. These manipulations in the model accurately reproduced the age-related characteristics of the MEG data, including larger amplitude oscillations in MA (compare **Figure 7A** to **Figure 2C**), a trend toward a TFR mu-alpha to mu-beta ratio >1 for YA and <1 for MA (compare **Figure 7B** to **Figure 1D**), a symmetry index that was not significantly different from zero for either group , and qualitatively similar PSDs (compare **Figure 7C** to **1C**) and individual trial waveforms and spectrograms (compare **Figure 7E** to **Figure 2E**). Further, analogous changes in the parameters of the evoked response inputs (increased postsynaptic conductances of the FF-FB-LFF inputs) created the differences in the tactile SI evoked response (compare **Figure 8** and **Figure 3**). Thus, the model showed that the predicted neurophysiological changes in MA accounted for the

changes in the spontaneous SI mu rhythm and in the evoked response and hence these neurophysiological changes explicitly link these phenomena.

Discussion

The present study compared the spontaneous SI mu rhythm and tactile evoked responses in YA and MA using MEG, and used a computationally realistic laminar model of SI to make specific predictions about the underlying neurophysiological bases for the observed age differences. To document changes that occur during middle age, we restricted our study to healthy participants between the ages of 23-43 years of age. Linear regression and group comparison analyses of the MEG data revealed a significant age-related increase in prestimulus mu power in SI calculated from TFRs, driven predominately by the emergence of greater mu-beta dominance in MA (**Figure 1**). In addition to this increase in TFR mu power, we found that the amplitude of the prestimulus oscillations was greater in MA, but that the symmetry of the oscillations was not affected by age: both YA and MA exhibited largely symmetric oscillations (**Figure 2**). We found that when averaging across groups the early evoked response in SI also showed age-related changes, with the MA showing a significantly larger and delayed M70 peak and a trend toward a greater M50 peak and slope from the M70 to M100 response (**Figure 3**). We emphasize that these data were not initially collected to address questions of aging. A more extensive data set will be required to elaborate the current findings and delineate more subtle aspects of the impact of aging on somatosensory rhythmogenesis and its correlation with tactile performance.

By testing a variety of biophysically interpretable parameters, we reproduced each of the age-related changes in our computational model of SI. Expanding on previous modeling results that showed MEG-measured SI mu rhythms could be reproduced by simulating ~10 FF input followed by FB input (Jones et al., 2009), our current results predicted that the delay between the rhythmic 10Hz FF and FB input remains nearly synchronous (~5 ms) in YA and MA. Further, the model predicted that by middle age there is a generalized strengthening of both the rhythmic FF and FB inputs and the variance of the FB inputs is decreased. In this manner, the model was able to reproduce oscillations that are largely symmetric, but that exhibit increased amplitude and a greater mu-beta dominance in MA, when compared to YA (**Figure 7**). Further, using the same parameter changes, the model was also able to reproduce the observed effects of age on the early evoked response (**Figure 8**), simulated as a sequence of FF – FB – LFF inputs (based on Jones et al., 2007). Thus, using a realistic computational model of laminar SI, we have derived specific predications about the neurophysiological changes that occur with healthy aging that give rise to differences in both MEG-measured SI rhythmic and evoked response activity between YA and MA.

Age-related changes in the mu rhythm

The present finding of an age-related increase in the power of the spontaneous somatosensory mu rhythm, driven primarily by the mu-beta component in our analysis, and to a lesser extent by mu-alpha, is consistent with prior studies that reported greater alpha and beta power in sensorimotor EEG electrodes in older adults during the execution of a motor task (Sailer *et al.*, 2000). In contrast, studies that have examined spontaneous alpha and beta rhythms in non-

somatosensory areas tend to report age-related decreases in alpha power and coherence in posterior cortices (Niedermeyer, 1997; Babiloni *et al.*, 2006; Rossini *et al.*, 2007). These contrasting results may arise from a critical difference in the age range of the participants examined in previous reports compared to the present study. We limited our age range to YA and MA, whereas previous studies have typically sought differences that occur much later in the lifespan (e.g., older adults above 60 years of age). Thus, the present study provides new information about changes in the somatosensory system that occur early in the course of healthy aging. Taken together with findings from past studies that examined older participants, our results raise the possibility that spontaneously occurring low frequency rhythms tend to exhibit an inverted U function, increasing in power during middle age and diminishing with advanced age.

In addition, prior studies tended to focus solely on changes in the alpha rhythm, rather than assessing both alpha and beta rhythms, and in fact, consistent with our results, one study that did examine spontaneous beta rhythms reported an increase in high-beta power (25-30 Hz) from 30 to 60 years (Roubicek, 1977). The general lack of investigation of beta frequency activity may be due, in part, to differences in recording techniques and data analysis methods: When measured using MEG and calculating TFRs of power, as in the present study, the somatosensory mu rhythm contained prominent mu-alpha and mu-beta subcomponents, whereas when measured using EEG, the dominant alpha component alone was typically observed (Kuhlman, 1978; Zhang & Ding, 2010).

A prior study by Nikulin and Brismar (2006) investigated the influence of age on cross-frequency phase-locking between alpha and beta activity measured with EEG across the brain. This study found that 10-20Hz phase-locking was strongest in middle age (defined as 25.7-45 yrs) compared to young (14.3-25.7 yrs) and older age (45.0-65.6 yrs). Further, these effects were most predominant in posterior areas, as compared to frontal and central areas. Cross frequency phase-locking between alpha and beta frequencies has also been shown to be a salient characteristic of MEG measured activity, including above rholandic regions, that increased with a mental arithmetic task (Palva et al., 2005). This effect was strongest over short inter-areal distances (Palva et al., 2005). Based on these findings, we investigated cross-frequency 10 to 20Hz phase-locking (measured with a phase-locking statistic (PLS) as in Lachaux et al., 2009) in our prestimulus SI signal and the influence of age on this measure (**Supplementary Figure 6**). We found that the PLS was more significant in the YA than MA groups (mean PLS YA=0.04, mean PLS MA=0.08) but that there was no significant difference between groups (p=0.39, **Supplementary Figure 6A**) nor a linear correlation with age (p=0.3, **Supplementary Figure 6B**). The model data showed a similar trend of YA simulations having smaller PLS than MA, but neither group reached significance in the model data, likely due to the smaller number of trials in each group (**Supplementary Figure 6C**). Our finding that the mean PLS value was less significant in MA age seems to contrast the finding of Nikulin and Brismar 2006. However, their middle age group contained participants with a range of ages that spans both our YA (23-31 yrs) and MA (33-43 yrs) classifications and a valid comparison between studies cannot be made.

Given that several subjects showed significant 10-20Hz phase-locking (**Supplementary Figure 6B**), it was also possible that our symmetry index measures where biased by this 2:1 phase-locking which can be sensitive to changes in alpha-beta phase differences and alpha-beta amplitude ratios. Therefore, we also tested if there was a correlation between symmetry indices and PLSs and found that there was no significant correlation (p=0.87, **Supplementary Figure 6D**).

Age-related changes in somatosensory evoked responses

Our analyses also revealed that the early components of the tactile SI evoked response differed between YA and MA. The most notable difference was a significantly increased magnitude of the M70 peak in MA, compared to YA, which the model predicted resulted from stronger post-stimulus feedback input in MA. This peak also occurred significantly later in MA and the slope between 70 and 100 ms was steeper than in YA. Other studies of somatosenory evoked potentials in MA and OA that used stronger median nerve stimulation also reported greater magnitudes and latencies of peaks in the first 100 ms following stimulus onset (Luders, 1970; Desmedt & Cheron, 1980; Adler & Nacimiento, 1988; Kakigi & Shibasaki, 1991; Ferri *et al.*, 1996; Stephen *et al.*, 2006). The present study is the first to report that these increases occur in a localized region of SI during delivery of threshold-level tactile stimuli and that they appear in middle age. Further, our study is the first to investigate concomitant changes in both the prestimulus and evoked response period using the same experimental paradigm.

Model-based predictions about the neural origin of age differences

The present study goes beyond previous work by employing a biophysically realistic model of laminar SI to make specific predictions about the neural substrates that give rise to the age-related changes in the MEG data. This model provides unprecedented insight into the putative neural substrates underlying age-related changes in the spontaneous mu rhythm and the evoked response. We have previously shown that the model can accurately reproduce spontaneous MEG SI mu rhythms from a combination of stochastic ~10Hz FF and FB inputs that arrive to the SI cortex with a nearly synchronous (5 ms) delay (Jones *et al.*, 2009). Further, the evoked response can be reproduced with a sequence of FF-FB-LFF inputs (Jones *et al.*, 2007). In addition, model analyses reported here indicated that the emergence of beta dominance in the mu rhythm in middle age arises from changes in the ongoing ~10Hz FF and FB input. The delay between these inputs remains fixed near synchrony (5ms) with age, but in MA, compared to YA, the variance of the FB inputs is decreased (e.g., increased synchrony in these inputs) and the strength of FF and FB inputs is increased (produced by increasing post-synaptic conductances). Similar changes in the evoked response inputs reproduced the observed differences in the MEG evoked response. Hence, the model predicts that a single set of neurophysiological changes intimately links the age-related differences in the prestimulus and evoked response SI activity.

Relation between model predictions and prior neurophysiological studies.

Our previous modeling results predicted that the neural mechanisms responsible for higher power spontaneous mu-alpha and mu-beta components directly influence the magnitude the early SI evoked response, and these predictions were confirmed in the MEG data (Jones et al,

2009). Specifically, the model predicted when the prestimlus mu power was higher, there was an increased ongoing depolarization in excitatory and inhibitory neurons, with a preferential effect on inhibitory interneurons, This prestimulus depolarization in turn led to an evoked response with an increased ~50 ms response (M50) and subsequently reduced M70 peak (Jones *et al.*, 2009). In the present study, the trend toward an increased ~50 ms response in MA with higher mu rhythms was consistent with the direct effect of increased mu power on this early evoked response. However, the increased strength of the post-stimulus ~70ms FB input in the MA model data effectively overrode the inhibitory depolarization during the ongoing rhythm and, rather than decreasing the M70 response, the heightened FB created a more pronounced M70 peak (**Figure 10**).

Previous studies often concluded that age-related increases in the somatosensory evoked response (near 70ms) arose from decreased levels of intracortical inhibition (Drechsler, 1978; Simpson & Erwin, 1983; Stephen *et al.*, 2006). Declines in inhibitory function are a cardinal feature of aging, with stereological studies in rats pointing toward a decreased ratio of presumptive inhibitory to excitatory synapses in sensorimotor cortices of old brains (Brunso-Bechtold *et al.*, 2000; Poe *et al.*, 2001), but no direct evidence exists that links these cellular changes to somatosensory evoked responses in humans. Our modeling results demonstrate an alternate prediction to the idea of decreased inhibition in creating the enhanced M70 peak, namely that it can be achieved simply by increasing the FB drive to SI. Further, the age related decline correlated with decreased inhibition is typically observed in participants who are above middle age and in whom the spontaneous rhythms may have decreased.

Based on the construction of our model of SI, the source of increased FB in MA could come from activity in high-order association cortices, or alternatively, from nonspecific thalamic inputs that contact supragranular layers (O'Sullivan *et al.*, 2001; Jones *et al.*, 2007). This prediction is consistent with a prominent theme that emerges from the fMRI literature on aging: When compared to YA, older adults tend to show increased activation of high-order association cortices, including prefrontal cortex, when performing a variety of cognitive and perceptual tasks (Grady *et al.*, 1994; Cabeza, 2002; Onozuka *et al.*, 2003). While it is difficult to bridge findings from fMRI and MEG/EEG studies, it is possible that a generalized increase in association cortex activity could provide the necessary FB enhancement to drive the greater M70 peak seen in our MEG and modeling data.

An important prediction from our model is that rhythmic feedback inputs to SI in MA need to be more synchronous, compared to YA, in order to generate an increased mu-beta rhythm that oscillates symmetrically around zero. Studies of task-related rhythms support this notion by showing a general posterior-to-anterior shift in the expression of low-frequency oscillations with age (Niedermeyer, 1997), which implies increased synchronous low frequency activity among these neurons. Further, phase-locking of alpha oscillations is increased in frontal electrodes in middle-aged adults (Yordanova *et al.*, 1998; Kolev *et al.*, 2002), and several studies have established that in young adults, SI mu rhythms are coupled, in terms of phase-locking and coherences, to alpha and beta rhythms in prefrontal and other association cortices (Palva *et al.*, 2005; Hanslmayr *et al.*, 2007; Schubert *et al.*, 2009; Zhang & Ding, 2010). It remains unknown

whether such coherence or phase-locking between frontal and somatosensory areas changes with age, but these earlier reports support our proposal that increased synchrony in frontal neurons results in greater FB drive to SI.

It is important to note, however, that the present results do not preclude the possibility that the FB inputs arise from a non-specific thalamic source that is oscillating with a slight phase-shift from that of the lemniscal thalamic driver (O'Sullivan *et al.*, 2001; Guillery & Sherman, 2002; Hughes & Crunelli, 2005). Indeed, the requirement that the inputs to the model be separated by a small delay (~ 5 ms, and thus nearly synchronous), may be more consistent with a thalamic source of feedback that is distinct from feedback inputs from high-order cortices onto SI. When compared to our knowledge of prefrontal and other association cortices, far less is known about the effects of age on the cellular and physiological integrity of the thalamus. In terms of gross volume, the thalamus shows significant age-related decline, with several studies reporting a linear trajectory of volume loss across the lifespan (Sullivan *et al.*, 2004; Walhovd *et al.*, 2005; Cherubini *et al.*, 2009). It is unclear, however, whether such changes emerge during middle age. The few histological studies that have examined the effects of age on individual nuclei in nonhuman animals have largely focused on the sensory nuclei of the thalamus, which tend to show subtle, but significant, age-related declines in neuron density (Ahmad & Spear, 1993), but not in total number of neurons (Satorre *et al.*, 1985; Ahmad & Spear, 1993). It is possible that the net effect of the age-related decrease in neural density diminishes inhibition in the thalamus and thus effectively increases the output to the cortex. Potentially inconsistent with our prediction of increased FB inputs with age, functional studies indicate an age-related

attenuation of fMRI signal in the thalamus, as measured using fMRI (Onozuka *et al.*, 2003), and increased peak-to-peak latencies (representing conduction times) from the medial lemniscus to the thalamus and to the sensory cortex (Kakigi, 1987). Such changes, however, are typically attributed to peripheral receptor deficits that result in decreased drive to sensory nuclei of the thalamus, and not nonspecific nuclei. Thus, additional research is needed to determine whether age-related changes exist in the anatomical and functional integrity of nonspecific thalamic nuclei that could translate into increased feedback of the sort implicated by our model.

Relation between mu rhythms and tactile detection.

Although the stimulus paradigm used here did not allow us to examine age-related differences in tactile perception (the stimulus intensity was maintained at a level that yielded a 50% detection rate, tailored to each individual participant), it is reasonable to speculate that age-related differences in spontaneous prestimulus mu power could directly influence somatosensory detection. Indeed, a vast literature documents age-related changes in somatosensory perceptual abilities (Schneider & Pichora-Fuller, 2000), including increases in tactile detection thresholds (Verrillo, 1982; Gescheider *et al.*, 1996; Verrillo *et al.*, 2002) and decreases in the subjective magnitude of vibrotactile sensation (Verrillo, 1982; Verrillo *et al.*, 2002). Older adults also show decreased tactile discrimination ability at suprathreshold levels, while discriminative capacities at the detection threshold appear to be less affected by age (Gescheider *et al.*, 1996). Several studies of healthy young adults have shown that prestimulus mu-alpha and mu-beta oscillations in somatosensory cortices predict subsequent detection of weak tactile stimuli (Linkenkaer-Hansen *et al.*, 2004; Schubert *et al.*, 2009; Zhang & Ding, 2010).

It is likely, therefore, that the age-related changes in the mu rhythm noted here are associated with differences in tactile detection. A thorough examination of this hypothesis may provide a deeper understanding of the mechanisms underlying sensory and perceptual deficits that are often seen with advanced age.

Acknowledgements: The authors wish to thank Michael Hines for excellent technical support in NEURON software code. This work was supported by NIH: P41RR14075, K25MH072941, 1RO1-NS045130-01, T32 GM007484, NSF: 0316933, the Athinoula A. Martinos Center for Biomedical Imaging, the McGovern Institute for Brain Research.

References

Adler G & Nacimiento AC (1988) Age-dependent changes of short-latency somatosensory evoked potentials in healthy adults. *Appl Neurophysiol* **51**, 55-59.

Ahmad A & Spear PD (1993) Effects of aging on the size, density, and number of rhesus monkey lateral geniculate neurons. *J Comp Neurol* **334**, 631-643.

Babiloni C, Binetti G, Cassarino A, Dal Forno G, Del Percio C, Ferreri F, Ferri R, Frisoni G, Galderisi S, Hirata K, Lanuzza B, Miniussi C, Mucci A, Nobili F, Rodriguez G, Luca Romani G & Rossini PM (2006) Sources of cortical rhythms in adults during physiological aging: a multicentric EEG study. *Hum Brain Mapp* **27**, 162-172.

Brunso-Bechtold JK, Linville MC & Sonntag WE (2000) Age-related synaptic changes in sensorimotor cortex of the Brown Norway X fischer 344 rat. *Brain Res* **872**, 125-133.

Cabeza R (2002) Hemispheric asymmetry reduction in older adults: the HAROLD model. *Psychol Aging* **17**, 85-100.

Cherubini A, Peran P, Caltagirone C, Sabatini U & Spalletta G (2009) Aging of subcortical nuclei: microstructural, mineralization and atrophy modifications measured in vivo using MRI. *Neuroimage* **48**, 29-36.

d'Onofrio F, Salvia S, Petretta V, Bonavita V, Rodriguez G & Tedeschi G (1996) Quantified-EEG in normal aging and dementias. *Acta Neurol Scand* **93**, 336-345.

Desmedt JE & Cheron G (1980) Somatosensory evoked potentials to finger stimulation in healthy octogenarians and in young adults: wave forms, scalp topography and transit times of parietal and frontal components. *Electroencephalogr Clin Neurophysiol* **50**, 404-425.

Drechsler F (1978) Quantitative analysis of neurophysiological processes of the aging CNS. *J Neurol* **218**, 197-213.

Felleman DJ & Van Essen DC (1991) Distributed hierarchical processing in the primate cerebral cortex. *Cereb Cortex* **1**, 1-47.

Ferri R, Del Gracco S, Elia M, Musumeci SA, Spada R & Stefanini MC (1996) Scalp topographic mapping of middle-latency somatosensory evoked potentials in normal aging and dementia. *Neurophysiol Clin* **26**, 311-319.

Fries P, Reynolds JH, Rorie AE & Desimone R (2001) Modulation of oscillatory neuronal synchronization by selective visual attention. *Science* **291**, 1560-1563.

Gescheider GA, Edwards RR, Lackner EA, Bolanowski SJ & Verrillo RT (1996) The effects of aging on information-processing channels in the sense of touch: III. Differential sensitivity to changes in stimulus intensity. *Somatosens Mot Res* **13**, 73-80.

Grady CL, Maisog JM, Horwitz B, Ungerleider LG, Mentis MJ, Salerno JA, Pietrini P, Wagner E & Haxby JV (1994) Age-related changes in cortical blood flow activation during visual processing of faces and location. *J Neurosci* **14**, 1450-1462.

Guillery RW & Sherman SM (2002) Thalamic relay functions and their role in corticocortical communication: generalizations from the visual system. *Neuron* **33**, 163-175.

Hanslmayr S, Aslan A, Staudigl T, Klimesch W, Herrmann CS & Bauml KH (2007) Prestimulus oscillations predict visual perception performance between and within subjects. *Neuroimage* **37**, 1465-1473.

Hari R (2006) Action-perception connection and the cortical mu rhythm. *Prog Brain Res* **159**, 253-260.

Hughes SW & Crunelli V (2005) Thalamic mechanisms of EEG alpha rhythms and their pathological implications. *Neuroscientist* **11**, 357-372.

Jones SR, Pritchett DL, Sikora MA, Stufflebeam SM, Hamalainen M & Moore CI (2009) Quantitative analysis and biophysically realistic neural modeling of the MEG mu rhythm: rhythmogenesis and modulation of sensory-evoked responses. *J Neurophysiol* **102**, 3554-3572.

Jones SR, Pritchett DL, Stufflebeam SM, Hamalainen M & Moore CI (2007) Neural correlates of tactile detection: a combined magnetoencephalography and biophysically based computational modeling study. *J Neurosci* **27**, 10751-10764.

Kakigi R (1987) The effect of aging on somatosensory evoked potentials following stimulation of the posterior tibial nerve in man. *Electroencephalogr Clin Neurophysiol* **68**, 277-286.

Kakigi R & Shibasaki H (1991) Effects of age, gender, and stimulus side on scalp topography of somatosensory evoked potentials following median nerve stimulation. *J Clin Neurophysiol* **8**, 320-330.

Kolev V, Yordanova J, Basar-Eroglu C & Basar E (2002) Age effects on visual EEG responses reveal distinct frontal alpha networks. *Clin Neurophysiol* **113**, 901-910.

Kononen M & Partanen JV (1993) Blocking of EEG alpha activity during visual performance in healthy adults. A quantitative study. *Electroencephalogr Clin Neurophysiol* **87**, 164-166.

Kuhlman WN (1978) Functional topography of the human mu rhythm. *Electroencephalogr Clin Neurophysiol* **44**, 83-93.

Linkenkaer-Hansen K, Nikulin VV, Palva S, Ilmoniemi RJ & Palva JM (2004) Prestimulus oscillations enhance psychophysical performance in humans. *J Neurosci* **24**, 10186-10190.

Luders H (1970) The effect of aging on the wave form of the somatosensory cortical evoked potential. *Electroencephalogr Clin Neurophysiol* **29**, 450-460.

Marciani MG, Maschio M, Spanedda F, Caltagirone C, Gigli GL & Bernardi G (1994) Quantitative EEG evaluation in normal elderly subjects during mental processes: age-related changes. *Int J Neurosci* **76**, 131-140.

Mazaheri A & Jensen O (2008) Asymmetric amplitude modulations of brain oscillations generate slow evoked responses. *J Neurosci* **28**, 7781-7787.

Murakami S, Hirose A & Okada YC (2003) Contribution of ionic currents to magnetoencephalography (MEG) and electroencephalography (EEG) signals generated by guinea-pig CA3 slices. *J Physiol* **553**, 975-985.

Murakami S & Okada Y (2006) Contributions of principal neocortical neurons to magnetoencephalography and electroencephalography signals. *J Physiol* **575**, 925-936.

Niedermeyer E (1997) Alpha rhythms as physiological and abnormal phenomena. *Int J Psychophysiol* **26**, 31-49.

Nikulin VV, Linkenkaer-Hansen K, Nolte G, Lemm S, Muller KR, Ilmoniemi RJ & Curio G (2007) A novel mechanism for evoked responses in the human brain. *Eur J Neurosci* **25**, 3146-3154.

O'Sullivan M, Jones DK, Summers PE, Morris RG, Williams SC & Markus HS (2001) Evidence for cortical "disconnection" as a mechanism of age-related cognitive decline. *Neurology* **57**, 632-638.

Ogata K, Okamoto T, Yamasaki T, Shigeto H & Tobimatsu S (2009) Pre-movement gating of somatosensory-evoked potentials by self-initiated movements: the effects of ageing and its implication. *Clin Neurophysiol* **120**, 1143-1148.

Okada YC, Wu J & Kyuhou S (1997) Genesis of MEG signals in a mammalian CNS structure. *Electroencephalogr Clin Neurophysiol* **103**, 474-485.

Onozuka M, Fujita M, Watanabe K, Hirano Y, Niwa M, Nishiyama K & Saito S (2003) Age-related changes in brain regional activity during chewing: a functional magnetic resonance imaging study. *J Dent Res* **82**, 657-660.

Palva S, Linkenkaer-Hansen K, Naatanen R & Palva JM (2005) Early neural correlates of conscious somatosensory perception. *J Neurosci* **25**, 5248-5258.

Poe BH, Linville C & Brunso-Bechtold J (2001) Age-related decline of presumptive inhibitory synapses in the sensorimotor cortex as revealed by the physical disector. *J Comp Neurol* **439**, 65-72.

Raz N & Rodrigue KM (2006) Differential aging of the brain: patterns, cognitive correlates and modifiers. *Neurosci Biobehav Rev* **30**, 730-748.

Rossini PM, Rossi S, Babiloni C & Polich J (2007) Clinical neurophysiology of aging brain: from normal aging to neurodegeneration. *Prog Neurobiol* **83**, 375-400.

Roubicek J (1977) The electroencephalogram in the middle-aged and the elderly. *J Am Geriatr Soc* **25**, 145-152.

Sailer A, Dichgans J & Gerloff C (2000) The influence of normal aging on the cortical processing of a simple motor task. *Neurology* **55**, 979-985.

Satorre J, Cano J & Reinoso-Suarez F (1985) Stability of the neuronal population of the dorsal lateral geniculate nucleus (LGNd) of aged rats. *Brain Res* **339**, 375-377.

Schneider BA & Pichora-Fuller MK (2000) Implications of perceptual deterioration for cognitive aging research. In *The Handbook of Aging adn Cognition*, pp. 155-219 [FI Craik and TA Salthouse, editors]. Mahwah, NJ: Lawrence Erlbaum Associates.

Schubert R, Haufe S, Blankenburg F, Villringer A & Curio G (2009) Now you'll feel it, now you won't: EEG rhythms predict the effectiveness of perceptual masking. *J Cogn Neurosci* **21**, 2407-2419.

Simpson DM & Erwin CW (1983) Evoked potential latency change with age suggests differential aging of primary somatosensory cortex. *Neurobiol Aging* **4**, 59-63.

Stephen JM, Ranken D, Best E, Adair J, Knoefel J, Kovacevic S, Padilla D, Hart B & Aine CJ (2006) Aging changes and gender differences in response to median nerve stimulation measured with MEG. *Clin Neurophysiol* **117**, 131-143.

Sullivan EV, Rosenbloom M, Serventi KL & Pfefferbaum A (2004) Effects of age and sex on volumes of the thalamus, pons, and cortex. *Neurobiol Aging* **25**, 185-192.

Tallon-Baudry C, Bertrand O, Delpuech C & Permier J (1997) Oscillatory gamma-band (30-70 Hz) activity induced by a visual search task in humans. *J Neurosci* **17**, 722-734.

Tesche CD, Uusitalo MA, Ilmoniemi RJ, Huotilainen M, Kajola M & Salonen O (1995) Signal-space projections of MEG data characterize both distributed and well-localized neuronal sources. *Electroencephalogr Clin Neurophysiol* **95**, 189-200.

Uusitalo MA & Ilmoniemi RJ (1997) Signal-space projection method for separating MEG or EEG into components. *Med Biol Eng Comput* **35**, 135-140.

Verrillo RT (1982) Effects of aging on the suprathreshold responses to vibration. *Percept Psychophys* **32**, 61-68.

Verrillo RT, Bolanowski SJ & Gescheider GA (2002) Effect of aging on the subjective magnitude of vibration. *Somatosens Mot Res* **19**, 238-244.

Walhovd KB, Fjell AM, Reinvang I, Lundervold A, Dale AM, Eilertsen DE, Quinn BT, Salat D, Makris N & Fischl B (2005) Effects of age on volumes of cortex, white matter and subcortical structures. *Neurobiol Aging* **26**, 1261-1270; discussion 1275-1268.

Walhovd KB, Westlye LT, Amlien I, Espeseth T, Reinvang I, Raz N, Agartz I, Salat DH, Greve DN, Fischl B, Dale AM & Fjell AM (2011) Consistent neuroanatomical age-related volume differences across multiple samples. *Neurobiol Aging* **32**, 916-932.

Yordanova JY, Kolev VN & Basar E (1998) EEG theta and frontal alpha oscillations during auditory processing change with aging. *Electroencephalogr Clin Neurophysiol* **108**, 497-505.

Zhang Y & Ding M (2010) Detection of a Weak Somatosensory Stimulus: Role of the Prestimulus Mu Rhythm and Its Top-Down Modulation. *J Cogn Neurosci* **22**, 307-322.

Ziegler DA, Piguet O, Salat DH, Prince K, Connally E & Corkin S (2010) Cognition in healthy aging is related to regional white matter integrity, but not cortical thickness. *Neurobiol Aging* **31**, 1912-1926.

Tables and Figures.

Table 1. Model parameters for ongoing exogenous drive to the SI network.

	YA	MA
Delay between ~10 Hz FF and FB input	5 ms	5 ms
Number of spikes in input burst	10	10
Variance of FF input burst	400	400
Variance of FB input burst	600 (less synchrony)	200 (more synchrony)
Post-synaptic conductance of FF and FB inputs	0.00002 pS	0.00004 pS

Table 2. Model parameters for evoked response inputs to the SI network.

Feedforward (FF) Feedback (FB) Late Feedforward (LFF)	Input times across trials (ms)	YA Maximal conductance (μS) Default AMPA/NMDA	MA Maximal conductance (μS) Default AMPA/NMDA
FF to L2/3e		0.0005	0.001
FF to L2/3i		0.001	0.002
FF to L5e		0.00025	0.0005
FF to L5i	25	0.0005	0.001
FB to L2/3e		0.0005/ 0.0005	0.001/ 0.001
FB to L2/3i		0.00025/ 0.00025	0.0005/ 0.0005
FB to L5e	7	0.0005/ 0.0005	0.001/ 0.001
LFF to L2/3e		0.00265	0.0053
LFF to L2/3i		0.00265	0.0053
LFF to L5e		0.00265	0.0027
LFF to L5i	135	0.00265	0.0027

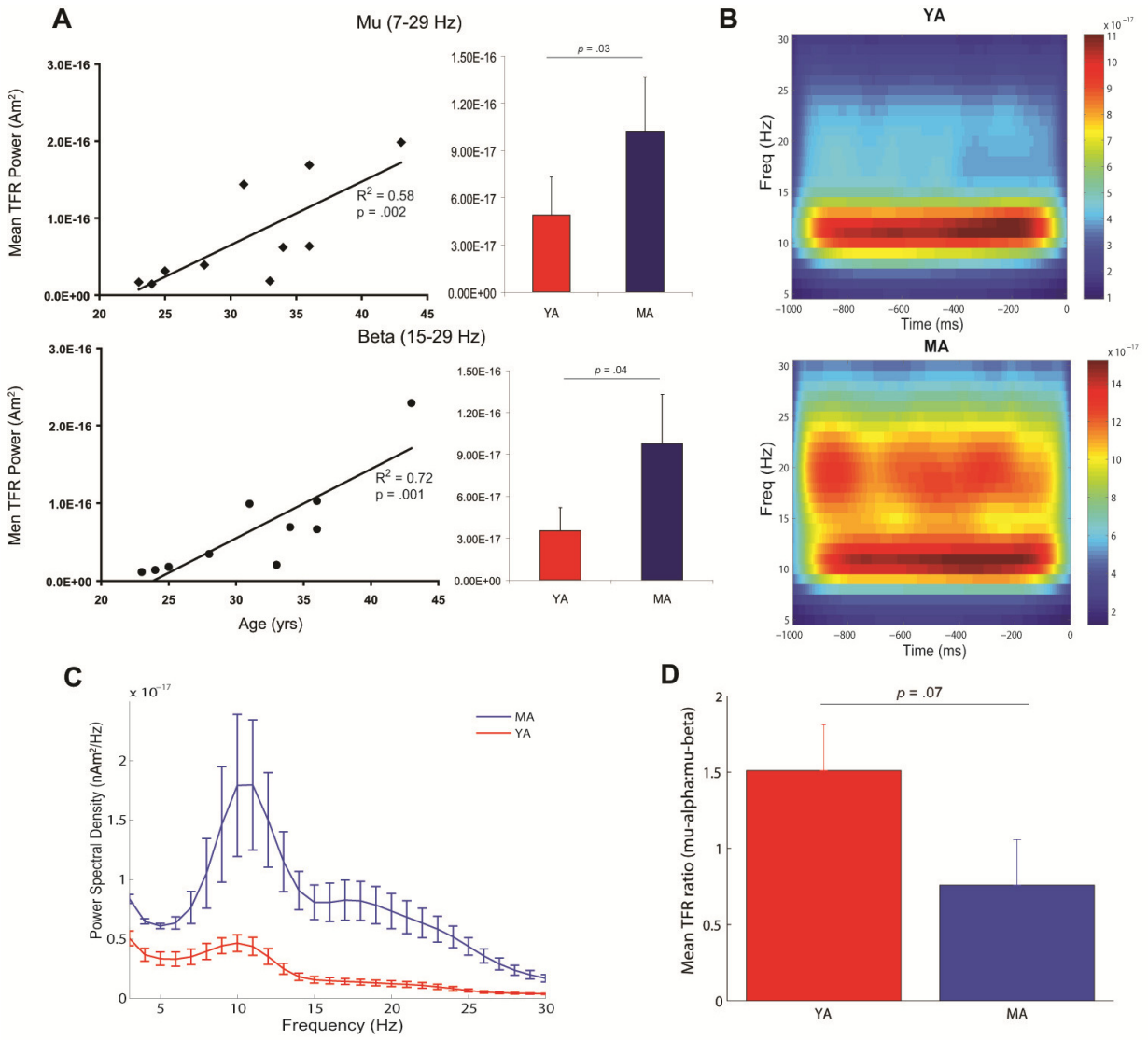

Figure 1. Age-related changes in MEG SI mu rhythms. A, Left panels Regression plots of prestimulus power in the mu (7-29 Hz, top) and mu-beta (15-29 Hz, bottom) ranges calculated from TFR spectrograms as a function of age. Significant correlations ($p < 0.05$) are indicated by solid regression lines. **Right panels.** Bar plots of mean and s.e. for time-averaged TFR power (1 sec, n=200 trials) in each frequency range for the YA (red) and MA (blue). **B.** Average prestimulus TFRs for the YA (top) and MA (bottom). The unit of power is $(Am)^2$. **C.** Average prestimulus power spectral density plots for the YA (blue) and MA (red), s.e. bars. **D.** Mean (+ s.e.) TFR ratios of mu-alpha to mu-beta power for the YA (red) and MA (blue). The TFR ratio was > 1 for YA and < 1 for MA ($p = 0.07$).

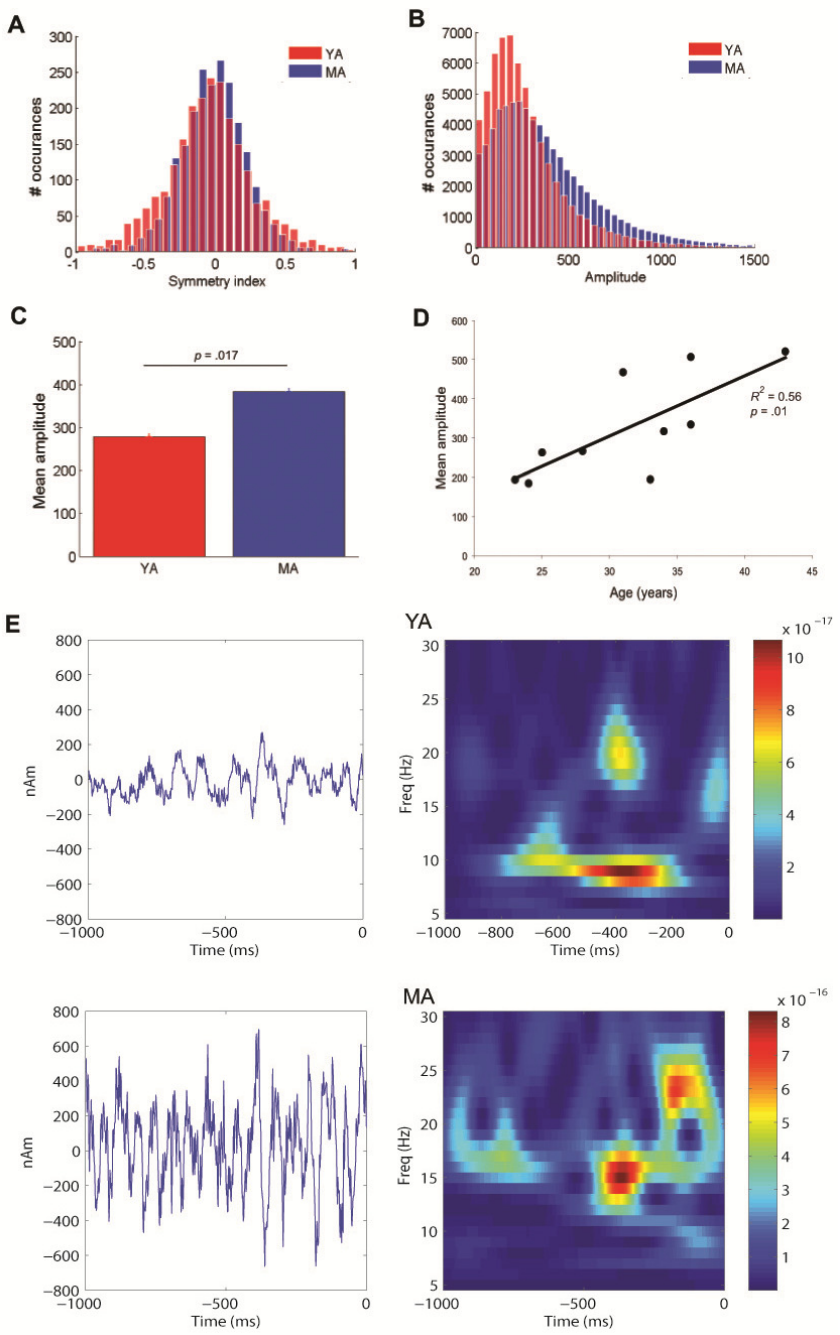

Figure 2. Symmetry and amplitude of prestimulus MEG oscillations. A. Histogram of symmetry indices for the prestimulus (1000 ms) period over all trials for the YA (red) and MA (blue). **B.** Histogram of peak-to-trough amplitudes during the prestimulus period for the YA and MA. **C.** Mean prestimulus peak-to-trough amplitudes for each group (s.e. bars). Amplitudes were significantly greater for the MA (p = 0.017) **D.** Regression plot of mean amplitudes by age (p = 0.01). **E.** Example single-trial prestimulus waveforms (left) and corresponding TFR plots (right) for one YA and one MA showing the single trial variability and symmetry of the oscillation around zero in both groups with greater amplitude oscillations in the MA. The unit of power in the TFR is $(Am)^2$.

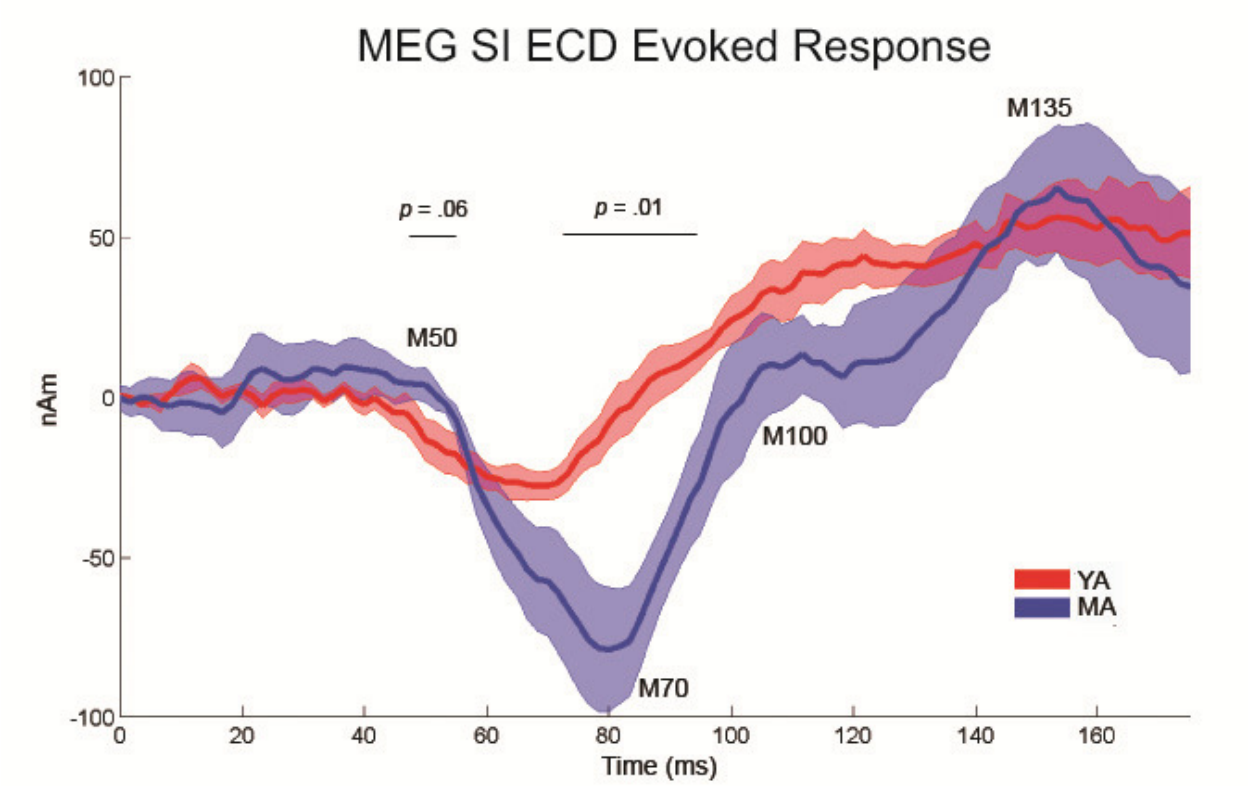

Figure 3. Age-related difference in the early MEG SI evoked response. Evoked SI ECD responses for the first 175 ms after stimulation for the YA (red) and MA (blue) (shaded region depicts s.e.). The MA group showed a significantly greater magnitude M70 peak (p = 0.01), longer latency of this peak (p = 0.03), and trends toward a greater ~50ms response (p = 0.06) and slope from the M70 to 100 ms response (p < 0.09*)*.

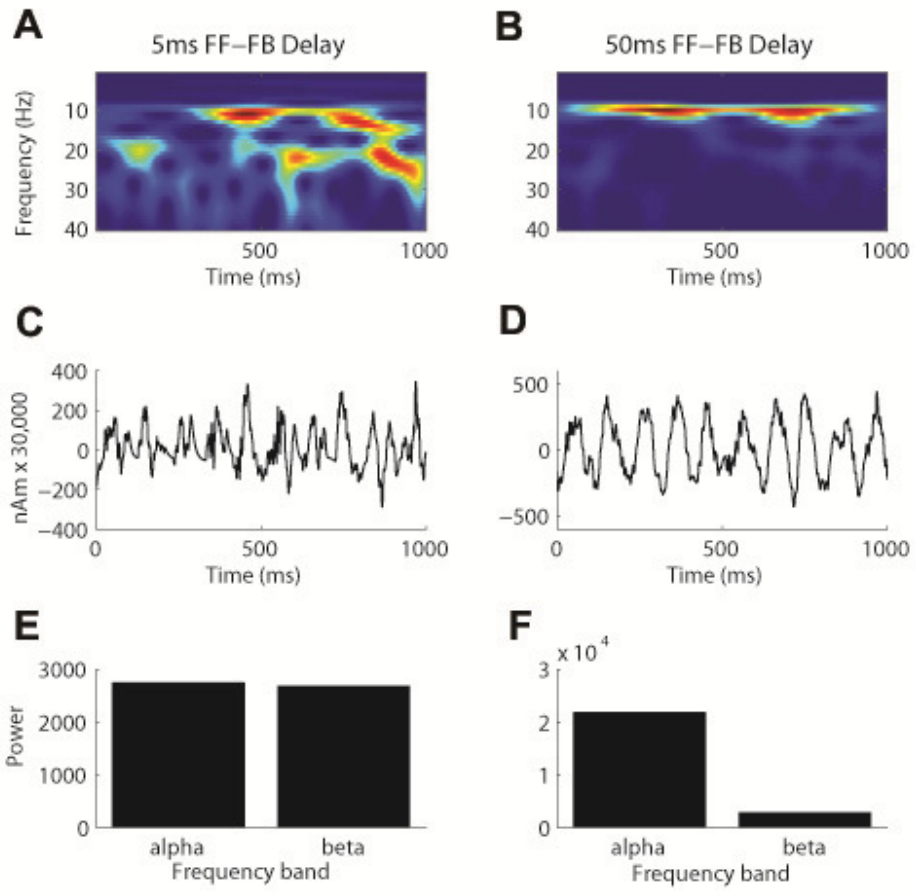

Figure 4. The effect of the delay between the rhythmic 10Hz FF and FB inputs on the simulated SI mu rhythm. A. A 5 ms FF-FB delay shows that both mu-alpha and mu-beta components emerge in the TFR. The unit of power is $(Am)^{2.}$ **B.** A 50 ms FF-FB delay shows that only mu-alpha emerges significantly in the TFR. **C.** Corresponding waveform for 5 ms delay. **D.** Corresponding waveform for 50 ms delay. **E.** The average mu-alpha and mu-beta power calculated from the TFR are approximately equal with a 5 ms delay. **F.** The average mu-alpha power is greater than mu-beta with a 50 ms delay.

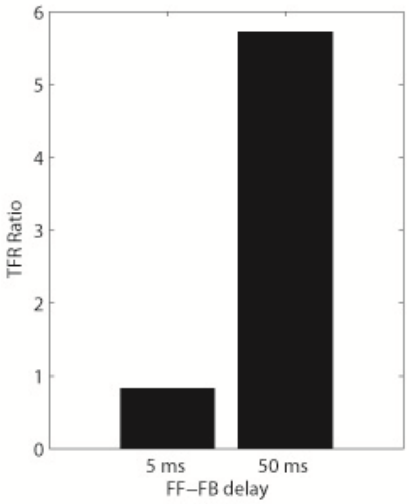

Figure 5. The effect of the delay between the rhythmic 10Hz FF and FB inputs on symmetry indices and TFR mu-alpha to mu-beta ratios. Increasing the FF-FB delay from 5 ms to 50 ms increased the TFR mu-alpha to mu-beta ratio from slightly <1 to a value >1. The increase to a 50ms delay, however, produced a nearly 5-fold increase in the TFR ratio, which was not consistent with changes from YA to MA (see Figure 1D), thus negating model prediction A.

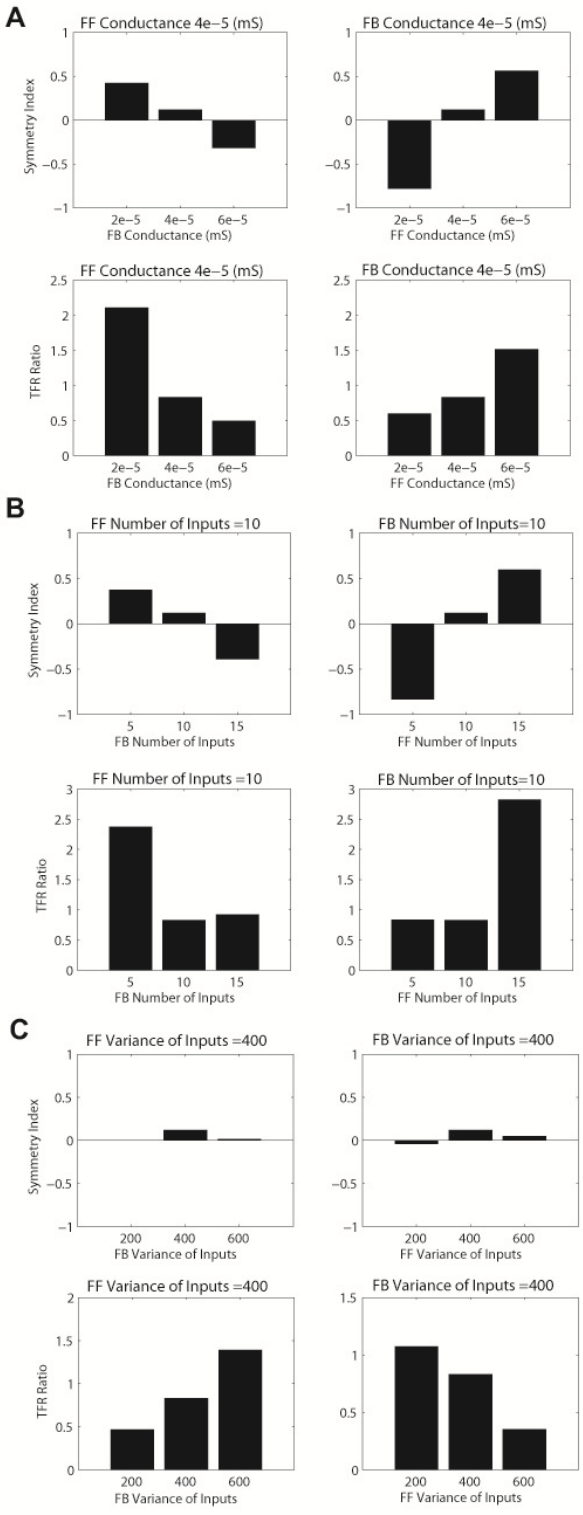

Figure 6. The effect of the strength of the 10Hz FF and FB input on symmetry indices and TFR mu-alpha to mu-beta ratios. For a fixed 5 ms delay between the rhythmic FF and FB input we manipulated the strength of the inputs via changes in the (**A**) post-synaptic conductance, (**B**) number of spike in the input burst on each cycle of the input, and (**C**) variance of spikes in the input burst on each cycle of the input (see **Supplementary Figure 3**). **A.** Increasing the post-synaptic conductances of the rhythmic FB input (left), while holding FF post-synaptic conductances constant, resulted in a decrease in the symmetry indices (top) and a decrease in the TFR mu-alpha to mu-beta ratio (bottom). The opposite pattern was found when the post-synaptic conductances of the FF input was increased, while holding FB conductances constant (right). **B.** Increasing the number of inputs on each cycle of the rhythmic FB input (left), while holding FF number constant, led to a decrease in symmetry indices and a decrease in the TFR ratio; the opposite pattern was found when the number of FF inputs were increased (right), while holding FB number constant. **C.** Increasing the variance of the inputs on each cycle the rhythmic FB input (left), while holding the FF variance constant, had a minimal effect on the symmetry indices, but resulted in a relative decrease in the TFR ratios. Increasing the variance of the rhythmic FF input (right), while holding the FB variance constant, again resulted in a relatively constant symmetry index, but led to an increase the TFR ratio.

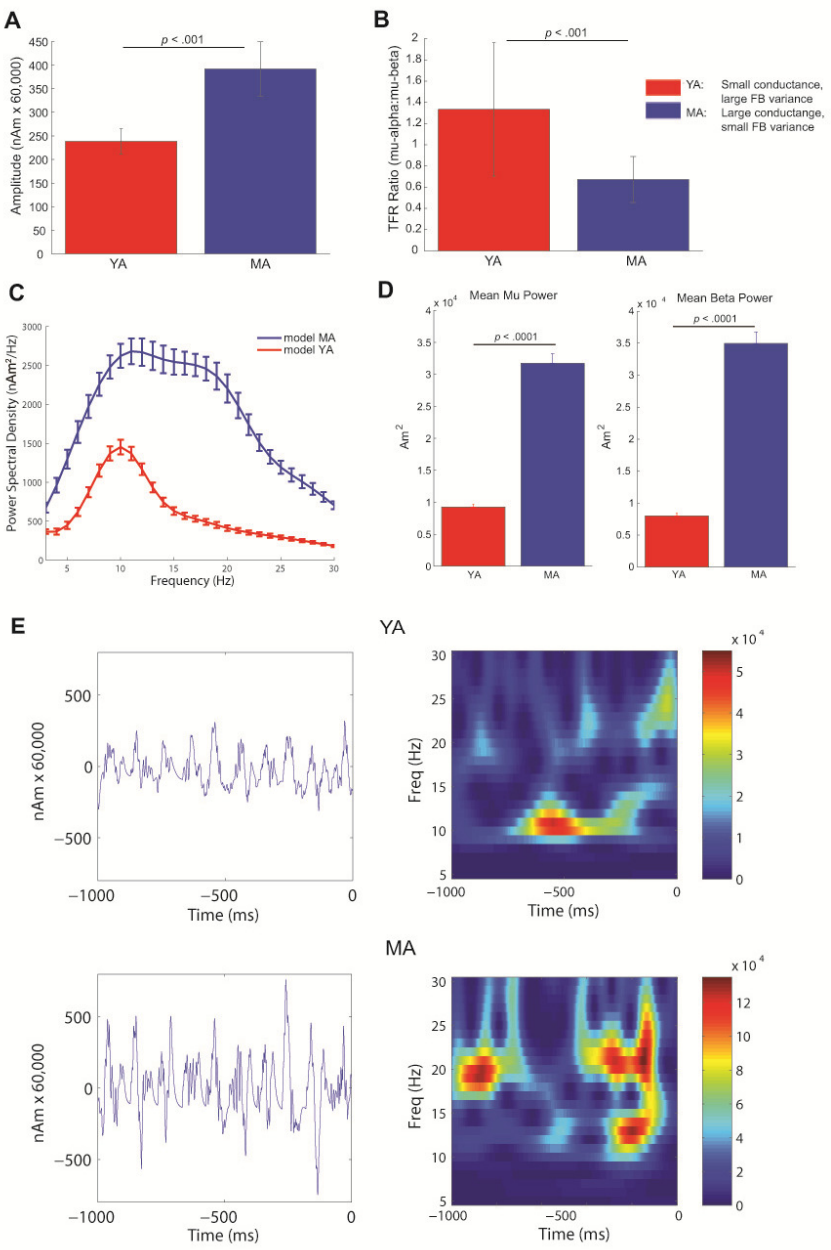

Figure 7. Simulating age-differences in the SI mu rhythm. Using the parameter regime outlined in **Table 1**, the computational model was able to reproduce each of the observed group comparison age-related characteristics of the MEG data: When averaging over multiple trials (n=25 each group), the model reproduced **A)** larger mean amplitudes of oscillations in the MA model data, and **B)** a TFR mu-alpha to mu-beta ratio >1 for YA and <1 for MA. **C**. Average power spectral density plots for the modeled YA (blue) and MA (red) data. **D.** Time-averaged TFR power estimates were significantly larger in the MA simulations in mu and mu-beta range ($p<0.001$). **E.** Individual trial waveforms and spectrograms showing single trial variability and symmetric oscillations, with increased amplitude oscillations and greater beta dominance in the simulated MA compared to YA model data (bottom). Panels A-D depict mean and s.e. across trials.

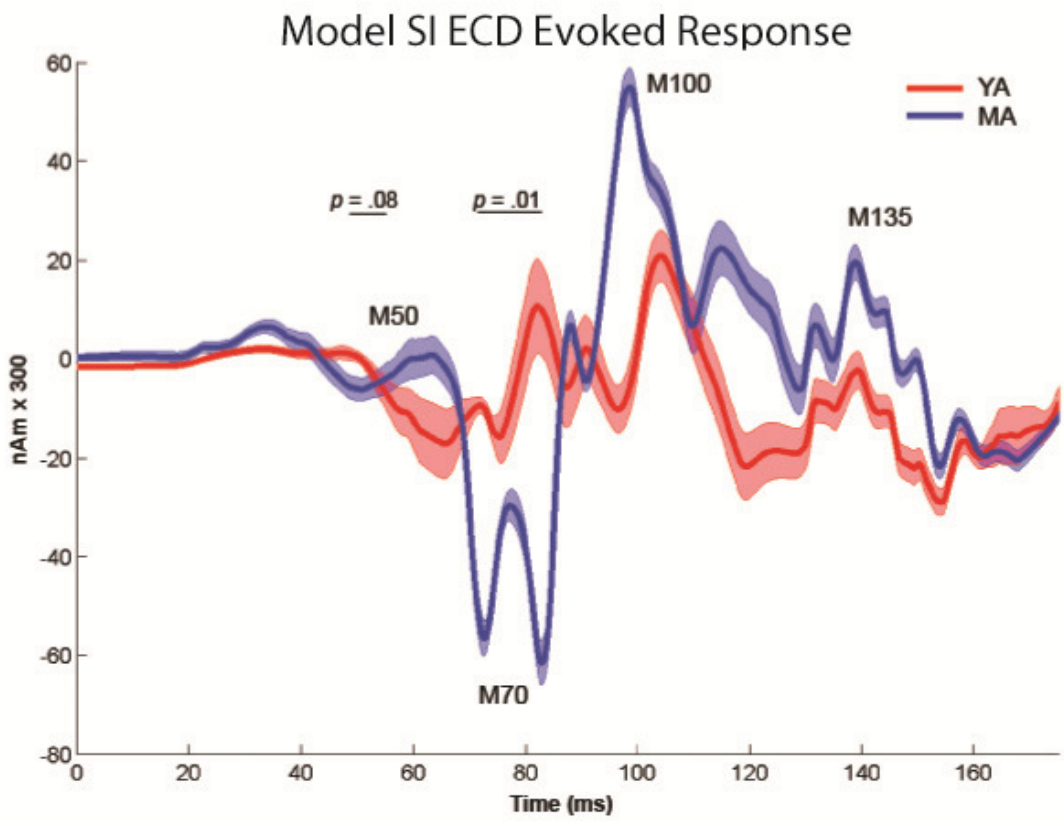

Figure 8. Simulating age-differences in the SI evoked response. Simulating an evoked response sequence with FF-FB-LFF input, as described in the results, during ongoing YA and MA mu rhythms reproduced the age-differences observed in the MEG evoked response, including a greater magnitude M70 peak (*p = 0.*01*),* a greater slope from the M70 to 100ms response (*p* < .0001*)* and a trend toward a decreased M50 response (*p = 0.*08*)* in the MA simulation. Mean and s.e. shown over n=30 trials per group.

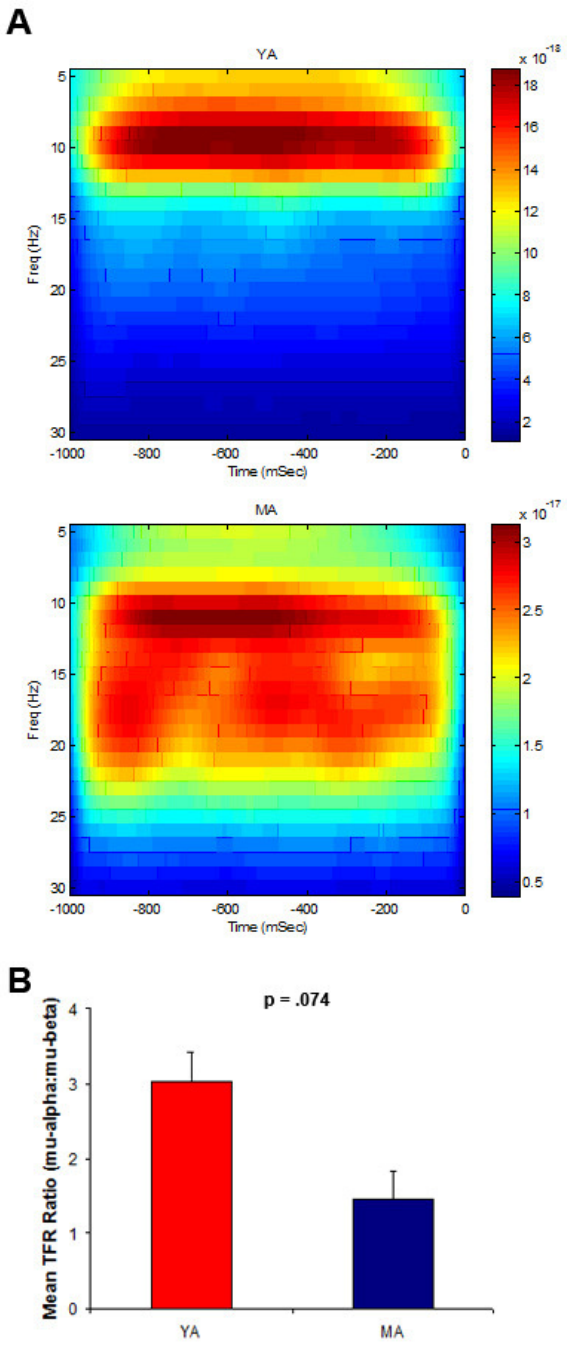

Supplementary Figure 1. TFRs calculated using the unit wavelet normalization (Tallon-Baudry et al. 1997). A) Prestimulus TFRs averaged across the YA (top) and MA (bottom) groups. The unit of power is $(Am)^2$. **B)** mean TFR ratios of prestimulus mu-alpha to mu-beta power in 100 ms time bins against age for the YA (red) and MA (blue).). The TFR ratio was > 1 for YA and < 1 for MA (p = 0.074). For each participant, ratios were averaged over all trials (n=200) and time (1 sec).

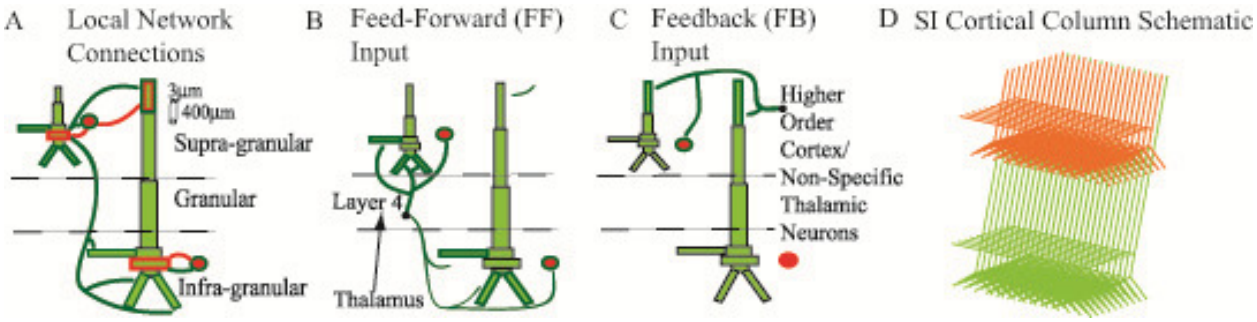

Supplementary Figure 2. Schematic illustration of SI model network A. Local network synaptic connections between multiple compartment pyramidal neurons (PNs, green) and single compartment inhibitory neurons (INs, red). 'Bold' outlined dendrites were contacted. Within layer PN-to-PN synapses (not shown) were also present on dark green outlined dendrites. **B**. Excitatory feedforward input connections. The black arrow is schematic, because lemniscal thalamic input was not explicitly modeled. **C.** Excitatory feedback-input connections from presumed higher order cortical or non-specific thalamic neurons. The feedforward and feedback inputs were modeled as spike train generators with a predetermined temporal profile and synaptic strength. **D.** Schematic of the Network Architecture*:* The network activity of 100 multi-compartment pyramidal neurons (PNs) in layers II/III and V (green), interconnected with 35 inhibitory interneurons (INs) per layer (not shown), were simulated using the software NEURON. (reproduced as in Jones et al., *in press* with permission from J. Neurophys.)

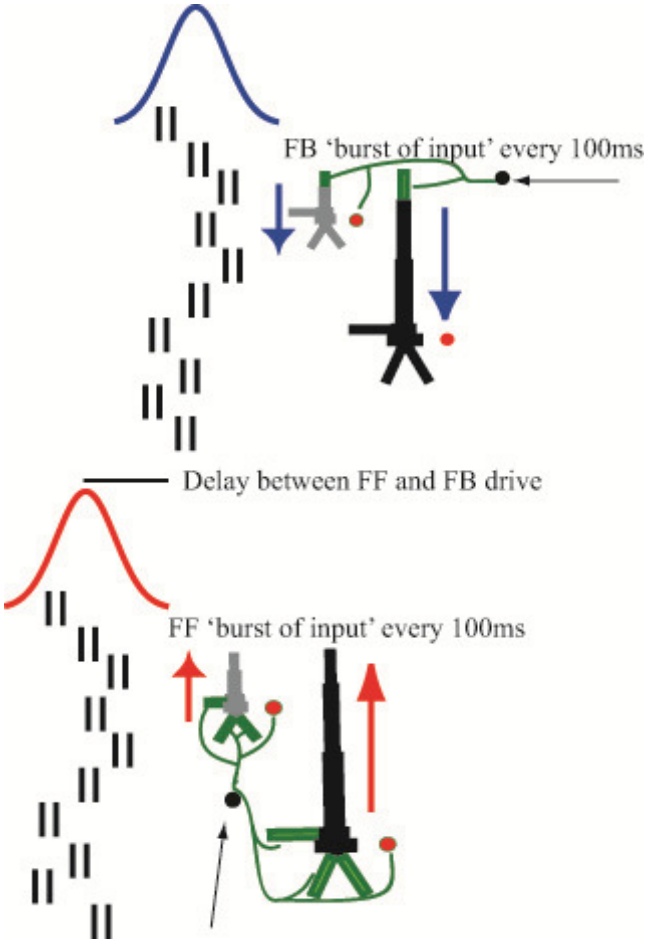

Supplementary Figure 3. Schematic illustration of alternating 10Hz FF and FB drive to the SI network that creates a mu rhythm. Every ~100ms (Gaussian, mean ISI 100ms, s.d.=20ms), 10 'bursts' of input (doublet spike trains, ISI 10ms) excite the SI network in a FF connection pattern followed by an analogous delayed FB input. Red and blue arrows depict intracellular current flow. FF inputs induce current flow up the dendrites and FB inputs current flow down the dendrites. (reproduced as in Jones et al., *in press* with permission from J. Neurophys.)

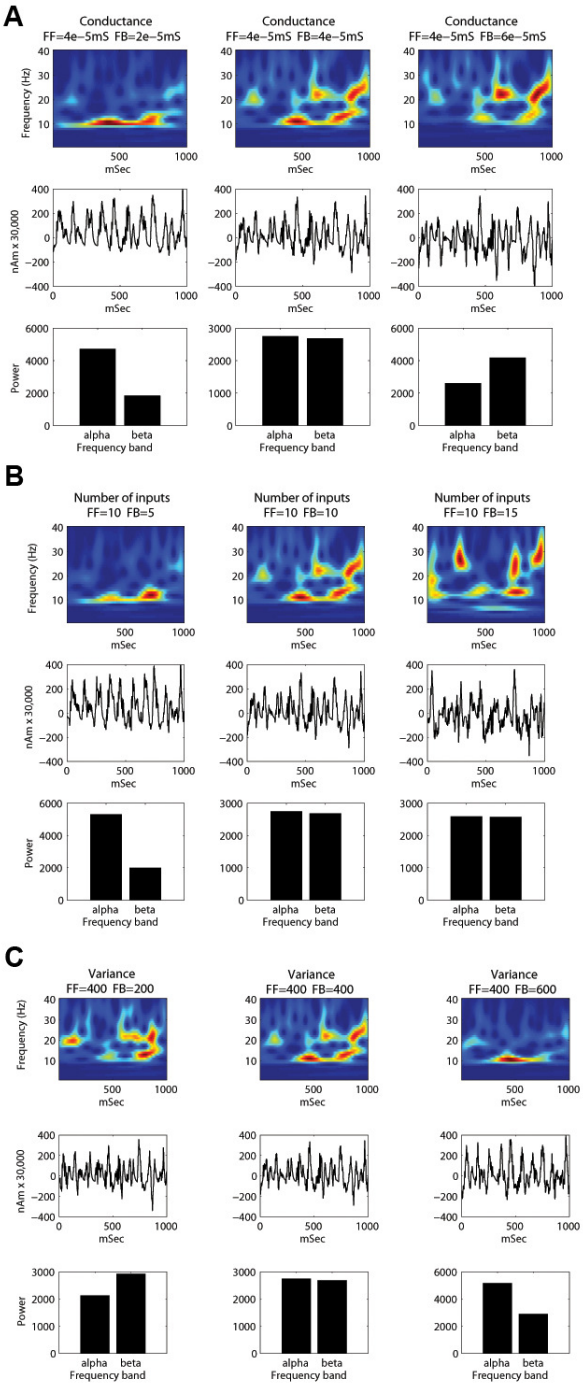

Supplementary Figure 4. The effect of the strength of the 10Hz FF and FB input on the SI mu rhythm. For a fixed 5 ms delay between the rhythmic FF and FB input we manipulated the strength of the inputs via changes in the (**A.**) post-synaptic conductance, (**B.**) number of spike in the input burst on each cycle of the input, and (**C.**) variance of spikes in the input burst on each cycle of the input (see **Supplimentary Figure 3**). TFR plots (top), example waveforms (middle), and mean mu-alpha and mu-beta power calculated from the TFRs (bottom) are shown, for three values of each parameter. The left columns show the effect of increased FF relative to FB parameters, the middle column shows the effect of equal FF and FB parameters, and the right column shows the effect of lower FF compared to FB parameters. In all cases, when the FF input strength is effectively increased compared to the FB input strength, mu-alpha power is increased. In contrast, when the FB input strength is effectively increased compared to the FF input strength, mu-beta power is increased. Further, when the strength of the FF and FB inputs are equal, the mu-alpha and mu-beta are approximately equal.

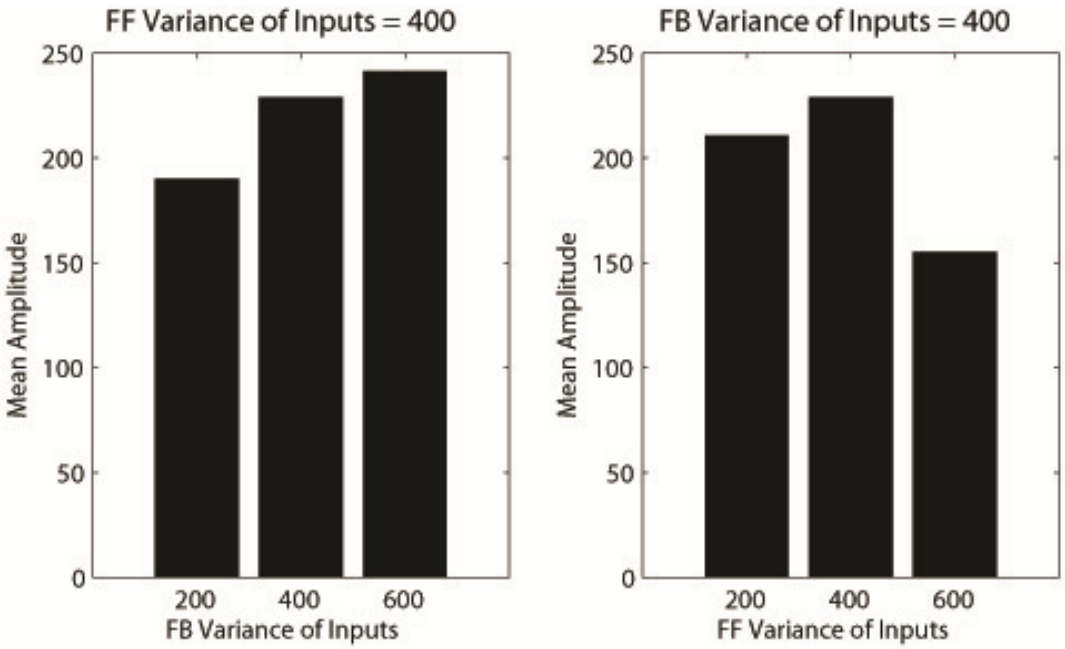

Supplementary Figure 5. The effects of the 10Hz FF and FB input variance on oscillation amplitude. With a fixed variance of the rhythmic FF inputs on each cycle of 400 ms, increasing the variance of the FB inputs (which increases relative mu-beta amplitude) resulted in a stepwise increase in the peak-to-trough amplitude of oscillations (left). In contrast, when the variance of the rhythmic FB input was fixed, increasing the FF variance (which increases mu-alpha amplitude) led to a decrease in the mean amplitude of oscillations.

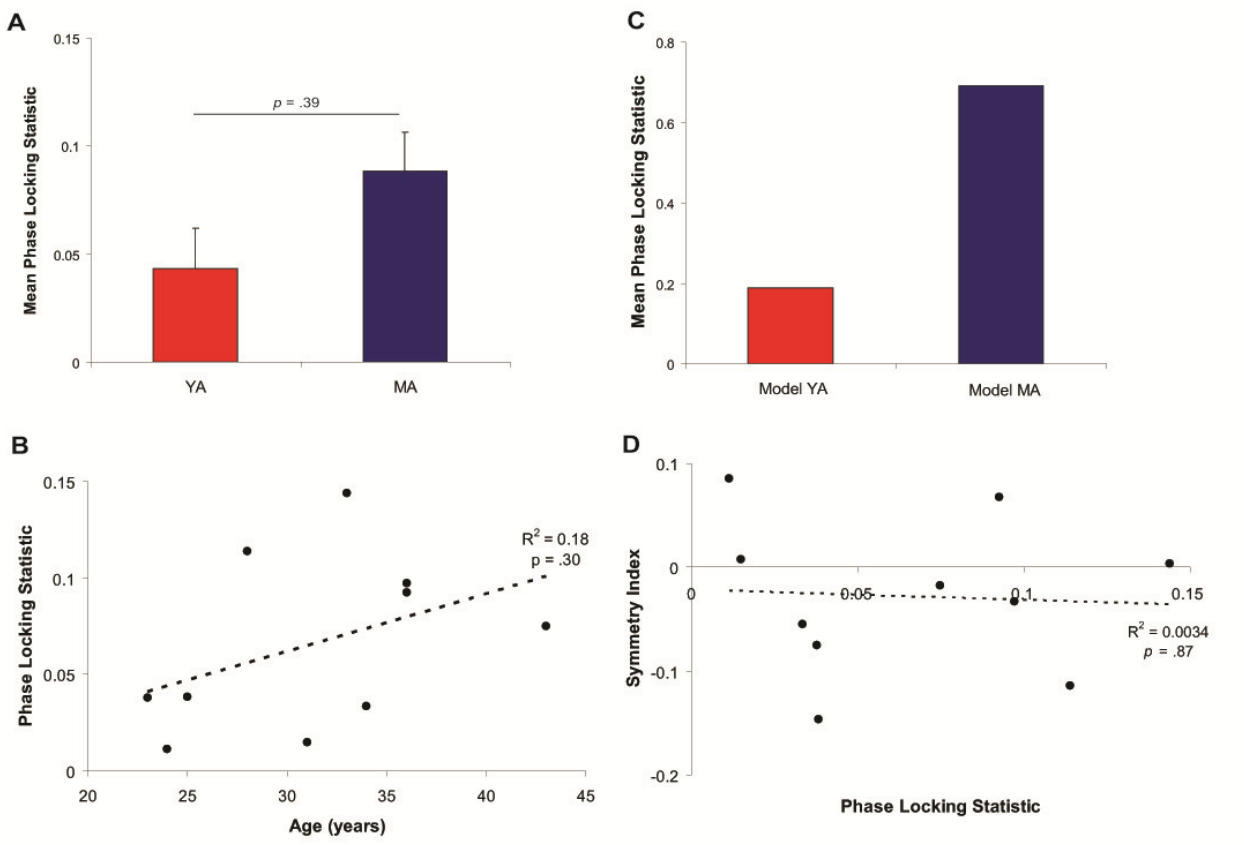

Supplementary Figure 6. Mu-alpha to mu-beta phase locking. We calculated10-20Hz phase-locking statistics (PLS) in our MEG and model SI data using methods as in Lachaux et al., 1999, where we first band passed the signal in the 7-29Hz mu range. **A)** The PLS was more significant in the YA than in the MA (mean PLS YA=0.04 ; mean PLS MA=0.08), but there was no significant difference between groups (p=0.39) nor was there **B**) a significant correlation between PLS and age (p = 0.30). **C)** The model data showed a similar trend of YA simulations having smaller PLS than MA but neither group reached significance likely due to the smaller sample size (n=25 trials) (model YA PLS =0.19 ; model MA PLS =.0.69). **D)** Phase locking statistics did not correlate significantly with symmetry indices (p = .87).

Chapter 5

New multispectral MRI tools reveal stage-dependent decreases in basal forebrain and substantia nigra volumes in early Parkinson's disease.

David A. Ziegler[1], Julien S. Wonderlick[1], Paymon Ashourian[1], Leslie A. Hansen[1], Jeremy C. Young[1], Alex J. Murphy[1], John H. Growdon[2], Suzanne Corkin[1]

1. Department of Brain & Cognitive Sciences, MIT, Cambridge, MA
2. Department of Neurology, Massachusetts General Hospital, Boston, MA

Abstract

While the principal neuropathologic feature of idiopathic Parkinson's disease (PD) is selective loss of dopaminergic neurons and accumulation of Lewy bodies in the substantia nigra pars compacta (SNc), degeneration also occurs in non-dopaminergic circuits, including the cholinergic basal forebrain (BF). Neuropathological studies suggest that degeneration begins in the brainstem and spreads rostrally. Thus, the SN should be affected earlier than the BF. This hypothesis has not been tested in living patients because reliable MRI-based biomarkers did not exist for imaging the SN and BF. The present study estimated the integrity of these structures in PD using new multispectral MRI methods to measure SN and BF volumes. We acquired multiecho T1, multiecho proton density, T2-SPACE, and T2-FLAIR sequences from 29 PD patients (Hoehn & Yahr Stages I-III) and 27 age-, sex-, and education-matched healthy controls. We then created a weighted average of the multiple echoes, yielding a single volume with a high contrast-to-noise ratio for the SN. We visualized the BF using the T2-FLAIR images. We manually labeled and calculated volumes for each structure. Relative to controls, H&Y Stage 1 PD patients had significantly decreased SN volumes. Patients in H&Y stages 2 & 3 showed relatively little additional volume loss. In contrast, the BF volume loss occurred later in the disease, with a significant decrease apparent in stage 2/3 patients compared to controls and stage 1 patients. The latter group did not differ significantly from controls. These results, consistent with the proposed neuropathological trajectory, suggest that our new multispectral methods provide advanced MRI biomarkers for tracking the degeneration of the SN and BF.

Introduction

Parkinson's disease (PD), a neurodegenerative disorder that causes motor, cognitive, and psychiatric symptoms, is typically characterized by a loss of nigrostriatal dopaminergic neurons in the substantia nigra pars compacta (SNc), accompanied by the aggregation of Lewy bodies throughout the brainstem (Fearnley & Lees, 1991; Wichmann & DeLong, 2002; Jellinger, 2005). While denervation of dopaminergic nigrostriatal projections may explain the cardinal motor symptoms of PD, as evidenced by the dramatic motor improvement associated with dopamine replacement therapy (Lang & Lozano, 1998; Poewe, 2009), abnormalities beyond the SNc (Pillon *et al.*, 1989; Dubois *et al.*, 1990a; Rye & DeLong, 2003; Calabresi *et al.*, 2006) may underlie the serious and potentially debilitating non-motor features, including cognitive and memory impairments and progression to dementia (Brooks & Pavese, 2010; Kehagia *et al.*, 2010). Notably, degeneration of the basal forebrain (BF) also occurs in PD (Javoy-Agid et al., 1981; Rogers et al., 1985; Mufson et al., 1991), and could contribute to these non-motor deficits.

The BF is a collection of cholinergic nuclei that contains the diagonal band of Broca, medial septum, and nucleus basalis of Meynert (Whitehouse et al., 1983). These nuclei constitute the primary source of cholinergic innervation of the entire cerebral cortex (Jones et al., 1976; Bigl et al., 1982; Mesulam et al., 1983) and are essential for a host of cognitive processes, including attention and long-term memory (Everitt & Robbins, 1997; Bentley *et al.*, 2004; Mesulam, 2004; Duzel *et al.*, 2010). Degeneration of the BF is often considered a hallmark of Alzheimer's disease

(AD) pathology (Whitehouse et al., 1982; Arendt et al., 1983; Candy et al., 1983; Mesulam, 2004), but some evidence suggests that cell loss and cholinergic dysfunction in PD is comparable or even greater (Arendt et al., 1983; Bohnen et al., 2003).

A prominent hypothesis regarding the neuropathological progression of PD posits that Lewy body deposition commences in the enteric and peripheral nervous system, prior to appearing in the brainstem, and then progresses anteriorly to the midbrain, forebrain, and neocortex (Del Tredici et al., 2002; Braak et al., 2004). Motor symptom onset is believed to become clinically significant between stages 3 and 4. While this staging scheme is based on careful neuropathological examination of a large sample of postmortem specimens, definitive confirmation of the hypothesis is lacking, with some researchers questioning the general utility of the Braak classification scheme (Jellinger, 2009; Lees, 2009). More direct measures of the timing and progression of neuronal degeneration in these areas would help to resolve this debate. In particular, according to this staging scheme, pathological changes in the SNc should precede degeneration of the more anterior BF (Braak et al., 2003; Braak et al., 2004; Shulman et al., 2011).

Indirect support for this hypothesis comes from PET studies that document altered cholinergic neurotransmission in patients with mild PD (Shimada *et al.*, 2009; Gilman *et al.*, 2010; Shinotoh & Hirano, 2010), but an in vivo comparison of the morphology of the SNc and BF in the early stages of PD is currently lacking because reliable MRI-based biomarkers do not exist for imaging

these structures (Schrag *et al.*, 1998; Marek & Jennings, 2009). The ineffectiveness of available MRI techniques stems predominantly from their lack of sufficient contrast to delineate subcortical structures. A few methods for imaging the SNc have met with some success, such as evaluation of T2 relaxation times (Kosta et al., 2006), inversion-recovery sequences (Hutchinson & Raff, 1999; Hutchinson & Raff, 2000), and proton density-weighted imaging (Oikawa et al., 2002). Other studies have resolved the BF/substantia innominata on T2-weighted images (Hanyu et al., 2002; Oikawa et al., 2004; Moon et al., 2008; Muth et al., 2009), demonstrating reduced thickness of this structure in mildly demented PD patients, compared to controls (Oikawa et al., 2004). A limitation of these structural neuroimaging studies, however, is that sequences were optimized to resolve one particular structure, and, therefore, were not well suited for visualizing other brain areas. Thus, each method failed to provide data about both of the implicated structures, and as a result, the morphology of the SNc and BF has been examined only in separate study groups using data collected at different times.

The purpose of the present study was to test the hypothesis that degeneration of the SNc precedes the BF. We used new multispectral structural MRI sequences (T2-SPACE, T2-FLAIR, multiecho T1, and multiecho proton density) to visualize and measure disease-related changes in these structures in a single sample of PD patients and controls. We previously showed that, for the purposes of morphometric analyses, high-bandwidth T1-weighted multiecho MPRAGE data are as good or better than are conventional T1-weighted images (Fischl et al., 2004; Wonderlick et al., 2009). Further, multiecho sequences are less prone to distortion, have a higher contrast-to-noise ratio for subcortical structures, and can be bandwidth-matched to

other multispectral sequences (T2-SPACE, T2-FLAIR, proton density), thereby facilitating coregistration across contrasts without distortion corrections. These scans provide a valuable new window on the subcortical structures that have been implicated in PD but are not readily visible on conventional MRI.

Methods.

Participants

We enrolled 29 patients with idiopathic PD in Hoehn and Yahr (H&Y) Stages 1-3 (13 stage 1, 13 stage 2, and 3 stage 3) and 27 healthy control participants (**Table 1**). In addition, a complete set of multispectral data was collected from a "training sample" of 5 young (mean age 21.4; SD 3.8; 1 male, 4 female) and 6 older (mean age 64.3; SD 12.2; 3 male, 3 female) healthy adults. With these training data, we established the MRI analysis protocols and anatomical definitions that we later applied to our study samples. All PD patients were referred to us by neurologists in the MGH/MIT Morris Udall Center of Excellence in Parkinson's Disease Research. Neurologists established the diagnosis of idiopathic PD by clinical examination according to research diagnostic criteria. We obtained Unified Parkinson's Disease Rating Scale (UPDRS) motor examination scores for 25 (86%) of the PD patients. All patients and controls were between the ages of 50 and 85 years, had completed at least 12 years of schooling, and were able to give informed consent. Exclusion criteria were Parkinsonian syndromes secondary to severe depression, reserpine or neuroleptic administration, progressive supranuclear palsy, multi-system atrophy, Lewy body disease, or the rigid form of Huntington's disease, a Mini-Mental

State Examination score below 26, a Beck Depression Inventory score above 18, history of a neurological disorder other than PD, cancer or serious chronic underlying medical illness, such as serious cardiac disease, untreated hypertension, or history of a psychiatric disorder, and any contraindication for MRI scanning, such as claustrophobia, mechanical or electromagnetic implants, ferromagnetic or non-static metal implants, or tattoos with metal ink.

MRI data acquisitions.

MRI data were aquired at the Athinoula A. Martinos Imaging Center at MIT's McGovern Institute for Brain Research using a Siemens 3 Tesla Trio MRI system with a 12-channel matrix head coil. For each PD patient and control, we collected a series of high-resolution (1 mm isotropic) multispectral data that included multiecho MPRAGE with T1-weighting (**Supplementary Figure 1A**), 3D T2-SPACE turbo spin echo (**Supplementary Figure 1B**), multiecho Fast Low-Angle Shot (FLASH) with proton density weighting (**Supplementary Figure 1C**), and 3D T2-SPACE FLAIR (Fluid-Attenuated Inversion Recovery) turbo spin echo (**Supplementary Figure 1D**) sequences. Each acquisition consisted of a 3D slab with 176 sagittal slices, 1.0 mm thick. In-plane field of view (FOV) was 256 mm sampled on a 256 x 256 matrix, giving an in-plane resolution of 1.0 x 1.0 mm. For *proton density weighting*, the flip angle was 3˚ and repetition time (TR) was 20 ms, during which six echoes were collected after a non-selective excitation. Echo times (TE) were evenly spaced at TE=1.85 + (n x 1.86) ms (n=0,..,5). A proton density volume was generated from a weighted linear average of acquisitions. For *T1-weighting*, flip angle=7˚, TR=2530 ms, and inversion time (TI)=1100 ms, during which four echoes were obtained after non-selective excitation, TE=1.58 + (n x 1.74) ms (n=0,..,3). A single

T1 volume was generated from a root mean square average of acquisitions. For *T2-SPACE*, we collected a 3D slab consisting of 176 sagittal slices, 1.0 mm thick. In-plane FOV was 256 mm sampled on a 256 x 256 matrix, giving an in-plane resolution of 1.0 x 1.0 mm, with TR=3200 ms and TE=444 ms. For *T2-FLAIR*, we obtained a 3D slab consisting of 176 sagittal slices, each 1.0 mm thick. In-plane FOV was 256 mm sampled on a 256 x 256 matrix, giving an in-plane resolution of 1.0 x 1.0 mm, with TR=6000 ms, TE=494 ms, and TI=2100 ms. All sequences were matched at a bandwidth of 698 Hz/pixel. To minimize head motion artifact and fatigue, we used parallel acquisition (GRAPPA) techniques, yielding scan times of 5:56 (multiecho MPRAGE), 4:08 (T2-SPACE), 8:13 (proton density), and 6:38 (T2-FLAIR) min. Each sequence was acquired twice for each participant and the two scans were averaged, yielding a single volume for each contrast.

Multispectral visualization of SNc and BF.

To differentiate the boundaries of the SNc from surrounding structures, we created a weighted average of the four contrasts to obtain a single volume with optimized contrast-to-noise ratio for the SNc, in which this structure was differentiable from the surrounding red nucleus and cerebral peduncles. Our choice of weighting parameters was guided by prior attempts at imaging the SNc, which largely employed T2- and proton density-weighted images. Using the MRI data from our training sample, we found that weighting coefficients of T1 = 11, T2-SPACE = 25, proton density = 94, and T2-FLAIR = 19 yielded excellent contrast for the SNc (**Figure 1A-B**). To generate this multispectral weighted average for each participant, we first performed motion correction and averaging of multiple acquisitions for each multispectral sequence.

Next, we coregistered the four averaged, motion-corrected multispectral volumes for each participant using a linear rigid-body transformation with trilinear interpolation, and then generated a weighted average of the multispectral images using the optimal weighting coefficients. Morphometric details of the SNc were not detectable in our high resolution T1-weighted images (**Supplementary Figure 1A**). In contrast, the SNc was clearly apparent in the average multispectral volume (**Figures 1A & 1B**, red arrows), emphasizing the contribution of the proton density and T2 data. The SNc was distinguished easily from the surrounding red nucleus, SNr, and cerebral peduncles (**Figure 1C**).

Having achieved excellent contrast for SNc, we manually labeled this structure in all PD and control brains (**Figure 1D**). The anatomical boundaries of the SNc were determined in consultation with two expert neuroanatomists using data from our training sample, and thus these participants were not included in the current study sample. The SNc was initially identified in axial sections through the midbrain at a plane where the red nucleus and cerebral peduncle were clearly apparent. The most superficial extent of the red nucleus was then identified and this section was used as the starting point for each label. We labeled the SNc in axial sections moving to the most inferior extent of the red nucleus. Labels were then checked for accuracy in the sagittal and coronal planes.

To visualize the BF, previous studies have typically used T2-weighted images (Moon et al., 2008; Muth et al., 2009). In the present study, we found that the contrast of our T2-FLAIR images (**Figure 2B**) far exceeded that obtained with T2-SPACE images (**Figure 2A**). In particular, the

inferior boundaries of the BF were more clearly defined in the T2-FLAIR images by virtue of the fact that this contrast negated the hyperintensity typically associated with CSF. Further, no additional boost in contrast was afforded by averaging the T2-FLAIR images with any other multispectral data. Thus, we manually labeled the BF on motion corrected, averaged, and intensity normalized T2-FLAIR images. We used a labeling convention similar to that of Muth et al. (2009), whereby the center of the label was identified as the coronal slice in which the anterior commisure was most prominent. The BF was apparent as a narrow band just inferior to the globus pallidus and superior to CSF (**Figure 2C**). We then traced the entire band in this slice and in two others: one anterior to the initial slice and one posterior to it.

Freesurfer-based segmentation of additional cortical and subcortical structures.

To obtain volumetric measures of cortical gray matter and selected subcortical structures, we performed cortical and subcortical segmentation using the FreeSurfer v4.5 software package (Athinoula A. Martinos Center at the Massachusetts General Hospital, Harvard Medical School; http://www.surfer.nmr.mgh.harvard.edu) (Dale et al., 1999; Fischl et al., 2002; Fischl et al., 2004). For each participant, the two multiecho-MPRAGE acquisitions were motion corrected, averaged, and resampled to create a single volume with greater SNR than either single acquisition. Preprocessing of volumes included an affine registration to Talairach space, B1 bias field correction, and removal of skull and dura voxels surrounding the brain. Each reconstructed volume underwent minimal manual editing by a single investigator to ensure that surfaces were properly registered to Talairach space and free of skull and dura. Other processing steps were fully automated using default parameters. After preprocessing, voxels in each hemisphere were

classified as either white matter or non-white matter based on local voxel intensity values. For subcortical segmentation, structures were determined by assigning each voxel of the preprocessed volume to one of 16 possible labels on the basis of voxel intensity, spatial evaluation against a probabilistic training atlas, and subsequent comparison to neighboring voxel labels. The resulting labels were comparable in accuracy to manually delineated subcortical segmentations (Fischl et al., 2002).

Statistical Analyses.

To ensure that the patient and control groups were well matched, we calculated independent *t* tests to detect any group differences in age, years of education, and MMSE scores. A χ^2 test for independence tested for differences in the sex distribution. We used multivariate general linear models (GLM) to test for volumetric differences between PD patients and controls. We performed two GLMs: in the first, the dependant variables were left and right hemisphere volumes of SNc and BF; in the second GLM, the dependant variables were the semi-automatically generated volumes for left and right cerebral cortex, thalamus, caudate, putamen, globus pallidus, hippocampus, and amygdala. To detect any stage dependence of the effects, we divided participants into three groups: controls, PD patients in H&Y stage 1, and PD patients in H&Y stages 2 and 3 (we combined stages 2 and 3 due to the small number of patients in stage 3). In all analyses, age, sex, years of education, and an estimate of intracranial volume (ICV) were included as covariates to help avoid any confounding effect of minor difference in these measures. ICV was estimated using a standard process implemented in the FreeSurfer morphometric processing stream; this process has been described previously

(Buckner et al., 2004). To test for covariance in the degeneration of SNc and BF, we calculated partial correlations, controlling for ICV, between left SNc and left BF and between right SNc and right BF.

Results

We found no significant differences between PD patients and controls in sex distribution (p = .83), age (p = .48), years of education (p = .26), or MMSE scores (p = .23). As expected, motor UPDRS scores were significantly higher in H&Y stage 2/3 patients (mean = 19.7, SD = 8.3), compared to stage 1 patients (mean = 9.2, SD = 5.4), confirming the expected increase in motor symptom severity (p = .002).

Volumes of SNc and BF. A multivariate GLM revealed a significant main effect of group for volumes of the left and right SNc and BF (F = 3.5, p = .001; **Figure 3**). Post-hoc tests confirmed that volumes of the SNc were smaller in H&Y stage 1 patients compared to controls on the left (p = .001); this difference exhibited a trend toward significance on the right (p = .08); H&Y stage 2/3 patients also showed significantly smaller volumes of the SNc, compared to controls, on both the left (p = .0002) and right (p = .02). We found no significant differences between patients in H&Y stage 1 and stages 2/3 for this structure (left, p = .9; right, p = .75). A comparison of multispectral averages from one PD patient and an age- and sex-matched control participant demonstrated the clearly visible signal loss in the SNc of this patient (**Figure 4**).

We observed a slightly different pattern for BF volumes: H&Y stage 1 patients did not differ significantly from controls on the left (p = .84) or right (p = .67), but patients in H&Y stages 2/3 showed significantly reduced volumes bilaterally, compared to controls (left, p = .008; right, p = .01). In addition, relative to patients in H&Y stage 1, those in H&Y stages 2/3 had significantly reduced volumes of the BF on the left (p = .04) and showed a trend toward smaller volumes on the right (p = .08).

Volumes of semi-automatically segmented structures.

In contrast to the significant disease-related changes found for volumes of SNc and BF, the multivariate GLM of cerebral cortex, thalamus, caudate, putamen, globus pallidus, hippocampus, and amygdala volumes did not reveal and significant differences between patients and controls (F = .7, p = .45). To ensure that no subtle differences in individual structures were washed out in the omnibus GLM, we performed exploratory post-hoc comparisons for each structure. The only comparison to even approach significance in this analysis were slightly reduced volumes of the left (p = .06) and right (p = .05) thalamus between stage 2/3 patients and controls. We found no other differences between patients in H & Y stage 1 or 2/3 and controls (all p > .13).

Discussion

This study made two significant contributions. First, we established the utility of new multispectral structural MRI methods for visualizing multiple brain regions affected by PD pathology, but which were poorly resolved with existing MRI techniques. Second, the

application of this new method to MRI data from PD patients and matched controls uncovered a volumetric reduction of the SNc in the earliest stages of the disease, followed by a decrease in BF volumes in later stages. This pattern of atrophy provides in vivo evidence in support of Braak's staging scheme by showing that volume loss in the SNc precedes degeneration of the BF, and is consistent with the putative rostral-to-caudal progression of pathological change (Del Tredici et al., 2002; Braak et al., 2003; Braak et al., 2004). These results underscore previous neuropathological studies showing a loss of cholinergic neurons in the BF (Javoy-Agid et al., 1981; Rogers et al., 1985; Mufson et al., 1991) in addition to degeneration of the SNc in idiopathic PD (Wichmann & DeLong, 2002; Jellinger, 2005). The present report complements the postmortem studies by establishing the temporal progression of degeneration of these structures in living patients. Further, the finding of decreased SNc volumes in H&Y Stage 1 PD patients, with relatively little additional volume loss in H&Y stages 2 & 3, supports the notion that cell loss in this area appears early in the disease course, with the bulk of SNc cell loss likely occurring prior to symptom onset (Lees, 2009). In contrast, the BF volume loss occurred later in the disease, with a significant decrease in volume in stage 2/3 patients relative to controls and stage 1 patients, who did not differ significantly from controls.

Disease-related changes in SNc.

This experiment took advantage of a broad range of MR contrasts, which for the first time could be easily coregistered, to achieve excellent contrast for the SNc. Based on previous MR studies, we generated weighted averages of scans with different contrasts, emphasizing the contribution of proton density- and T2-weighted images, with a lesser, but important,

contribution from T1-weighted and T2-FLAIR images. This method allowed reliable delineation the SNc in a relatively large sample of PD patients and matched controls. The fact that the anatomical location of the SNc in our images corresponded well to those described in the most accurate MRI studies performed to date (Oikawa *et al.*, 2002; Sasaki *et al.*, 2006; Hutchinson & Raff, 2008; Menke *et al.*, 2009), increased our confidence in the utility of this method for distinguishing SNc from SNr. As a result, we were able to detect a significant decrease in the volume of the SNc in the earliest stage of the disease.

The present finding of significantly reduced SNc volumes in stage 1 patients is consistent with the known neuropathological trajectory. Numerous postmortem studies have established that PD is associated with a significant loss of dopaminergic neurons in the SNc (Jellinger, 1987; German *et al.*, 1989; Fearnley & Lees, 1991; Ma *et al.*, 1997; Jellinger, 2004). The degree of cell loss correlates with severity of motor symptomology (Rinne et al., 1989; Ma et al., 1997; Greffard et al., 2006), and dopamine replacement therapy remains the gold standard treatment for motor symptoms (Lang & Lozano, 1998; Poewe, 2009). Further, neuropathological studies indicate that a large percentage of dopamineric neurons in the SNc are lost prior to symptom onset or formal diagnosis, with estimates ranging from 30-70% (Fearnley & Lees, 1991; Gaig & Tolosa, 2009; Lees, 2009).

Because the borders of the SNc are nearly impossible to visualize on conventional T1-weighted MRI, many attempts have been made to develop new sequences that would provide indices of nigral degeneration in PD (Massey & Yousry, 2010). Results from these studies, however, are

wrought with contradictions. Early attempts at visualizing the SNc capitalized on the relative distribution of iron in the midbrain, which causes magnetic susceptibility and signal loss on T2-weighted images (Drayer et al., 1986). The SNr has relatively high levels of iron, and thus appears as a hypointense region, whereas the dopamineric SNc, which contains neuromelanin, appears as a hyperintense region between the SNr and red nucleus on axial images (Sasaki et al., 2008). While the majority of studies report signal loss or reduced size of the SNc in PD patients compared to controls (Duguid et al., 1986; Braffman et al., 1989; Huber et al., 1990; Antonini et al., 1993; Gorell et al., 1995), some failed to find disease-related changes (Stern et al., 1989; Adachi et al., 1999), and others pointed out potential confounds in prior studies (Doraiswamy et al., 1991). Possible limitations of visualizing the SNc on T2-weighted images were that the anatomical location of the SNc appeared to be inconsistent with histological reports and these methods were not able to reliably differentiate SNc from SNr (Sasaki et al., 2008). A subsequent study used proton density weighted MRI in combination with short inversion-time recovery images to more accurately distinguish the SNc and SNr, but did not find a significant decrease in SNc size in PD patients (Oikawa et al., 2002). Newer methods, such as the use of MR sequences sensitive to neuromelanin (Sasaki et al., 2006) and segmented inversion recovery ratio imaging (Hutchinson *et al.*, 2003; Minati *et al.*, 2007; Hutchinson & Raff, 2008) have achieved greater success in differentiating SNr and SNc and have documented disease-related changes in the SNc. An emerging method, connectivity-based segmentation of the SN using diffusion tensor imaging, may prove useful for delineating SNc and SNr, but an initial report failed to find a significant different in SNc size between PD patients and controls, possibly due to a limited sample size (Menke et al., 2009).

Somewhat surprisingly, we found no additional significant loss of SNc volume in patients in stages 2/3. This lack of further volumetric decrease presents a paradox considering that the progression from stage to stage necessitates a worsening of motor symptoms, and motor symptom severity has been linked to pathology in the SNc. In addition, neuropathological studies have shown continued cell loss over the course of the disease (Fearnley & Lees, 1991). One possible explanation is that our group of patients in stages 2/3 was almost entirely composed of stage 2 patients (we were only able to acquire usable MRI data from 3 PD patients in stage 3), and thus the difference between these two early stages may be small in terms of both pathological change in the SNc and motor symptom worsening, compared to transitioning into the end-stages of the disease, often coinciding with the onset of dementia.

Basal forebrain degeneration in PD.

In addition to using our new multispectral MRI methods to measure the SNc, we also found that our T2-FLAIR images provided superior contrast for the BF than that achieved in previous MRI studies. We were, therefore, able to examine the morphology of this structure in this same set of PD patients and controls. Previous evidence of cholinergic degeneration in PD comes directly from pathological studies and indirectly from PET measurements of cholinergic markers. Neuropathological studies have documented a pronounced loss of cholinergic neurons in the BF of patients with PD (Arendt *et al.*, 1983; Whitehouse *et al.*, 1983; Nakano & Hirano, 1984; Tagliavini *et al.*, 1984; Rogers *et al.*, 1985). In addition to direct cell counts, evidence for a loss of BF cholinergic function in PD brains comes from other postmortem studies that documented

decreases in biochemical markers of cholinergic function, including choline acetyltransferase (ChAT) and acetylcholinesterase (AChE) (Ruberg et al., 1986). Several of these studies reported a link between non-motor cognitive impairments and cholinergic dysfunction (Perry et al., 1985; Mattila et al., 2001).

Complementary in vivo evidence for a loss of cholinergic function in PD comes from PET studies showing a marked reduction of AChE activity in cortical regions (Bohnen et al., 2006; Shimada et al., 2009; Gilman et al., 2010). Based on our knowledge of the patterns of cholinergic projections (Jones et al., 1976; Bigl et al., 1982; Mesulam et al., 1983), it appears likely that a decrease in cortical AChE activity would result from a specific loss of cholinergic neurons in the BF. This decrease in AChE function appears relatively early in PD (Bohnen & Albin, 2009; Gilman *et al.*, 2010), but the magnitude of the disruption is greater and more widespread in PD patients with dementia than in non-demented patients (Bohnen et al., 2006; Shimada et al., 2009). The present finding of greater BF volume loss at later stages of the disease is consistent with these PET studies, as well as with reports of a more dramatic degree of BF cell loss in PD patients with dementia, compared to non-demented patients (Whitehouse et al., 1983). None of the patients in the present study was demented.

MRI studies of the BF have generally relied on T2-weighted images. In contrast to studies of the SNc, relatively few studies have attempted to use MRI to measure disease-related changes in the BF of PD patients, although reports exist of BF changes on MRI in AD (Moon et al., 2008) and mild cognitive impairment (Muth et al., 2009). One study reported a small, but significant,

decrease in the thickness of the BF, measured in a single coronal section from a T2-weighted image, in cognitively intact PD patients, as well as a more substantial reduction in demented patients (Oikawa et al., 2004). Another report showed decreased BF thickness in patients with dementia with Lewy bodies, but this study did not include a non-demented idiopathic PD group (Hanyu et al., 2007).

The volume of the BF has also been measured using T1-weighted images collected at 3T, in which the borders of the BF are more visible than in lower field strength images (George et al., 2009). This method revealed a significant decrease in volume of the BF between non-demented PD patients and controls, with further volume loss in demented patients (Choi et al., 2011). The present finding of reduced BF forebrain volumes in stage 2/3 PD patients is in accord with these previous reports. No other studies, to our knowledge, have examined differences between stages 1 and 2/3, but the reports of more extreme cell and volume loss in demented patients is consistent with the trajectory of volume loss reported here.

The fact that cholinergic degeneration in PD worsens with disease progression and is exacerbated in PD patients with dementia (Whitehouse *et al.*, 1983; Gaspar & Gray, 1984; Bohnen *et al.*, 2006; Shimada *et al.*, 2009) suggests parallels between PD and AD. While disruption of cholinergic function appears to be linked to the development of cognitive impairments and dementia, explicit evidence for a shared pathogenic mechanism between PD and AD remains equivocal. In PD, neuron loss or Lewy body deposition in the BF can occur in the absence of the hallmark neuropathological features of AD—amyloid plaques and

neurofibrillary tangles (Nakano & Hirano, 1984; Tagliavini *et al.*, 1984; Kosaka *et al.*, 1988; Yoshimura, 1988; Sudarsky *et al.*, 1989). Other studies have failed to find a significant correlation between level of cognitive impairment and degree of cell loss (Jellinger & Paulus, 1992) or Lewy body burden (Kalaitzakis et al., 2009) in the BF in PD, leading to the hypothesis that the degree of cholinergic degeneration must reach a critical threshold before the symptoms of dementia emerge (Jellinger, 2004). Thus, while some have proposed a common mechanism underlying BF degeneration in AD and PD with dementia, direct support for this hypothesis is lacking. An alterative proposal is that BF degeneration is primary in PD, whereas cholinergic cell loss in AD is secondary to cortical pathology which then leads to depleted retrograde transport of critical growth factors to BF neurons (Jellinger, 2004).

Whether a bona fide pathological parallel exists between PD and AD, the disruption of cholinergic function in PD has real and important clinical implications that are not limited to dementia. Cholinergic dysfunction has been linked to a number of non-motor symptoms in PD, including decreased performance on tests of working memory (Bohnen et al., 2006), set-shifting (Dubois et al., 1990b; Bedard et al., 1999), and free recall (Bedard et al., 1999). In addition, administration of anticholinergic drugs led to the development of executive (Bedard et al., 1999) and memory (Dubois et al., 1987) impairments in PD patients who did not previously show these deficits. Some of these symptoms were partially ameliorated by treatment with central cholinesterase inhibitors (Olin et al., 2010; Schmitt et al., 2010a; Schmitt et al., 2010b), and indeed, cholinesterase inhibitors have become a staple in the treatment of PD (Burn, 2010; Wood et al., 2010).

Comparison of SNc and BF changes in PD

This study provided the first direct in vivo comparison of volumes of the SNc and BF in the same sample of PD patients, supporting the predominant view that the neuropathological progression in PD begins in the medulla and then spreads in a topographical fashion up the brainstem, to the midbrain, forebrain, and then finally neocortex (Del Tredici et al., 2002; Braak et al., 2004). In this neuropathological staging scheme, Lewy body deposition appears to occur in the SNc in stage 3 and in the BF in stage 4. Consistent with this proposal, our analysis of MRI-derived volumetric data revealed an earlier decrease in the volume of the SNc, followed by a later loss of BF volumes in H&Y stages 2/3. Our MRI data add to the neuropathological studies, which are based entirely on measures of α-synuclein inclusions and not on cell or volume loss, with uncertainty regarding the correspondence between α-synuclein pathology and loss of volume (Ma et al., 1997).

Some researchers have called into question the usefulness of the neuropathological staging scheme (Jellinger, 2009; Lees, 2009), arguing that idiopathic PD is not the result of a unitary pathogenic mechanism. Indeed, a longitudinal study of pathological progression revealed three distinct subgroups of patients (Halliday et al., 2008; Jellinger, 2009). While the largest subgroup, patients with onset in their 50s and 60s and slow disease progression, showed pathological changes consistent with the Braak staging scheme, other patients did not show this pattern. These differences in patterns of neurodegeneration may represent subgroups of PD patients with fundamentally distinct disease processes and trajectories of disease progression, and an emerging view is that heterogeneity may be the rule in PD.

This heterogeneity likely reflects the existence of biological subtypes, with groups of patients showing unique patterns of disease progression and cognitive change. PD patients who show early pathological insults in non-dopaminergic nuclei may be more likely to show deficits in attention and cognitive control in the early stages of the disease. Support for this view comes from studies that have identified groups of patients with distinct patterns of cognitive impairment (Mortimer et al., 1987; Lewis et al., 2003; Locascio et al., 2003). This finding raises the possibility that a subgroup of idiopathic PD patients may be at greater risk for developing memory impairments and dementia, which may correspond to a greater degree of BF degeneration, resulting in a more extensive disruption of cholinergic innervation of the neocortex. Evidence of such heterogeneity comes from the observation that some advanced PD patients without dementia actually showed higher levels of AchE activity than a sample of drug-naïve patients in the earliest stages of the disease (Shimada et al., 2009). Further, PD patients who show postural and gait disturbances, which are associated with increased risk of falling, are at greater risk for developing dementia (Taylor et al., 2008). Pharmaceutical augmentation of cholinergic activity led to a significantly reduced frequency of falling in some PD patients (Chung et al., 2010).

Somewhat surprisingly, volumes of the SNc and BF did not correlate significantly with each other in our sample of PD patients or controls. One possibility is that our sample is heterogeneous with respect to disease subgroups, and thus a larger sample might reveal a subset of patients in which degeneration of these structures is more tightly linked. Longitudinal

studies on a larger sample will be necessary to determine with confidence whether such subgroups exist. The development of new in vivo measures of subcortical brain structures, such as those described here, will be essential to document expected anatomical changes. The future identification and characterization of PD subgroups will provide clinicians and researchers more focused therapeutic targets.

Volumes of semi-automatically segmented structures

In contrast to volumes of SNc and BF, we did not find any significant reductions of volume for any of the striatal, forebrain, or neocortical structures that we examined. This result is largely consistent with the Braak neuropathological staging scheme, which posits that PD initially targets brainstem medullary, pontine, and olfactory nuclei, and then the SNpc, BF and limbic structures. The disease affects other forebrain and neocortical areas in the latest stages of the disease (Braak et al., 2004), which is often associated with severe cognitive impairments and frank dementia. Our study explicitly excluded demented patients and only included three patients in H&Y stage 3. It is, therefore, not surprising that we did not find structural correlates of pathological changes that occur very late in the disease course. Because Lewy body pathology affects limbic structures in the same pathological stage as the BF (Braak et al., 2004; Shulman et al., 2011), we might have expected to see evidence of disease-related changes in the hippocampus and amygdala in our stage 2/3 patients, in whom we observed a volumetric decline of BF volumes. While we cannot fully explain this discrepancy, we note that some neuropathological studies failed to find a correlation between α-synuclein pathology and volumetric loss (Ma et al., 1997; Harding et al., 2002b), which may be more tightly coupled to

an actual loss of neurons. Postmortem studies have documented a loss of neurons in the amygdala (Double *et al.*, 1996; Churchyard & Lees, 1997; Harding *et al.*, 2002b), hippocampus (Rinne et al., 1987; Harding et al., 2002a), and thalamus (Brooks & Halliday, 2009; Halliday, 2009; Kusnoor *et al.*, 2009), but these changes, observed postmortem, are typically seen in patients in more advanced stages than those in our study. Thus, it is possible that the patterns of Lewy body pathology and neuronal degeneration do not follow parallel trajectories.

Further complicating the interpretation of these findings are several prior MRI studies that examined cortical and subcortical volumes between PD patients and controls. Results from these studies are mixed and often contradictory. Consistent with the present results, several studies reported no differences in regional cortical or subcortical volumes between PD and controls (Schulz et al., 1999; Barber et al., 2002; Almeida et al., 2003). Also in accordance with our findings was a longitudinal study that used voxel-based morphometric methods to detect a decrease in volumes of hippocampus and amygdala in demented PD patients, with smaller, but nonsignificant decreases in nondemented patients, compared to controls (Junque et al., 2005). In contrast, others reported selective decreases of midbrain and striatal volumes in PD (Lisanby et al., 1993; Geng et al., 2006), while another group reported increased intracranial volumes in PD, accompanied by decreased volume of the putamen (Krabbe et al., 2005). To build a consensus in the literature, future experiments will need to recruit large samples of well-characterized PD patients and integrate their MRI data, derived from advanced imaging and analysis tools, with scores from a broad spectrum of cognitive tests.

Conclusion

The present study introduced powerful multispectral MRI tools to examine the temporal progression of degeneration in SNc and BF, as well as in other forebrain and neocortical structures. Although some aspects of the Braak neuropathological staging scheme remain a topic of debate and continued research, results from this study provide in vivo support for the Braak staging scheme, in which Lewy body pathology affects SNc prior to BF, before spreading anteriorly to the neocortex. A critical outstanding question is whether subgroups of patients exist that do not show this temporal progression of pathological change, and if so, what are the frequencies and clinical ramifications. The multispectral methods presented here provide new MRI biomarkers that will allow future studies to test this hypothesis on a larger sample of PD patients studied longitudinally.

References

Adachi M, Hosoya T, Haku T, Yamaguchi K & Kawanami T (1999) Evaluation of the substantia nigra in patients with Parkinsonian syndrome accomplished using multishot diffusion-weighted MR imaging. *AJNR Am J Neuroradiol* 20, 1500-1506.

Almeida OP, Burton EJ, McKeith I, Gholkar A, Burn D & O'Brien JT (2003) MRI study of caudate nucleus volume in Parkinson's disease with and without dementia with Lewy bodies and Alzheimer's disease. *Dement Geriatr Cogn Disord* 16, 57-63.

Antonini A, Leenders KL, Meier D, Oertel WH, Boesiger P & Anliker M (1993) T2 relaxation time in patients with Parkinson's disease. *Neurology* 43, 697-700.

Arendt T, Bigl V, Arendt A & Tennstedt A (1983) Loss of neurons in the nucleus basalis of Meynert in Alzheimer's disease, paralysis agitans and Korsakoff's Disease. *Acta Neuropathol* 61, 101-108.

Barber R, McKeith I, Ballard C & O'Brien J (2002) Volumetric MRI study of the caudate nucleus in patients with dementia with Lewy bodies, Alzheimer's disease, and vascular dementia. *J Neurol Neurosurg Psychiatry* 72, 406-407.

Bedard MA, Pillon B, Dubois B, Duchesne N, Masson H & Agid Y (1999) Acute and long-term administration of anticholinergics in Parkinson's disease: specific effects on the subcortico-frontal syndrome. *Brain Cogn* 40, 289-313.

Bentley P, Husain M & Dolan RJ (2004) Effects of cholinergic enhancement on visual stimulation, spatial attention, and spatial working memory. *Neuron* 41, 969-982.

Bigl V, Woolf NJ & Butcher LL (1982) Cholinergic projections from the basal forebrain to frontal, parietal, temporal, occipital, and cingulate cortices: a combined fluorescent tracer and acetylcholinesterase analysis. *Brain Res Bull* 8, 727-749.

Bohnen NI & Albin RL (2009) Cholinergic denervation occurs early in Parkinson disease. *Neurology* 73, 256-257.

Bohnen NI, Kaufer DI, Hendrickson R, Ivanco LS, Lopresti BJ, Constantine GM, Mathis Ch A, Davis JG, Moore RY & Dekosky ST (2006) Cognitive correlates of cortical cholinergic denervation in Parkinson's disease and parkinsonian dementia. *J Neurol* 253, 242-247.

Bohnen NI, Kaufer DI, Ivanco LS, Lopresti B, Koeppe RA, Davis JG, Mathis CA, Moore RY & DeKosky ST (2003) Cortical cholinergic function is more severely affected in parkinsonian dementia than in Alzheimer disease: an in vivo positron emission tomographic study. *Arch Neurol* 60, 1745-1748.

Braak H, Del Tredici K, Rub U, de Vos RA, Jansen Steur EN & Braak E (2003) Staging of brain pathology related to sporadic Parkinson's disease. *Neurobiol Aging* 24, 197-211.

Braak H, Ghebremedhin E, Rub U, Bratzke H & Del Tredici K (2004) Stages in the development of Parkinson's disease-related pathology. *Cell Tissue Res* 318, 121-134.

Braffman BH, Grossman RI, Goldberg HI, Stern MB, Hurtig HI, Hackney DB, Bilaniuk LT & Zimmerman RA (1989) MR imaging of Parkinson disease with spin-echo and gradient-echo sequences. *AJR Am J Roentgenol* 152, 159-165.

Brooks D & Halliday GM (2009) Intralaminar nuclei of the thalamus in Lewy body diseases. *Brain Res Bull* 78, 97-104.

Brooks DJ & Pavese N (2010) Imaging non-motor aspects of Parkinson's disease. *Prog Brain Res* 184, 205-218.

Buckner RL, Head D, Parker J, Fotenos AF, Marcus D, Morris JC & Snyder AZ (2004) A unified approach for morphometric and functional data analysis in young, old, and demented adults using automated atlas-based head size normalization: reliability and validation against manual measurement of total intracranial volume. *Neuroimage* 23, 724-738.

Burn DJ (2010) The treatment of cognitive impairment associated with Parkinson's disease. *Brain Pathol* 20, 672-678.

Calabresi P, Picconi B, Parnetti L & Di Filippo M (2006) A convergent model for cognitive dysfunctions in Parkinson's disease: the critical dopamine-acetylcholine synaptic balance. *Lancet Neurol* 5, 974-983.

Candy JM, Perry RH, Perry EK, Irving D, Blessed G, Fairbairn AF & Tomlinson BE (1983) Pathological changes in the nucleus of Meynert in Alzheimer's and Parkinson's diseases. *J Neurol Sci* 59, 277-289.

Choi SH, Jung TM, Lee JE, Lee SK, Sohn YH & Lee PH (2011) Volumetric analysis of the substantia innominata in patients with Parkinson's disease according to cognitive status. *Neurobiol Aging*.

Chung KA, Lobb BM, Nutt JG & Horak FB (2010) Effects of a central cholinesterase inhibitor on reducing falls in Parkinson disease. *Neurology* 75, 1263-1269.

Churchyard A & Lees AJ (1997) The relationship between dementia and direct involvement of the hippocampus and amygdala in Parkinson's disease. *Neurology* 49, 1570-1576.

Dale AM, Fischl B & Sereno MI (1999) Cortical surface-based analysis. I. Segmentation and surface reconstruction. *Neuroimage* 9, 179-194.

Del Tredici K, Rub U, De Vos RA, Bohl JR & Braak H (2002) Where does parkinson disease pathology begin in the brain? *J Neuropathol Exp Neurol* 61, 413-426.

Doraiswamy PM, Shah SA, Husain MM, Rodrigo Escalona P, McDonald WM, Figiel GS & Krishnan KR (1991) Magnetic resonance evaluation of the midbrain in Parkinson's disease. *Arch Neurol* 48, 360.

Double KL, Halliday GM, McRitchie DA, Reid WG, Hely MA & Morris JG (1996) Regional brain atrophy in idiopathic parkinson's disease and diffuse Lewy body disease. *Dementia* 7, 304-313.

Drayer B, Burger P, Darwin R, Riederer S, Herfkens R & Johnson GA (1986) MRI of brain iron. *AJR Am J Roentgenol* 147, 103-110.

Dubois B, Danze F, Pillon B, Cusimano G, Lhermitte F & Agid Y (1987) Cholinergic-dependent cognitive deficits in Parkinson's disease. *Ann Neurol* 22, 26-30.

Dubois B, Pillon B, Sternic N, Lhermitte F & Agid Y (1990a) Age-induced cognitive disturbances in Parkinson's disease. *Neurology* 40, 38-41.

Dubois B, Pilon B, Lhermitte F & Agid Y (1990b) Cholinergic deficiency and frontal dysfunction in Parkinson's disease. *Ann Neurol* 28, 117-121.

Duguid JR, De La Paz R & DeGroot J (1986) Magnetic resonance imaging of the midbrain in Parkinson's disease. *Ann Neurol* 20, 744-747.

Duzel S, Munte TF, Lindenberger U, Bunzeck N, Schutze H, Heinze HJ & Duzel E (2010) Basal forebrain integrity and cognitive memory profile in healthy aging. *Brain Res* 1308, 124-136.

Everitt BJ & Robbins TW (1997) Central cholinergic systems and cognition. *Annu Rev Psychol* 48, 649-684.

Fearnley JM & Lees AJ (1991) Ageing and Parkinson's disease: substantia nigra regional selectivity. *Brain* 114 (Pt 5), 2283-2301.

Fischl B, Salat DH, Busa E, Albert M, Dieterich M, Haselgrove C, van der Kouwe A, Killiany R, Kennedy D, Klaveness S, Montillo A, Makris N, Rosen B & Dale AM (2002) Whole brain segmentation: automated labeling of neuroanatomical structures in the human brain. *Neuron* 33, 341-355.

Fischl B, Salat DH, van der Kouwe AJ, Makris N, Segonne F, Quinn BT & Dale AM (2004) Sequence-independent segmentation of magnetic resonance images. *Neuroimage* 23 Suppl 1, S69-84.

Gaig C & Tolosa E (2009) When does Parkinson's disease begin? *Mov Disord* 24 Suppl 2, S656-664.

Gaspar P & Gray F (1984) Dementia in idiopathic Parkinson's disease. A neuropathological study of 32 cases. *Acta Neuropathol* 64, 43-52.

Geng DY, Li YX & Zee CS (2006) Magnetic resonance imaging-based volumetric analysis of basal ganglia nuclei and substantia nigra in patients with Parkinson's disease. *Neurosurgery* 58, 256-262; discussion 256-262.

George S, Mufson EJ, Leurgans S, Shah RC, Ferrari C & Detoledo-Morrell L (2009) MRI-based volumetric measurement of the substantia innominata in amnestic MCI and mild AD. *Neurobiol Aging*.

German DC, Manaye K, Smith WK, Woodward DJ & Saper CB (1989) Midbrain dopaminergic cell loss in Parkinson's disease: computer visualization. *Ann Neurol* 26, 507-514.

Gilman S, Koeppe RA, Nan B, Wang CN, Wang X, Junck L, Chervin RD, Consens F & Bhaumik A (2010) Cerebral cortical and subcortical cholinergic deficits in parkinsonian syndromes. *Neurology* 74, 1416-1423.

Gorell JM, Ordidge RJ, Brown GG, Deniau JC, Buderer NM & Helpern JA (1995) Increased iron-related MRI contrast in the substantia nigra in Parkinson's disease. *Neurology* 45, 1138-1143.

Greffard S, Verny M, Bonnet AM, Beinis JY, Gallinari C, Meaume S, Piette F, Hauw JJ & Duyckaerts C (2006) Motor score of the Unified Parkinson Disease Rating Scale as a good predictor of Lewy body-associated neuronal loss in the substantia nigra. *Arch Neurol* 63, 584-588.

Halliday G, Hely M, Reid W & Morris J (2008) The progression of pathology in longitudinally followed patients with Parkinson's disease. *Acta Neuropathol* 115, 409-415.

Halliday GM (2009) Thalamic changes in Parkinson's disease. *Parkinsonism Relat Disord* 15 Suppl 3, S152-155.

Hanyu H, Asano T, Sakurai H, Tanaka Y, Takasaki M & Abe K (2002) MR analysis of the substantia innominata in normal aging, Alzheimer disease, and other types of dementia. *AJNR Am J Neuroradiol* 23, 27-32.

Hanyu H, Shimizu S, Tanaka Y, Hirao K, Iwamoto T & Abe K (2007) MR features of the substantia innominata and therapeutic implications in dementias. *Neurobiol Aging* 28, 548-554.

Harding AJ, Lakay B & Halliday GM (2002a) Selective hippocampal neuron loss in dementia with Lewy bodies. *Ann Neurol* 51, 125-128.

Harding AJ, Stimson E, Henderson JM & Halliday GM (2002b) Clinical correlates of selective pathology in the amygdala of patients with Parkinson's disease. *Brain* 125, 2431-2445.
Huber SJ, Chakeres DW, Paulson GW & Khanna R (1990) Magnetic resonance imaging in Parkinson's disease. *Arch Neurol* 47, 735-737.
Hutchinson M & Raff U (1999) Parkinson's disease: a novel MRI method for determining structural changes in the substantia nigra. *J Neurol Neurosurg Psychiatry* 67, 815-818.
Hutchinson M & Raff U (2000) Structural changes of the substantia nigra in Parkinson's disease as revealed by MR imaging. *AJNR Am J Neuroradiol* 21, 697-701.
Hutchinson M & Raff U (2008) Detection of Parkinson's disease by MRI: Spin-lattice distribution imaging. *Mov Disord* 23, 1991-1997.
Hutchinson M, Raff U & Lebedev S (2003) MRI correlates of pathology in parkinsonism: segmented inversion recovery ratio imaging (SIRRIM). *Neuroimage* 20, 1899-1902.
Javoy-Agid F, Taquet H, Ploska A, Cherif-Zahar C, Ruberg M & Agid Y (1981) Distribution of catecholamines in the ventral mesencephalon of human brain, with special reference to Parkinson's disease. *J Neurochem* 36, 2101-2105.
Jellinger K (2005) The pathology of Parkinson's disease-recent advances. In *Scientific basis for the treatment of parkinson's disease.*, pp. 53-86 [N Galvez-Jimenez, editor]. New York: Taylor & Francis.
Jellinger KA (1987) The pathology of Parkinson's disease. In *Movement Disorders 2* [CD Marsden and S Fahn, editors]. UK: Butterworth & Co.
Jellinger KA (2004) The pathology of Parkinson's disease - recent advances. In *Scientific basis for the treatment of Parkinson's disease* [N Galvez-Jimenez, editor]: Taylor & Francis.
Jellinger KA (2009) A critical evaluation of current staging of alpha-synuclein pathology in Lewy body disorders. *Biochim Biophys Acta* 1792, 730-740.
Jellinger KA & Paulus W (1992) Clinico-pathological correlations in Parkinson's disease. *Clin Neurol Neurosurg* 94 Suppl, S86-88.
Jones EG, Burton H, Saper CB & Swanson LW (1976) Midbrain, diencephalic and cortical relationships of the basal nucleus of Meynert and associated structures in primates. *J Comp Neurol* 167, 385-419.
Junque C, Ramirez-Ruiz B, Tolosa E, Summerfield C, Marti MJ, Pastor P, Gomez-Anson B & Mercader JM (2005) Amygdalar and hippocampal MRI volumetric reductions in Parkinson's disease with dementia. *Mov Disord* 20, 540-544.
Kalaitzakis ME, Christian LM, Moran LB, Graeber MB, Pearce RK & Gentleman SM (2009) Dementia and visual hallucinations associated with limbic pathology in Parkinson's disease. *Parkinsonism Relat Disord* 15, 196-204.
Kehagia AA, Barker RA & Robbins TW (2010) Neuropsychological and clinical heterogeneity of cognitive impairment and dementia in patients with Parkinson's disease. *Lancet Neurol* 9, 1200-1213.
Kosaka K, Tsuchiya K & Yoshimura M (1988) Lewy body disease with and without dementia: a clinicopathological study of 35 cases. *Clin Neuropathol* 7, 299-305.
Kosta P, Argyropoulou MI, Markoula S & Konitsiotis S (2006) MRI evaluation of the basal ganglia size and iron content in patients with Parkinson's disease. *J Neurol* 253, 26-32.
Krabbe K, Karlsborg M, Hansen A, Werdelin L, Mehlsen J, Larsson HB & Paulson OB (2005) Increased intracranial volume in Parkinson's disease. *J Neurol Sci* 239, 45-52.

Kusnoor SV, Muly EC, Morgan JI & Deutch AY (2009) Is the loss of thalamostriatal neurons protective in parkinsonism? *Parkinsonism Relat Disord* 15 Suppl 3, S162-166.

Lang AE & Lozano AM (1998) Parkinson's disease. Second of two parts. *N Engl J Med* 339, 1130-1143.

Lees AJ (2009) The Parkinson chimera. *Neurology* 72, S2-11.

Lewis SJ, Cools R, Robbins TW, Dove A, Barker RA & Owen AM (2003) Using executive heterogeneity to explore the nature of working memory deficits in Parkinson's disease. *Neuropsychologia* 41, 645-654.

Lisanby SH, McDonald WM, Massey EW, Doraiswamy PM, Rozear M, Boyko OB, Krishnan KR & Nemeroff C (1993) Diminished subcortical nuclei volumes in Parkinson's disease by MR imaging. *J Neural Transm Suppl* 40, 13-21.

Locascio JJ, Corkin S & Growdon JH (2003) Relation between clinical characteristics of Parkinson's disease and cognitive decline. *J Clin Exp Neuropsychol* 25, 94-109.

Ma SY, Roytta M, Rinne JO, Collan Y & Rinne UK (1997) Correlation between neuromorphometry in the substantia nigra and clinical features in Parkinson's disease using disector counts. *J Neurol Sci* 151, 83-87.

Marek K & Jennings D (2009) Can we image premotor Parkinson disease? *Neurology* 72, S21-26.

Massey LA & Yousry TA (2010) Anatomy of the substantia nigra and subthalamic nucleus on MR imaging. *Neuroimaging Clin N Am* 20, 7-27.

Mattila PM, Roytta M, Lonnberg P, Marjamaki P, Helenius H & Rinne JO (2001) Choline acetytransferase activity and striatal dopamine receptors in Parkinson's disease in relation to cognitive impairment. *Acta Neuropathol* 102, 160-166.

Menke RA, Jbabdi S, Miller KL, Matthews PM & Zarei M (2009) Connectivity-based segmentation of the substantia nigra in human and its implications in Parkinson's disease. *Neuroimage* 52, 1175-1180.

Mesulam MM (2004) The cholinergic innervation of the human cerebral cortex. *Prog Brain Res* 145, 67-78.

Mesulam MM, Mufson EJ, Levey AI & Wainer BH (1983) Cholinergic innervation of cortex by the basal forebrain: cytochemistry and cortical connections of the septal area, diagonal band nuclei, nucleus basalis (substantia innominata), and hypothalamus in the rhesus monkey. *J Comp Neurol* 214, 170-197.

Minati L, Grisoli M, Carella F, De Simone T, Bruzzone MG & Savoiardo M (2007) Imaging degeneration of the substantia nigra in Parkinson disease with inversion-recovery MR imaging. *AJNR Am J Neuroradiol* 28, 309-313.

Moon WJ, Kim HJ, Roh HG & Han SH (2008) Atrophy measurement of the anterior commissure and substantia innominata with 3T high-resolution MR imaging: does the measurement differ for patients with frontotemporal lobar degeneration and Alzheimer disease and for healthy subjects? *AJNR Am J Neuroradiol* 29, 1308-1313.

Mortimer JA, Jun SP, Kuskowski MA & Webster DD (1987) Subtypes of Parkinson's disease defined by intellectual impairment. *J Neural Transm Suppl* 24, 101-104.

Mufson EJ, Presley LN & Kordower JH (1991) Nerve growth factor receptor immunoreactivity within the nucleus basalis (Ch4) in Parkinson's disease: reduced cell numbers and co-localization with cholinergic neurons. *Brain Res* 539, 19-30.

Muth K, Schonmeyer R, Matura S, Haenschel C, Schroder J & Pantel J (2009) Mild cognitive impairment in the elderly is associated with volume loss of the cholinergic basal forebrain region. *Biol Psychiatry* 67, 588-591.

Nakano I & Hirano A (1984) Parkinson's disease: neuron loss in the nucleus basalis without concomitant Alzheimer's disease. *Ann Neurol* 15, 415-418.

Oikawa H, Sasaki M, Ehara S & Abe T (2004) Substantia innominata: MR findings in Parkinson's disease. *Neuroradiology* 46, 817-821.

Oikawa H, Sasaki M, Tamakawa Y, Ehara S & Tohyama K (2002) The substantia nigra in Parkinson disease: proton density-weighted spin-echo and fast short inversion time inversion-recovery MR findings. *AJNR Am J Neuroradiol* 23, 1747-1756.

Olin JT, Aarsland D & Meng X (2010) Rivastigmine in the treatment of dementia associated with Parkinson's disease: effects on activities of daily living. *Dement Geriatr Cogn Disord* 29, 510-515.

Perry EK, Curtis M, Dick DJ, Candy JM, Atack JR, Bloxham CA, Blessed G, Fairbairn A, Tomlinson BE & Perry RH (1985) Cholinergic correlates of cognitive impairment in Parkinson's disease: comparisons with Alzheimer's disease. *J Neurol Neurosurg Psychiatry* 48, 413-421.

Pillon B, Dubois B, Cusimano G, Bonnet AM, Lhermitte F & Agid Y (1989) Does cognitive impairment in Parkinson's disease result from non-dopaminergic lesions? *J Neurol Neurosurg Psychiatry* 52, 201-206.

Poewe W (2009) Treatments for Parkinson disease--past achievements and current clinical needs. *Neurology* 72, S65-73.

Rinne JO, Rummukainen J, Paljarvi L & Rinne UK (1989) Dementia in Parkinson's disease is related to neuronal loss in the medial substantia nigra. *Ann Neurol* 26, 47-50.

Rinne UK, Rinne JO, Rinne JK & Laakso K (1987) Chemical neurotransmission in the parkinsonian brain. *Med Biol* 65, 75-81.

Rogers JD, Brogan D & Mirra SS (1985) The nucleus basalis of Meynert in neurological disease: a quantitative morphological study. *Ann Neurol* 17, 163-170.

Ruberg M, Rieger F, Villageois A, Bonnet AM & Agid Y (1986) Acetylcholinesterase and butyrylcholinesterase in frontal cortex and cerebrospinal fluid of demented and non-demented patients with Parkinson's disease. *Brain Res* 362, 83-91.

Rye D & DeLong MR (2003) Time to focus on the locus. *Arch Neurol* 60, 320.

Sasaki M, Shibata E, Tohyama K, Kudo K, Endoh J, Otsuka K & Sakai A (2008) Monoamine neurons in the human brain stem: anatomy, magnetic resonance imaging findings, and clinical implications. *Neuroreport* 19, 1649-1654.

Sasaki M, Shibata E, Tohyama K, Takahashi J, Otsuka K, Tsuchiya K, Takahashi S, Ehara S, Terayama Y & Sakai A (2006) Neuromelanin magnetic resonance imaging of locus ceruleus and substantia nigra in Parkinson's disease. *Neuroreport* 17, 1215-1218.

Schmitt FA, Aarsland D, Bronnick KS, Meng X, Tekin S & Olin JT (2010a) Evaluating rivastigmine in mild-to-moderate Parkinson's disease dementia using ADAS-cog items. *Am J Alzheimers Dis Other Demen* 25, 407-413.

Schmitt FA, Farlow MR, Meng X, Tekin S & Olin JT (2010b) Efficacy of rivastigmine on executive function in patients with Parkinson's disease dementia. *CNS Neurosci Ther* 16, 330-336.

Schrag A, Kingsley D, Phatouros C, Mathias CJ, Lees AJ, Daniel SE & Quinn NP (1998) Clinical usefulness of magnetic resonance imaging in multiple system atrophy. *J Neurol Neurosurg Psychiatry* 65, 65-71.

Schulz JB, Skalej M, Wedekind D, Luft AR, Abele M, Voigt K, Dichgans J & Klockgether T (1999) Magnetic resonance imaging-based volumetry differentiates idiopathic Parkinson's syndrome from multiple system atrophy and progressive supranuclear palsy. *Ann Neurol* 45, 65-74.

Shimada H, Hirano S, Shinotoh H, Aotsuka A, Sato K, Tanaka N, Ota T, Asahina M, Fukushi K, Kuwabara S, Hattori T, Suhara T & Irie T (2009) Mapping of brain acetylcholinesterase alterations in Lewy body disease by PET. *Neurology* 73, 273-278.

Shinotoh H & Hirano S (2010) Emerging in vivo evidence of subcortical cholinergic dysfunction in Parkinsonian syndromes. *Neurology* 74, 1406-1407.

Shulman JM, De Jager PL & Feany MB (2011) Parkinson's disease: genetics and pathogenesis. *Annu Rev Pathol* 6, 193-222.

Stern MB, Braffman BH, Skolnick BE, Hurtig HI & Grossman RI (1989) Magnetic resonance imaging in Parkinson's disease and parkinsonian syndromes. *Neurology* 39, 1524-1526.

Sudarsky L, Morris J, Romero J & Walshe TM (1989) Dementia in Parkinson's disease: the problem of clinicopathological correlation. *J Neuropsychiatry Clin Neurosci* 1, 159-166.

Tagliavini F, Pilleri G, Bouras C & Constantinidis J (1984) The basal nucleus of Meynert in idiopathic Parkinson's disease. *Acta Neurol Scand* 70, 20-28.

Taylor JP, Rowan EN, Lett D, O'Brien JT, McKeith IG & Burn DJ (2008) Poor attentional function predicts cognitive decline in patients with non-demented Parkinson's disease independent of motor phenotype. *J Neurol Neurosurg Psychiatry* 79, 1318-1323.

Whitehouse PJ, Hedreen JC, White CL, 3rd & Price DL (1983) Basal forebrain neurons in the dementia of Parkinson disease. *Ann Neurol* 13, 243-248.

Whitehouse PJ, Struble RG, Clark AW & Price DL (1982) Alzheimer disease: plaques, tangles, and the basal forebrain. *Ann Neurol* 12, 494.

Wichmann T & DeLong MR (2002) Neurocircuitry of Parkinson's disease. In *Neuropsychopharmacology: the difth generation of progress* [K Davis, D Charney, J Coyle and C Nemeroff, editors]. Philadelphia: Lippincott, Williams and Wilkins.

Wonderlick JS, Ziegler DA, Hosseini-Varnamkhasti P, Locascio JJ, Bakkour A, van der Kouwe A, Triantafyllou C, Corkin S & Dickerson BC (2009) Reliability of MRI-derived cortical and subcortical morphometric measures: effects of pulse sequence, voxel geometry, and parallel imaging. *Neuroimage* 44, 1324-1333.

Wood LD, Neumiller JJ, Setter SM & Dobbins EK (2010) Clinical review of treatment options for select nonmotor symptoms of Parkinson's disease. *Am J Geriatr Pharmacother* 8, 294-315.

Yoshimura M (1988) Pathological basis for dementia in elderly patients with idiopathic Parkinson's disease. *Eur Neurol* 28 Suppl 1, 29-35.

Tables and figures.

Table 1. Characteristics of PD and control groups: means ± SD

	N	Age	Edu	MMSE	H&Y Stage (n)
PD	29 (11F)	65.3 ± 8.8	17.1 ± 2.0	28.0 ± 1.6	1 (13); 2 (13); 3 (3)
Control	27 (11F)	63.7 ± 7.2	17.8 ± 2.4	28.6 ± 1.7	--

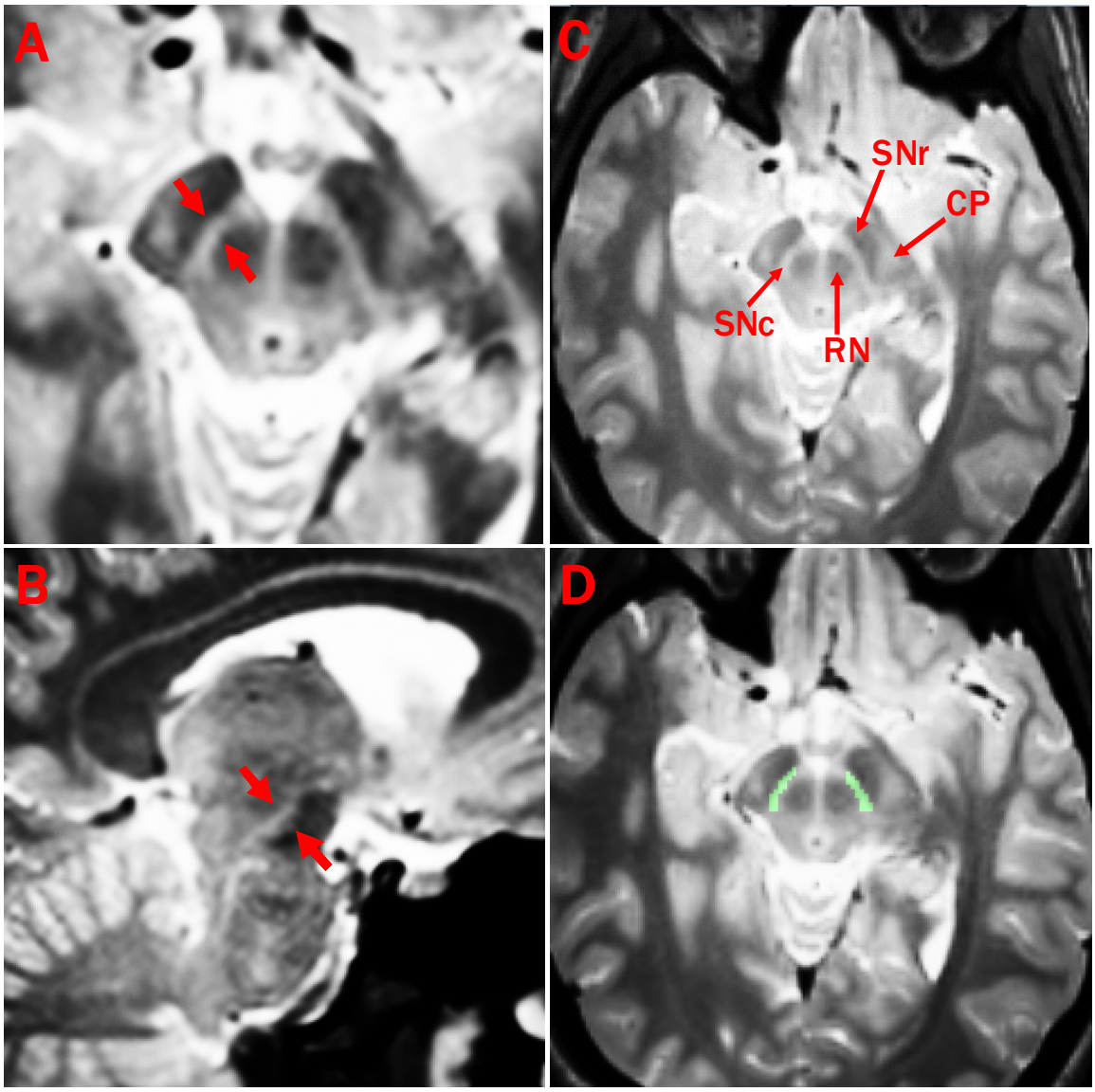

Figure 1. Representative **A**) axial and **B**) sagittal views of the midbrain of a control participant's multispectral weighted average showing the **C**) substantia nigra, pars compacta (SNc), substantia nigra, pars reticulata (SNr), red nucleus (RN), and cerebral peduncles (CP); **D**) example of a manually delimited label of SNc (green).

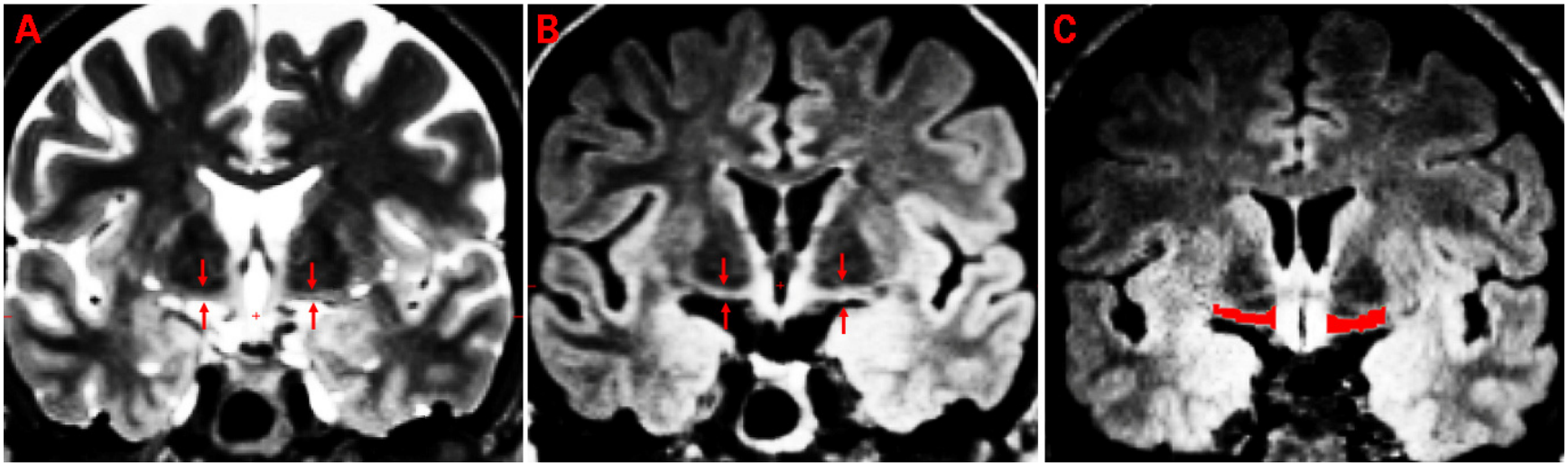

Figure 2. Coronal images at the level of the anterior commisure showing the basal forebrain in **A**) a T2-weighted image and in **B**) a T2-FLAIR image. These images clearly deomonstrate the improved contrast for both the superior and inferior boundaries in the T2-FLAIR images. **C**) example of a manually delimited label of BF (red).

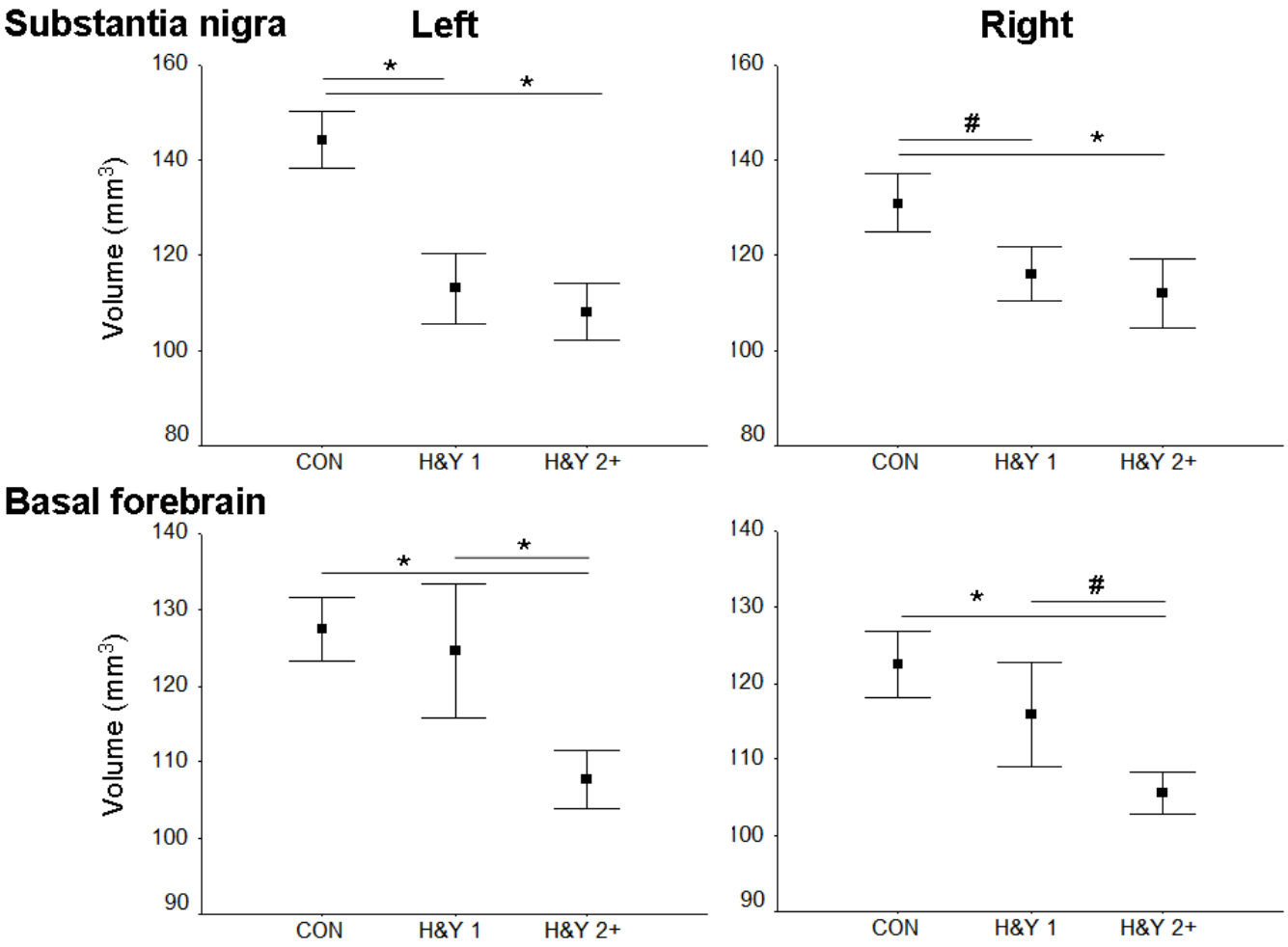

Figure 3. Mean volumes of the substantia nigra (top) and basal forebrain (bottom) for the left and right hemispheres for controls, patients in H&Y stage 1, and patients in H&Y states 2/3. Bars are means ±se; * denotes $p < .05$, # denotes $p < .1$.

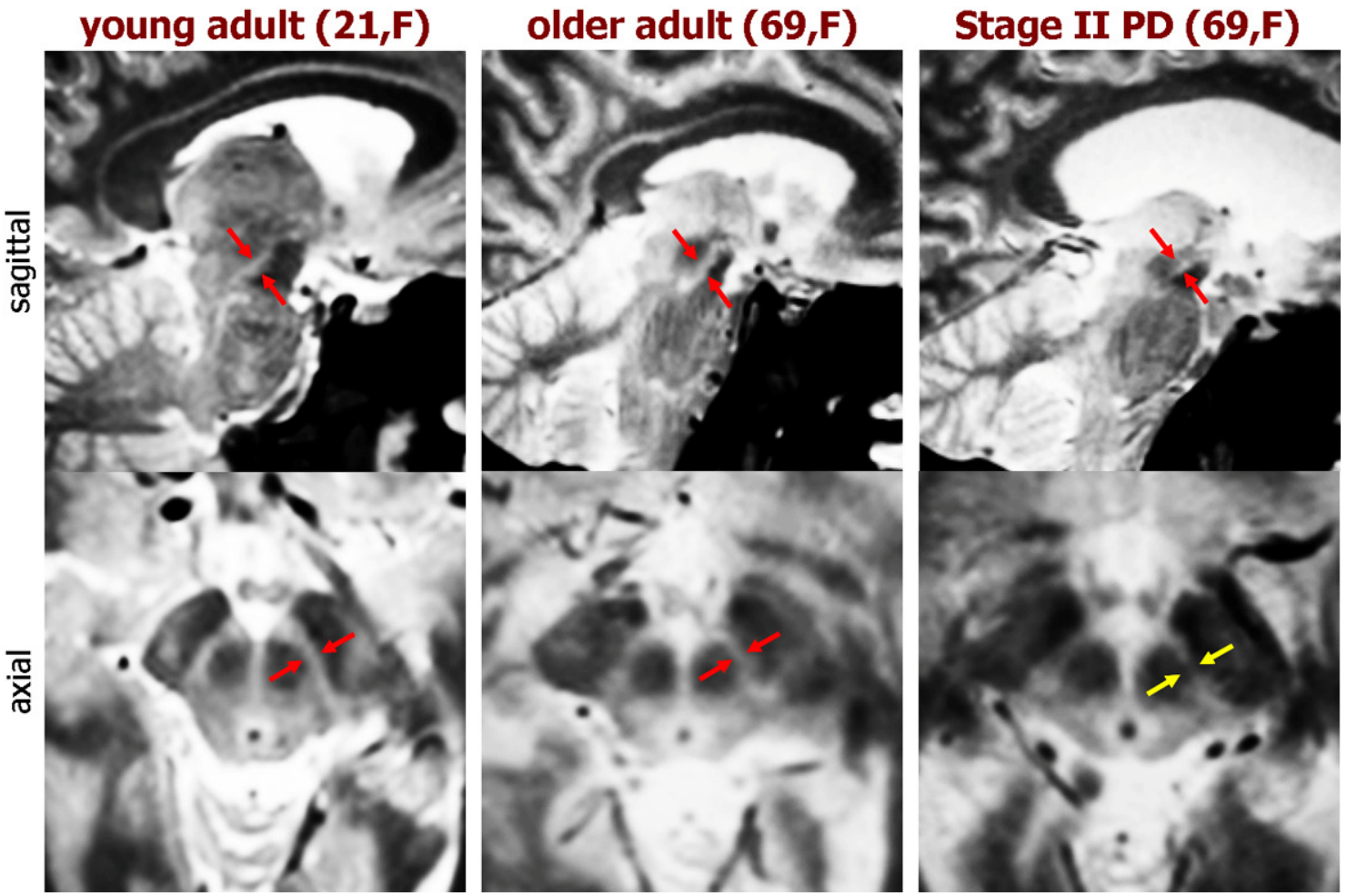

Figure 4. Multispectral weighted averages showing the substantia nigra (red arrows) in saggital (top) and axial views (bottom) for a young adult (left), a healthy control (middle), and an age- and sex-matched PD patient (right). Signal loss is readily apparent in the PD brain (yellow arrows).

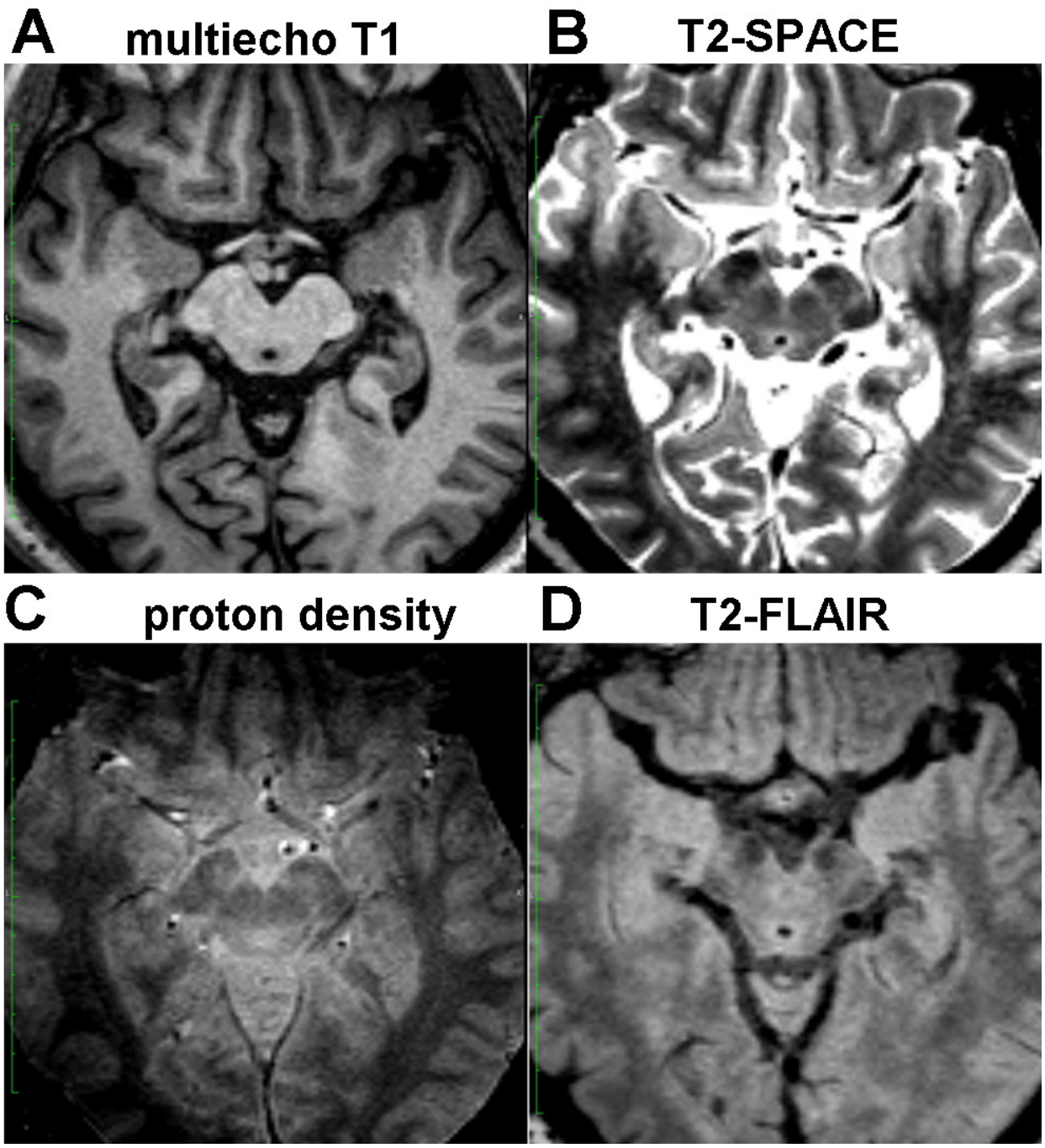

Supplementary Figure 1. Representative axial sections from one training subject showing the different multispectral contrasts: **A**) T1, **B**) T2-SPACE, **C**) Proton Density, and **D**) T2-FLAIR.

Acknowledgments

It was a privilege to have Suzanne Corkin as a graduate mentor. Ever since our first meeting, when she persuaded me to try my first cherrystone clam, Sue has encouraged me to broaden my perspective and to pursue new research avenues, even when they were outside my comfort zone. She taught me the value of striking a balance between collaboration and independent thinking and the importance of effective scientific communication. She has been a great mentor and a good friend, and I look forward to raising many more glasses of chardonnay together as we ponder scientific questions in the future.

I was extremely fortunate to have an outstanding committee. I want to thank John Gabrieli, Matti Hämäläinen, Earl Miller, and Chris Moore for their advice and constructive criticism of my research and for their enthusiasm and support of my professional development.

The Corkin Lab was an incredible place to spend my time as a graduate student, and I was lucky to have the opportunity to work with the many remarkable scientists that passed through the lab during my time at MIT. I am especially thankful to have shared the bulk of this journey with my fellow graduate student, Paymon Ashourian. I can't think of a better scientific collaborator, and I am truly grateful for his help with experimental design and data analysis and for the insightful comments he always provided about my experiments and interpretation. I was also lucky to work with a remarkably gifted group of postdocs, technical assistants, administrative assistants, and visiting faculty in the Corkin lab. This research would not have been possible without the hard work of Meredith Brown, Emily Connally, Colleen Koperek, Bettiann McKay, Olivier Piguet, Keyma Prince, Ivar Reinvang, Julien Wonderlick, and Jeremy Young.

One of the best parts of being at MIT was having the chance to work with some of its amazing undergraduate students. A number of UROPs made important contributions to this research, and I am proud to have worked with them: Erica Griffith, Leslie Hansen, Nicolas Harrington, Emma Jefferies, Cecily Koppuzha, and Alex Murphy.

Every chapter in this thesis is the result of collaborations with numerous colleagues, and I am indebted to them for their assistance. I would like to thank Stephanie Jones for sharing MEG data and for providing the computational modeling expertise that made Chapter 4 possible. Early on, David Salat gave me a crash course in DTI analysis, and this knowledge laid the foundation upon which the bulk of this thesis rests. Thanks to the MRI team at the Athinoula A. Martinos Center Imaging at the McGovern Institute for all of their technical support with the MRI components of my research: Sheeba Arnold, Steve Shannon, and Christina Triantafyllou. At the Athinoula A. Martinos Center for Biomedical Imaging at MGH, Brad Dickerson, Bruce Fischl, Allison Stevens, and Anastasia Yendiki created some of the most sophisticated MRI sequences and analysis tools available, which I used extensively in my research. I am indebted to John Growdon at MGH and Clemens Scherzer at BWH for their guidance on my research on Parkinson's disease and their help with patient recruitment.

I am also grateful for Jim Freeman, Susan Kennedy, and Jeff Pollard who were influential in my academic journey leading up to MIT. They showed me early on how rewarding scientific research could be and just how cool the brain is. Without Martha Herbert's open embrace and

contagious enthusiasm for science, I may not have persevered down the path of neuroscience research.

I never could have completed this undertaking without the unwavering support of my family and friends. I want to thank my mom, dad, and brother for always being there when I needed them and for encouraging me to make the big choices myself, all the while knowing I could lean on them if the path I chose proved tougher than anticipated. To my best friend and life partner, Peter—words cannot express how grateful I am for you. Having you by my side each and every day made it possible for me to complete this journey, and I am so excited to embark on our next adventure together. Thanks to my little man Swiffer, who provided countless hours of moral support and love from under my desk at MIT. He may not have made it to the end of this road with me, but he made the bulk of the journey immeasurably more enjoyable. Thanks to Roxie for wiggling her way into my life and making the last six months of my graduate career much more fun—I will miss you. And of course, I've got to include a quick shout-out to all of my friends at the MIT Libraries—not for the reference or metadata support, but because sometimes you just need a Muddy lunch.

Completion of this thesis depended greatly on the financial support of a number of funding sources: The HST-Martinos Catalyst Fund, The Advanced Multimodal Neuroimaging Training Program, the Singleton family, and numerous grants from the NIH, including T32 GM007484, T32 MH082718, and AG021525.